

Influenza A virus interferes with innate immune signaling in avian cells

by

Yanna Xiao

A thesis submitted in partial fulfillment of the requirements for the degree of

Doctor of Philosophy

in

Virology

Department of Medical Microbiology and Immunology
University of Alberta

© Yanna Xiao, 2019

Abstract

Retinoic Acid-Inducible Gene I (RIG-I) plays an essential role in the host innate immune response to influenza A viruses. RIG-I is present in ducks, but absent in chickens. Our previous work suggests that it might be worthwhile to make chickens transgenic for duck RIG-I under the control of its own promoter to improve their ability to detect and respond to influenza infection. However, it was not known whether the duck RIG-I promoter would function in chicken cells. Here, I identified the duck RIG-I promoter and showed that activation of the MAVS pathway by the constitutively active N-terminal region of RIG-I or poly (I:C) led to stimulation of duck RIG-I promoter activity. Two essential *cis*-regulatory elements in the core promoter region, a GC-box and an interferon-sensitive response element (ISRE) were responsible for the basal and inducible expression of duck RIG-I, respectively. Chicken IRF7 rather than chicken IRF1 induced duck RIG-I promoter activity using the putative ISRE. Thus, I have identified the minimal necessary promoter for basal and inducible expression of RIG-I, which can be used in transgenes.

PB1-F2 from influenza virus PR8 (H1N1) was reported to inhibit RIG-I mediated type I IFN production via interaction with MAVS in mammals, as the critical adaptor protein, duck MAVS was still not well characterized, but is very different from mammalian MAVS. PB1-F2 contributes to the high pathogenesis of A/Vietnam/1203/04 (H5N1) (VN1203) in ducks, but the underlying mechanism by which PB1-F2 increases the virulence of VN1203 was yet unknown. The multiple roles of PB1-F2 were mainly characterized in the mammalian system, and in a virus strain-, cell type-, and species-specific manner. Limited information about PB1-F2 is available in avian cells. Here, I characterized duck MAVS and PB1-F2 proteins from PR8 and three similar highly pathogenic avian influenza viruses: VN1203, reverse-genetics recombinant VN1203

(rgVN1203), and A/duck/Thailand/71.1/2004 (D4AT) in avian cells, and further investigated the association of these two proteins. DuMAVS and PR8 PB1-F2 were distributed in the mitochondria of DF-1 cells, while, H5N1 PB1-F2 proteins were distributed throughout the cells. Like human MAVS, overexpression of duck MAVS could stimulate IFN- β promoter activity and it associated with duck RIG-I 2CARD. All tested PB1-F2 proteins inhibited IFN- β promoter activities stimulated by duck RIG-I 2CARD and they all showed similar staining patterns and were co-immunoprecipitated by duck MAVS, suggesting interactions between these PB1-F2 proteins and duck MAVS are likely. These studies lead to greater understanding of the role of PB1-F2 in the contribution to viral virulence in the reservoir host.

Acknowledgements

Firstly, I would like to thank my supervisor, Dr. Kathy Magor for providing me with this Ph.D. opportunity and giving me the continuous support, right direction and kind encouragement throughout my degree. I will remember forever how kind of you to have me stay at your home, to introduce the local supermarkets, and to help me move into my first residence during the first week I landed in Canada. It was a huge help to me, a new arrival international student. More importantly, it is you who helped me get a big improvement of the language and presentation skills, which made me feel more confident during the usual life. Many thanks to you! Besides, here I must express my gratitude to Dr. Paul Melancon for your wonderful coordination skills, your consideration and your sacrifice of your leisure time, and to the leaders of MMI department, without you, I cannot stand here today.

I would like to thank my committee members, Dr. Hanne Ostergaard and Dr. David Marchant for your time, your guidance, and your valuable comments on my research and my thesis. I am also grateful to Dr. Brad Magor for your excellent experimental suggestions and critical reading of the manuscript of my first project. Additionally, thank you to the graduate coordinators, Dr. Deborah Burshtyn, Dr. Edan Foley and Dr. Kevin Kane for your concern and kind advice on my progress in the program.

I would also like to thank my lab mates Graham, Danyel, Ximena, Lee, Luke, David, Laura, Janet and Eric for their assistance, insightful feedback, cooperation and friendship. Graham, thank you for picking me up from the airport, touring me around the campus, and giving me useful suggestions on my experiments. Danyel, many thanks to your help in technical skills, constructive feedback to my writing, valuable suggestions on my research and job application, and of course your patience and kind friendship. Ximena and Lee, thank you for your emotional support, sharing life experiences with me, and your advice on all kinds of things, except for the research. I feel so lucky to have you guys during this long tough journey.

I would like to express my gratitude to all office staff in the MMI department and FGSR, particularly to Anne and Tabitha for your emotional and administrative support. Thank you also to Stephen Ogg, Gerry Barron and Dr. Xuejun Sun for your help with my confocal images.

Thanks to Li Ka Shing Sino-Canadian Exchange Program and Canadian Institutes of Health Research (CIHR) for supporting me financially to complete this program and thank you to CIHR for funding my Ph.D. projects.

Finally, I would like to give the most profound gratitude to my dear parents for providing me with unfailing support throughout all these years. To my beloved husband, Gangtao Peng, for your faith in me, constant support, and ongoing encouragement as a lover, a friend, and a wise senior. Without your company, I cannot go so far. To my adorable baby daughter, Annie Peng, for your coming into my life as the most precious gift from God and giving me the wonderful experience as a mom. Thank you! I love you all!

Table of Contents

Chapter 1 Introduction	1
1.1 Influenza A virus	2
1.1.1 Virology of Influenza A virus	2
1.1.2 Influenza A virus evolution, pandemic flu and H5N1	9
1.1.3 Treatment and prophylaxis of influenza infection.....	11
1.2 Overview of innate immune recognition of influenza A virus	14
1.2.1 Toll-like receptors.....	15
1.2.2 RIG-I like receptors	15
1.2.3 NOD-like receptors.....	17
1.3 RIG-I/MDA5 signaling pathway.....	18
1.3.1 Ligand recognition and activation of RIG-I and MDA5	18
1.3.2 Activation of MAVS and the downstream signaling pathway	21
1.4 Overview of suppression of host innate immune responses by influenza A virus.....	23
1.4.1 NS1	23
1.4.2 PB2, PA	25
1.4.3 PB1-F2 (polymerase basic protein 1-frame 2)	25
1.5 Ducks and influenza A virus	31
1.5.1 Ducks are the relevant species for influenza	31
1.5.2 Duck innate immune responses to influenza A virus	34
1.5.3 Influenza A virus evasion from duck innate immune responses.	38
1.6 Research objectives	39
Chapter 2 Materials and Methods	48
2.1 Cells and viruses.....	49
2.1.1 Primary duck embryonic fibroblast (DEF) and DF-1	49

2.1.2 HeLa cell line.....	49
2.1.3 AD293T cell line	49
2.1.4 Viruses	49
2.2 Amplification and identification of duck RIG-I promoter	50
2.2.1 PCR.....	50
2.2.2 Gel electrophoresis, gel extraction, and ligation to pCR2.1- TOPO vector	50
2.2.3 Transformation	51
2.2.4 Colony selection, mini-culture, and mini-prep	52
2.2.5 PCR or restriction digestion to identify the correct clones.....	52
2.2.6 Big Dye sequencing.....	52
2.2.7 Sequence analysis and alignment of amplified duck RIG-I promoter.....	53
2.2.8 Amplification and cloning the full-length duck RIG-I promoter (from -2024 to -1) ...	53
2.3 Bioinformatics	54
2.4 General procedure of plasmid construction	54
2.5 Specific plasmid construction	55
2.5.1 The full-length promoter reporter vector of duck RIG-I (p2024)	55
2.5.2 Serial deletion promoter vectors.....	56
2.5.3 Transcription factor (TF) binding site deletion mutants.....	57
2.5.4 TF binding site point mutation vectors (site-directed mutagenesis).....	58
2.5.5 pmCherry-chIRFI and pmCherry-dIRF1	58
2.5.6 No-tag/Flag/GST/GFP-PB1-F2 (PR8/ Rg/D4AT/VN) vectors.....	59
2.5.7 Flag-PB1-F2 (VN) point mutation vectors (site-directed mutagenesis).....	60
2.6 Cell seeding and transfection	60
2.7 Dual luciferase assay.....	61
2.7.1 To investigate RIG-I promoter activity	61

2.7.2 To investigate PB1-F2 influence in IFN- β reporter activity.	62
2.8 Quantitative RT-PCR analysis of transcription factor (TF) genes in DF-1 cells.	62
2.8.1 RNA extraction.....	62
2.8.2 cDNA synthesis	62
2.8.3 Real-time PCR.....	63
2.9 Statistical analysis	63
2.10 General procedures of immunofluorescence (IF) staining.....	63
2.10.1 Visualization of mCherry-tagged IRF proteins.	64
2.10.2 Investigation of the distribution of duck MAVS and PB1-F2 in DF-1 cells or HeLa cells.....	65
2.10.3 Investigation of the colocalization between duck MAVS and RIG-I 2CARD or PB1-F2 in DF-1 cells or HeLa cells.....	65
2.11 Protein extraction from cell culture and GST-pull downs	65
2.12 Co-immunoprecipitation (Co-IP).....	66
2.13 Western Blotting (WB)	67
Chapter 3 Results-Part I: The Core Promoter Controls the Basal and Inducible Expression of Duck Retinoic Acid Inducible Gene-I (RIG-I)	75
3.1 Rationale.....	76
3.2 Results	76
3.2.1 The identification and cloning of the duck RIG-I promoter sequence.....	76
3.2.2 The alignment of the full-length promoter sequence of duck RIG-I with the published RIG-I genome sequence in Ensembl.	77
3.2.3 Unlike RIG-I proteins, RIG-I promoters do not show an expected phylogenetic relationship.	78
3.2.4 The duck RIG-I promoter is inducible by RIG-I signaling and poly (I:C).....	78
3.2.5 The time frame of basic and inducible expression of duck RIG-I.....	79

3.2.6 The core promoter of duck RIG-I is inducible.	79
3.2.7 Identification of putative transcription factor binding sites.....	80
3.2.8 Neither IRF1 nor IRF7 was upregulated at the transcriptional level by the stimulation by RIG-I 2CARD.....	81
3.2.9 Chicken IRF7 induces promoter activity of duck RIG-I in DF-1 cells.	82
3.3 Summary	83
3.4 Discussion	83
Chapter 4 Results-Part II: Duck MAVS Signaling and Inhibition by PB1-F2.....	100
4.1 Rationale.....	101
4.2 Results	102
4.2.1 Duck MAVS has only 27.82% amino acid sequence identity to human MAVS.	102
4.2.2 Duck MAVS is most closely related to chicken MAVS.	102
4.2.3 Duck MAVS is localized on mitochondria of DF-1 cells.	103
4.2.4 Overexpression of duck MAVS stimulates IFN- β promoter activity in DF-1 cells... ..	103
4.2.5 Human RIG-I 2CARD is not able to interact with avian MAVS to stimulate IFN- β promoter activity in DF-1 cells.....	104
4.2.6 Duck MAVS has a similar staining pattern to duck RIG-I 2CARD and it can be pulled down by GST tagged duck RIG-I 2CARD.....	104
4.2.7 PB1-F2 (PR8) inhibits duck RIG-I 2CARD and duck MAVS mediated IFN- β promoter activity.....	105
4.2.8 PB1-F2 (PR8) is localized to the mitochondria of DF-1 cells.....	106
4.2.9 PB1-F2 (PR8) has a similar staining pattern to duck MAVS and immunoprecipitated with V5-MAVS.	106
4.3 Summary	107
4.4 Discussion	107

Chapter 5 Results-Part III: Inhibition of MAVS Signaling by PB1-F2 from H5N1 Highly Pathogenic Avian Influenza Viruses in Avian Cells.....	120
5.1 Rationale.....	121
5.2 Results.....	122
5.2.1 The amino acid alignment of PB1-F2 from three similar HPAI H5N1 and PR8 (H1N1).....	122
5.2.2 Expression levels of different tagged PB1-F2 vectors in DF-1 cells.	123
5.2.3 PB1-F2 (Rg/D4AT/VN) are distributed throughout DF-1 cells.	124
5.2.4 VN1203 PB1-F2 is the most potent inhibitory factor to RIG-I 2CARD mediated IFN- β promoter activity.....	124
5.2.5 T51M point mutation alone does not change the function of wild-type PB1-F2 (VN)	125
5.2.6 The indicated point mutations do not change the inhibiting function of wild-type VN1203 PB1-F2 to RIG-I 2CARD mediated IFN- β promoter activity.	126
5.2.7 PB1-F2 has a similar staining pattern to duck MAVS.	126
5.2.8 PB1-F2 was immunoprecipitated by duck MAVS.	127
5.3 Summary	129
5.4 Discussion	129
Chapter 6 Summary, Discussion and Future Directions.....	145
6.1 Summary of results.....	146
6.2 Discussion and future directions	147
References.....	156
Appendix I-Commonly Used Buffers and Solutions	193
Appendix II-Sequence ID	197

List of Tables

Table 2-1 Primers used for the full-length duck RIG-I promoter amplification.....	68
Table 2-2 Primers used for generating serial truncated constructs of duck RIG-I promoter.....	68
Table 2-3 Primers used for TF binding site deletion or point mutation constructs of duck RIG-I promoter.....	68
Table 2-4 Primers used for generating various expression vectors	69
Table 2-5 Primers used for sequencing.....	70
Table 2-6 Primer and probe sequences used in quantitative real-time PCR (qPCR).....	70
Table App-1 The sequence ID of RIG-I proteins	197
Table App-2 The sequence ID of RIG-I promoters	197
Table App-3 the sequence ID of MAVS proteins.....	198

List of Figures

Figure 1.1 A schematic of the spherical influenza A virus particle.....	40
Figure 1.2 A schematic illustration of the eight RNA segments of influenza A virus and the viral proteins encoded by each segment.....	41
Figure 1.3 Nomenclature of influenza viruses.....	42
Figure 1.4 Influenza A virus life cycle.	43
Figure 1.5 A model of signal activation by full-length RIG-I and MAVS.....	44
Figure 1.6 Schematic of MAVS.....	45
Figure 1.7 RIG-I/MDA5 signaling pathway stimulated by influenza A virus.	46
Figure 1.8 Overview the multiple roles of PB1-F2.....	47
Figure 2.1 The schematic generation of the full-length duck RIG-I promoter TOPO vector.	72
Figure 2.2 The schematic of inverse PCR for site-directed deletion mutagenesis.	72
Figure 2.3 The schematic of the primer binding sites in the full-length RIG-I promoter vector..	73
Figure 2.4 The point mutations in the RIG-I core promoter region.....	74
Figure 3.1 The nucleotide sequences of the amplified fragments and CpG island prediction	86
Figure 3.2 The alignment of the identified full-length promoter sequence of duck RIG-I with the published duck RIG-I genome sequence in Ensemble.	89
Figure 3.3 Phylogenetic analysis of RIG-I proteins and <i>DDX58</i> promoters.	90
Figure 3.4 The duck RIG-I promoter activity is induced by MAVS signaling downstream of RIG-I 2CARD or poly (I:C) stimulation.....	92
Figure 3.5 RIG-I promoter activity at different time points post-transfection.	93
Figure 3.6 The region between -250 and -73 confers basal and IFN- β inducible activity of the duck RIG-I promoter.....	94
Figure 3.7 Deletion of the GC-box and ISRE <i>cis</i> elements decreased the basal and inducible RIG-I promoter activity, respectively.	96
Figure 3.8 Neither IRF1 nor IRF7 was upregulated at the transcriptional level by the stimulation of RIG-I 2CARD.....	97
Figure 3.9 Chicken IRF7 and duck IRF1 induce RIG-I promoter activity.....	99
Figure 4.1 MAVS amino acid alignment.....	111
Figure 4.2 Phylogenetic analysis of MAVS proteins.....	112

Figure 4.3 Duck MAVS localizes to mitochondria of DF-1 cells.	113
Figure 4.4 Duck MAVS overexpression promotes the IFN- β promoter activity.	114
Figure 4.5 The RIG-I 2CARD interaction with MAVS to stimulate IFN- β promoter activity is species-specific.	115
Figure 4.6 Duck MAVS has a similar staining pattern to duck RIG-I 2CARD and can be pulled down by GST tagged duck RIG-I 2CARD.	116
Figure 4.7 PB1-F2 (PR8) inhibits duck RIG-I 2CARD and duck MAVS mediated IFN- β promoter activity.	117
Figure 4.8 PB1-F2 (PR8) is co-localized with the mitochondria of DF-1 cell.	118
Figure 4.9 PB1-F2 (PR8) has a similar staining pattern to duck MAVS and can be immunoprecipitated with V5-MAVS.	119
Figure 5.1 Amino acid alignment of PB1-F2.	132
Figure 5.2 Expression levels of PB1-F2 fusion proteins in DF-1 cells.	134
Figure 5.3 The distribution of HPAI H5N1 PB1-F2 in DF-1 cells.	137
Figure 5.4 Among three tested H5N1 PB1-F2, VN1203 PB1-F2 has the strongest inhibitory activity to RIG-I 2CARD induced IFN- β reporter activity.	139
Figure 5.5 T51M point mutation alone does not change the function of wild-type VN PB1-F2.	140
Figure 5.6 The indicated point mutations do not change the inhibiting function of wild-type VN PB1-F2 on RIG-I 2CARD mediated IFN- β reporter activity.	141
Figure 5.7 PB1-F2 co-localizes with duck MAVS.	143
Figure 5.8 PB1-F2 was immunoprecipitated by duck MAVS.	144
Figure 6.1 Overview of my findings and questions left unanswered	155

List of Abbreviations

AIV	Avian Influenza Virus
ALR	AIM2-Like Receptor
ANOVA	One-Way Analysis of Variance
ANT3	Adenine Nucleotide Translocator 3
ARDS	Acute Respiratory Distress Syndrome
BIR	Baculovirus Inhibitor Repeat
CARD	Caspase Activation and Recruitment Domain
Cardif	CARD Adaptor Inducing IFN- β
CD	Circular Dichroism
cDNA	Complementary DNA
ChIFN- β	Chicken IFN- β
CLR	C-Type Lectin Receptors
Co-IP	Co-Immunoprecipitation
CPSF	Cleavage and Polyadenylation Specificity Factor
CRM1	Chromosomal Region Maintenance 1
cRNA	Complementary Genomic RNA
CTD	C-Terminal Domain
CYLD	Cylindromatosis
DAMP	Danger Associated Macular Pattern
dATP	Deoxyadenosine Triphosphate
ddH ₂ O	Double-Distilled Water
DEF	Duck Embryoic Fibroblast
DF1	Chicken Embryonic Fibroblast Cell Line
DMEM	Dulbecco's Modified Eagle Medium
DNA	Deoxyribonucleic Acid
DRV	Duck Reovirus
DUBA	De-Ubiquitinating Enzyme A
ER	Endoplasmic Reticulum
FADD	Fas-Associated Death Domain
FAO	Food and Agriculture Organization
FBS	Fetal Bovine Serum
GAF	Gamma Interferon Activation Factor
GAPDH	Glyceraldehyde 3-Phosphate Dehydrogenase
GAS	Gamma Interferon Activation Site
GST	Glutathione-S-Transferase
HA	Hemagglutinin
HMW	High Molecular Weight
HPAI	Highly Pathogenic Avian Influenza

IF	Immunofluorescence
IFITMs	Interferon-Induced Transmembrane Protein
IFN	Interferon
IFNAR	IFN- α Receptor
IKK α /IKK β /IKK γ /IKK ϵ	Inhibitor of Kappa B Kinase Subunit Alpha/Beta/Gamma/Epsilon
IMP β	Importin β
IMP α	Importin α
IPS-1	IFN-B Promoter Stimulator 1
IRFs	Interferon-Regulatory Factors
ISG	Interferon-Stimulated Gene
ISGF3	IFN-Stimulated Gene Factor 3
ISRE	IFN-Stimulated Response Elements
I κ B	Inhibitory κ B
JAK-STAT	Janus Activated Kinase-Signal Transducer and Activator of Transcription
LB	Lysogeny Broth
LPAI	Low Pathogenicity Avian Influenza
LRR	Leucine-Rich Repeat
M1	Matrix 1
M2	Matrix 2
MAM	Mitochondrial-Associated Endoplasmic Reticulum Membrane
MAVS	Mitochondrial Antiviral Signaling
MCA	Mander's Coefficient A
MCB	Mander's Coefficient B
MDA5	Melanoma Differentiation-Associated Gene-5
MDCK	Madin-Darby Canine Kidney
MMP	Mitochondrial Membrane Potential
mRNA	Messenger RNA
MS	Mass Spectrometric
Mx	Myxovirus Resistance Proteins
MyD88	Myeloid Differentiation Primary-Response Protein 88
NA	Neuraminidase
NCBI	National Centre For Biotechnology
NEMO	NF- κ B Essential Modulator
NEP	Nuclear Export Protein
NES	Nuclear Export Signal
NF- κ B	Nuclear Factor-Kappa B
NLR	Nucleotide Oligomerization Domain (NOD)-Like Receptor
NLS	Nuclear Localization Signals
NMR	Nuclear Magnetic Resonance
NP	Nucleoprotein

NPC	Nuclear Pore Complex
NS1	Non-Structural Protein 1
NS2	Non-Structural Protein 2
NSP1	Non-Structural Protein 1
OAS	2', 5'-Oligoadenylate Synthetase
OIE	World Organization for Animal Health
ORF	Open Reading Frame
PA	Polymerase Acidic Protein
PABPII	Poly(A) Binding Protein II
PAMP	Pathogen-Associated Molecular Pattern
PB1	Polymerase Basic Protein 1
PB1-F2	Polymerase Basic Protein 1 – Frame2
PB2	Polymerase Basic Protein 2
PBMCs	Peripheral Blood Mononuclear Cells
PCC	Pearson's Correlation Coefficient
PCR	Polymerase Chain Reaction
PKC	Protein Kinase C
PKR	Protein Kinase R
PNK	Polynucleotide Kinase
Poly (I:C)	Polyinosinic–Polycytidylic Acid
PP1 α	Phosphoprotein Phosphatase 1 α
PP1 γ	Phosphoprotein Phosphatase 1 γ
PR8	A/Puerto Rico/8/1934 (H1N1)
PRR	Pattern Recognition Receptor
PTPC	Permeability Transition Pore Complex
PYD	Pyrin Domain
qPCR	Quantitative Real-Time Polymerase Chain Reaction
RA	Retinoic Acid
RanGAP	Ran GTPase Activating Protein
RBD	RNA Binding Domain
RdRp	RNA Dependent RNA Polymerase
RIG-I	Retinoic Acid-Inducible Gene I
RIP1	Receptor Interacting Protein 1
RLR	RIG-I Like Receptor
RLU	Relative Luciferase Units
RNA	Ribonucleic Acid
RT-PCR	Reverse Transcription-Polymerase Chain Reaction
SA	Sialic Acid
SDS	Sodium Dodecyl Sulfate
SMs	Synonymous Mutations
SOC	Super Optimal Broth with Catabolite repression

TBK1	TANK-Binding Kinase 1
TF	Transcription Factor
TIMs	TRAF-Interacting Motifs
TIR	Toll/IL-1 Receptor
TLR	Toll-Like Receptor
TOM 40	Translocase of The Outer Membrane 40 Channels
TRADD	TNF Receptor-Associated Death Domain
TRAF	Tumor Necrosis Factor Receptor-Associated Factor
TRIF	TIR Domain-Containing Adaptor Protein Inducing IFN- β
TRIM	Tripartite-Motif Family
VDAC1	Voltage-Dependent Anion Channel 1
VISA	Virus-Induced Signaling Adaptor
VN1203	A/Vietnam/1203/04 (H5N1)
vRNPs	Viral Ribonucleoproteins
WB	Western Blotting
WCL	Whole Cell Lysate
WHO	World Health Organization
$\Delta\psi_m$	Change in Mitochondrial Inner Membrane Potential

Chapter 1 Introduction

1.1 Influenza A virus

Influenza A virus, along with three other influenza viruses (B, C, and D), compose the four influenza virus genera in the family of Orthomyxoviridae. They are different in host range and pathogenicity. Influenza A viruses infect a wide variety of species, including humans, horses, pigs, waterfowl and other hosts, and cause recurrent epidemics and occasionally massive outbreaks known as pandemics. Whereas, influenza B viruses are only seen in humans and cause mild seasonal epidemics, though they have a similar structure and genome composition to influenza A viruses. Influenza C and D viruses are more divergent than influenza B. Although influenza C viruses predominantly infect humans, they are detected less frequently and generally cause mild respiratory disease and are not thought to lead to epidemics. Influenza D viruses, the most recently isolated influenza viruses, primarily infect cattle and are not known to infect or cause illness in humans (Ferguson et al., 2016; Hause et al., 2014; Taubenberger and Kash, 2010).

1.1.1 Virology of Influenza A virus

1.1.1.1 Influenza A virus structure, genome and viral proteins

Influenza A virus is an enveloped virus and its outer lipid layer is derived from host cellular membrane during budding (Noda, 2011). Numerous glycoproteins, hemagglutinin (HA) and neuraminidase (NA) form spike structures inserted into the lipid membrane, and matrix 2 (M2) proteins make up proton channels in it. Among these three transmembrane proteins, HA is the most abundant, accounting for about 80 percent, followed by NA, around 17 percent, the minor component is M2, with only 16-20 molecules per virion (Nayak et al., 2009; Schroeder et al., 2005). Beneath the outer lipid layer is the peripheral membrane protein, matrix 1 (M1), which forms a shell to maintain virion morphology. The genome of influenza A viruses is associated with multiple copies of nucleoproteins (NPs) and the polymerase complexes; all three are in the core of virions. Additionally, limited amounts of nuclear export proteins (NEPs) are also observed in the interior of virions (Yasuda et al., 1993) (Figure 1.1)

Typically, the shape of the influenza A virus particle (also called a virion) is roughly spherical with the diameter ranging from approximately 80–120 nanometers, but occasionally, it forms a filamentous shape with the length more than 20 micrometers (Noda, 2011; Sugita et al., 2011).

Most lab-adapted influenza A virus strains show a spherical phenotype, whereas the clinical isolates are predominantly filamentous (Kilbourne and Murphy, 1960). There are several factors that determine virion morphology, including M1 and M2 proteins, polarized cell phenotype, and actin cytoskeleton networks (Elleman and Barclay, 2004; Roberts and Compans, 1998). Nevertheless, the significance of filamentous morphology in viral pathogenesis or replication is still unclear.

The genome of influenza A viruses consists of eight negative single-stranded RNA segments. Each segment contains conserved and partially complementary sequences at the 3' and 5' ends, which form the core promoter of vRNA (Desselberger et al., 1980; Robertson, 1979; Skehel and Hay, 1978). The sizes of these eight segments range from 890 to 2341 bp. From the longest to the shortest, the segments are numbered from segment 1 to segment 8 or named based on the main protein they code for. For instance, segments from 1 to 8 are also named PB2 (Polymerase basic subunit 2), PB1 (Polymerase basic subunit 1), PA (Polymerase acidic subunit), HA (Hemagglutinin), NP (Nucleoprotein), NA (Neuraminidase), M (Matrix), and NS (Non-Structural), respectively. Each viral RNA (vRNA) segment is associated with multiple NPs and a heterotrimeric polymerase complex (PB1, PB2, and PA) to form individual ribonucleoprotein complexes (RNP) composed of a flexible rod-like structure folded back and coiled on itself (Compans et al., 1972). RNP complex is the fundamental unit for transcription and replication of the viral genome (Eisfeld et al., 2015). The heterotrimeric polymerase complex is bound to the base-paired genomic end, also known as the promoter region of vRNA to form a hook conformation, which has been crystallized and illustrated in recent experiments (Pflug et al., 2014; Reich et al., 2014). NP binds to a unique segment of negative single strand RNA (vRNA) at a ratio of 1:24 (NP: RNA nucleotides) along the entire length with high affinity and without sequence specificity. It bears nuclear localization signals (NLS) to import the viral genome into cell nucleus (Baudin et al., 1994; Compans et al., 1972; Scholtissek and Becht, 1971).

Each segment codes for at least one essential viral protein. To date, up to 16 viral proteins encoded by these eight segments have been reported (Jagger et al., 2012; Muramoto et al., 2013; Wise et al., 2009; Wise et al., 2012). Segments 1, 4, 5, and 6 encode a single protein, while segments 2, 3, 7, and 8 code for 3 (PB1, PB1-F2 and PB1-N40), 4 (PA, PA-X, PA-N155, and

PA-N182), 3 (M1, M2, and M42), and 2 (NS1 and NEP) viral proteins, respectively (Schrauwen et al., 2014). The schematic illustration of the eight individual segments, as well as the proteins encoded by each segment is shown in Figure 1.2.

1.1.1.2 Influenza A virus classification and nomenclature

Based on the genetic and antigenic properties of surface glycoproteins, HA and NA, influenza A virus is classified into different subtypes. To date, there have been 18 different HA antigens (H1-H18), and 11 different NA antigens (N1-N11) reported. Therefore, a variety of different combinations of HA and NA are possible. Such as H1N1, H5N1, H7N9, and so on. Of these, H17N10 and H18N11 were recently discovered in Central and South American fruit bats, and only found in this species (Tong et al., 2012; Tong et al., 2013). All other remaining 16 HA and 9 NA subtypes can be isolated from wild aquatic birds. H1N1 and H3N2 are the only two subtypes currently circulating among humans (Fouchier and Munster, 2009; reviewed by Olsen et al., 2006).

According to the predominantly infected species, influenza A virus is classified into avian and mammalian influenza A virus. Avian influenza A virus is further divided into highly pathogenic avian influenza (HPAI) or low pathogenicity avian influenza (LPAI) based on molecular characteristics of the virus (presence of HA polybasic cleavage site) and the severity of the disease in chickens in a laboratory setting (Mishra et al., 2017). HPAI and LPAI designation only refer to the illness severity in chickens, not in other species. For example, both HPAI and LPAI have caused severe illness in humans, but some HPAI is not lethal in other avian species, such as ducks. All mammalian influenza A virus genes are thought to originate from avian influenza viruses. However, the direct infection of humans by avian influenza viruses via contact with infectious secretions or contaminated poultry products is infrequent. Fortunately, there is still no documentation of sustained transmission of avian influenza A viruses in humans.

The currently used nomenclature system of influenza viruses was established by the World Health Organization (WHO) in 1980. The first designation is influenza virus type, which is determined by the antigenicity of the conserved viral protein, NP. The next one is to designate the host and geographic sources of the isolated influenza viruses, followed by the strain number

and the isolated year. Finally, it indicates the subtype of influenza virus based upon the classification rule by HA and NA surface proteins (1980b). If the influenza viruses are isolated from humans, the host can be omitted. The diagram of influenza nomenclature is shown in Figure 1.3.

1.1.1.3 The life cycle of influenza A virus

The life cycle of influenza A virus can be divided into several steps: entry into the host cells; vRNPs getting released and imported into nucleus; transcription and replication of vRNA; vRNPs exportation from the nucleus; assembly and budding. The details of each step will be discussed below and are illustrated in Figure 1.4.

Entry into the host cells

As the first step in the virus life cycle, entry into the host cells is initiated by the recognition of sialic acid (SA) receptors on the surface of susceptible host cells by HA. Two significant linkages between SA and the carbohydrates they bind to in cellular membrane glycoprotein or glycolipid can be recognized by HA, α 2,3-linkage and α 2,6-linkage. These two types of SA receptors determine the host and cell type specificity of influenza A viruses. For example, human influenza A viruses recognize α 2, 6-linked SA receptors that are mainly found on epithelial cells in the upper respiratory tract of humans, whereas avian influenza A viruses recognize α 2,3-linked SA receptors which are abundantly expressed on epithelial cells in the avian intestine and the human lower respiratory tract.

The initial synthesized form of HA is a single polypeptide precursor HA0, which is non-functional. To become biologically active, HA0 needs to be cleaved by cellular proteases into H1 and H2 subunits, which are linked by disulfide bonds. HA1 contains the functional domain that binds to SA receptors, and HA2 has a fusion peptide which mediates the fusion of the virus with the host endosomal membrane (reviewed by Huang et al., 2003; reviewed by Skehel and Wiley, 2000). The proteolytic character contributes to the tropism and pathogenicity of influenza A virus. For instance, a hallmark of HPAI is acquiring a multi-basic cleavage site at HA0. Unlike the mono-basic cleavage site, only cleaved by trypsin-like protease, which is limited to the intestinal and respiratory system, the multi-basic cleavage site can be cleaved by ubiquitous

proteases, thus, the virus has the potential to infect and grow systemically in the host (reviewed by Bertram et al., 2010; Straus and Whittaker, 2017).

Upon binding to the SA receptors by HA1, influenza A viruses are internalized via receptor-mediated endocytosis (Matlin et al., 1981) and sequentially exposed to early endosome (pH 6.0-6.5), late endosome (pH 5.0-5.5), and lysosome (pH 4.6-5.0) (reviewed by Mellman et al., 1986). The low pH triggers significant conformation changes of HA proteins, leading to the fusion between viral and the endosomal membranes. Additionally, the acidic environment in the endosome compartment also opens up the M2 proton-selective ion channel to acidify the virion core, leading to vRNPs becoming dissociated from M1 proteins and released into host cytoplasm (Pinto et al., 1992; Sansom and Kerr, 1993; Takeuchi et al., 1994).

vRNPs trafficking into the nucleus

Following release into the cytoplasm, vRNPs must be shuttled to the nucleus where the viral replication and transcription take place. Small molecules and proteins are able to cross the nuclear envelope through the nuclear pore complexes (NPCs) via passive diffusion, whereas, the large molecules greater than 40 kDa, including vRNPs, have to be actively transported across NPC, which involves nuclear localization signal (NLS) motifs in cargo proteins and transportation factors or carrier molecules cycling between cytoplasm and nucleus (Eisfeld et al., 2015; Stewart, 2007). There are a few nuclear transport pathways that use different carriers (Fahrenkrog and Aebi, 2003; reviewed by Pemberton and Paschal, 2005). In the early stage of the viral life cycle, vRNPs are believed to utilize the classical nuclear import pathway to enter the nucleus. In brief, the primary NLS motifs in vRNP protein components (NP, PB1, PB2, and PA) are recognized by the adaptor protein, importin α (IMP α) (Neumann et al., 1997; Nieto et al., 1994; Tarendeau et al., 2007; Wang et al., 1997), which is further associated with the transport receptor, importin β (IMP β) to form IMP α -IMP β -cargo complex before entering the nucleus across NPC. Once inside the nucleus, IMP β and IMP α are sequentially dissociated from the complex using RanGTPase and CAS protein and release the vRNP cargo into the nuclear plasma. The carriers themselves will be recycled back to the cytoplasm (Eisfeld et al., 2015).

Transcription and replication of vRNA

Once in the nucleus, parental vRNPs are first transcribed into viral mRNA (primary transcription) and are replicated into the full-length complementary genomic RNA (cRNA) serving as the template to amplify vRNA. The mRNA transcripts are in turn exported into the cytoplasm to direct the translation of viral proteins. The amplified vRNAs are subsequently associated with the newly generated viral NPs and polymerase proteins to generate progeny vRNPs, that can be used as templates again to transcribe (the secondary transcription) and replicate, and eventually be incorporated into large numbers of progeny virions.

The primary transcription is initiated by a cap-snatching process involving the viral PB2 and PA. In brief, the viral polymerase proteins PB2 and PA recognize and snatch the 7-methylguanosine cap structure of cellular pre-mRNAs (Plotch et al., 1981) or noncoding RNA (Gu et al., 2015; Koppstein et al., 2015) to use as primers to copy its own RNA genome. At the end of transcription, poly-A tails are produced via a stuttering copying of oligo-uracil sequences located at the conserved 5'-end of vRNA. The viral polymerase protein, PB1, mediates this process. Once the first transcription is done, the produced viral mRNAs are exported to the cytoplasm and translated into various viral proteins, including NP and the viral polymerase proteins (PB1, PB2, and PA). Subsequently, these proteins are imported into the nucleus and used to generate progeny vRNPs together with the replicated vRNAs (Jorba et al., 2009; Plotch et al., 1979; Poon et al., 1999; Robertson et al., 1981).

Unlike viral transcription, viral replication is a primer-independent process and catalyzed by soluble viral RNA dependent RNA polymerase (RdRp), also known as the viral polymerase protein complex. Whereas, the viral transcription is dependent on the resident polymerase protein complex (Fodor, 2013; Jorba et al., 2009). Additionally, the newly translated viral NP is responsible for protecting viral genome RNA from degradation (Vreede et al., 2004). However, the full mechanism of viral replication is still unknown, such as: how does vRNA cooperate with the polymerase protein complex and NPs to form the final vRNP structure?

Exportation of vRNPs from the nucleus

The assembly and budding processes occur on the cellular plasma membrane. Therefore, as a prerequisite, the newly synthesized progeny vRNPs must be exported from the cell nucleus into

the cytoplasm. This transportation is mediated by CRM1 (chromosomal maintenance 1)-dependent nuclear export pathway. In brief, the nuclear export receptor, CRM1, also known as exportin 1, recognizes the leucine-rich nuclear export signal (NES) motifs in cargo proteins and binds to GTP-loaded Ran GTPase, which transports cargo proteins across NPC in a complex form. On the cytosolic face of NPC, Ran-GTP is hydrolyzed to Ran GDP by Ran GTPase activating protein (RanGAP), which stimulates the dissociation of CRM1-Ran GTPase-cargo protein complex. The cargo is released into the cytoplasm. Ran-GDP and CRM1 are transported back into the nucleus for another round of nuclear export (Eisfeld et al., 2015). The NES motifs are only found in NP proteins among the vRNP complexes, and there is evidence to show the direct interaction between NP and CRM1 (Elton et al., 2001). While, another two viral proteins, M1 and NEP, are also requisite in this process because NP cannot be exported out of nucleus lack either of them (Bui et al., 2000; Martin and Helenius, 1991). M1 is known to interact with NEP (Akarsu et al., 2003; Shimizu et al., 2011), which in turn interacts with CRM1 via the NES motif in its N-terminal (Huang et al., 2013a; O'Neill et al., 1998). Additionally, M1 interacts directly with vRNPs (Shimizu et al., 2011), herein, vRNP-M1-NEP-CRM1 formed a “daisy-chain” complex, through which vRNPs are exported. Next, the exported vRNPs have to be transported to the plasma membrane, using the microtubule network (Momose et al., 2007) and Rab11-positive recycling endosome (Amorim et al., 2011; Momose et al., 2011), which have been observed via tracking fluorescently tagged vRNP components (Eisfeld et al., 2011; Momose et al., 2011).

Assembly and budding

At the end, the virus has to get the newly synthesized viral proteins and viral genome assembled into virions and get them detached from the infected cells to infect the adjacent or neighboring cells. This complicated process is initiated by HA and NA, which are targeted to the lipid raft domains on the membrane of the infected cells and are capable of altering membrane curvature (Chen et al., 2007; Chen et al., 2005). Additionally, the cytoplasmic tails of these two proteins serve as the docking sites recruiting M1 to the membrane, where they can polymerize and form the inner layer of the viral envelope. M1 can further mediate cell membrane curvature, and recruit vRNPs and M2 to the budding site (Arzt et al., 2001; Arzt et al., 2004). Subsequently, M2 mediates membrane scission by altering the membrane curvature at the neck of the budding

virus to complete the budding process (Iwatsuki-Horimoto et al., 2006; Nayak et al., 2009). So far, the virions are still attached to the cell membrane through the interaction between HA and sialic acid. Finally, the virions have to use NA proteins to cleave sialic acids off of glycoproteins or glycolipids on the cellular membrane to get free from the original infected cells, to further infect the neighboring cells (Calder et al., 2010; Jagadesh et al., 2016).

The mechanism for how many and which segments will be packed into the virion is controversial. Two models have been hypothesized. One packing model believes that the viral genome segments are randomly packed into the virion. Whereas, the other one predicts that packing signals exist, which have been observed in PB1, PB2, and PA segments (Fujii et al., 2003; Liang et al., 2005).

Overall, the life cycle of influenza A virus is an extremely complicated process, which requires the tight organization of various viral proteins to play their roles at precise spots and time. Besides, it also involves substantial host factors at different steps. A better understanding of this process guides us to develop novel strategies to prevent and control influenza infection.

1.1.2 Influenza A virus evolution, pandemic flu and H5N1

Influenza A virus has a high mutation rate due to using RNA dependent RNA polymerase for replication, which lacks proofreading capability and makes point mutations more likely. If the mutation occurs in the two surface glycoproteins, HA and NA, their antigenic features change, resulting in the viruses avoiding pre-existing host immunity. This is known as antigenic drift, which is the main reason for the generation of new viral strains and annual influenza epidemics. Moreover, the segmented nature of the influenza genome makes possible re-assortment between two or more different viral strains infecting the same cell, resulting in the generation of new viral strains or subtypes. This case is known as genetic shift, which can lead to influenza pandemics if the novel virus strain acquires the ability for efficient and sustained human to human transmission (1980a; Marintcheva, 2016; Nakajima, 2003; Weber and Elliott, 2002).

In the 20th century, three influenza pandemics occurred in the years of 1918, 1957, and 1968, respectively. The 1918 "Spanish flu" caused by H1N1 subtype has been recorded as the most severe pandemic influenza. One-third of the world's population was estimated infected with this

virus, and up to 50 million people died from it. Moreover, this virus strain was the “mother” of all following pandemics. The origin of this virus is yet still unknown (Gershen, 2006; Soper, 1918; Taubenberger and Morens, 2006). The pandemic strains in 1957 and 1968 were H2N2 and H3N2, respectively. The key segments of these two virus strains are from the 1918 virus, and the new surface protein genes originate from avian influenza viruses. 1957 pandemic flu was first detected in Yunnan Province of China, later, sequentially spread to Hong Kong, Singapore, Taiwan, and Japan, and finally all over the world. Thus, it was known as "Asian flu" (Fukumi, 1959; Glezen, 1996). The global mortality was comparatively less than that of the 1918 pandemic flu, causing about 1-2 million deaths worldwide (Anderson, 1958; Viboud et al., 2016; Vynnycky and Edmunds, 2008). Ten years later, the Asian flu evolved into 1968 pandemic flu, also known as "Hong Kong flu", because it started from Hong Kong and spread to the rest of the world within half a year. Despite a high transmission ability, it led to the lowest mortality rate among these three influenza pandemics. The number of human deaths was estimated to range from 500,000 to 2 million (Cockburn et al., 1969; Reperant et al., 2016; Zdanov and Antonova, 1969).

Currently, we have much better medical conditions than before, but there are still 3-5 million cases of severe illness and approximately 250,000–500,000 deaths worldwide because of influenza (Schrauwen et al., 2014). Moreover, another pandemic flu emerged from Mexico at the beginning of the 21st century, April 2009, and spread to more than 214 countries within a year, and led to 18449 deaths (http://www.who.int/csr/don/2010_08_06/en/). The genome of 2009 pandemic H1N1 is the combination of segments from North American and Eurasian swine lineages. Thus, it is also known as "swine pandemic" (Garten et al., 2009; Masoodi et al., 2012).

H5N1 was first isolated from domestic geese in Guangdong province of China in 1996. Since then, it has become of global concern because H5N1 viral strains have caused epizootic and panzootic infections in many species of birds all over the world (Li et al., 2014a; Xu et al., 1999). Additionally, H5N1 viruses have broken the barrier of host species and been introduced into humans since 1997 in Hong Kong (1998; Lavanchy, 1998). Fortunately, they only cause sporadic infections with limited human-to-human transmission (Ungchusak et al., 2005; Wang et al., 2008). H5N1 can cause severe pneumonia and progress quickly to acute respiratory distress

syndrome (ARDS) and multiple organ failure. According to WHO report, it had caused 454 deaths out of 860 infected cases from year 2003 to 2017, with significantly high mortality (around 53%)

(http://www.who.int/influenza/human_animal_interface/2017_10_30_tableH5N1.pdf). Given the feature of rapid evolution via point mutation and genome re-assortment, it is possible that H5N1 achieves the capacity of efficient human to human transmission, resulting in worldwide spread. Therein, H5N1 poses a potential pandemic threat to human health (Liu et al., 2009; Taubenberger and Morens, 2009).

1.1.3 Treatment and prophylaxis of influenza infection

1.1.3.1 Treatment of influenza A virus infection

Based on the knowledge of the virus life cycle, several antiviral compounds have been developed against influenza viruses by inhibiting the crucial steps in this cycle. Three classes of these antiviral drugs are currently available: 1) M2 ion channel inhibitors, including amantadine and rimantadine 2) Neuraminidase (NA) inhibitors, including oseltamivir (Tamiflu), zanamivir (Relenza) and peramivir (Rapivab) 3) PA (polymerase acidic subunit) inhibitor, baloxavir marboxil (Xofluza).

Amantadine and rimantadine were approved for clinical use by the U.S. Food and Drug Administration (FDA) in 1966 and 1993, respectively (Hay et al., 1985; Quilligan et al., 1966; reviewed by Suzuki et al., 2003; Wendel et al., 1966). They function by blocking hydrogen ion passage through M2 ion channel on the viral envelope, hence, inhibiting viral uncoating and vRNPs releasing into the cytoplasm (Cady et al., 2010; Schnell and Chou, 2008; Stouffer et al., 2008). Initially, both drugs were highly efficacious (with the efficacy rate up to 90%) in prevention and inhibition of influenza A virus infection caused by different subtypes, such as H1N1, H2N2, and H3N2 (Dolin et al., 1982; Reuman et al., 1989). Nevertheless, influenza A viruses gradually became drug resistant by introducing adamantane resistance-associated mutations in M2 protein. During 2005-2006, prevalence of resistance to M2 ion channel inhibitors among H3N2 and H1N1 global isolates was up to 90.6% and 15.6%, respectively. Astonishingly, the H3N2 isolates from many Asia countries, including China, Japan, and South Korea evolved to become 100% adamantane resistant (Deyde et al., 2007). For this reason, use of

M2 ion channel blockers have been discouraged for treatment and chemoprophylaxis of currently circulating influenza viruses by the United States Centers for Disease Control and Prevention (CDC) (Fiore et al., 2011).

NA inhibitors, which were first approved for the prophylaxis and treatment of influenza by FDA in 1999 (Moscona, 2005), were the only recommended anti-influenza drugs used worldwide before baloxavir marboxil (Xofluza) was approved by FDA very recently, October 24th, 2018 (https://www.accessdata.fda.gov/drugsatfda_docs/nda/2018/210854Orig1s000TOC.cfm), even though there are still populations of drug-resistant influenza viruses circulating (Nguyen et al., 2012). Unlike adamantane-resistance, which progressed quickly and predominantly in the H3N2 subtype, oseltamivir-resistance was predominantly in the H1N1 subtype. During 2006-2007, less than 1% of investigated global circulating H1N1 viruses had reduced sensitivity to NA inhibitors (Escuret et al., 2008). Over time, NA inhibitor-resistant variants consistently increased. The amount of oseltamivir-resistant seasonal H1N1 had increased to 7% and 90% in 2008 and 2009, respectively (Hurt et al., 2016; Okomo-Adhiambo et al., 2010). Both H5N1 and H7N9 harbored the two most common oseltamivir-resistance-associated mutations, H274Y and R292K, respectively (Hai et al., 2013).

Baloxavir marboxil (Xofluza) is a novel anti-influenza drug, targeting the polymerase acidic subunit and inhibiting virus replication. It gained first global approval to treat acute, uncomplicated influenza in people 12 years of age and older in Japan on Feb 23rd, 2018 (Heo, 2018), and received the FDA approval in the US most recently, October 24th, 2018 (https://www.accessdata.fda.gov/drugsatfda_docs/nda/2018/210854Orig1s000TOC.cfm). Xofluza has shown efficacy against a wide range of influenza viruses, including influenza A and influenza B virus, particularly, oseltamivir-resistant strains and avian strains (H7N9, H5N1) (Noshi et al., 2018).

In the last several decades, several categories of novel antiviral drugs or strategies have been developed to combat these issues: 1) Viral component inhibitors 2) Host factor inhibitors 3) Antibody therapy. 4) Host immunomodulation 5) Small interfering RNA target the viral RNA.

Among these, except for baloxavir marboxil, all the others are still in different clinical experimental stages.

1.1.3.2 Influenza vaccine

Given the limited effectiveness of currently available antiviral drugs, vaccines are of critical importance, particularly for persons who are likely to develop influenza-related complications, such as children under 5, seniors, pregnant women, and residents of nursing homes or long-term care facilities. Immunization not only prevents people from getting flu but also effectively constrains the spread of influenza viruses. Currently, a few types of influenza vaccines are available, but the conventional inactivated influenza and live attenuated influenza virus vaccines are still most commonly used. The traditional flu vaccine recommended annually by WHO is a trivalent vaccine, composed of inactivated influenza viruses from two current circulating subtypes of influenza A virus (H1N1 and H3N2) and one circulating influenza B virus. Since 2009, in order to reduce the lineage mismatch rate between trivalent vaccine B strain and the circulating B strain, another influenza B virus has been added to the traditional vaccine to make a quadrivalent vaccine (reviewed by Kumar et al., 2018).

“Antigenic drift” or rarely “antigenic shift” results in the high mutation rate of influenza antigens (HA and NA). Thus, annual updates of influenza vaccines become necessary (Gerdil, 2003). Moreover, it is extremely challenging to produce large-scale vaccine rapidly, which is hampered by a high frequency of adaptive mutations of HA in embryonated chicken eggs and low yields of production in cultured cells (Wong and Webby, 2013). As a result, many new approaches of vaccines have been investigated, including the development of a DNA vaccine (Kumar et al., 2012), universal vaccine and influenza-like particles (reviewed by Khanna et al., 2014; Schwartzman et al., 2015). FP-01.1 and M2e based peptides are two newly synthesized universal influenza vaccine candidates (Francis et al., 2015; Ma et al., 2013). In addition to inducing strong humoral immune responses, the induction of cellular immune responses also plays a vital role in the prophylaxis of influenza infection, such as, Multimeric 001, which can activate both cellular and humoral host immune response to a wide variety of influenza A and B strains (Atsmon et al., 2014). Theoretically, all these novel vaccine candidates are up-and-coming. In fact, making appropriate vaccines to prevent all the circulating influenza virus strains faces many challenges,

such as constant viral mutation, antibody selection pressure, high cost of clinical trials, and scale of distribution. However, many promising avenues are being explored, and chances for success could be further improved with the further study of influenza antigenic proteins.

1.2 Overview of innate immune recognition of influenza A virus

Due to a wide variety of host species and a high mutation rate, influenza A viruses are major pathogens that pose ongoing threats to human and animal health, causing seasonal or pandemic flu. Except for utilizing vaccination and antiviral drugs as the most common strategies to prevent and treat influenza infection in the human population, all host species have developed defense mechanisms consisting of innate immunity and adaptive immunity against the invading pathogens, including influenza A virus. As the first line of host defense against infection, innate immune responses are rapid and non-specific. In contrast, the adaptive immune responses are slow and specific with the key feature of memory. It typically takes 5-7 days for antibodies and effector T cells to arrive at the target sites and clear novel pathogens. To prevent causing undue damage to the infected host, the innate immune system is exceptionally critical for controlling influenza infection in the first few days (Hufford et al., 2012; White et al., 2008).

Innate immunity is a complex system, containing initial soluble inhibitors (such as defensins) which are present in respiratory mucosal secretions prior to viral infection, the recognition of conserved pathogen-associated molecular patterns (PAMPs) by many kinds of pattern recognition receptors (PRRs), and the limitation or resolution of infection by various innate immune effectors, such as hundreds of interferon-stimulated genes (ISGs), autophagy, and inflammasome activation. Besides these innate immune factors, the innate immune cells (dendritic cells, macrophage, monocytes, and natural killer cells) also play a significant role in defense against infection (White et al., 2008).

The recognition of PAMPs by various PRRs initiates a series of innate immune responses. PAMPs are conserved components of invading pathogens or produced during infection (Janeway, 1989). PRRs can be subdivided into several classes: Toll-like receptors (TLRs), RIG-I like receptors (RLRs), Nucleotide oligomerization domain (NOD)-like receptors (NLRs), AIM2-like receptors (ALRs), C-type lectin receptors (CLRs), and intracellular DNA sensors

(Akira et al., 2006). Among these, TLRs, RLRs, and NLRs are the three principal PRR families involved in influenza A virus infection (Pizzolla et al., 2017).

1.2.1 Toll-like receptors

TLRs were the first identified PRRs and are most well characterized (De Nardo, 2015). To date, 13 TLRs (TLR1-13) have been identified from mice, but only 10 TLRs (TLR1-10) were reported in humans. They are generally expressed in innate immune cells, such as dendritic cells, macrophage, and monocytes. Nevertheless, they are also found in adaptive immune cells (B and T cells) and non-immune cells (epithelial and fibroblast cells) (Delneste et al., 2007). TLR3, TLR7, TLR8, and TLR9 are localized to the intracellular compartments, such as endosomes, endolysosomes, lysosomes and the endoplasmic reticulum (ER) and recognize nucleic acids derived from various viruses. Whereas, the remaining ones are expressed in the cell membrane and recognize the PAMPs present on the surface of bacteria, fungi, and parasites (reviewed by Kawai and Akira, 2011). As RNA sensors, TLR3 and TLR7 can recognize influenza A virus and in turn activate the signaling pathways via binding to the adaptor proteins, TIR (Toll/IL-1 receptor) domain-containing adaptor protein inducing IFN- β (TRIF) and myeloid differentiation primary-response protein 88 (MyD88), respectively. Finally, they promote the production of type I interferon and proinflammatory cytokines through activating the downstream transcription factors: interferon-regulatory factors (IRF3 and IRF7), and nuclear factor- κ B (NF- κ B). TLR8 is also involved in influenza A virus detection and promotes the production of IL-12, rather than type I interferon. However, further research on the relationship between TLR8 and influenza infection is still needed (Ablasser et al., 2009; Berger et al., 2009).

1.2.2 RIG-I like receptors

The second family of PRRs are RIG-I like receptors (RLRs), which are regarded as the essential pattern recognition receptors for host recognition of various families of RNA viruses, such as Paramyxoviridae, Rhabdoviridae, Orthomyxoviridae, Filoviridae, and Coronaviridae (Loo and Gale, 2011). They are DExD/H box RNA helicases encoded by the genes *DDX58*, *IFIH1*, and *DHX58*, which are, respectively retinoic acid-inducible gene I (RIG-I), melanoma differentiation-associated gene-5 (MDA5), and laboratory of genetics and physiology 2 (LGP2) (Barral et al., 2009; Kawai and Akira, 2009). RIG-I and MDA5 are composed of a tandem N-

terminal caspase activation and recruitment domain (CARD), a central DExD/H box helicase domain responsible for RNA-dependent ATP hydrolysis, and a C-terminal domain (CTD). N-terminal tandem CARD-domain is the functional domain, which triggers the downstream signaling cascade that induces the production of proinflammatory cytokines and type I interferons. Overexpression of 2CARD constitutively stimulates the signaling pathway independent of viral infection (Yoneyama and Fujita, 2004). The CTD is an RNA binding domain and is also a repressor domain. Overexpression of this domain inhibits RIG-I mediated signaling pathways (Saito et al., 2007). RIG-I and MDA5 share about 25% and 40% homology within their 2CARD and CTD, respectively. Whereas LGP2 lacks the N-terminal 2CARD-domain (reviewed by Yoneyama et al., 2005), and thus also any direct signaling capacity. With the CTD also known as the repressor domain (RD), LGP2 was initially identified as a negative regulator of RIG-I and MDA5 via competitively binding to dsRNA (Rothenfusser et al., 2005) or blocking the multimerization of RIG-I and its interaction with the adaptor protein (Saito et al., 2007). However, Satoh and colleagues later found that LGP2 promoted the viral RNA recognition by RIG-I and MDA5, suggesting it also acts as a positive regulator of RLRs (Satoh et al., 2010).

RLRs are broadly expressed in the cytoplasm of a variety of cell types in most tissues, including epithelial, endothelial and immune cells (Matsumiya and Stafforini, 2010). RIG-I localization in membrane ruffles of non-polarized epithelial cells has been observed, thought to occur through the association of CARD domain with F-actin cytoskeleton, whereas, MDA5 did not co-localize with F-actin (Mukherjee et al., 2009). Both RIG-I and MDA5 can induce type I interferon production through MAVS (mitochondrial antiviral signaling) signaling pathway. More interestingly, they are also inducible by type I interferon (IFN) (Kang et al., 2004). Hence, they amplify type I IFN signaling via this positive feedback loop. The molecular mechanism underlying this regulation is still not fully clear. While RIG-I was initially identified as a novel retinoic acid (RA) inducible gene (Liu et al., 2000), how RA regulates RIG-I expression is also still unclarified. It has been shown that RIG-I is inducible by LPS (Imaizumi et al., 2002), IFN- γ (Cui et al., 2004), Type I interferons (Matikainen et al., 2006) and poly (I:C) (Kubota et al., 2006). Su and colleagues carried out a deletion analysis of the human RIG-I promoter and showed that IRF1 was critical for the basal and inducible expression of RIG-I via direct

interaction with the element in the range from -166 to -1 of the RIG-I promoter (Su et al., 2007). Recently, using STAT1-null mouse cells U3A, or Type I IFN receptor (IFNAR)-null cells U5A, it was shown that the early induction of RIG-I in response to a viral mimic poly (I:C), involves IRF3 (Hayakari et al., 2016). The promoter of human MDA5 is still uncharacterized.

1.2.3 NOD-like receptors

NOD-like receptors (NLRs) are another cytoplasmic PRR family that recognize infection and stress of intracellular compartments and regulate the innate immune response. To date, over 20 NLRs have been identified, but, many of them have not been characterized yet (Chen and Ichinohe, 2015; Latz et al., 2013). Structurally, NLRs comprise three domains. The N-terminal interaction domain varies by subfamily and may be either a caspase recruitment domain (CARD), an acidic transactivating domain, a pyrin domain (PYD), or a baculovirus inhibitor repeat (BIR) domain. The common central NOD domain or nucleotide binding domain is conserved in all subfamilies, and the C-terminal domain consists of a variable number of leucine-rich repeat (LRR) motifs, which is proposed to bind to PAMPs or danger associated molecular patterns (DAMPs) (Petrilli et al., 2007). The N-terminal domain is the effector domain.

According to the type of N-terminal domain, NLRs are divided into four subfamilies: NLRA (A for acidic transactivating domain), NLRB (B for BIRs), NLRC (C for CARD) and NLRP (P for PYD) (Ting et al., 2008). NOD1 and NOD2 belong to NLRC subfamily and play a pivotal role in innate immune responses to bacterial infection (Philpott et al., 2014), whereas, NLRP3 belongs to the NLRP subfamily and forms a sizeable multiprotein inflammasome complex associated with the adaptor protein ASC (apoptosis-associated speck-like protein containing caspase recruitment domain), and procaspase 1. NLRP3 inflammasome is the best-characterized inflammasome complex and is implicated in the response to influenza infection.

NLRP3 is expressed predominantly in monocytes, DCs and macrophages, and also in human bronchial epithelial cells (Guarda et al., 2011). The activation of NLRP3 inflammasome complex is responsible for the maturation of the prototypic inflammatory cytokines IL-1 β and IL-18 and induction of pyroptosis of infected cells (reviewed by Prochnicki et al., 2016). Two signals are required for the full activation of this inflammasome complex. The recognition of PAMPs by PRRs (TLR, NLR, or RLRs) provides the first signal, which upregulates the production of pro-

IL-1 β , pro-IL-18, procaspase 1 and NLRP3. The second signal is the autocatalysis of inactivated procaspase-1 triggered by cell damage to form activated caspase-1, which in turn cleaves pro-IL-1 β and pro-IL-18 to generate mature IL-1 β and IL-18 (reviewed by Abderrazak et al., 2015; reviewed by Martinon et al., 2009).

The caspase 1 mediated secretion of IL-1 β and IL-18 was reported in influenza-infected macrophages many years ago, NLRP3 inflammasome was not identified as an essential component of host defence against influenza until recent years when inflammasome deficient (NLRP3 $^{-/-}$, or ASC $^{-/-}$, or caspase 1 $^{-/-}$) mice were found to be more sensitive to mouse-adapted pathogenic H1N1 A/Puerto Rico/8/1934 (PR8) strain than the wild-type mice (Allen et al., 2009; Thomas et al., 2009). In addition to ssRNA of influenza A virus, two influenza viral proteins (M2 ion channel protein and PB1-F2) also act as stimuli of the NLRP3 inflammasome (Ichinohe et al., 2010; McAuley et al., 2013).

1.3 RIG-I/MDA5 signaling pathway

1.3.1 Ligand recognition and activation of RIG-I and MDA5

Although both RIG-I and MDA5 are principally cytoplasmic RNA sensors, they recognize structurally distinct RNA ligands. RIG-I preferentially detects short double strand RNA (dsRNA) segments (<300 bp) (Kato et al., 2008) bearing a blunt-ended panhandle structure and a 5' triphosphate (5'-ppp) structure, which exists in most viral genomes or antigenomes, and the host RNA molecules before being processed and modified in the nucleus and released to the cytoplasm (Hornung et al., 2006; Nallagatla et al., 2008; Pichlmair et al., 2006; Schlee et al., 2009). A recent study found that 5'diphosphate moiety (5'-pp) in the viral RNA could also be detected by RIG-I, and served as a self/non-self-discriminator (Goubau et al., 2014).

Interestingly, Liu et al. most recently identified a nuclear-resident RIG-I fraction that recognizes nuclear replication of influenza vRNAs, extending the non-self RNA sensing paradigm by RIG-I to the nucleus (Liu et al., 2018). On the other hand, due to the apparently unstable interaction between MDA5 and its ligand, the ligand features of MDA5 have not been well characterized (Runge et al., 2014). MDA5 preferentially binds to longer dsRNA segments (> 1000 bp), and specific structure at the end is unnecessary (Kato et al., 2008; reviewed by Reikine et al., 2014). Thus, the unique RNA structural features of different RNA viruses determine their recognition by RIG-I or MDA5. For instance, orthomyxoviruses, rhabdoviruses, and arenaviruses are

preferentially detected by RIG-I, whereas, picornaviruses are predominantly recognized by MDA5 (Goubau et al., 2013).

To better understand the molecular basis of RIG-I activation by its ligand, a crystal structure of RIG-I in complex with dsRNA was elucidated (Jiang et al., 2011; Kowalinski et al., 2011; Luo et al., 2011). In the absence of dsRNA ligand, RIG-I is in an auto-repressed state: the functional N-terminal 2CARD is folded back to the CTD and contacts either the helicase domain, the CTD, or both, which prevents 2CARD from interacting with polyubiquitin and the CARD domain of its adaptor protein. Upon binding of dsRNA ligand by the C-terminal domain, RIG-I undergoes an extensive conformational change. CTD and helicase domain forms a more compact configuration to encompass the dsRNA, which facilitated ATP binding and hydrolysis, RIG-I was in turn fully activated and 2CARD exposed. Subsequently, RIG-I transitioned from monomer into a filamentous state in an ATP dependent manner, and the de-repressed 2CARD forms a homotetramer, which interacts with the adapter protein MAVS to initiate the downstream signaling cascade (Peisley et al., 2013). Unlike RIG-I, MDA5 2CARD is not masked by its own parts, such as the helicase domain or CTD. Upon binding to dsRNA, MDA5 cooperatively forms a helical filament in a head to tail arrangement along the long dsRNA, independent of ATP (Berke and Modis, 2012; Berke et al., 2012; Wu et al., 2013). Similar to RIG-I, MDA5 2CARD also forms oligomers providing a platform for the downstream immune signaling factors. But, the length of the linker between the 2CARD and the helicase domain of MDA5 is two-fold of that in RIG-I. Therefore, it was speculated that MDA5 2CARD probably forms an octamer consisting of two helical tetramers (Wu et al., 2013).

In addition to RNA recognition and conformational changes, posttranslational modifications (including phosphorylation and ubiquitination) are involved in the complicated activation process of RIG-I and MDA5. In the absence of triggers, residues S8 and T170 (in RIG-I 2CARD), T770, S854 and S855 (in RIG-I CTD), and S88 (in MDA5 2CARD) are kept phosphorylated to prevent unwanted immune signaling that may be harmful to the host (Gack et al., 2010). Upon infection, these sites are dephosphorylated by a phosphatase, which in turn triggers the K63-linked ubiquitination of RIG-I 2CARD and CTD, mediated by two major E3 ubiquitin ligases, TRIM25 and Riplet. K63-linked ubiquitination of RIG-I stabilizes the

CARD helical tetramer configuration, which is required for activation of the downstream signaling cascade (Gack et al., 2007; Oshiumi et al., 2013; Peisley et al., 2013). Unlike RIG-I, the molecular mechanism of MDA5 activation is poorly understood, although the importance of K63-ubiquitination was also confirmed in both cell-based and cell-free systems (Jiang et al., 2012; Lang et al., 2017).

Several factors are implicated in the initiation and restriction of RIG-I/MDA5 mediated immune signaling pathways by interfering with the phosphorylation and ubiquitination process. Phosphoprotein phosphatase 1 α (PP1 α) and phosphoprotein phosphatase 1 γ (PP1 γ), two highly homologous isoenzymes, are known as the activators of both RIG-I and MDA5 via dephosphorylating residues in the 2CARD of both receptors (Wies et al., 2013). Additionally, de-ubiquitinating enzyme A (DUBA) (Kayagaki et al., 2007; Wertz et al., 2004), the tumor suppressor CYLD (cylindromatosis) (Friedman et al., 2008) and the anti-apoptotic protein A20 are known as the inhibitors of RIG-I/MDA5 signaling pathways via removing the ubiquitin chains from RIG-I/MDA5 or the downstream factors. However, the phosphatases responsible for dephosphorylating of residues in CTD of RIG-I are still unknown.

Some other studies suggested a ubiquitin-independent mechanism to induce the tetramer formation of 2CARD of RIG-I (Patel et al., 2013; Peisley et al., 2013). This mechanism is also known as the proximity-induced oligomerization model, in which, upon binding to dsRNA and with ATP hydrolysis (Kohlway et al., 2013; Schlee et al., 2009), the helicase-CTD of RIG-I forms a filamentous oligomer along dsRNA, consequently, the proximal 2CARD also forms an oligomer. Due to the length of the linker between 2CARD and the helicase-CTD, a tetramer is generated. These two mechanisms do not necessarily conflict, and may complement each other to allow a broad variety of viral RNAs being recognized by RIG-I. Ubiquitin-dependent mechanism plays a critical role in short dsRNA mediated activation of RIG-I, whereas, the filament dependent model becomes more important in response to longer dsRNA (Wu and Hur, 2015) (Figure 1.5).

1.3.2 Activation of MAVS and the downstream signaling pathway

The 2CARD helical tetrameric structure of activated RIG-I serves as a platform for the recruitment and activation of the adaptor protein, MAVS (mitochondrial antiviral signaling) (Seth et al., 2005), also known as IPS-1 (IFN- β promoter stimulator 1) (Kawai et al., 2005), VISA (virus-induced signaling adaptor) (Xu et al., 2005) and Cardif (CARD adaptor inducing IFN- β) (Meylan et al., 2005). MAVS is 540 amino acids long and is composed of an N-terminal CARD domain, a proline-rich region and a C-terminal transmembrane domain (Figure 1.6), which anchors it to the membranes of mitochondria and peroxisomes (Dixit et al., 2010; Seth et al., 2005), as well as mitochondrial-associated endoplasmic reticulum membranes (MAM) (Horner et al., 2011). The MAVS CARD domain performs an essential function in the activation of the signaling cascade by interacting with the 2CARD of RIG-I or MDA5 to form the functional prion-like aggregates (Hou et al., 2011). The crystal structure analysis shows MAVS CARD filament formation is nucleated by RIG-I 2CARD helical tetramer which serves as a platform to recruit single MAVS CARD structures to extend this helical trajectory (Wu et al., 2014) (Figure 1.5).

In addition to the three domains, three tumor necrosis factor receptor-associated factor (TRAF)-interacting motifs (TIMs) are also found within MAVS, two (aa143-147 and aa153-158) in the proline-rich region and one (aa455-460) close to the transmembrane domain (Vazquez and Horner, 2015) (Figure 1.6). Upon activation of MAVS by switching conformation from monomer to polymer, TRAF3 (Saha et al., 2006), TRAF5 (Tang and Wang, 2010), TRAF2 and TRAF6 will be recruited and directly associated with TIMs in MAVS. TRAFs, as E3 ligases for K63-linked polyubiquitination, ubiquitinate not only MAVS signaling components, but also themselves. The auto-ubiquitinated TRAFs interact with the downstream NF- κ B essential modulator (NEMO), also known as inhibitory κ B (I κ B) kinase gamma (IKK γ), an essential regulator of IKK canonical (IKK α /IKK β) and non-canonical (IKK ϵ and TANK-binding kinase 1 (TBK1)) complex. TRAF3 and TRAF5 predominantly direct NEMO to physically interact with TANK (TRAF family member-associated NF- κ B activator) and further recruit the non-canonical IKK complex (IKK ϵ and TBK1), resulting in phosphorylation and translocation of IRF3 and IRF7. This cascade promotes the production of type I interferon: IFN- α , and IFN- β (Tang and Wang, 2010). The secreted type I IFNs from infected cells initiates autocrine or paracrine JAK-

STAT (Janus activated kinase-signal transducer and activator of transcription) signaling after binding to the cell membrane IFN receptors, consisting of two subunits: IFNAR1 and IFNAR2. The activated STAT1, STAT2, and IRF-9 form a heterotrimeric transcription factor complex called IFN-stimulated gene factor 3 (ISGF3), which binds to IFN-stimulated response elements (ISRE) in the promoter region of hundreds of interferon-stimulated genes (ISGs) (Horner and Gale, 2013). Activated STAT1 can also form a homodimer called gamma interferon activation factor (GAF), which binds to gamma interferon activation site (GAS) to induce ISGs expression (Wu and Chen, 2014). ISGs encode a wide range of proteins with different biological functions. Some ISGs encode proteins that play a crucial role in defending against viral infection, such as dsRNA dependent protein kinase R (PKR), myxovirus resistance proteins (Mx), interferon-induced transmembrane proteins (IFITMs), and 2', 5'-oligoadenylate synthetase (OAS). Some others encode proteins like IRF7, IRF3, and RIG-I to form a positive feedback loop to induce more IFN production. Accordingly, type I IFNs are the most critical innate immune factors against viral infection.

TRAF2 and TRAF6 associate with NEMO and canonical IKK complex (IKK α /IKK β), triggering phosphorylation and degradation of I κ B, and translocation of NF- κ B (Nuclear Factor kappa-light-chain-enhancer of activated B cells). This axis upregulates the production of proinflammatory cytokines, such as TNF- α , IL-1, IL-6, and chemokines. They are involved in various inflammatory processes.

Additionally, several death-domain containing proteins are also involved in these two axes, including TRADD (TNF receptor-associated death domain), FADD (Fas-associated death domain) and RIP1 (receptor interacting protein 1). FADD and RIP1 have been known to interact with MAVS CTD (Balachandran et al., 2004; Matsumiya and Stafforini, 2010). The direct association between TRADD and TRAF3 or FADD/RIP1 has been reported recently. Herein, the activation of MAVS recruits TRAFs, FADD and RIP1, which form a central molecular signaling unit with TRADD to activate IRF3 and NF- κ B (Michallet et al., 2008). However, the precise mechanisms remain to be elucidated (Barral et al., 2009).

In summary, following the activation of MAVS, two principal signaling axes are involved and eventually lead to the activation and translocation of transcription factors IRF3/IRF7, and NF- κ B, which serve different functions through inducing production of type I IFN and proinflammatory cytokines, respectively. The first axis is TRAF3/5 \rightarrow NEMO \rightarrow TANK \rightarrow IKK ϵ /TBK1 \rightarrow IRF3/IRF7 \rightarrow IFN- α /IFN- β \rightarrow JAK-STATs \rightarrow ISGs. The second axis is TRAF2/6 \rightarrow TRADD/FADD/RIP1 \rightarrow NEMO \rightarrow IKK α /IKK β \rightarrow I κ B \rightarrow NF- κ B \rightarrow proinflammatory cytokines. (Figure 1.7)

1.4 Overview of suppression of host innate immune responses by influenza A virus

As a consequence of host-virus coevolution, influenza A viruses have developed several strategies to counteract host immune responses for their survival and efficient replication. Here, I will discuss several key immune antagonist proteins of influenza A virus, particularly IFN antagonists.

1.4.1 NS1

Non-structural protein 1 (NS1) is the most important, and best characterized IFN antagonist protein of influenza A viruses (reviewed by Chen et al., 2018). It is widely distributed in the cytoplasm and the nucleus of infected cells, where it interacts with different cellular components to inhibit type I IFN production at different levels, including viral RNA detection and signal transduction. It can also interfere with the activities of several key ISGs, such as PKR, and OAS (reviewed by Hale et al., 2008).

NS1 contains two distinct functional domains: an N-terminal RNA binding domain (RBD) and a C-terminal effector domain (ED), which predominantly interacts with host cellular proteins (Wang et al., 2002). NS1 can shield viral dsRNA from being recognized by RIG-I/ MDA5 via non-specific binding to dsRNA but with low affinity (Hatada and Fukuda, 1992). Additionally, the direct interaction between NS1 and RIG-I has been reported by several groups, and the IFN inhibitory property was also confirmed in these studies (Guo et al., 2007; Mibayashi et al., 2007; Opitz et al., 2007). Moreover, it has been found that NS1 associates with both TRIM25 and Riplet, both E3 ubiquitin ligases, to prevent K63-linked polyubiquitination of RIG-I, and consequently, inhibit RIG-I activation through abolishing 2CARD tetramer formation (Gack et

al., 2009; Rajsbaum et al., 2012). In a recent study, evidence was obtained for the interaction between NS1 C-terminal ED (126-225) and TRAF3 (Qian et al., 2017). Due to this interaction, NS1 blocked K63-linked polyubiquitination of TRAF3 and disrupted the MAVS-TRAF3 complex, in turn, impaired the signal transduction, and eventually, attenuated the production of type I IFNs. Thus, TRAF3 is as another important target of NS1.

The antagonistic property to host innate immunity appears to be due to not only the inhibitory effect on type I IFN production but also the interference with ISG function, such as PKR and OAS. Upon activation by binding to dsRNA, PKR acts as a protein kinase to phosphorylate translation initiation factor, eIF2, resulting in the inhibition of viral and cellular protein synthesis, further inhibiting virus replication (Gale and Katze, 1998). Initially, NS1 was believed to inhibit PKR through sequestering dsRNA (Lu et al., 1995), whereas, later on, data indicated that PKR activation was still blocked in the cells, which were infected with a recombinant influenza A virus expressing NS1 proteins without dsRNA-binding activity. This finding suggests the binding between NS1 and dsRNA is not required for the inhibitory effect of NS1 to PKR activation during influenza A virus infection (Li et al., 2006). Several studies provided the evidence that the inhibition of PKR activation by NS1 protein is solely attributed to the direct binding between these two proteins (Bergmann et al., 2000; Li et al., 2006; Min et al., 2007).

OAS is another interferon-stimulated gene inhibited by NS1. Like PKR, the activation of this ISG is also triggered by dsRNA binding, and promotes the production of poly "A" chains with 2' -5'-phosphodiester bonds, which bind to and activate RNase L. The activated RNase L then degrades viral and host cellular single-stranded RNAs, blocking protein production in the cells, which is necessary for viral replication (Silverman, 2007). Interestingly, the RNA cleavage products can be recognized by RIG-I to augment IFN production (Min and Krug, 2006). The primary role of N-terminal RBD of NS1 is dsRNA binding, that inhibits OAS activation by sequestering dsRNA, in turn, inhibits RNase L activation and the cleavage of single strand viral and cellular RNAs. Consequently, NS1 prevents viral RNA from degradation, and in turn, restricted the augmentation of type I IFN synthesis (Min and Krug, 2006).

Another mechanism by which NS1 counteracts host innate immune responses is binding and sequestering the 30kDa subunit of the cellular cleavage and polyadenylation specificity factor (CPSF30) away from 3' end processing of cellular pre-mRNAs, resulting in the accumulation of unprocessed pre-mRNA in the nucleus and the general inhibition of the cellular mRNA production, including both interferon mRNAs and other antiviral mRNAs (Noah et al., 2003). In contrast, it does not interfere with the production of viral mRNAs, the maturation of which is dependent on viral polymerase proteins rather than host CPSF30.

The multiple IFN-antagonistic functions of NS1 mentioned above are strain-specific. Most previous studies focused on NS1 derived from the laboratory-generated PR8 (A/Puerto Rico/8/34(H1N1)) virus strain, which is different from the counterparts of the circulating influenza viruses. The variable sequences in the C-terminal effector domain might contribute to this difference (reviewed by Hale et al., 2008).

1.4.2 PB2, PA

PB2 derived from A/WSN/33 (H1N1) was found to interact with MAVS and inhibit MAVS-mediated IFN- β production, which suggested PB2 was another potentially IFN antagonistic protein, that determines influenza virulence (Graef et al., 2010). Another group confirmed this immune-inhibitory activity of PB2 in the 2009 pandemic H1N1 virus subtype and identified a mutation, T588I, that exacerbated the inhibitory effect of PB2 to type I interferon, which in turn enhanced the virulence of 2009 pandemic H1N1 (Zhao et al., 2014). Most recently, another subunit of the influenza polymerase complex, PA, was also found to suppress IFN- β production through binding and blocking IRF3 activation, providing a new strategy by which virus evades host antiviral signaling (Iwai et al., 2010; Yi et al., 2017). Interestingly, although the direct interaction of polymerase components with RIG-I has been observed, its contribution to the suppression of the IFN signaling was not observed in the study (Li et al., 2014b). Further investigation is needed to determine the biological significance of these observations.

1.4.3 PB1-F2 (polymerase basic protein 1-frame 2)

PB1-F2 genome, subtypes and subcellular distribution

PB1-F2 is encoded by the +1 alternate open reading frame and translated from the 4th start codon, located in 120bp downstream of the first start codon of PB1 gene (Chen et al., 2001). PB1-F2 is a small molecule with a full-length of 87 or 90 amino acids and a molecular weight of 10.5 kDa, and is seen in almost all avian influenza A virus subtypes (Zell et al., 2007) and three pandemic virus strains: Spanish H1N1 (1918), Asian H2N2 (1957), and Hong Kong H3N2 (1968) (McAuley et al., 2010a), however, it has evolved into various truncated versions as the avian influenza viruses become adapted to mammalian hosts (Pancucharova and Russ, 2006). Particularly, PB1-F2 derived from 2009 pandemic H1N1, has two C-terminally truncated forms (11 and 57 amino acids in total length) (Hai et al., 2010; Smith et al., 2009). Even so, these truncations do not appear to affect the virulence of the strain due to the remaining of C-terminus, which contributes to some functions of PB1-F2 (Hai et al., 2010). The subcellular distribution of PB1-F2 is virus strain-specific. PB1-F2 from mammalian influenza virus subtypes, such as PR8 (H1N1) and A/TW/3355/1997 (H1N1), was predominantly localized to the mitochondria of infected cells via a short mitochondrial targeting sequence (MTS) in the C-terminus (Gibbs et al., 2003; Yamada et al., 2004), although the distribution of PB1-F2 in the cytoplasmic and nuclear fractions was also seen in the cells infected with PR8 (Mazur et al., 2008). Whereas, PB1-F2 derived from avian influenza subtypes, such as H5N1 and H7N7, is found distributed throughout the cells, including the cytoplasm and the nucleus (Chen et al., 2010; Chen et al., 2001).

PB1-F2 structure

The molecular structure of a full-length synthetic PB1-F2 (PR8) was first characterized using nuclear magnetic resonance (NMR) and circular dichroism (CD) spectroscopy by Bruns and co-workers (Bruns et al., 2007). This study revealed the structural features of PB1-F2 depend on the solvent conditions. In pure aqueous solution, PB1-F2 is in a random coil state, whereas, under membrane mimicking solution conditions, PB1-F2 is capable of forming two independent structural domains: two N-terminal closely linked short helices and a C-terminal extended α -helix, which are connected by an unstructured hinge region. According to the study, PB1-F2 molecule tends to form oligomeric structures (Bruns et al., 2007). These discoveries were confirmed by research investigating the structural characteristics of PB1-F2 from seven influenza subtypes, including three H1N1 (A/WSN/33 (H1N1), A/PR/8/1934 (H1N1), A/BrevigMission/1/1918 (H1N1)), one H3N2 (A/Udorn/1972 (H3N2)), one H6N2

(A/Tu/Mass/3740/1965 (H6N2)) and two highly pathogenic H5N1 (A/HK/156/1997 (H5N1) and A/Swan/FR/06299/2006 (H5N1)). The study showed that the conformational changes in response to different solvent conditions were not only seen in PR8 PB1-F2, but also in other tested strains. Under certain conditions, such as 80% acetonitrile, 0.01% sodium dodecyl sulfate (SDS), and 0.1 mg/ml asolectin liposomes, a β -sheet was also adopted by PB1-F2 to form insoluble oligomeric amyloid fibers or amorphous aggregates. More importantly, the amyloid fibers were also observed in membranes of infected cells (Chevalier et al., 2010). To investigate whether the secondary structure of PB1-F2 is highly related to its functions, Solbak and co-workers characterized and compared the secondary structures of PB1-F2 from pandemic flu 2009 H1N1, 1918 Spanish flu H1N1, Bird flu H5N1, and PR8 H1N1 by NMR and CD spectroscopy. In contrast to the previous report, the C-terminal structure of PB1-F2 from the less virulent viral strains (pandemic 2009 H1N1 and PR8 H1N1) consists of an extensive α -helix, whereas, the counterpart from the highly virulent viral strains (Spanish H1N1 and Bird H5N1) harbours two shorter helices divided by a loop region. This structural discrepancy at the C-terminus might contribute to the different pathogenicity of influenza A viruses. Unfortunately, due to the signal overlap in the spectra, the N-terminal structure of PB1-F2 was not well characterized by NMR (Solbak et al., 2013). Taken together, these data indicated that the secondary structure of PB1-F2 is highly dependent on the surrounding environment and more insight needs to be gained in understanding the relationship between structure and specific functions of PB1-F2.

PB1-F2 interferes with type I IFN production

Similar to NS1, PB1-F2 is a non-structural protein, not packaged into the virion, but expressed in host cells to modulate innate immune responses at multiple stages, resulting in impaired antiviral responses and increased inflammation. The overview of the reported roles PB1-F2 plays is illustrated in Figure 1.8. In 2011, a study by Varga et al. described an interaction of PB1-F2 derived from PR8 with the adaptor protein, MAVS, in human embryonic kidney (293T) cells. This interaction inhibited RIG-I mediated IFN- β promoter activity as well as IFN- β production in a bioassay. The C-terminal portion of PB1-F2 was indispensable for the interaction (Varga et al., 2011). The mechanism of this inhibitory activity relies on decreasing the mitochondrial membrane potential (MMP), which is essential for the structural rearrangement of the MAVS complex and further propagation of the downstream signaling (Koshihara et al., 2011; Varga et al.,

2012). Another study also demonstrated that PB1-F2 impaired RIG-I signaling by reducing mitochondrial inner membrane potential ($\Delta\psi_m$). Interestingly, the reduction of $\Delta\psi_m$ is not due to the interaction with MAVS, but rather the translocation of PB1-F2 into the mitochondrial inner membrane via translocase of the outer membrane (TOM) 40 channels, not TOM20 and TOM22, which generally transport host-proteins (Yoshizumi et al., 2014).

In comparison with the wild-type PR8, the modified PB1-F2-deficient PR8 induced a significant increase of IFN- β and ISGs in human pulmonary epithelial cells (A549) and had lower virulence in mice. In the study, they observed PB1-F2 only inhibited the IRF3 promoter activity, not NF- κ B reporter activity, suggesting PB1-F2 inhibits IFN- β signaling pathway involving IRF3 rather than NF- κ B (Dudek et al., 2011). On the contrary, knocking out the PB1-F2 gene from A/WSN/33 (H1N1) strongly reduced IFN- β expression through the NF- κ B signaling pathway, rather than the IRF3 pathway in A549 cells. Interestingly, they only observed this activity in epithelial cells, not in immune cells (Le Goffic et al., 2010).

PB1-F2 induces the apoptosis of innate immune cells

A cell-specific pro-apoptotic function of PB1-F2 was first described in U937 monocyte cells by Chen and colleagues (Chen et al., 2001). Subsequent studies confirmed this function in macrophages (Jaworska et al., 2014) and monocytes (Mitzner et al., 2009). The direct association of NLRX1 (nucleotide-binding oligomerization domain-like receptor X1), another host innate immune sensor, with PB1-F2 can protect macrophages from viral-induced apoptosis (Jaworska et al., 2014). Furthermore, the phosphorylation of PB1-F2 by protein kinase C (PKC) plays a crucial role in PB1-F2 mediated apoptotic cell death (Mitzner et al., 2009). Intriguingly, the pro-apoptotic activity of PB1-F2 is also viral strain-specific, since Chen et al. found that PB1-F2 from PR8, a subtype of influenza H1N1, possessed this activity, but not PB1-F2 from H3N2 and H5N1 strains (Chen et al., 2010). Zamarin and colleagues proposed a mechanism for this pro-apoptotic function using glutathione-S-transferase (GST) pulldowns followed by mass spectrometric (MS) analysis. They identified two proteins on the mitochondrial membrane that interact with PB1-F2: adenine nucleotide translocator 3 (ANT3) and voltage-dependent anion channel 1 (VDAC1). These two proteins constitute the permeability transition pore complex (PTPC), which is implicated in the

mitochondrial permeabilization and the mitochondrial-mediated cell apoptosis. It was proposed that by binding to ANT3 and VDAC1, PB1-F2 impaired the mitochondrial integrity, leading to apoptosis of infected immune cells. This study provides insight into the molecular mechanism by which PB1-F2 promotes cell apoptosis (Zamarin et al., 2005). Intriguingly, both ANT3 and VDAC1 proteins are expressed in a tissue-specific manner (Doerner et al., 1997; Stepien et al., 1992), which might account for the different apoptotic responses mediated by PB1-F2 in different cell types infected with influenza virus.

PB1-F2 increases the production of proinflammatory cytokines

In addition to inhibiting interferon production by the RIG-I pathway and promoting apoptosis, there are conflicting reports about PB1-F2 modulation of proinflammatory signaling. Using yeast two-hybrid assay and co-immunoprecipitation studies in Vero cells, Reis et al. identified an interaction between IKK β and PB1-F2 proteins from four different influenza strains: A/Quail/Hong Kong/G1/97(H9N2), A/Puerto Rico/8/34(H1N1) (PR8), A/turkey/England/50-92/91(H5N1), and A/turkey/Turkey/1/2005(H5N1). They found that PB1-F2 severely impaired NF- κ B activation triggered by the overexpression of IKK β . However, they concluded that PB1-F2 was not altering the kinase activity of IKK β nor the translocation of NF- κ B but was preventing NF- κ B from binding to the promoter region of the regulated genes. Using truncated PB1-F2 constructs, the full-length protein was shown to be necessary for inhibition of NF- κ B signaling (Reis and McCauley, 2013). In contrast, using the yeast two-hybrid approach and screening human spleen cDNA, Leymarie *et al.* discovered a novel interactor of PB1-F2 from A/WSN/33 (H1N1): calcium-binding and coiled-coil domain 2 (CALCOCO2, also known as NDP52). By interacting with this molecule, PB1-F2 enhanced MAVS-mediated NF- κ B reporter activity, while inhibiting TBK1-dependent ISRE reporter activity (Leymarie et al., 2017). This suggests PB1-F2 has the capacity to simultaneously exacerbate NF- κ B-mediated inflammatory responses and attenuate host antiviral signaling.

PB1-F2 also induces the secretion of proinflammatory cytokines, IL-1 β and IL-18, by activating the NLRP3 inflammasome in human peripheral blood mononuclear cells (PBMCs) (McAuley et al., 2013) and in mice (Pinar et al., 2017). Several studies investigated the underlying mechanisms by which PB1-F2 activates NLRP3 inflammasome. In human cells, McAuley et al.

showed that PB1-F2 from PR8 (H1N1), but not from A/Wuhan/359/1995 (Wuhan) (H3N2), formed high molecular weight aggregates and activated the NLRP3 inflammasome, while soluble PB1-F2 was unable to do so (McAuley et al., 2013). Another study demonstrated that upon being incorporated into the phagolysosome, PB1-F2 undergoes acidification, and in turn induces assembly of ASC into a large speck-like complex, which is known as a simple upstream readout for the activation of NLRP3 inflammasome (Stutz et al., 2013). Additionally, PB1-F2 derived from avian H7N9 upregulated mitochondrial reactive oxygen species (ROS), leading to the activation of NLRP3 inflammasome (Pinar et al., 2017). Thereby, as a major activator of NLRP3 inflammasome, PB1-F2 is essential to the excessive production of proinflammatory cytokines, also known as a “cytokine storm”, which plays a pivotal role in the pathogenesis of influenza, especially the highly pathogenic subtypes.

PB1-F2 exacerbates secondary bacterial infection

In addition to regulating host innate immune responses, PB1-F2 also promotes secondary bacterial infections. A primary contributor to influenza mediated severe morbidity and mortality is bacterial pneumonia caused by secondary bacterial infections following influenza (Harford and Leidler, 1947; Tsigrelis et al., 2010). PB1-F2 has been identified in the 1918 pandemic H1N1 virus strain as a potentially critical virulence factor (Conenello et al., 2007). To investigate whether PB1-F2 has an effect on secondary bacterial infections, which contributed to the remarkable lethality of Spanish flu (1918 pandemic H1N1), McAuley et al. (McAuley et al., 2007) challenged mice with wild-type mouse-adapted PR8 and isogenic mutant PR8 viruses, which were engineered to largely decrease PB1-F2 expression. Seven days post infection, the mice were infected with *Streptococcus pneumoniae*. The results showed the presence of PB1-F2 greatly enhanced the frequency and severity of secondary bacterial pneumonia in the mouse model, which in turn caused mice significant weight loss and death due to the increased parenchymal inflammation and inflammatory cell infiltration. They further engineered PB1-F2 from 1918 Spanish flu virus into the PR8 sequence without changing other viral elements and inoculated these viruses and wild-type PR8 into mice with subsequent bacterial challenge. The 1918 PB1-F2 performed more efficiently than that of wild-type PR8 in exacerbating secondary bacterial pneumonia, as reflected by an entire versus patchy distribution of consolidated foci in the lungs of infected mice. This observation indicated PB1-F2 likely contributed to the

remarkable lethality of the 1918 Spanish pandemic flu not only by regulating host immune responses, but also by exacerbating secondary bacterial infections. Another group subsequently identified several amino acids contributing to this cytotoxic function of PB1-F2, including I68, L69, and V70 (Alymova et al., 2014).

PB1-F2 promotes the replication of influenza A virus

PR8 and WSN viruses with PB1-F2 knocked out, compared to wild-type, formed strikingly smaller plaques in Madin-Darby Canine Kidney (MDCK) cell monolayer due to reduced viral replication and spread (Mazur et al., 2008). Using a recombinant polymerase system and protein-protein interaction assays (co-localization, yeast two-hybrid assay, and co-immunoprecipitation (co-IP)), Mazur et al. found that the underlying mechanism was a direct interaction between PB1-F2 and PB1 increasing polymerase activity in HEK293T cells (Mazur et al., 2008). Subsequently, McAuley and colleagues confirmed and extended this knowledge by investigating several significant influenza virus strains in different cell types. In HEK293T cells, the knocking-out of PB1-F2 from Spanish 1918 and H5N1 also resulted in a considerable decrease of polymerase activity. However, knocking-out of PB1-F2 from an H3N2 did not make any difference in polymerase activity. Intriguingly, the difference was not detected in A549 cells for any tested influenza isolates, which indicates the impact of PB1-F2 on polymerase activity was virus-specific and cell type-specific (McAuley et al., 2010b).

Interestingly, Mazel-Sanchez and co-workers most recently showed that PB1-F2 isolated from avian H5N1 (VN1203), but not from mammalian H1N1 and H3N2, competitively bound to a poorly characterized host restrictor protein, known as HCLS1-associated protein X1 (HAX-1), and counteracted its restriction of PA nuclear entrance, promoting, in turn, polymerase activity and virus replication (Hsu et al., 2013; Mazel-Sanchez et al., 2018).

1.5 Ducks and influenza A virus

1.5.1 Ducks are the relevant species for influenza

Wild aquatic waterfowl has been considered as the natural reservoir of almost all known subtypes of influenza A virus (H1 to H16 and N1 to N9) (Hinshaw et al., 1980; Webster et al., 1992), except for the recent isolates H17N10 and H18N11, which are derived from bats (Tong et

al., 2012; Tong et al., 2013). Serving as carriers and transmitters of avian influenza A virus, they are responsible for the continuous global circulation of influenza A virus by migration. According to surveillance over several decades, the vast majority of avian influenza viruses (AIV) were isolated from two taxonomic orders: Anseriformes (ducks, geese, and swans) and Charadriiform (gulls, terns, and shorebirds). Moreover, it was more frequent to isolate AIV from dabbling ducks, especially mallards (*Anas platyrhynchos*), compared to any other wild birds (Krauss et al., 2004; Olsen et al., 2006; reviewed by Stallknecht and Shane, 1988). According to recent data from a large-scale surveillance of AIV in wild birds throughout USA over 5 years (2007-2011), the prevalence of AIV in the collected samples of dabbling ducks was disproportionately high (86.4%), and most highly pathogenic AIVs, 91.5% H5 and 89.7% H7 were also from the samples of dabbling ducks (Bevins et al., 2014). In addition to maintaining influenza A viruses, wild ducks also transmit them to domestic poultry and mammals, including humans (Kim et al., 2009; Krauss and Webster, 2010). Moreover, they play a vital role in generating novel influenza viruses since they host diverse subtypes of influenza A virus, allowing reassortments of the infected influenza viruses occur easily (Deng et al., 2013).

Additionally, ducks, especially mallards, are essential to study because they have a unique relationship with influenza A virus. Upon infection with LPAI, gallinaceous birds may present clinical disease characterized by high morbidity (>50%), and low mortality (<5%), and the influenza viruses predominantly replicate in the epithelium of nasal cavity, followed by respiratory and intestinal tracts. Whereas, the clinical symptoms and tissue lesions are rarely observed in ducks infected with LPAI naturally (Daoust et al., 2011) or experimentally (Jourdain et al., 2010), despite with a higher viral shedding. The primary replication site of LPAI in ducks are the enterocytes lining the intestinal tract. A comparative study by Costa *et al.* has shown that wood ducks, laughing gulls, and redheads have primarily oropharyngeal shedding of LPAI viruses, whereas, mallards shed the most virus from the cloaca (Costa et al., 2011). Furthermore, infection with HPAI H5N1 causes gallinaceous poultry systemic diseases characterized by multiple organ failure and central nervous system damage. In chicken and turkey, the mortality rate increases to 100% within hours or days (Brown et al., 2006), and humans show similar symptoms as seen in gallinaceous birds with a mortality rate of approximately 60% (reviewed by Swayne and Suarez, 2000). In contrast, the same highly pathogenic viral strains may only cause

mild or no symptoms in some duck species, especially mallards, allowing them to spread the viruses more efficiently as a “Trojan horses” (Alexander et al., 1986; Cooley et al., 1989; Kim et al., 2009; Shortridge et al., 1998). Intriguingly, compared to the taxonomically related species (wood ducks, laughing gulls, and redheads), mallards also appear less susceptible to HPAI-Eurasian lineage H5N1 viruses (Brown et al., 2006). The subsequent research demonstrated that Pekin ducks (domestic *Anas platyrhynchos*), a descendant of the mallard duck, had less morbidity and mortality than Muscovy ducks after challenge with HPAI H5N1 (Cagle et al., 2011). The difference was attributed to lower antibody titers and higher level of the proinflammatory cytokine (IL-6) in Muscovy duck, versus higher antibody titers and greater induction of RIG-I in Pekin ducks.

To date, most human cases of infection with HPAI H5N1 have resulted from a direct transmission from poultry to human. Traditional agricultural practices (backyard farming or open houses) allow infected wild ducks to interact with free-grazing ducks, which, in turn, further spread H5N1 influenza viruses to chickens (Gilbert et al., 2006). Additionally, the live poultry markets in Asia also provide an ideal environment for interspecies transmission and genetic mixing of influenza viruses (Short et al., 2015). To restrain the spread of HPAI to other species, particularly, to avoid posing threat to humans, 60 million domestic fowl were slaughtered in 2004 in Thailand and over a 200 million birds were culled from 1996 to 2005 in Asian countries, which resulted in a disruption of the poultry industry and dramatic economic losses (Songserm et al., 2006; reviewed by Swayne, 2006). Thus, the successful control of HPAI infection of ducks plays an essential role in preventing and eradicating infection in poultry and humans.

The application of poultry vaccination in ducks and chickens has dramatically reduced the incidence of H5N1 infection in humans and poultry, and successfully decreased viral shedding (Beato et al., 2007; Pfeiffer et al., 2010). However, poultry vaccination does not provide “sterilizing immunity” and influenza infection may still occur in vaccinated populations without clinical signs (reviewed by Capua and Alexander, 2008; reviewed by Swayne, 2006). Additionally, poultry vaccination remains highly controversial. Both the United Nations Food and Agriculture Organization (FAO) and the World Organisation for Animal Health (OIE) do not support the long-term use of poultry vaccination without additional preventive measures

(reviewed by Domenech et al., 2009). Thus, further studies of the host-pathogen interaction between ducks and AIV are needed to facilitate a better understanding of molecular pathogenesis of the flu infection and better guidance for designing efficient strategies to prevent and treat influenza (Fauci, 2006; reviewed by Herold et al., 2015).

1.5.2 Duck innate immune responses to influenza A virus

The rapid lethality in chickens, but mildness or absence of symptoms in ducks suggest differential contributions of avian innate immune responses to the outcome of HPAI infection. Mammalian innate immune responses to influenza A virus have been comprehensively overviewed above. Here I will shed light on avian innate immune responses to influenza viruses, mainly those of ducks.

TLRs

To date, 10 chicken TLRs (chTLR1La, chTLR1Lb, chTLR2a, chTLR2b, chTLR3-5, chTLR7, chTLR15, and chTLR21) and 4 duck TLRs (duTLR3-5 and duTLR7) have been characterized (reviewed by Chen et al., 2013a). Among these, chTLR3-5 and chTLR7 recognize the same PAMPs as the homologous mammalian TLRs (Velova et al., 2018). While, TLR9 is missing in birds (chicken, duck, and goose) (reviewed by Brownlie and Allan, 2011; reviewed by Magor et al., 2013; Temperley et al., 2008). TLR8 is disrupted by a 6-kilobase insertion containing chicken repeat 1 (CR1) retroviral-like insertion elements to form a pseudogene TLR8 in chicken (Philbin et al., 2005). Some TLRs are unique to birds, such as TLR1La, TLR1Lb, TLR15, and TLR21, which have never been reported in mammals (Chen et al., 2013a; Kestra et al., 2013). Interestingly, avian specific TLR15, only reported in chickens, turkeys, quails, geese and zebra finches (Chen et al., 2013a), gained a novel function as a sensor recognizing secreted fungal and bacterial proteases (de Zoete et al., 2011). TLR21 was reported to be similar to mammalian TLR9, recognizing CpG DNA (Brownlie et al., 2009). Therefore, it has been proposed to functionally compensate for the missing TLR9 in birds (reviewed by Magor et al., 2013). Despite the disruption in birds of TLR8, an ssRNA detector, the other two RNA sensors, TLR3 and TLR7, are present and functionally conserved in chickens and ducks. chTLR3, sharing approximately 48% amino acid identity with human TLR3, detects the dsRNA analog poly (I:C) and rapidly induces type I IFN production like human TLR3 (Iqbal et al., 2005; Karpala et al.,

2008). Additionally, the upregulation of chTLR3 and IFN- β mRNA after challenging chickens with HPAI H5N1 and LPAI H7N1 has been observed, indicating they might play a significant role in host antiviral innate immune responses (Cornelissen et al., 2012). Duck TLR3 has been identified and characterized separately in Pekin ducks and Muscovy ducks. Pekin duck TLR3 shares 86.3 % amino acid identity with chTLR3 and is abundantly expressed in various tissues. Muscovy duck TLR3 shares 97.1% amino acid identity with Pekin duck TLR3 and is also constitutively expressed in a variety of tissues. The mRNA levels of TLR3, Mx, and IFN- α were significantly increased in Pekin duck livers, spleens, lungs, and brain tissues upon being challenged with duck reovirus (DRV) (Zhang et al., 2015). Nonetheless, the relationship between Pekin duck TLR3 and avian influenza is still unclear, although the rapid upregulation of TLR3 has been observed in the brain tissue of Muscovy ducks which were challenged with A/Duck/Guangdong/212/2004 (H5N1) (Jiao et al., 2012).

Sharing 62% amino acid identity with human TLR7, chTLR7 mRNA is also alternatively spliced in chickens, consistent with the characteristic of TLR7 in mice and humans. Unexpectedly, the activation of chTLR7 by TLR7 agonists, particularly R848 and poly (U), induced the up-regulation of IL-1 β and IL-8 rather than IFN- α and IFN- β in the chicken HD11 cell line and primary chicken splenocytes. However, stimulation of chicken cells with TLR3 agonist, poly (I:C), induced both IFN- α and IFN- β (Philbin et al., 2005). Pekin duck TLR7 shares 85% amino acid identity with chTLR7 but appears to function differently. Unlike chTLR7, which failed to induce IFN- α production by TLR7 agonists (R848 and loxoribine) in chicken splenocytes and cell lines (Philbin et al., 2005), Pekin duck TLR7 stimulated the upregulation of both pro-inflammatory cytokines (IL-1 β and IL-6) and IFN- α in duck splenocytes triggered by loxoribine and imiquimod (MacDonald et al., 2008). Functional differences like this may help to explain the differential susceptibility of ducks and chickens to avian influenza.

RLRs

RIG-I has been identified and characterized in ducks, but, is absent in chickens (Barber et al., 2010; Chen et al., 2013b). Duck RIG-I is 933 amino acids long with 53% amino acid identity to human RIG-I. Consistent with mammalian RIG-I, duck RIG-I also contains three domains: An N-terminal 2CARD, a helicase domain, and a C-terminal regulatory domain. The rapid induction

of abundant RIG-I and downstream immune factors, such as IFNs (IFN- α , IFN- β) and proinflammatory cytokines (IL-1 β , IL-18, and IL-6), were observed in lung tissues of ducks infected with HPAI H5N1 (Barber et al., 2010; Saito et al., 2018). More interestingly, duck RIG-I transfection rescued the recognition of 5'triphosphate RNA (5'ppp RNA), in turn, stimulated IFN response, consequently, significantly reduced the replication of either LPAI or HPAI in a chicken embryonic fibroblast cell line (DF-1), which initially could not detect RIG-I ligand. Hence, the absence of RIG-I in chicken is another plausible explanation for its higher susceptibility to AI, especially HPAI (Barber et al., 2010). Using microarray, Barber et al. identified many upregulated antiviral innate immune genes by comparing the transcriptional profiles of DF-1 cells transfected with duck RIG-I or empty vector and challenged with both HPAI VN1203 (H5N1) and LPAI BC500 (H5N2). Using real time-PCR, they confirmed the induction of a subset of the above identified antiviral genes, including *MX1*, *PKR*, *IFIT5*, *OASL*, and *IFNB* (Barber et al., 2013). In the same year, compared to the control ducks, Huang and co-workers also showed the remarkable induction of some antiviral innate immune genes, including *DDX58*, *IFITM3* and *AvIFIT* in H5N1 infected ducks with a transcriptome analysis (Huang et al., 2013c). Subsequently, upregulation of *MX1*, *PKR*, *IFNA* and *IFNB* were also seen in DF-1 cells transfected with duck RIG-I and infected with H9N2 avian influenza virus (Shao et al., 2014). Several other important immune response genes, such as *TRIM25*, *USP18*, *STAT1*, *STAT2*, *IRF1*, *IRF7* and *IRF8* were also identified and confirmed with RNA-seq and real-time PCR, respectively, in DF-1 cells transfected with duck RIG-I and challenged with a synthetic ligand (5'ppp-dsRNA) (Chen et al., 2016). Taken together, these data suggest that duck RIG-I is structurally and functionally homologous to mammalian RIG-I and appears to conserve some of this function also in chicken cells.

The other two members of the RLR family, MDA5 and LGP2, have been identified both in ducks and in chickens. Like mammalian LGP2, chicken LGP2 also lacks the CARD domain and negatively regulated chicken IFN- β promoter activation by influenza A virus infection (Liniger et al., 2012). The mRNA of duck LGP2 was ubiquitously detected in a variety of duck tissues. Jiao *et al.* infected ducks with HPAI H5N1 and observed a significant increase of LGP2 in the brain, lung, and spleen tissues at 1-day post infection (dpi). However, further investigation is

needed to determine whether duck LGP2 functions as a positive or negative regulator of the RIG-I and MDA5 pathways (Jiao et al., 2015).

Similarly, duck MDA5 is also widely expressed in a variety of duck tissues. Infection with A/Duck/Guangdong/212/2004(H5N1) remarkably increased the mRNA level of MDA5 in duck brain, lung, and spleen tissues at 1 dpi. Overexpression of the functional CARD domain of MDA5 strongly enhanced the IFN- β promoter activity, and in turn resulted in the elevation of mRNA levels of antiviral molecules and proinflammatory cytokines in primary duck embryonic fibroblast (DEF) cells. In the same study, they further investigated the transcriptional factors involved in this signaling pathway using dual-luciferase assay after co-transfecting duck MDA5 CARD and duck IRF7 or duck NF- κ B reporter vector into DEF cells. They observed duck MDA5 stimulated the promoter activity of duck IRF7 rather than duck NF- κ B (Wei et al., 2014). Karpala *et al.* first identified chicken MDA5 and functionally characterized it in chicken cells. They found chicken MDA5 was inducible by type-I IFN or a dsRNA agonist, as well as influenza infection (H5N1) in DF-1 cells. Importantly, knocking down chicken MDA5 largely decreased chicken IFN responses triggered by dsRNA, but did not affect the proliferation of influenza viruses (Karpala et al., 2011). An alternative transcript of chicken MDA5, which can be detected in various chicken tissues, could also induce chicken IFN- β after activation by the overexpression or poly (I:C) stimulation (Lee et al., 2012). Taken together, these findings indicate that MDA5 and LGP2 function is probably highly conserved among vertebrates, and that chicken MDA5 is less effective than duck RIG-I at restricting influenza virus replication.

NLRs

To date, two bacterial ligand detectors, NOD1 (Tao et al., 2015) and NLRC5 (Guo et al., 2016; Lian et al., 2012; Qiu et al., 2016), and one influenza associated sensor (NLRP3) (Ye et al., 2015) in NLRs family have been identified in chickens, but the only available information about chNLRP3 is the tissue-specific distribution pattern, with nothing mentioned about its function. Nothing is yet known about duck NLRP3 and its potential role in influenza response, although a recent study demonstrated the upregulation of proinflammatory cytokines, IL-1 β and IL-18, in HPAI H5N1 infected duck lung and spleen. (Saito et al., 2018). Whether the NLRP3 inflammasome mediates the activation of these proinflammatory cytokines requires further

investigation. So far, duNOD1, most recently characterized by Li et al., is the only documented duck NLR (Li et al., 2017).

Immune factors involved in RIG-I/MDA5 signaling pathway

In addition to the above mentioned PRRs, the homologues of several protein intermediates in mammalian RIG-I/MDA5 signaling have also been described in ducks. As discussed above, human TRIM25 mediates human RIG-I activation via generating either anchored or unanchored K63-linked polyubiquitin chains. Similarly, duck TRIM25 also activates duck RIG-I, albeit without necessarily covalently attaching the K63-linked polyubiquitin chain (Miranzo-Navarro and Magor, 2014). A unique TRIM27-like (TRIM27-L) gene is found in ducks, thought to be a result of gene duplication, which is absent in chickens and turkeys. The upregulation of this gene was detected in Pekin ducks at 1 dpi with HPAI H5N1, and its overexpression in DF-1 cells strongly increased duRIG-I 2CARD-mediated upregulation of chMx1 and chIFN- β mRNA (Blaine et al., 2015). Additionally, overexpressing or knocking down duTRAF6 resulted in increased or decreased expression of dsRNA mediated NF- κ B and IFN- β in duck embryonic fibroblasts (DEFs), indicating duTRAF6 is also involved in the duck innate immune response (Zhai et al., 2015). Further studies are needed to address how these molecules are involved in modulating duck innate immune system.

1.5.3 Influenza A virus evasion from duck innate immune responses.

Influenza virus evasion from host innate immune responses has been thoroughly examined in mammalian systems, but limited information is available in avian species, and particularly ducks. So far, NS1 is the only influenza immune-antagonist protein to be investigated in ducks (Wei et al., 2014). Overexpression of NS1 (H5N1) inhibited duck MDA5 mediated promoter activities of chIFN- β and chIRF7, as well as the expression of downstream immune factors in DEF cells. On the contrary, a genetically engineered H5N1 virus with NS1 deleted demonstrated a stronger induction of the promoter activities and downstream immune factors, compared to wild-type H5N1 in DEF cells (Wei et al., 2014). However, the molecular mechanism through which NS1 inhibits duck innate immune response remains to be elucidated. Whether and how the other immune antagonist viral proteins impact the innate immune system of the natural reservoir (ducks) is not yet clear. PB1-F2 was regarded as a virulence factor of HPAI H5N1 (VN1203) in

ducks through enhancing the viral polymerase activity and increasing the replication of influenza viruses (Marjuki et al., 2010). Interestingly, Leymarie *et al.* reported that PB1-F2 attenuated the virulence of H5N1 (A/duck/Niger/2090/2006 (H5N1)) in chickens (Leymarie et al., 2014), in contrast to VN1203 in ducks. These findings further indicated the species and viral strain-specificity of PB1-F2 function.

1.6 Research objectives

When I started my project, the duck RIG-I promoter and duck MAVS were still uncharacterized. Additionally, limited information about PB1-F2 is available in an avian system. Hence, three objectives were developed: 1) Characterization of the duck RIG-I promoter 2) Functional characterization of duck MAVS and inhibition by PB1-F2 3) to examine interactions between PB1-F2 from highly pathogenic strains with avian MAVS.

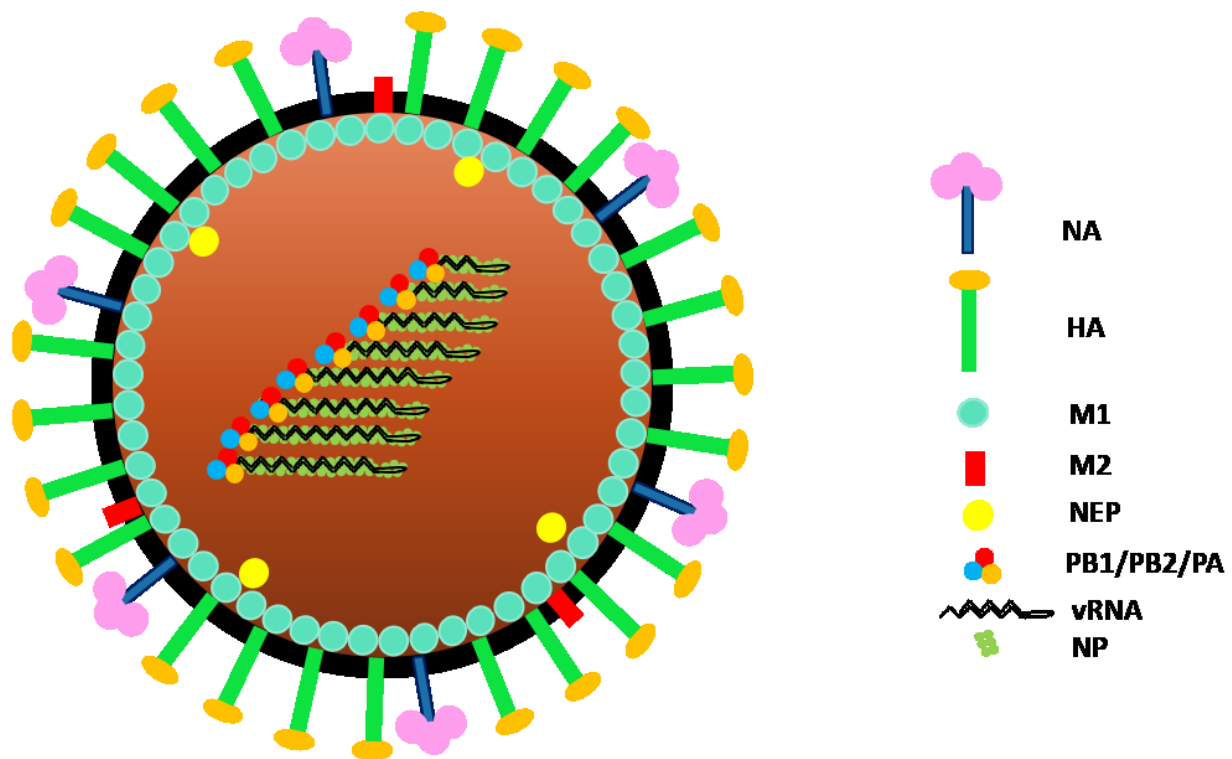


Figure 1.1 A schematic of the spherical influenza A virus particle.

Influenza A virus consists of the outer membrane envelope with two types of surface glycoproteins (HA and NA) as well as M2 ion channel protein, an inner M1 shell, and the eight ribonucleoprotein complexes (RNPs) in the core of each viral particle. Some nuclear export proteins (NEPs) are also distributed inside it. Each viral RNA segment is associated with a heterotrimeric polymerase complex (PB1/PB2/PA) and multiple copies of NP to form the fundamental replication and transcription unit, also known as RNP.

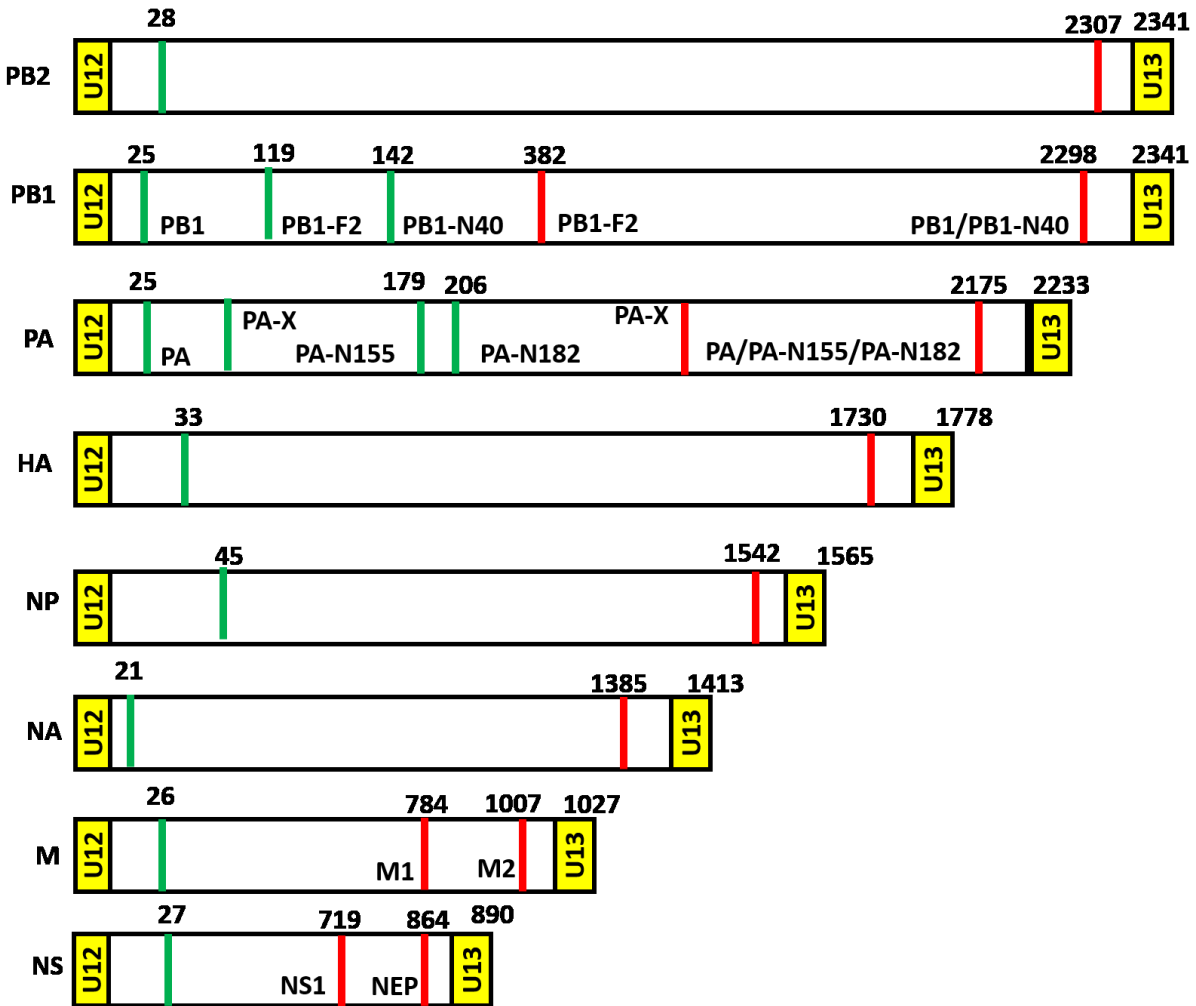


Figure 1.2 A schematic illustration of the eight RNA segments of influenza A virus and the viral proteins encoded by each segment.

U12/U13 are the conserved sequences in each segment. The green and red lines indicate the start and stop codons, respectively. The numbers above each segment indicate the positions of the start and stop codons.

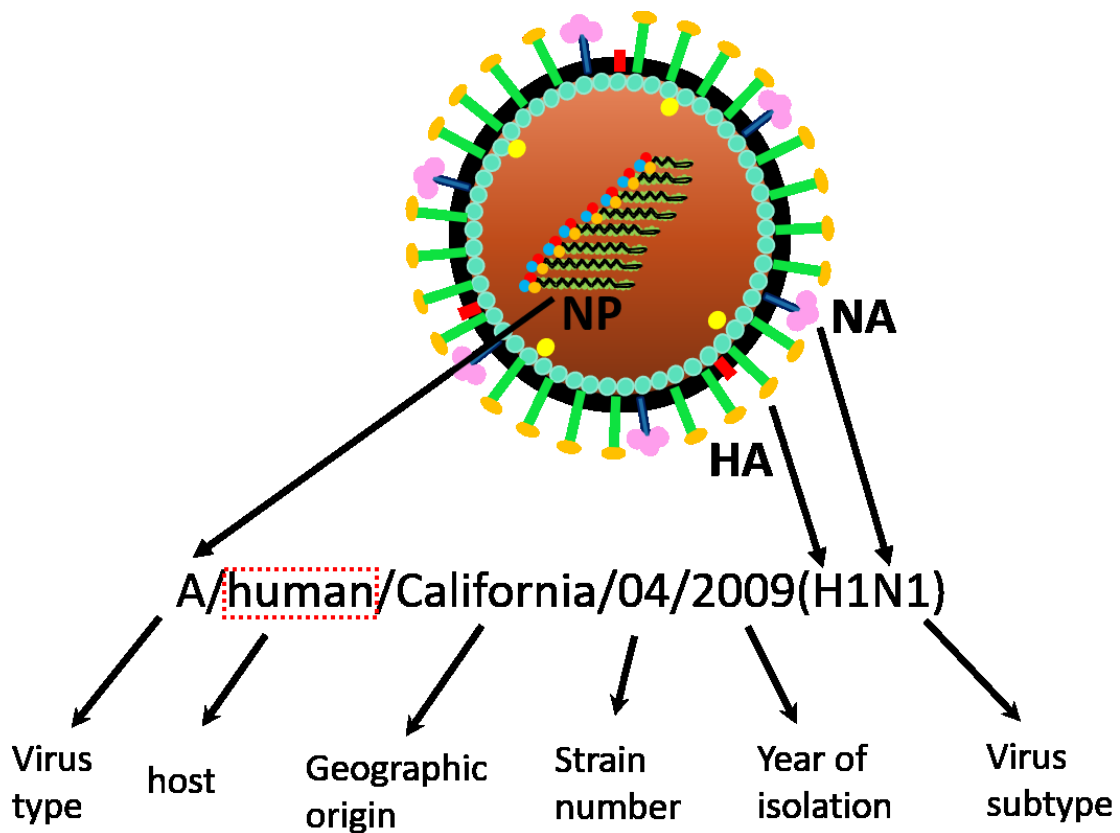


Figure 1.3 Nomenclature of influenza viruses.

The name consists of virus type, host origin, geographic origin, strain number and the year of isolation. At the end, the subtype of the isolated influenza virus is bracketed. The virus type is determined by the conserved nuclear protein (NP) as the arrow shows. If the viruses are isolated from humans, the host designation is optional, which is illustrated by the red dotted box.

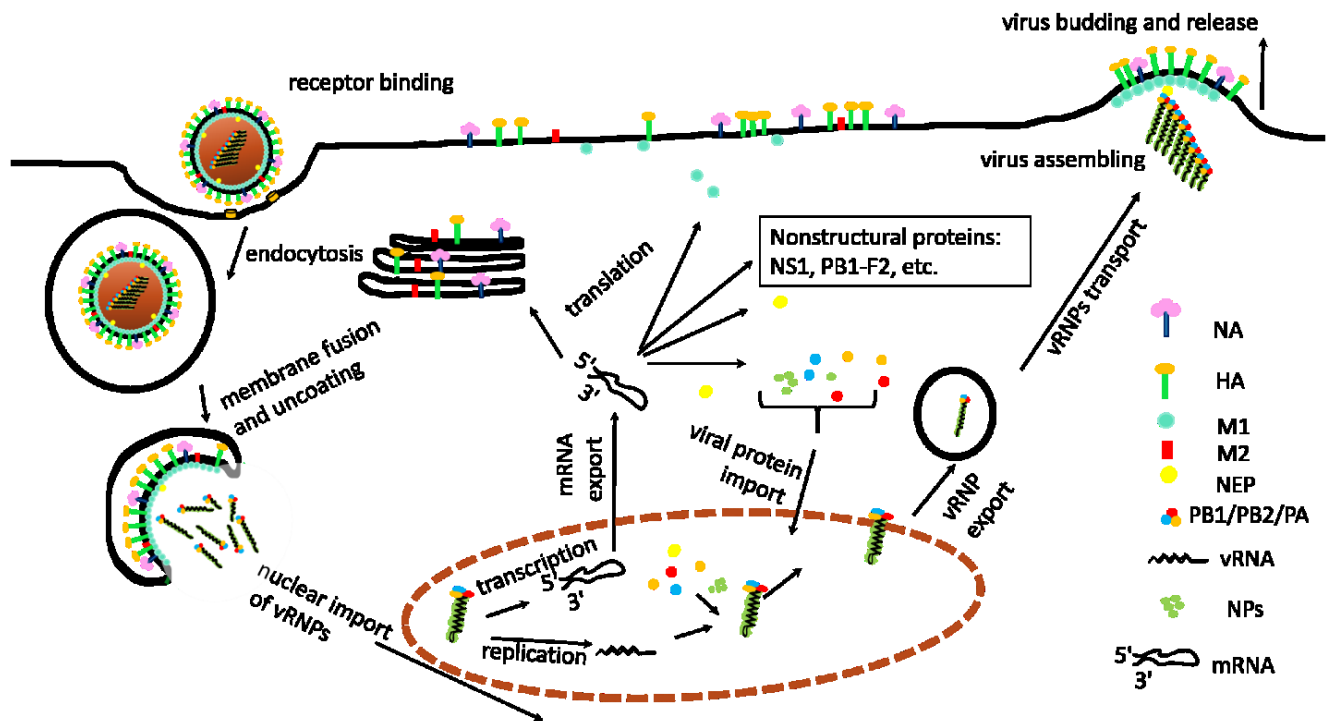


Figure 1.4 Influenza A virus life cycle.

The crucial steps of the viral life cycle are denoted, including receptor binding and endocytosis, membrane fusion, uncoating, nuclear import of vRNPs, viral genome replication, transcription, mRNA nuclear export, viral protein translation, nuclear import of newly synthesized viral protein, nuclear export of vRNPs, vRNPs transport to cell membrane, virus assembly, virus budding and release.

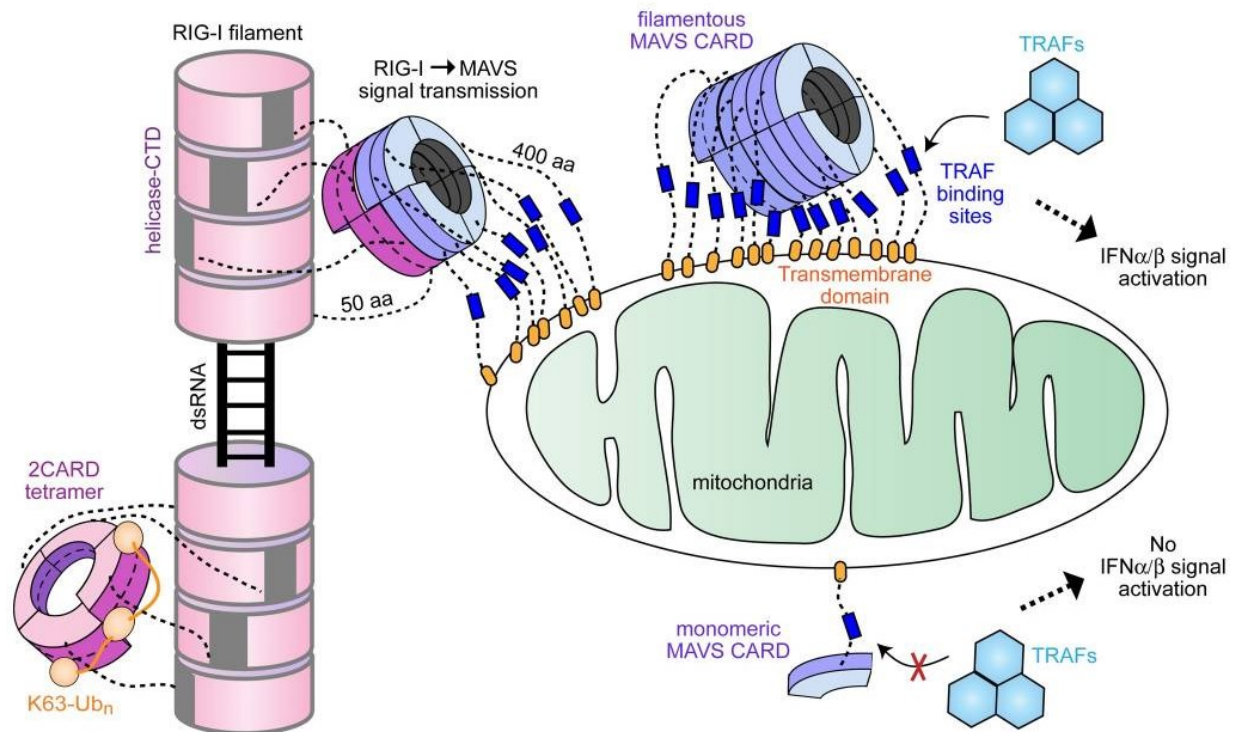


Figure 1.5 A model of signal activation by full-length RIG-I and MAVS

“Upon encountering viral dsRNA with 5' ppp and the blunt end, the RNA binding domain (helicase-CTD) of RIG-I forms filamentous oligomers along the length of dsRNA in an ATP-dependent manner. This filament formation brings together 2CARDs into proximity and induces tetramerization of 2CARD while being tethered to the core filament via a 50 aa flexible linker (Peisley et al., 2013). Tetramerization of 2CARD may also be induced by K63-Ub_n, which stabilizes the 2CARD tetramer by bridging between adjacent 2CARDs and wrapping around the tetramer (Peisley et al., 2014). The 2CARD tetramer resembles the lock-washer (helical ring) structure, which serves as a helical template that nucleates the MAVS CARD filament. MAVS CARD is anchored to the mitochondrial outer membrane via a ~400 aa long linker, which contains the TRAF binding sites. Filament formation of MAVS CARD would bring together multiple TRAF binding sites into proximity, which appears to be important for efficient recruitment of TRAF molecules and activation of the further downstream signaling pathway (Hou et al., 2011; Takamatsu et al., 2013).” The figure is cited from (Wu et al., 2014), and permitted by CellPress, open access.

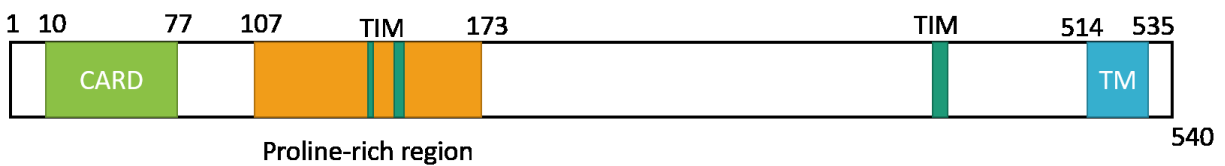


Figure 1.6 Schematic of MAVS.

MAVS is 540 amino acids long and contains an N-terminal caspase activation and recruitment domain (CARD), a proline-rich region and a C-terminal transmembrane domain (CTD or TM). Three tumor necrosis factor receptor-associated factor (TRAF)-interacting motifs (TIMs) are also within MAVS, two in the proline-rich region (aa143-147 and aa153-158) and one close to the transmembrane domain (aa455-460).

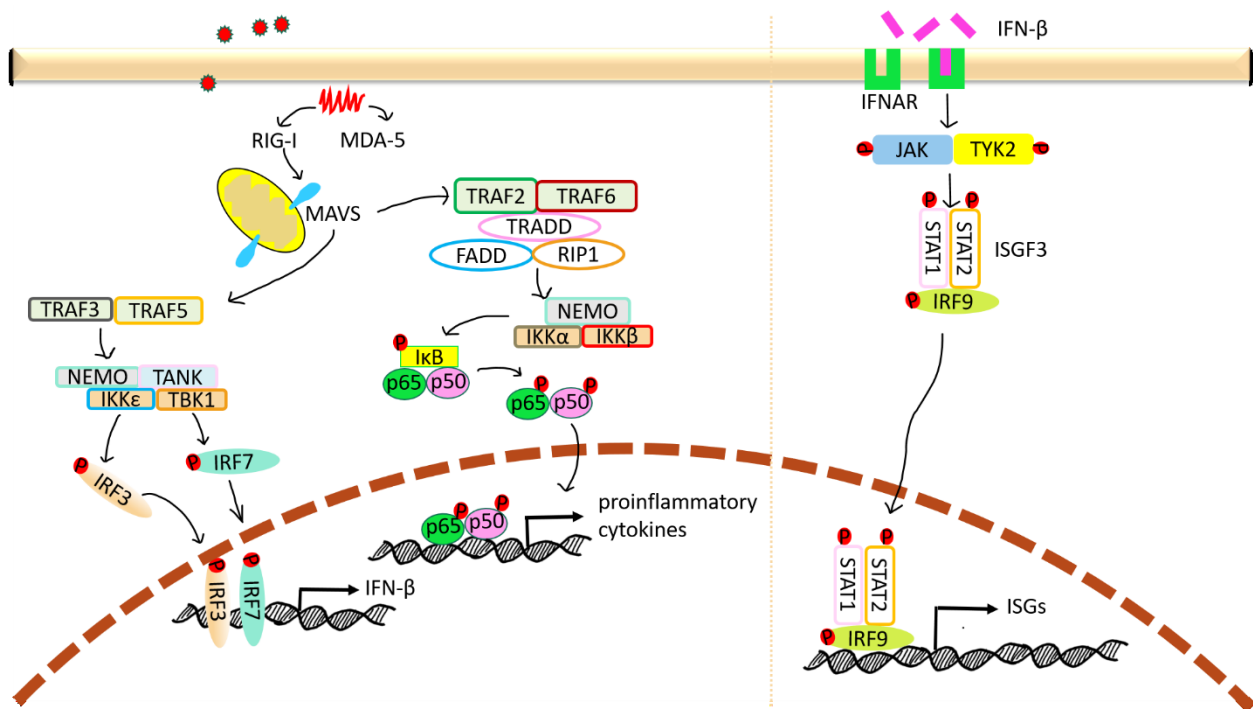


Figure 1.7 RIG-I/MDA5 signaling pathway stimulated by influenza A virus.

Upon detection of influenza viral RNA (PAMP) by RIG-I/MDA5, the adaptor protein, MAVS, is activated, resulting in the activation of a sequential signaling cascade, followed by phosphorylation and translocation of transcription factors (IRF3, IRF7, and NF- κ B). IRF3 and IRF7 mediated the induction of IFN- β , which subsequently binds to interferon receptors (IFNAR) on the cell membrane, triggering the JAK-STAT signaling cascade, and finally promoting the production of a variety of ISGs by the activated ISGF3 complex consisting of STAT1, STAT2, and IRF9. Upon being activated, NF- κ B (p50/p65) is imported into the nucleus and upregulates the expression of proinflammatory cytokines.

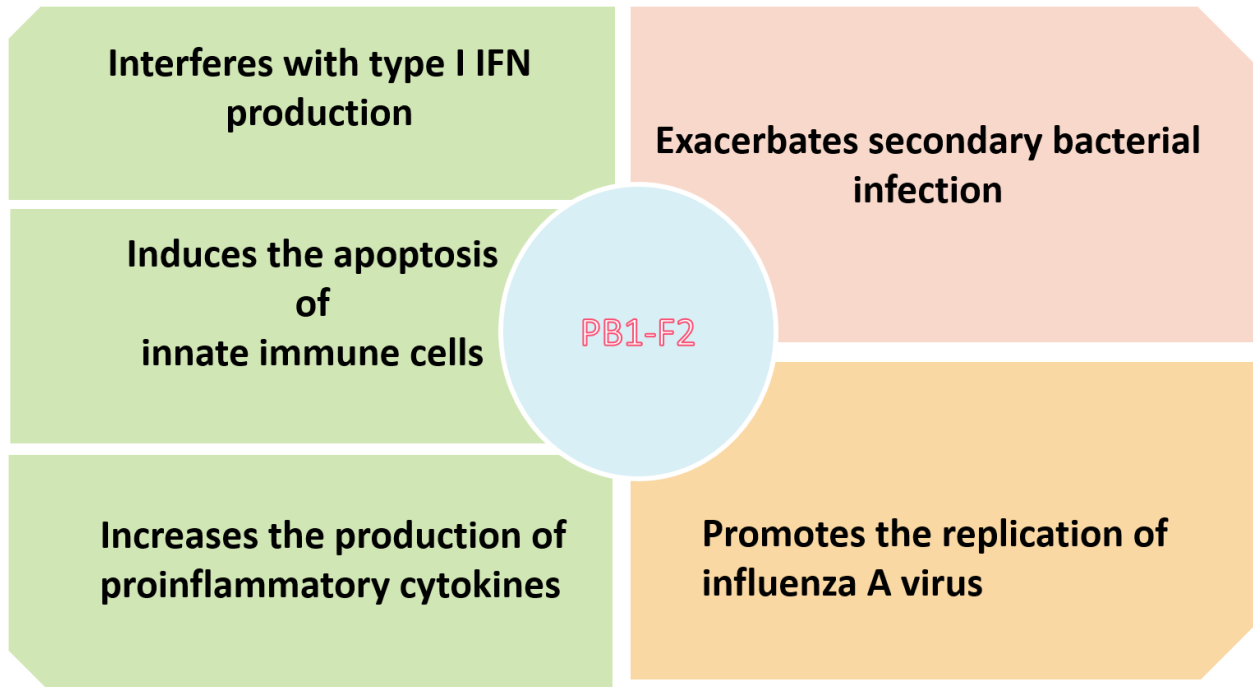


Figure 1.8 Overview the multiple roles of PB1-F2

Three primary functions of the PB1F2 protein have been identified: (I) Modulates host innate immune responses, including interfering with type I IFN production, inducing the apoptosis of innate immune cells and increasing the production of proinflammatory cytokines (II) exacerbates secondary bacterial infection (III) promotes the replication of influenza A virus

Chapter 2 Materials and Methods

2.1 Cells and viruses

2.1.1 Primary duck embryonic fibroblast (DEF) and DF-1

Primary duck embryonic fibroblasts (DEFs) were isolated from 11-day old embryonated mallard duck eggs purchased from Duckcetera, Canada. DF-1 cells are spontaneously immortalized chicken embryonic fibroblast cells, derived from East Lansing Line (ELL-0) chicken embryos (Schaefer-Klein et al., 1998) and were purchased from ATCC (ATCC® CRL-12203™). Both DEF and DF-1 cells were maintained in Dulbecco's Modified Eagle Medium (DMEM) (Gibco) with sodium pyruvate (110 mg/L), sodium bicarbonate (1.8 g/L), and 10% fetal bovine serum (FBS) (Sigma) in a 5% CO₂ incubator at 37 °C and 39 °C, respectively. Approximately every three to four days, the confluent cells were rinsed with 1×PBS and digested with 0.25% trypsin/EDTA (HyClone) for 5-10 minutes to detach adherent cells. Trypsin was inactivated by adding complete growth medium. Cells were sub-cultivated at a 1:6 dilution as recommended by the ATCC instructions.

2.1.2 HeLa cell line

The HeLa cell line was purchased from ATCC (ATCC® CCL-2™). Cells were cultured in DMEM (as DF-1 growth medium) in a 5% CO₂ incubator at 37 °C. The medium was renewed twice a week. Every four to five days, the cells would become confluent and be passed at a 1:5 dilution ratio as recommended by the ATCC instructions.

2.1.3 AD293T cell line

The AD293T cell line, derived from the commonly used HEK293T cell line with improved cell adherence and plaque formation properties, was purchased from Stratagene. AD293T cells were cultured in DMEM (as DF-1 growth medium) in the presence of 5% CO₂ at 37 °C.

Approximately every 3-4 days, cells were rinsed with 1×PBS and treated with 0.25% trypsin/EDTA to detach when cells became confluent. Trypsin was inactivated by adding complete growth medium. Cells were passed at a 1:6 dilution ratio.

2.1.4 Viruses

PB1-F2 proteins used in the projects were cloned from four different influenza A virus strains. Three of them were from highly pathogenic avian influenza (HPAI) H5N1:

A/Vietnam/1203/2004 (H5N1) (VN1203), reverse-genetics recombinant VN1203 (rgVN1203), and A/duck/Thailand/71.1/2004 (D4AT). VN1203 and D4AT were isolated from a fatal human and an infected duck, respectively. VN1203 is one of the most lethal influenza A viruses tested in laboratories (Marjuki et al., 2010). D4AT was reported as the most lethal strain to ducks with 100% lethality (Sturm-Ramirez et al., 2005). RgVN1203 was the reverse-genetics recombinant VN1203 with 14 inadvertently introduced synonymous mutations (SMs): 11 SMs in PB1, 2 in NP, and 1 in NA. But, it was found that 3 out of 11 SMs in PB1 localized in PB1-F2 open reading frame and changed the encoded amino acids (T51M, V56A, and E87G) (Marjuki et al., 2010). The remaining virus was a mammalian influenza strain: A/Puerto Rico/8/1934 (H1N1) (PR8). PR8 was isolated from a human case, but it is a mouse-adapted strain.

2.2 Amplification and identification of duck RIG-I promoter

2.2.1 PCR

We previously cloned the complete cDNA sequence of duck RIG-I in 2010 (Barber et al., 2010), and the duck genome was also sequenced in 2013 (Huang et al., 2013b). However, the translational start site (TSS) and the promoter region of duck RIG-I could not be identified in the genome sequence because the 5'UTR and the first exon was unassembled and the intervening sequence partially undefined. Using a forward primer (RIG-I promoter F1 as in Table 2-1) based on the genome sequence and a reverse primer (RIG-I promoter R1 as in Table 2-1) in exon 2, we amplified duck RIG-I promoter from blood genomic DNA of a male White Pekin duck #26 (Moon and Magor, 2004). A 20 µl PCR amplification system was prepared and run as the instruction of KAPA HiFi PCR Kit (Kapa biosystems). PCR reactions were performed in a GeneAmp PCR System 9700 (Applied Biosystem). The general thermocycling program consisted of an initial denaturation step of 95°C for 3 minutes, followed by 25 cycles of 98°C for 20 seconds, 65°C for 15 seconds, 72°C for 1.5 minutes, and a final extension of 72°C for 7 minutes.

2.2.2 Gel electrophoresis, gel extraction, and ligation to pCR2.1- TOPO vector

Gel electrophoresis: PCR products mixed with Orange G loading buffer (6×) were loaded into a 1% agarose gel with 0.5 µg/ml ethidium bromide and run in 1× TBE buffer under 100 V voltage

for 45 minutes, finally, visualized under UV light. A fragment of approximately 1.5 kb was obtained from this PCR reaction.

Gel extraction: A 50 μ l PCR reaction system was performed using the same conditions as the 20 μ l reaction system, except the amount of each buffer was increased up to 2.5 times. Followed by gel electrophoresis, the band of interest (around 1.5 kb) was excised from the agarose gel with a clean, sharp scalpel, and purified using the Gel Extraction kit (Qiagen) according to the manufacturer's instruction. In the final step, the DNA fragment of interest was eluted from QIAquick membrane with 30 μ l double-distilled water (ddH₂O).

Ligation to pCR2.1-TOPO vector: Before ligating to TOPO vector, the purified DNA fragment was modified to have an A-tail added. The protocol was as follows: 17 μ l eluted DNA fragment was mixed and incubated with 5 μ l dATP (1mM), 2.5 μ l Taq Buffer (10 \times), and 0.5 μ l homemade Taq DNA polymerase (5 units/ μ l) at 72 $^{\circ}$ C for 20 minutes. Two microliters of A-tailed DNA fragment were transferred to a 1.5 ml tube, followed by adding 0.5 μ l salt solution (1.2 M NaCl, 0.06 M MgCl₂) and 0.5 μ l pCR2.1-TOPO vector provided by pCR2.1- TOPO kit (Invitrogen) and gently mixing by swirling the pipette tip in the mixture. The tube was left at room temperature for 30 minutes to allow the A-tailed DNA fragment to ligate to TOPO vector.

2.2.3 Transformation

During the final 5-10 minutes of the above incubation, One-Shot Top 10 *E. coli* competent cells were taken out from -80 $^{\circ}$ C and placed on ice to thaw. The entire 3 μ l above ligated product was added to the thawed competent cells and mixed gently. The mixture was incubated on ice for 30 minutes, followed by being heat-shocked at 42 $^{\circ}$ C for precisely 30 seconds and allowed to recover on ice for 2 minutes. 250 μ l Super Optimal broth with Catabolite (SOC) media was added to the cells and incubated at 37 $^{\circ}$ C for 1 hour with shaking speed at 225 rpm. 100 μ l of the cells with 40 μ l X-gal (20ng/ μ l) was plated on lysogeny broth (LB) agar plate containing 100 μ g/ml ampicillin and incubated at 37 $^{\circ}$ C overnight.

2.2.4 Colony selection, mini-culture, and mini-prep

On the day after transformation, white (cells transformed with vectors containing recombinant DNA) and blue (cells transformed with non-recombinant plasmids, only vector) colonies could be visualized on the plate. I picked five white colonies from the plate with sterilized pipette tips and incubated them separately in 2 ml LB bacterial culture media with ampicillin (100ug/ml) or carbenicillin (100ug/ml) at 37°C overnight (around 16 hours) with the shaking speed at 225 rpm. The next day, the plasmid was extracted from *E. coli* cells using Presto Mini Plasmid Kit (Geneaid) as described in the manufacturer's protocol. In the last step, the plasmid was eluted from the column with 30 µl ddH₂O and the concentration was measured using NanoDrop® ND-1000 UV/Vis Spectrophotometer (NanoDrop Technologies).

2.2.5 PCR or restriction digestion to identify the correct clones

The presence of inserted sequence of interest was screened with PCR or EcoRI restriction digestion of TOPO vectors. For the above sample, I performed a 25 µl reaction system of PCR to screen the extracted plasmids from the picked 5 colonies with Platinum Taq DNA Polymerase kit (Invitrogen) as described in the manufacturer's instruction. The primers used were M13F and M13R (Table 2-1). The general thermocycling program consisted of an initial denaturation step of 94°C for 2 minutes, followed by 28 cycles of 94°C for 30 seconds, 55°C for 30 seconds, 72°C for 4 minutes, and a final extension of 72°C for 7 minutes. Followed by gel electrophoresis and visualizing the amplified sequence bands under UV light, two or three samples with the expected size were used for sequencing.

2.2.6 Big Dye sequencing

To amplify the sequence, a PCR was performed using a single primer (M13F or M13R) according to the protocol: 1 µl BigDye™ Terminator 3.1 ready reaction mix (Thermo Fisher), 3 µl 2.5× sequence buffer (200 mM Tris, pH 9.0 5 mM MgCl₂), 1 µl primer (2.5 pM), and 50-200 ng plasmid DNA as the template, adding sterilized Milli-Q H₂O to a final volume of 10 µl. The thermocycling program: 30 cycles of 95°C for 20 seconds, 50°C for 15 seconds, 61°C for 1 minute.

The sequenced samples were cleaned by ethanol precipitation prior to the standard Sanger sequencing on ABI 3730 in Molecular Biology Facility (MBSU) of University of Alberta. The protocol of ethanol precipitation was as follows: 1.5 μ L 1.5M NaAc/250 mM EDTA (pH 8.0) was added to the 10 μ L sequencing reaction and mixed by pipetting up and down. 11.5 μ l isopropanol (1:1 volume) was added to the tube and mixed. The samples were left on ice for 30 min, then centrifuged at 4°C for 15 minutes to ensure all precipitated product was pelleted. The supernatant was aspirated, and the pellets were washed with 500 μ L of 70% EtOH by being vortexed thoroughly and spin down at 13,000 rpm (the maximum speed) for 10 minutes. In the last step, the supernatant was aspirated, and the pellets were air dried for 5 min.

2.2.7 Sequence analysis and alignment of amplified duck RIG-I promoter

Upon receiving the sequencing results, I did sequence analysis and alignment using the Clustal Omega (<http://www.ebi.ac.uk/Tools/msa/clustalo/>) and BoxShade Server (http://www.ch.embnet.org/software/BOX_form.html). The approximately 1.5 kb amplified segment was confirmed to be the right sequence containing 1140 bp nucleotides upstream of the start codon (ATG) and 338 bp nucleotides covering exon 1, intron 1, and partial exon 2. So far, I have identified the proximal promoter, the complete first exon and first intron of duck RIG-I. The next step is to amplify and clone approximately 2 kb sequence upstream of the start codon as the full-length promoter.

2.2.8 Amplification and cloning the full-length duck RIG-I promoter (from -2024 to -1)

Due to a GC rich region in close proximity to the start codon of duck RIG-I, it was difficult to directly amplify the promoter region (-2024 to -1). Therefore, firstly, a reverse primer was designed to amplify a more extended segment containing part of exon 1. Going through serial experiments (PCR, gel electrophoresis, gel extraction, A-tailing, ligation, transformation, sequencing, sequence analysis, and cloning) described above, a TOPO vector with the sequence range from -2024 to +63 was successfully generated. The primers used in this PCR were RIG-I promoter F2 and RIG-I promoter R2-1 (Table 2-1). The template of PCR was the genomic DNA extracted from the male White Pekin duck #26.

Then, taking the above generated TOPO vector (with -2024 to +63 sequence segment) as the template, the promoter (from -2024 to -1) sequence was amplified using primers RIG-I promoter F2 and RIG-I promoter R2-2 (Table 2-1) with Q5 High-Fidelity PCR Kit (NEB) according to the manufacturer's instruction. The general thermocycling program consisted of an initial denaturation step of 98°C for 30 seconds, followed by 30 cycles of 98°C for 10 seconds, 65°C for 30 seconds, 72°C for 1 minutes, and a final extension of 72°C for 7 minutes. Followed by gel electrophoresis, gel extraction, A-tailing, ligation, transformation, sequencing, sequence analysis, and cloning, the TOPO vector with the full-length duck RIG-I promoter (pTOPO-2024) was finally successfully constructed. To help understand, the schematic diagram of the complicated process of generating pTOPO-2024 from duck genomic DNA was shown in the Figure 2.1.

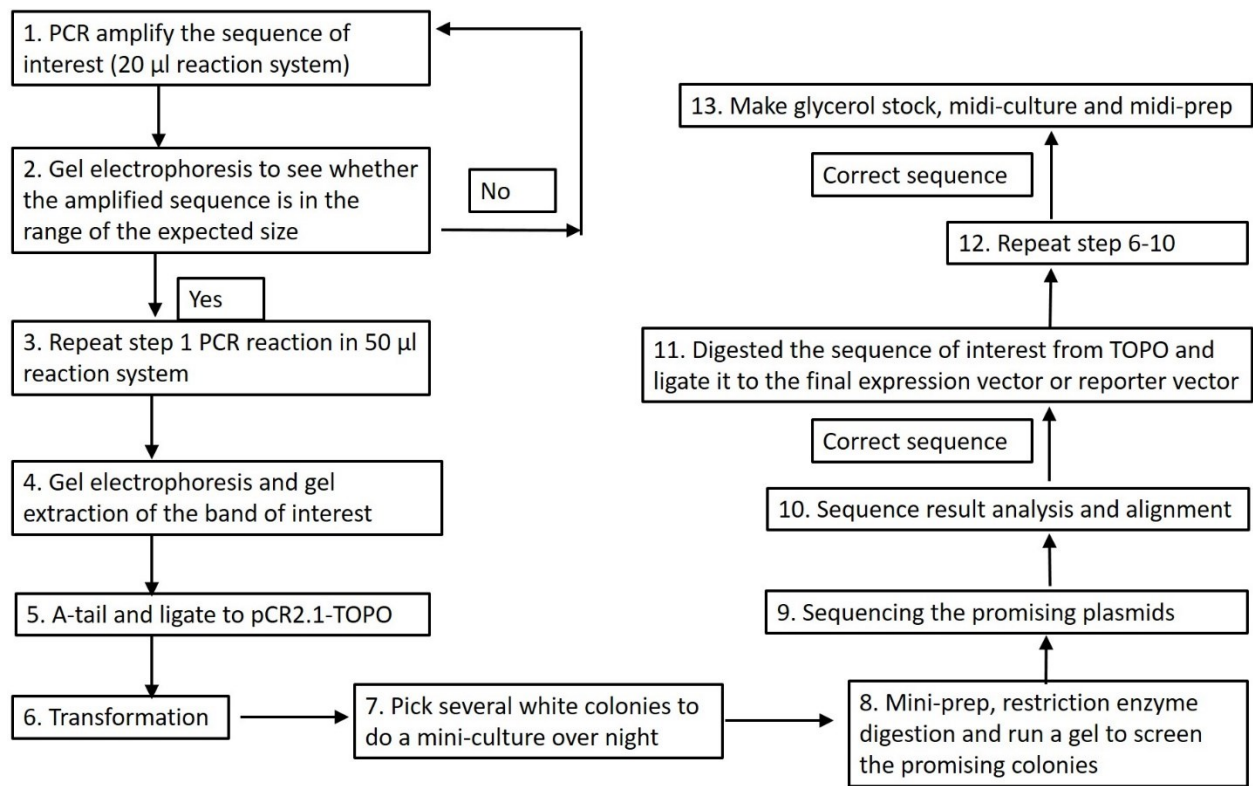
2.3 Bioinformatics

RIG-I proteins and promoters from other vertebrates were recovered from GenBank, Ensembl, or using the UCSC Genome Browser <http://genome.ucsc.edu/> (Kent et al., 2002) (sequence IDs listed in Appendix II). The bootstrap consensus trees of RIG-I promoters, RIG-I proteins, and MAVS proteins were generated by MEGA7 through the bootstrap analysis of 1000 replicates using Neighbor-Joining method and Maximum Composite Likelihood model or Poisson model, respectively. Branches corresponding to partitions reproduced in less than 50% bootstrap replicates were collapsed. All positions containing gaps and missing data were eliminated.

To analyze the core promoter sequence, putative transcription factors (TFs) and their binding sites in this region were predicted using the JASPAR online server (<http://jaspar.binf.ku.dk/>). The database used was JASPAR Core Vertebrata (Mathelier et al., 2016) and the relative profile score threshold was set as 85%.

2.4 General procedure of plasmid construction

The flowchart of molecular clone generation



2.5 Specific plasmid construction

2.5.1 The full-length promoter reporter vector of duck RIG-I (p2024)

The full-length sequence of duck RIG-I promoter was digested out of pTOPO-2024 (generated in section 2.2.8) by KpnI and XhoI (NEB) and ligated to pGL3-basic luciferase reporter vector (Promega), which was previously digested with the same restriction enzymes (KpnI and XhoI), to generate p2024 as step 11 to step 13 in the flowchart of section 2.4. This vector was then used as the backbone plasmid to construct serial truncated duck RIG-I promoter plasmids presented in this work.

T4 Ligation: The ligation was performed using T4 DNA ligase (NEB) according to the manufacturer's instructions. Briefly, 0.020 pmol digested pGL3-basic vector and 0.060 pmol inserted RIG-I full-length promoter sequence were added into a microcentrifuge tube containing 4 µl 5×T4 DNA ligase buffer, adjusting the mixture volume to 19 µl with ddH₂O. Finally, 1 µl T4 DNA ligase (400,000 units/ml) was added into the mixture and incubated at 16 °C overnight.

Transformation: 5 µl ligation product was transformed into 50 µl DH5α competent cells (NEB) according to the protocol of section 2.2.3. In the last step, 100 µl transformed competent cells were plated on the LB agar plate containing 50 µg/ml carbenicillin and incubated at 37°C overnight. X-gal was not necessary for this transformation.

Sequencing: The primers used for p2024 sequencing were RV primer 3, GLprimer 2, RIG-I promoter F, and RIG-I promoter R (Table 2-1). Around 600 ng of each promising plasmid was mixed with 1 µl above individual primer (2.5 µM) and sent to sequence in Molecular Biology Facility (MBSU) of University of Alberta.

2.5.2 Serial deletion promoter vectors

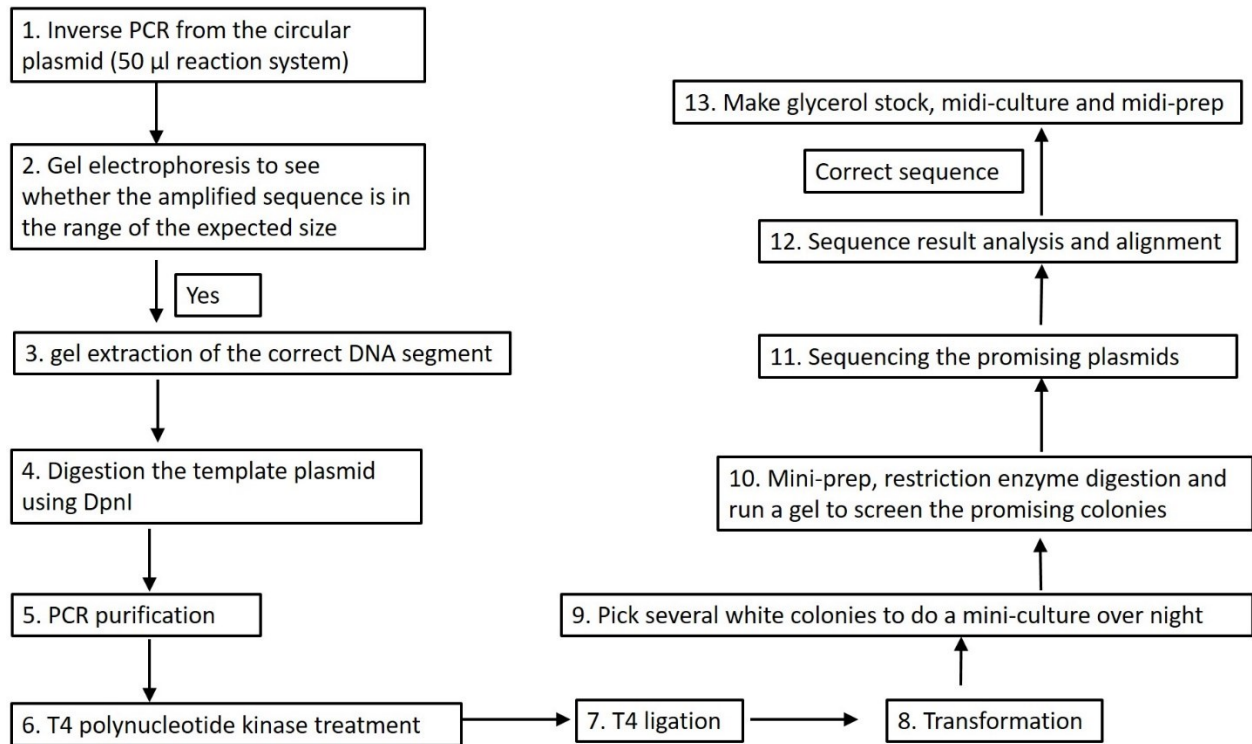
The inverse PCR was run to amplify the entire circular plasmid with a targeted deletion (Figure 2.2). The above generated p2024 was used as the template of this reaction. The primers and their binding sites in the circular p2024 were shown in the schematic diagram (Figure 2.3). The PCR reaction was performed as the manufacturer's instructions using Phusion High-Fidelity DNA polymerase (NEB). The amount of template used for each reaction was 10 ng and the final concentration of each primer in a PCR reaction was 0.5 µM. The thermocycling conditions consisted of an initial denaturation step of 98°C for 30 seconds, followed by 30 cycles of 98°C for 10 seconds, 60°C for 30 seconds, 72°C for 3 minutes, and a final extension of 72°C for 7 minutes. PCR products were loaded into 1% agarose gel to run gel electrophoresis and gel extraction. Followed by PCR purification using QIAquick PCR Purification Kit (QIAGEN) according to the manufacturer's instructions. In the last step, the purified DNA was eluted with 30 µl ddH₂O.

15 µl of purified PCR sample was treated with 1 µl T4 polynucleotide kinase (PNK) (10,000 units/ml) (NEB) in 4 µl 5×T4 ligase buffer (NEB) at 37 °C for 1 hour for phosphorylation prior to ligation using T4 ligase (NEB) at 16 °C overnight.

On the following day, 10 µl ligation product was transformed into DH5α competent cells as the protocol in section 2.2.3. Followed by picking colonies, mini-culture, mini-prep, and restriction digestion. The restriction enzyme used for digestion was EcoRI (NEB). The sequencing method

was described in section 2.5.1. The sequencing primers were RV primer 3 and GLprimer 2. The analysis of sequencing results was as section 2.2.7.

The whole procedure of generating the deletion constructs is shown in the following flowchart.



2.5.3 Transcription factor (TF) binding site deletion mutants

I created constructs with the deletion of specific transcription factor binding sites in the duck RIG-I promoter by site-directed mutagenesis (NEB) using the promoter constructs (p250 and p125) as template and the Phusion High-Fidelity PCR kit (NEB). The gel extracted products were treated with Dpn I (NEB) to eliminate the original template plasmid, purified with the QIAquick PCR purification kit (QIAGEN) before the addition of 5'-phosphates with T4 Polynucleotide Kinase (NEB) and the two ends of the amplified strands ligated together with T4 DNA ligase to form the mutant constructs. The primers were designed to hybridize to either side of deleted TF binding sites (Table 2-1). A random deletion vector was constructed as the negative control. The predicted TF binding sites and deleted parts in p250 or p125 were shown in Figure 3.7A and Figure 3.7B.

2.5.4 TF binding site point mutation vectors (site-directed mutagenesis)

The primers used in this part (Table 2-1) were designed on the website <http://bioinformatics.org/primerx/> following the protocol in the QuikChange Manual. Basically, the primers are designed with a T_m of at least 78°C and centering the mutation in the middle.

Site-directed mutagenesis was performed according to the protocol provided in AML Version 1.2 (2005.11.06). Briefly, a linear amplification was first implemented as the recommended reaction system. The polymerase used was Phusion High-Fidelity DNA polymerase (NEB), and the template was p250. The PCR thermocycling program consisted of an initial denaturation step of 95°C for 5 minutes, followed by 18 cycles of 95°C for 50 seconds, 60°C for 50 seconds, 72°C for 2.5 minutes, and a final extension of 72°C for 7 minutes. Followed by DpnI treatment to digest the template plasmids and transformation of the final reaction product into DH5 α competent cells. Finally, the point mutated RIG-I promoter plasmids were recovered through standard procedures.

In some constructs, more than 3 nucleotides required changing, so two cycles of site-directed mutagenesis were implemented with two pairs of site-directed mutated primers. The mutated plasmids generated in the first cycle were used as the templates in the second cycle. For generation of mutation of the GC box and ISRE, the introduced mutations were shown in Figure 2.4.

2.5.5 pmCherry-chIRF1 and pmCherry-dIRF1

Chicken IRF1 was amplified from cDNA prepared from chicken DF-1 cells, and duck IRF1 was amplified from duck spleen cDNA using Phusion High Fidelity DNA polymerase and cloned into pCR2.1-TOPO vector. PCR reactions were implemented according to the manufacturer's instructions for Phusion High-Fidelity DNA polymerase (NEB). The thermocycling condition consisted of an initial denaturation step of 98°C for 30 seconds, followed by 32 cycles of 98°C for 10 seconds; 62°C for 30 seconds; 72°C for 1 minute, and a final extension of 72°C for 7 minutes. dIRF1 was digested from pCR2.1-TOPO with EcoR1 and KpnI (NEB) and ligated into pmCherry-C1 vector (ClonTech) to generate pmCherry-dIRF1. Because of an internal EcoR1 site, chicken IRF1 was amplified from pTOPO-chIRF1 using primers (HindIII-chIRF1 F and

chIRF1-KpnI R2 as in Table 2-1) to introduce a HindIII site. The protected nucleotides were added on either side of HindIII-chIRF1-KpnI segment. Followed by digestion of HindIII-chicken IRF1-Kpn I segment and ligating into pmCherry-C1. Chicken IRF7 was amplified from chicken lung cDNA using Phusion (NEB) using primers including an EcoR1 and KpnI restriction enzyme site. These primers amplified the full-length IRF7 gene. The product was digested with restriction enzymes and introduced into pmCherry-C1. All constructs were verified by sequencing and confirmed to introduce the IRF proteins in-frame downstream of mCherry.

2.5.6 No-tag/Flag/GST/GFP-PB1-F2 (PR8/ Rg/D4AT/VN) vectors

I took over this project from Man Rao, who had constructed pTOPO-PB1-F2 (Rg/D4AT/VN) without any tag. I digested the PB1-F2 (Rg/D4AT/VN) segment out of TOPO vectors using BamH I and Not I (NEB) and ligated them into pGST vector to generate GST tagged PB1-F2 expression vectors, pGST-PB1-F2 (Rg/D4AT/VN). However, it turned out the GST tag influenced the following luciferase assay experiments. Thus, Flag and GFP tagged PB1-F2 (Rg/D4AT/VN) expression vectors were further constructed.

Taking pTOPO-PB1-F2 (Rg/D4AT/VN) as the templates, Flag-PB1-F2 (Rg/D4AT/VN) was amplified using primers BamHI-PB1-F2 (Rg/ D4AT /VN) F, PB1-F2 (Rg)-NotI R and PB1-F2 (D4AT /VN)-NotI R (Table 2-15) with Q5 High-Fidelity PCR Kit (NEB) as the manufacturer's instruction. The general thermocycling program consisted of an initial denaturation step of 98°C for 30 seconds, followed by 30 cycles of 98°C for 10 seconds; 62°C for 30 seconds; 72°C for 30 seconds, and a final extension of 72°C for 7 minutes. Followed by the standard cloning procedures. The sequencing results showed pTOPO-Flag-PB1-F2 (Rg/D4AT/VN) correct but lacking the start codon “ATG” at the beginning of Flag sequence. Hence, “ATG” was further inserted in front of Flag sequence of pTOPO-Flag-PB1-F2 (Rg/D4AT/VN) with primers BamH1-Flag F and pcDNA3.1 R (Table 2-1) to finally generate the correct pTOPO-Flag-PB1-F2 (Rg/D4AT/VN) expression vectors. Followed by digesting Flag-PB1-F2 (Rg/D4AT/VN) out of TOPO vectors with BamH I and Not I (NEB) and ligating them to predigested pcDNA3.1 using the same restriction digestion enzymes to construct pcDNA3.1-Flag-PB1-F2 (Rg/D4AT/VN) expression vectors.

For PB1-F2 (PR8) vectors, I first reverse transcribed cDNA from extracted RNA of PR8 virus (David Tetrault) as the protocols in section 2.8.1 and 2.8.2. The BamH I-Flag-PB1-F2 (PR8)-Not I segment was amplified from cDNA using primers BamHI-Flag-PB1-F2 (PR8) F and PB1-F2 (PR8) NotI R (Table 2-15) with Phusion High-Fidelity DNA polymerase (NEB) according to the manufacturer's instructions.

Prior to constructing pGFP-PB1-F2 (PR8), un-tagged BamH I-PB1-F2 (PR8)-Not I segment was amplified from the gel extracted product of Flag-PB1-F2 (PR8) segment, which was digested out of pcDNA3.1-Flag- PB1-F2 (PR8) with BamH I and Not I (NEB). The primers used in this PCR were BamHI-PB1-F2 (PR8) F and PB1-F2 (PR8)-NotI R (Table 2-1). The PCR product was inserted into TOPO vector.

To make GFP tagged PB1-F2 (PR8/Rg/D4AT/VN) fusion vectors, PB1-F2 segments were digested out of pTOPO- PB1-F2 (PR8/Rg/D4AT/VN) vectors using Kpn I and Apa I (NEB) and ligated to pEGFP-C vector (Addgene).

2.5.7 Flag-PB1-F2 (VN) point mutation vectors (site-directed mutagenesis)

Flag-PB1-F2 (VN) point mutation vectors were generated by site directed mutagenesis. The primers, PB1-F2 (VN) T51M/V56A/V42C/R79Q/E87G F or R (Table 2-1) were designed on the website <http://bioinformatics.org/primerx/>. Flag-PB1-F2 (VN) was used as the template to amplify the linear Flag-PB1-F2 (VN) plasmids containing the indicated single point mutation. While, Flag-PB1-F2 (VN) (T51M) was the template to amplify the linear Flag-PB1-F2 (VN) plasmids containing two-point mutations (T51M with another indicated point mutation). The other steps were the same as previously described.

2.6 Cell seeding and transfection

DEF, DF-1 or AD293T cells were seeded into 24-well plates at 2×10^5 /well or 6-well plates at 8×10^5 /well, while, HeLa cells were seeded into 6-well plates at 4×10^5 /well. If the cells were used to do immunofluorescence (IF) or MitoTracker Red staining, prior to seeding the cells, an 18×18 mm sterilized coverslip (Fisher Scientific) would be put into each well of 6-well plates.

24h after plate-seeding, the cells (70-90% confluency) were transfected with the indicated DNA constructs using Lipofectamine 2000TM reagent (Invitrogen) at a ratio of 1: 2.5 (DNA: Lipofectamine). The brief transfection protocol for 6-well plates is as follows: Lipofectamine 2000 was diluted with 250 μ l Opti-MEM medium and let stand for 5 minutes at room temperature. Meanwhile, DNA or plasmid was diluted with 250 μ l Opti-MEM medium as well, followed by mixing and incubating the diluted DNA or plasmid with the diluted lipofectamine 2000 for 20 minutes before they were added to the 1 \times PBS washed cells. Finally, 500 μ l of cell culture medium was added into each well and the cells maintained in the cell incubator for 24h before using them to do the following experiments. The amount of Opti-MEM medium used to dilute DNA or lipofectamine 2000 for 24-well plate transfection was 50 μ l per well.

2.7 Dual luciferase assay

2.7.1 To investigate RIG-I promoter activity

DEF or DF-1 cells in a 24-well plate were transfected with the duck RIG-I promoter plasmids (150 ng/well) and the *Renilla* luciferase control vector (10 ng/well) with or without the stimulators (the constitutively active duck RIG-I N-terminal domain (2CARD) or high molecular weight (HMW) poly (I:C) (InvivoGen). The GST (control) or GST-2CARD were transfected at 20 ng/well. The concentration of HMW poly (I:C) used was 2 μ g/ml. The promoter activity of duck RIG-I was measured at 24 h post transfection using the Dual Luciferase Reporter Assay (Promega) according to manufacturer's instructions. Briefly, the cells were lysed with 100 μ l 1 \times passive lysis buffer at room temperature for 15 min. 20 μ l of cell lysate was transferred to 1.5 ml Eppendorf tube, followed by adding 100 μ l luciferase assay reagent II and 100 μ l 1 \times Stop & Glo[®] reagent to cell lysate, in sequence, and measuring the luciferase activity using the GloMax 20/20 Luminometer (Promega). The firefly luminescence from the test reporters was normalized to the *Renilla* luminescence from the control vector, and the normalized relative luciferase units (RLU) were divided by the mean RLU of the control cells (pGL3 Basic). For each construct, transfections were done in triplicate. Assays were performed at least twice.

2.7.2 To investigate PB1-F2 influence in IFN- β reporter activity.

DF-1 cells in a 24-well plate were transfected with 150 ng chicken IFN- β reporter vector (chIFN- β), 10 ng *Renilla* luciferase control vector, and 500 ng of the pcDNA3.1, Flag-PB1-F2 plasmid or Flag-NS1 with 20 ng GST (control) or GST-2CARD vector (stimulator). 24 h post transfection, type I IFN- β reporter activity was measured using the Dual Luciferase Reporter Assay System (Promega) according to the above protocol.

2.8 Quantitative RT-PCR analysis of transcription factor (TF) genes in DF-1 cells.

2.8.1 RNA extraction

DF-1 cells were seeded into 24-well plates and transfected with 150 ng pGL3-Basic or p2024 with or without 20 ng GST-2CARD per well, 24 h post transfection, cellular RNA was extracted using Trizol (Invitrogen) according to the manufacturer's instructions. Briefly, cells were lysed directly in the culture plate by adding 250 μ l of Trizol reagent per well and passing the cell lysate several times through a pipette. The homogenized sample was transferred to RNase free 1.5 ml Eppendorf tube and allowed to sit at room temperature for 5 minutes prior to adding 50 μ l of chloroform. The tubes were vigorously shaken and allowed to settle for 2 to 3 minutes at room temperature prior to being centrifuged at 10,000 \times g for 15 minutes at 4 $^{\circ}$ C. The aqueous phase was transferred to a fresh 1.5 ml Eppendorf tube containing 125 μ l of isopropyl alcohol and allow the sample to sit at room temperature for 10 minutes prior to being centrifuged at 10,000 \times g for 10 minutes at 4 $^{\circ}$ C. The supernatant was removed, and the RNA pellet was washed once with 500 μ l 75% ethanol by vortexing and centrifugation at 7,500 \times g for 5 minutes at 4 $^{\circ}$ C. At the end of the procedure, the RNA pellet was air-dried for 5-10 minutes and dissolved in 30 μ l RNase-free water. The concentration of the extracted RNA was measured with the NanoDrop[®] ND-1000 UV/Vis Spectrophotometer (NanoDrop Technologies).

2.8.2 cDNA synthesis

cDNA synthesis from RNA was performed using Superscript III first-strand synthesis kit (Invitrogen) according to the manufacturer's protocol. Briefly, 1 μ g of the extracted RNA was treated with 1 μ l DNase I (1U/ μ l) at room temperature for 15 minutes to remove any contaminating genomic DNA, followed by being heat treated at 65 $^{\circ}$ C for 10 minutes to

inactivate the DNase enzyme prior to being incubated with 1 μ l of random primer and 1 μ l dNTP at 65 °C for 5 minutes. In the last step, 1 μ l Superscript III (200 U/ μ L), 1 μ l RNase OUT (40 U/ μ L), and 2 μ l DTT (0.1M) were added into the mixture to synthesize cDNA at 50 °C for 50 minutes and 70 °C for 15 minutes in the thermocycler. The quality of synthesized cDNA was roughly estimated by running a traditional PCR of GAPDH before being used to do real-time PCR.

2.8.3 Real-time PCR

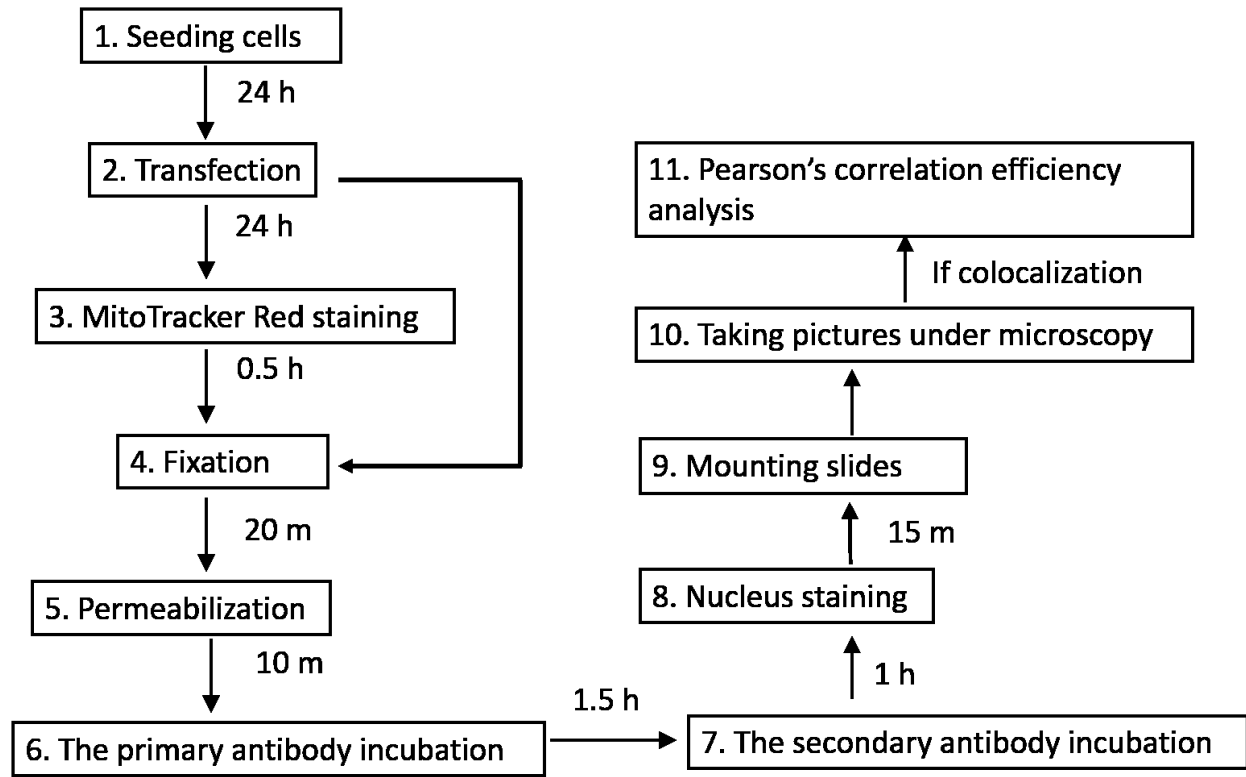
The synthesized cDNA was diluted ten-fold in nuclease-free water before use. The mRNA transcripts were amplified by adding 2.5 μ l diluted cDNA, 1 μ l of the indicated primer/probe mix (10 μ M) (Table 2.2), and 1.5 μ l ddH₂O to 5 μ l of the TaqMan master mix reagent (Roche). The reaction was performed in 7500 fast real-time PCR system (Applied Biosystems). The thermocycling program consisted of an initial denaturation step of 95°C for 2 minutes, followed by 40 cycles of 95°C for 15 seconds and 60°C for 1 minute. The qPCR primer and probe were designed using online Real-Time PCR design tool (IDT) and ordered as mixes (qPCR assays, IDT). Fold difference of gene expression was determined with the method of $2^{-\Delta\Delta CT}$ in the 7500 fast system software (Applied Biosystems). The fold change for each target gene was normalized to the endogenous control gene GAPDH. For each sample and each gene, the experiment was done in triplicate.

2.9 Statistical analysis

Values indicated the means \pm standard deviation and the statistical analysis among multiple experimental groups or two groups was performed by Tukey's multiple comparison under one-way analysis of variance (ANOVA) or Student's t-test using GraphPad Prism 6 software. $P < 0.05$ was considered significant.

2.10 General procedures of immunofluorescence (IF) staining

The general procedures of immunofluorescence (IF) were shown in the flowchart:



After each step, the cells will be washed with 1×PBS

2.10.1 Visualization of mCherry-tagged IRF proteins.

DF-1 cells were seeded into 6-well plates containing a glass coverslip in each well. Twenty-four hours later, 2 µg mCherry, mCherry-chIRF1, mCherry-chIRF7 or mCherry-dIRF1 were transfected separately into wells of the seeded DF-1 cells. Twenty-four hours post transfection, the cells were washed once with 1 × PBS and fixed with 4 % paraformaldehyde (PFA)/PBS at room temperature for 20 minutes. Nuclei were stained with 2 µg/ml Hoechst and the coverslips mounted onto microscope slides (1.0 mm thick) using Mowiol mounting medium (in Appendix I). The slides were examined using a Zeiss fluorescence microscope and the images taken with the AxioVision software.

2.10.2 Investigation of the distribution of duck MAVS and PB1-F2 in DF-1 cells or HeLa cells.

DF-1 or HeLa cells were seeded into 6-well plates containing a glass coverslip per well. 24 hours later, 2 µg V5-dMAVS, Flag-PB1-F2 (PR8) and GST-PB1-F2 (Rg/D4AT/VN) were transfected separately into the seeded cells. 24 hours post transfection, the cells were washed once with 1×PBS and stained with 200 nM MitoTracker Red (Invitrogen) in cell incubators for 30 minutes. The stained cells were washed with 1×PBS twice, fixed with 4% PFA, and permeabilized with 0.2% Triton X-100. The primary antibodies used for V5-dMAVS, Flag-PB1-F2 and GST-PB1-F2 were mouse anti-V5 (Invitrogen), mouse anti-Flag-M2 (Sigma-Aldrich) and mouse anti-GST (Thermo Fisher) in 1: 500 dilution, respectively. The secondary antibody was goat-anti-mouse-Alexa 488 (1: 500 dilution) (Thermo Fisher). The nucleus staining, and mounting procedures were the same as previously described. The slides were examined under Confocal Microscope Zeiss LSM 710 and the captured images were processed with Zen 2011 software.

2.10.3 Investigation of the colocalization between duck MAVS and RIG-I 2CARD or PB1-F2 in DF-1 cells or HeLa cells.

DF-1 or HeLa cells were seeded into 6-well plates containing a glass coverslip per well. 24 hours later, 1 µg V5-dMAVS and 1 µg GST-2CARD or 1 µg Flag-PB1-F2 (PR8/Rg/D4AT/VN) were co-transfected into the seeded cells. 24 hours post transfection, the cells were washed with 1×PBS, fixed with 4% PFA, and permeabilized with 0.2% Triton X-100. The primary antibodies were rabbit anti-V5 (Abcam) and mouse anti-Flag-M2 (Sigma-Aldrich) or rabbit anti-V5 (Abcam) and mouse anti-GST (Thermo Fisher) mixture in 1×PBS in 1: 500 dilution. The secondary antibody was goat-anti-mouse-Alexa 488 (Thermo Fisher) and goat-anti-rabbit-Alexa 594 (Thermo Fisher) mixture in 1×PBS in 1: 500 dilution. The other steps were the same as previously described.

2.11 Protein extraction from cell culture and GST-pull downs

Protein extraction: The seeded DF-1 cells in 6-well plate were co-transfected with 1 µg V5-dMAVS and 1 µg GST (control) or GST-2CARD. Protein extraction was performed 24 h post transfection. Briefly, the transfected cells were washed once with ice-cold 1x PBS, aspirated and

transferred from the cell plate immediately to ice. The cells were lysed using 200 μ l 1% Triton X-100 lysis buffer with cOmplete Mini, EDTA-free proteinase inhibitor cocktail pellets (Roche Diagnostics) per well, rocked on ice for at least 15 minutes. The cells were scraped in the lysis buffer (1000 μ l) and the lysate was collected into 1.5 ml micro centrifuge tubes and centrifuged at 12,000 g at 4 °C for 10 minutes to pellet the cell debris.

GST-pull down: 30 μ l of whole cell lysate (WCL) was boiled for 10 minutes in 10 μ l of 4 \times Laemmli buffer to be used for Western Blotting (WB). The remaining WCL was incubated with equilibrated glutathione-coated sepharose beads (GE Healthcare) overnight at 4 °C with constant agitation to allow the GST-tags to bind to glutathione. The pellet was discarded. During the time of centrifugation, 100 μ l GST beads had been equilibrated according to the manufacturer's instruction (GE Healthcare). The next day, the beads were spun down and washed three times with 1 ml ice-cold lysis buffer with the protease inhibitor cocktail (Sigma-Aldrich). The beads were resuspended in 60 μ l Laemmli buffer and processed by boiling for 10 minutes prior to being used to do Western Blotting (WB).

2.12 Co-immunoprecipitation (Co-IP)

The seeded DF-1 cells in 6-well plates were co-transfected with 1 μ g V5-dMAVS and 1 μ g Flag-PB1-F2 (PR8) or transfected with 2 μ g V5-dMAVS or 2 μ g Flag-PB1-F2 (PR8/Rg/D4AT/VN) per well separately. Protein extraction was performed 24 h post transfection as outlined in the protocol in section 2.2.9. 30 μ l WCL of each sample was boiled for 10 minutes in 10 μ l of 4 \times Laemmli buffer to be used for WB. The remaining WCL of V5-dMAVS and Flag-PB1-F2 (PR8) or the mixture of 500 μ l WCL of V5-dMAVS and 500 μ l WCL of Flag-PB1-F2 (PR8/Rg/D4AT/VN) was incubated with equilibrated mouse anti-V5 coated agarose beads (Sigma) overnight at 4 °C with constant agitation. 50 μ l beads were used for each sample and equilibrated as described in the manufacturer's instruction (Sigma). The second day, the beads were washed three times with ice-cold lysis buffer and eluted with 4 X Laemmli buffer, followed by boiling for 10 minutes before being used for WB.

2.13 Western Blotting (WB)

Equal amounts (20 μ l or 15 μ l) of prepared protein samples, with 6 μ l PageRuler™ Plus prestained ladder (Pierce), were loaded into a 12% SDS-PAGE gels (Table 2-4) for separation at 100 V under reducing conditions. The proteins were transferred from SDS-PAGE gel to Trans-Blot Nitrocellulose transfer membrane (BioRad) at 100 mA for 1.5 hours. Membranes were blocked in 5% (w/v) skim milk/PBS for 30 minutes at room temperature. This was followed by incubating with the primary antibodies (mouse anti-Flag M2 (Sigma-Aldrich) and rabbit anti-V5 (Abcam)) at 1: 5000 dilution for 1.5 hours at room temperature and the secondary antibodies (goat anti-mouse-HRP (BioRad) and goat anti-rabbit-HRP (BioRad)) for 1 hour at room temperature. The membranes were developed using Pierce ECL Western Blotting Substrate (Thermo scientific) according to the manufacturer's instruction.

Table 2-1 Primers used for the full-length duck RIG-I promoter amplification

Name	sequence (5' to 3')
RIG-I promoter F1	CCAAGTAAAAATGCCTCTCTGCT
RIG-I promoter R1	GCATCGCGTCCAGCATCCCTCGGA
RIG-I promoter F2	AGCTGATGACCTGCAAAAAGTT
RIG-I promoter R2-1	GTTGAGGCTCCGCTCGATGTA
RIG-I promoter R2-2	GGCTGGGCTCTGCCGCGCCG

F: forward primer; R: reverse primer

Table 2-2 Primers used for generating serial truncated constructs of duck RIG-I promoter

Name	sequence (5' to 3')	Application
SDM R	AAGGGCGAATTCCAGCACACTG	SDM construction
1kb F	CTTACTGAAAATGCAGGGTGGA	p1000 construction
500bp F	GAGCGGCGGAGACAAAGTGCCA	p500 construction
250bp F	CTGGACCCAGGCCCGTGCTC	p250 construction
125bp F	ATCTCCACACCCCGCGGGGCC	p125 construction
73bp F	GCTGCCTTCTGTGCCGAGCCG	p73 construction

F: forward primer; R: reverse primer; SDM is short for "serial deletion mutation"

Table 2-3 Primers used for TF binding site deletion or point mutation constructs of duck RIG-I promoter

Name	sequence (5' to 3')	Application
ΔRandom F	TCACGAAGCTGCGAGCCGCTG	random deletion mutation
ΔRandom R	AGACACGGCCTGGGGTCCAG	random deletion mutation
ΔNHLH1 F	GCCGCTGCCTATGCCCGCTGG	NHLH1 BSDM
ΔISRE F	TTCCCGCCGGGCCTCGCT	ISRE deletion mutation
ΔISRE R	GGCCCCGCGGGGTGTGGA	ISRE deletion mutation
mGC F1	CGGCCAGAGGGCTTGCTGCGGATGG	GC point mutation 1
mGC R1	CCATCCGCAGCAAGCCCTCTGGCCG	GC point mutation 1
mGC F2	CTGGCGGCCAGAGTTCTTGCTGCGGATG	GC point mutation 2
mGC R2	CATCCGCAGCAAGAACTCTGGCCGCCAG	GC point mutation 2
mISRE F1	CGCGGGGGCCGCTAACGTTTTCCATTC	ISRE point mutation 1
mISRE R1	GAATGGA AACGTTAGCGGCCCGCG	ISRE point mutation 1
mISRE F2	GGCCGCTAACGTGAGCCATTCGCCCG	ISRE point mutation 2
mISRE R2	CGGCGGGGAATGGCTCACGTTAGCGGCC	ISRE point mutation 2

F: forward primer; R: reverse primer; Δ: deletion mutation; BSDM: binding site deletion mutation; m: point mutation

Table 2-4 Primers used for generating various expression vectors

Name	sequence (5' to 3')	Application
EcoRI-chIRF1 F	GAATTC AATGCCCGTCTCAAG	chIRF1 amplification
chIRF1-KpnI R	GGTACCTTACAAGCTGCAGGA	chIRF1 amplification
EcoRI-dIRF1 F	GAATTC AATGCCCGTCTCCAG	dIRF1 amplification
dIRF1-KpnI R	GGTACCTTACAAGCCACAGGA	dIRF1 amplification
HindIII-chIRF1 F	CCCAAGCTTCGAATTC AATGCCCGTCT	chIRF1 amplification 2
chIRF1-KpnI R2	CGGGGTACCTTACAAGCTGCAGGAGC	chIRF1 amplification 2
BamHI-PB1-F2(PR8) F	GGATCCATGGGACAGGAACAGG	PB1-F2 (PR8) amplification
PB1-F2 (PR8)-NotI R	GCGGCCGCCTACTCGTGTTTG	PB1-F2 (PR8) amplification
BamHI-PB1-F2 (Rg/D4AT/VN) F	GGATCCATGGAACAGGGACAGGATACAC	PB1-F2 (Rg/D4AT/VN) amplification
PB1-F2 (Rg)-NotI R	GCGGCCGCTCAGTTTATCCACCCTTGTTT	PB1-F2 (Rg) amplification
PB1-F2 (D4AT/VN)-NotI R	GCGGCCGCTCAGTTTATCCACTCTTGTTT	PB1-F2 (D4AT/VN) amplification
BamHI-Flag-PB1-F2(PR8) F	GGATCCGCCACCGATTATAAAGATGATGAT GATAAAGGAATGGGACAGGAACAGGATACA	Flag-PB1-F2 (PR8) amplification
PB1-F2 (PR8) NotI R	GCGGCCGCCTACTCGTGTTTGCTGAACAAC	PB1-F2 (PR8) amplification
BamHI -Flag-PB1-F2 (Rg/D4AT/VN) F	GGATCCGCCACCGATTATAAAGATGATGAT GATAAAGGAATGGAACAGGGACAGGATACA	Flag-PB1-F2 (Rg/D4AT/VN) amplification
BamH1-Flag F	GGATCCGCCACCATGGATTATAAAGATGA	Flag-PB1-F2 (pcDNA3.1) correction
pcDNA3.1 R	GAGCTCGGTACCAAGCTTAAGTTTAAAC	Flag-PB1-F2 (pcDNA3.1) correction
T51M F	GAGCCAGTGGGTATGCACAAACAGATTG	VN PB1-F2 point mutation
T51M R	CAATCTGTTTGTGCATACCCACTGGGCTC	VN PB1-F2 point mutation
V56A F	CGCACAAACAGATTGCGTATTGGAAGCAATG	VN PB1-F2 point mutation
V56A R	CATTGCTTCCAATACGCAATCTGTTTGTGCG	VN PB1-F2 point mutation
V42C F	GATTGATGGACCACTGCCTGAGGATAATGAG	VN PB1-F2 point mutation
V42C R	CTCATTATCCTCAGGCAGTGGTCCATCAATC	VN PB1-F2 point mutation
R79Q F	CTCGTGTCTTGAAACAATGGAAATTGTTCAAC	VN PB1-F2 point mutation
R79Q R	GTTGAACAATTTCCATTGTTTCAAGACACGAG	VN PB1-F2 point mutation
E87G F	GAAATTGTTCAACAAACAAGGGTGGATAAA CTGAGCGGCC	VN PB1-F2 point mutation
E87G R	GGCCGCTCAGTTTATCCACCTGTTTGTGAAACA ATTTC	VN PB1-F2 point mutation

F: forward primer; R: reverse primer; d: duck; ch: chicken

Table 2-5 Primers used for sequencing

Name	sequence (5' to 3')	Target to be sequenced
M13F	CAGGAAACAGCTATGAC	pCR2.1-TOPO vector
M13R	GTAAAACGA CGGCCAGT	pCR2.1-TOPO vector
RVprimer 3	CTAGCAAAATAGGCTGTCCC	pGL3-Basic vector
GLprimer 2	CTTTATCTTTTTGGCGTCTTCCA	pGL3-Basic vector
RIG-I promoter F	CTCTTCTCAGGTGAAGGACAAG	The full-length RIG-I promoter
RIG-I promoter R	TTCTCTCACATTTTCTCACTCT	The full-length RIG-I promoter
pmCherry F	AACATCAAGTTGGACATCACC	mCherry vector
pmCherry R	GAAATTTGTGATGCTATT	mCherry vector
pGEX F	GGGCTGGCAAGCCACGTTTGGTG	pGEX-6P-1 vector
T7	TAATACGACTCACTATAGGG	pcDNA3.1 vector
BGHR	TAGAAGGCACAGTCGAGG	pcDNA3.1 vector
pEGFP-C	CATGGTCCTGCTGGAGTTCGTG	pEGFP vector
pEGFP-N	CGTCGCCGTCCAGCTCGACCAG	pEGFP vector

F: forward primer; R: reverse primer

Table 2-6 Primer and probe sequences used in quantitative real-time PCR (qPCR)

Gene	Primer and probe sequence (5' to 3')
GAPDH	FW: AGG CTG TGG GAA AAG TCA TC RV: GCC TTC ACT ACC CTC TTA ATG TC PR: FAM-/CGT CTC TGT/ZEN/CGT GGA CCT GAC C/-3IABkFQ
IRF1	FW: GTT GTA TGA GGA TAT GAG GAT GGA G RV: AGG ACG AGA GGT CTA AGG TG PR: FAM-/CGT GTA GTC /ZEN/GTG AGC GGT GTA GC/3IABkFQ
STAT-2	FW: ACA TTC ACA TCG ACA GGG AC RV: CTT CTG CTC CTT CAG TGT GAG PR: FAM-/CGA GGG TTC /ZEN/CGC AAA TTC AAC ATC C/3IABkFQ
STAT-3	FW: TCA GCT CTG TTT TCC CTT CG RV: GTA AGC CCT GAA ACT CCC TG PR: FAM-/AGC ACA GTA /ZEN/AAG CCC TCC ACA TCA C/3IABkFQ

FW: forward; RV: reverse; PR: probe



Amplified full length promoter sequence (-2024 to -1)

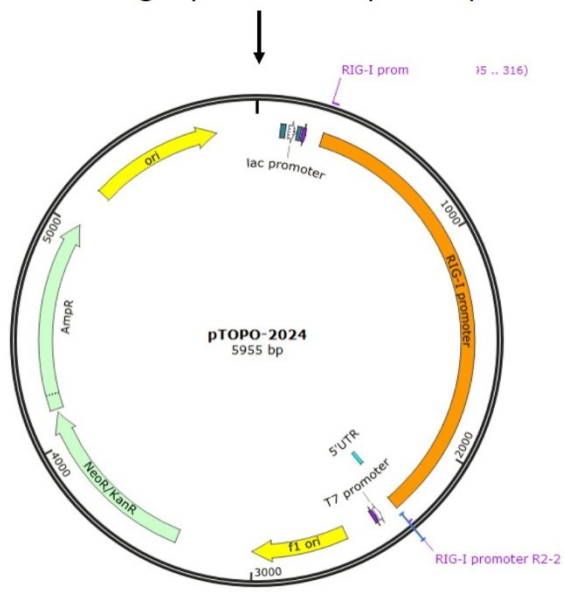


Figure 2.1 The schematic generation of the full-length duck RIG-I promoter TOPO vector.

The first exon of RIG-I in duck genome was identified by PCR using primers RIG-I promoter F1 and RIG-I promoter R1. Due to high “GC” content in 5'UTR region, a piece of segment consisted of the full-length RIG-I promoter and partial first exon (-2024 to + 63) was amplified from duck genome using primers RIG-I promoter F2 and RIG-I promoter R2-1. Finally, the exact full-length of RIG-I promoter was amplified from pTOPO (-2024 to +63) using primers RIG-I promoter F2 and RIG-I promoter R2-2 and inserted into TOPO vector.

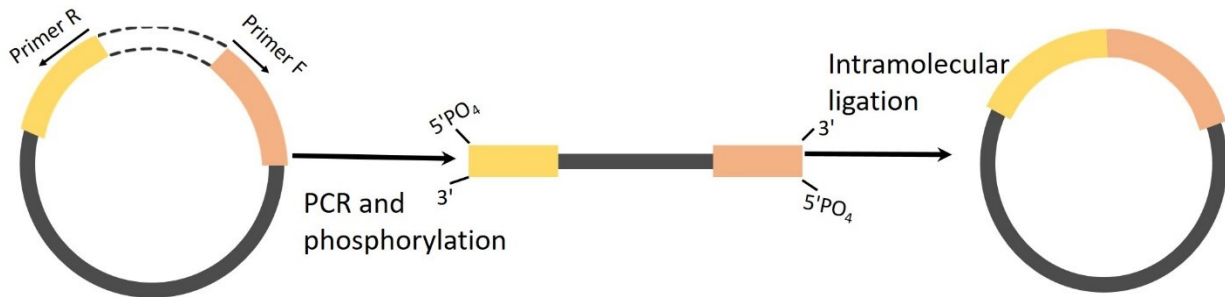


Figure 2.2 The schematic of inverse PCR for site-directed deletion mutagenesis.

The primers were designed to hybridize to either side of the deletion region as shown in the left plasmid. PCR was performed to form a linearized fragment missing the deleted part and this fragment was phosphorylated by T4 polynucleotide kinase (PNK) prior to recircularization by performing ligation using T4 ligase.

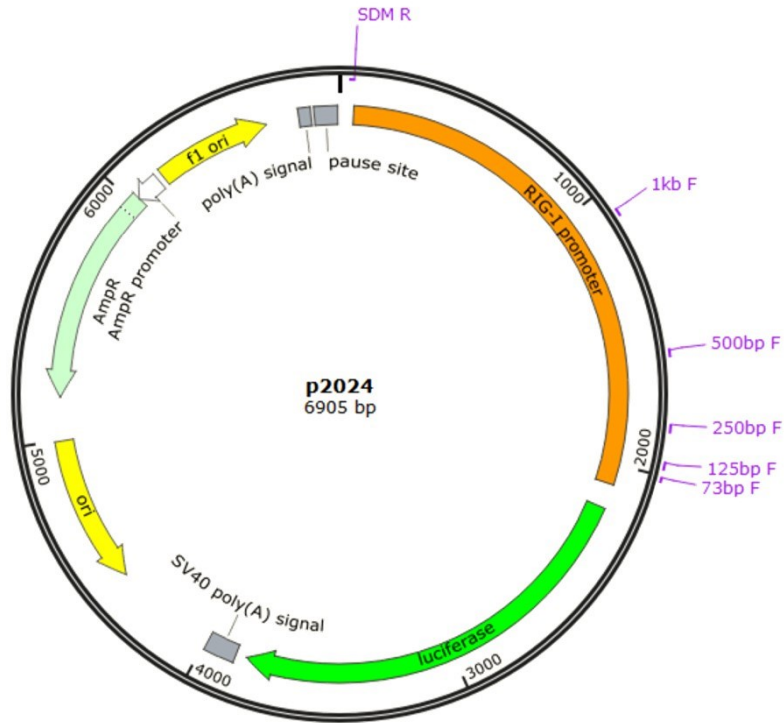
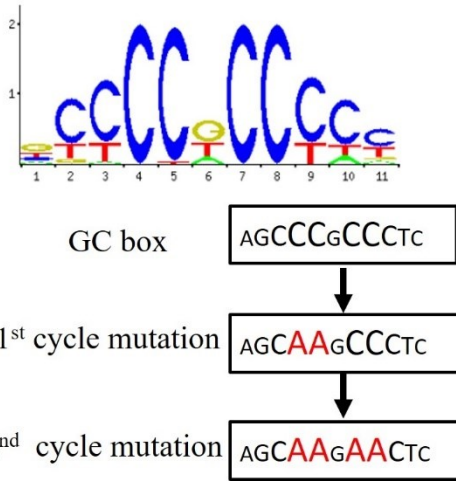


Figure 2.3 The schematic of the primer binding sites in the full-length RIG-I promoter vector.

The sequence of primers used to make serial deletion mutated RIG-I promoter vectors can be found in Table 2.1. The reverse primer, SDM R, and each forward primer indicated in the image were combined to make serial deletion mutants (p1000, p500, p250, p125 and p73). “SDM R” is short for serial deletion mutation reverse primer. “F” is short for the forward primer.

A Sp1/Sp2 binding site (ID: MA0079.3)



B IRF-1 binding site (ID: MA0050.2)

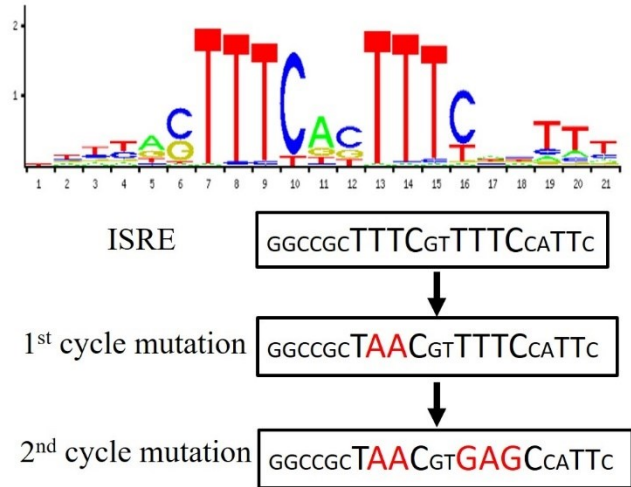


Figure 2.4 The point mutations in the RIG-I core promoter region.

The binding site sequences with ID in JASPAR database, the predicted binding sequences in the core promoter region of duck RIG-I (GC box and ISRE), and the mutated nucleotides in the 1st and 2nd mutagenesis cycles of GC box and ISRE were shown in (A) and (B), respectively.

Chapter 3 Results-Part I: The Core Promoter Controls the Basal and Inducible Expression of Duck Retinoic Acid Inducible Gene-I (RIG-I)

Parts of this chapter are published (Xiao et al., 2018).

3.1 Rationale

We previously cloned duck RIG-I and showed that it is critically involved in innate immunity of ducks to influenza virus (Barber et al., 2010). We also showed that overexpressed duck RIG-I could functionally compensate for the lack of RIG-I in chicken cells and turn on interferon and interferon stimulated genes, and in turn, reduce the replication of both LPAI and HPAI (Barber et al., 2013). Duck RIG-I itself is highly induced by infection HPAI H5N1, presumably through the action of interferons produced during infection in a positive feedback loop. Overexpression of the N-terminal end of duck RIG-I 2CARD constitutively induces expression of an interferon reporter construct and downstream interferon-stimulated genes (Miranzo-Navarro and Magor, 2014). Together our work suggests that it might be worthwhile to make chickens transgenic for duck RIG-I to improve their ability to detect and respond to influenza infection. However, the expression of RIG-I must be strictly controlled, as an inappropriate production of inflammatory cytokines will lead to inflammation-related autoimmune diseases or failure in viral clearance. To serve as a pattern recognition receptor, RIG-I must be expressed in cells at a basal level and be highly induced during infection. Ducks and chickens diverged early in avian evolution (Hackett et al., 2008), so, it is not known whether the duck RIG-I promoter will function in chicken cells and whether appropriate basal and inducible expression can be achieved. Therefore, in this part, my aims are 1) to identify the duck RIG-I promoter and analyze its phylogenetic relationship 2) to characterize the basal and inducible activity of duck RIG-I promoter in chicken cells 3) to identify the core promoter via deletional analysis 4) to identify the essential *cis* elements required for basal and inducible expression within this core promoter 5) to determine whether chicken IRF factors can induce the duck RIG-I gene in chicken cells.

3.2 Results

3.2.1 The identification and cloning of the duck RIG-I promoter sequence

We aimed to identify and characterize the duck *DDX58* (RIG-I) promoter. As an initial approach, I tried to recover the promoter sequence from the predicted duck genome sequence in Ensembl. However, the 5' UTR and the first exon of duck RIG-I were missing in the genome sequence, which made the direct identification impossible. To identify the promoter sequence, several pairs of primers were designed to cover a part of the putative upstream promoter sequence and a part of the second or third exon of duck RIG-I. Finally, a fragment around 1.5 kb long was amplified

and sequenced. The sequencing result showed this fragment included the 5' UTR (19 bp), its upstream 1121 bp nucleotides, and its downstream 338 bp nucleotides consisting of the complete first exon (106 bp), the entire first intron (108 bp), and partial second exon (124 bp) (Figure 3.1A). Around 2 kb upstream of the start codon were taken as the full-length promoter sequence for study. Due to a rich GC region sitting in close proximity to the start codon of duck RIG-I, it was difficult to directly amplify the promoter region (-2024 to -1). To solve this problem, a more extended fragment ranging from -2024 to +63 was first amplified. Using the TOPO vector with this segment (from -2024 to +63) as the template, the full-length promoter sequence (from -2024 to -1) (including 5' UTR) was finally amplified and cloned into TOPO vector (Figure 3.1B). The identified promoter sequence has been submitted to Genbank (accession number: KY093012). Moreover, a predicted CpG island with 229 bp length was localized between -284 bp and -55 bp of the full-length duck RIG-I promoter by MethPrimer (<http://www.urogene.org/cgi-bin/methprimer/methprimer.cgi>) with the criteria of the island size over 100 and GC content over 50% (Figure 3.1C). In this project, the position of nucleotide “A” in the start codon was regarded as “+1” and the position of the most proximal upstream nucleotide in the promoter region was regarded as “-1” and one nucleotide further was “-2”, and so forth.

3.2.2 The alignment of the full-length promoter sequence of duck RIG-I with the published RIG-I genome sequence in Ensembl.

To verify the reliability of the above amplified 2024 bp segment taken as duck RIG-I promoter sequence, I did an alignment of this sequence with the predicted duck RIG-I genome sequence in Ensembl using the online Clustal Omega interface and the BoxShade server. It demonstrated that the amplified 2024 bp sequence was nearly the same as the predicted duck RIG-I genome sequence, except for the terminal region, which was close to and included 5' UTR region (Figure 3.2). In fact, this region was not well assembled in the predicted duck RIG-I genome sequence consisting of approximately 300 bp of unreadable nucleotides. Including this region, the overall percent identity between the identified RIG-I full-length promoter sequence and the published RIG-I genome sequence was still high, up to 96.51%, which indicated the above identified duck RIG-I promoter sequence was reliable.

3.2.3 Unlike RIG-I proteins, RIG-I promoters do not show an expected phylogenetic relationship.

To determine whether the evolutionary relationship of RIG-I promoters was consistent with that of the RIG-I proteins, we created phylogenetic trees to compare vertebrate RIG-I proteins and RIG-I promoters using MEGA7. RIG-I protein and promoter sequences were downloaded from the NCBI protein database and UCSC database, respectively. As expected, the mallard duck RIG-I amino acid sequence is closer in evolutionary distance to other bird RIG-I sequences than to mammalian proteins (Figure 3.3 A). In contrast, RIG-I promoters do not follow the expected phylogenetic relationship between different species. In fact, the mouse RIG-I promoter appears relatively closest to the duck RIG-I promoter compared to other species, albeit the bootstrap values are low (Figure 3.3B).

3.2.4 The duck RIG-I promoter is inducible by RIG-I signaling and poly (I:C).

To determine whether the amplified 2024 bp sequence upstream of the duck RIG-I gene has promoter activity this segment was inserted into the multiple cloning site (MCS) in the pGL3-basic vector to generate a promoter reporter vector, p2024. We transfected p2024 into chicken DF-1 cells and primary duck embryonic fibroblasts (DEF) and tested its promoter activity using the dual luciferase assay. The empty pGL3-basic vector was transfected as negative or background control. The inserted 2024 bp promoter sequence significantly increased the relative luciferase activity compared to the empty pGL3-basic vector in DF-1 chicken (Figure 3.4A), and DEF cells (Figure 3.4B), indicating that the inserted segment has promoter activity.

According to the previous reports, the activation of RIG-I or MDA5 induces type I IFN production, and these two molecules are ISGs, also being regulated by type I IFN (Kang et al., 2004; Kang et al., 2002; Su et al., 2007). Therefore, RIG-I induces type I IFN which induces RIG-I (an interferon stimulated gene) in a positive feedback loop. We previously showed that overexpression of the constitutively active N-terminal region of duck RIG-I, the two CARD domains (2CARD), can stimulate the MAVS signaling pathway and induce type I IFN and ISG upregulation in chicken DF-1 cells (Miranzo-Navarro and Magor, 2014). Hence, to determine whether the promoter activity of duck RIG-I is inducible by type-I IFN, we co-transfected RIG-I promoter vector (p2024) with or without duck RIG-I 2CARD. The relative activity of the RIG-I

promoter upon stimulation for 24 hours following transfection with RIG-I 2CARD was significantly higher than the p2024 promoter with GST in DF-1 cells (Figure 3.4C) and DEF (Figure 3.4D). Though chickens lack the RIG-I gene, they have MDA5 (Liniger et al., 2012), which can be effectively activated by longer RNA molecules (>2kb) such as HMW poly (I:C) (Kato et al., 2008). The relative luciferase activity of duck RIG-I promoter co-transfected with poly (I:C) is significantly increased compared to the p2024 RIG-I promoter alone (Figure 3.4E). As expected, the firefly luciferase activities remain unchanged for the pGL3-Basic control, either unstimulated or stimulated by co-transfection with 2CARD or poly (I:C). Stimulation with co-transfected 2CARD or poly (I:C) indirectly demonstrates that the duck RIG-I promoter is inducible by type-I IFN. Because the promoter activity in chicken DF-1 cells provided comparable results to primary duck cells, and transfection efficiency was much higher, further promoter analysis was performed in DF-1 cells.

3.2.5 The time frame of basic and inducible expression of duck RIG-I

To determine whether the timepoint post-transfection influenced the reporter activity, the RIG-I promoter reporter vector (p2024) was transfected into DF-1 cells with or without duck RIG-I 2CARD (stimulator). The relative luciferase activity was measured by Dual Luciferase Assay at three different time points (12h, 24h, and 48h) post-transfection. In this experiment, the empty pGL3-basic vector was used as negative control. The result showed that the basic promoter activity of duck RIG-I at 12 hours post-transfection was around 1.5 times of the activity in 24 hours and 48 hours, whereas, the strongest inducible promoter activity of duck RIG-I was obtained at 24 hours post-transfection (Figure 3.5). Based on the above results, we decided to set the time point at 24 hours post-transfection for subsequent experiments.

3.2.6 The core promoter of duck RIG-I is inducible.

To identify the core promoter and the essential elements for duck RIG-I inducible activity, we constructed a series of deletion mutants of the duck RIG-I promoter and transfected them into DF-1 cells (Figure 3.6A). At 24 hours post-transfection, we tested the relative promoter activity by dual luciferase assay. Compared with the full-length promoter p2024 and deletion mutants, p250 had the highest basal promoter activity, whereas p73, the most proximal region to the

translation start site, had the lowest activity (Figure 3.6A). Duck RIG-I appears to be a TATA-less promoter, however, a sequence at -121 (CCACACC) matches the mammalian initiator (INR) canonical sequence YYANWYY (Yang et al., 2007). Thus p250 includes the core promoter of duck RIG-I. Since several longer fragments had lower activity than the p250 fragment, some suppressive elements may be located between -250 bp and -2024 bp. Our deletion analysis confirms the recent prediction of the -301~+14 region as the core duck RIG-I promoter (Zhang et al., 2018).

To identify the location of elements responsible for interferon inducible promoter activity, we tested all constructs with co-transfected GST or GST-2CARD. All promoter constructs were inducible by RIG-I 2CARD except p73. Construct p125 had the highest inducible activity following transfection of RIG-I 2CARD in DF-1 cells (Figure 3.6B). This result suggests that the core promoter region contains all the necessary elements for the interferon inducible expression of duck RIG-I. Therefore, the core promoter lies between -250 bp and -1 and controls both basal and inducible expression.

3.2.7 Identification of putative transcription factor binding sites

To examine the core promoter sequence for transcription factor (TF) binding sites, we examined the proximal promoter sequence with the transcription factor search program, “JASPAR” (<http://jaspar.binf.ku.dk/>). There are 121 putative sites predicted with this setting in the core promoter sequence. Transcription factors NHLH1, Sp1, and Sp2 are predicted to bind between -125 bp and -250 bp, and two of them (Sp1 and Sp2) bind the same position in this region, which is identified as a GC-box. Additionally, other transcription factors (IRF1, STAT1:: STAT2, and IRF7) are predicted to bind to the same position between -125 bp and -73 bp, identifying an interferon-sensitive response element (ISRE) (Figure 3.7A).

To confirm the importance of these binding sites to the basal and inducible expression of duck RIG-I, we constructed promoter mutants with the NHLH1 binding site or GC-box deleted from the p250 promoter construct, and the ISRE deleted from p125, and finally, a control construct deleting a random sequence in p250 (Figure 3.7B). We transfected the mutant or wild-type promoter constructs into DF-1 cells. At 24 h post-transfection, we determined the relative

promoter activities by dual luciferase assay. Compared to the wild-type promoter vectors (p250 or p125), the deletion of the GC-box significantly decreased the basal promoter activity (Figure 3.7C). To identify the location of the interferon responsive element, the same promoter constructs were co-transfected with GST or GST-2CARD to stimulate MAVS signaling. Notably, the deletion of the putative ISRE resulted in the loss of inducible activity for p125. Because all other deletion constructs of p250 still bear the ISRE, their promoter activities could be induced by RIG-I 2CARD (Figure 3.7D). The comparison of wild-type and deletion constructs of the predicted GC-box and the ISRE suggests that these binding sites contribute to duck RIG-I basal and inducible expression, respectively.

To confirm that the GC-box controls constitutive expression, we created a promoter with a mutated version of the site GC-box in the p250 backbone. Mutation of the canonical GC-box BYYCCDCCYHY involved changing the key cytidines involved in binding to adenines, AGCAAGAACTC. We transfected DF-1 cells with the deleted or mutated constructs and showed that the GC-box is required for the basal transcription activity, which is also affected by the mutation or deletion of the ISRE (Figure 3.7E). To confirm that the putative ISRE is necessary for interferon induction, we transfected promoter constructs with deleted or mutant ISREs, together with GST or GST-2CARD. The canonical ISRE predicted by JASPAR as YYRSTTTTCDBTTTTYCNNTTT was mutated to GGCCGCTAACGTGAGCCATTC to alter the key nucleotides involved in binding. The inducible promoter activity of duck RIG-I is lost with deletion or mutation of the ISRE (Figure 3.7F).

3.2.8 Neither IRF1 nor IRF7 was upregulated at the transcriptional level by the stimulation by RIG-I 2CARD.

To determine whether IRF1 and IRF7 transcripts are upregulated in RIG-I 2CARD stimulated DF-1 cells, the mRNA levels in RIG-I 2CARD stimulated and untreated DF-1 cells transfected with the p2024 promoter construct were measured using qPCR. The mRNA transcript level of the housekeeping gene (GAPDH) was used as the internal reference for normalization. IFN- β and Mx1 were measured as indicators of activation of these cells. Compared to RIG-I 2CARD untreated group, the mRNA level of IFN- β and Mx1 in RIG-I 2CARD treated group was upregulated by 1.67 and 17.1 times, respectively (Figure 3.8A). Whereas, the transcript for IRF1

and IRF7 were induced 1.12 and 0.96 times in comparison to the untreated cells (Figure 3.8B), which indicated neither IRF1 nor IRF7 were significantly upregulated at the transcriptional level by the stimulation of RIG-I 2CARD. However, it is not necessary to increase the expression level for transcription factors to regulate gene transcription. In fact, upon phosphorylation, TFs are activated and translocated from cytoplasm to the nucleus to perform their function of regulating gene transcription. Thus, despite no observed upregulation, these transcription factors may be responsible for duck RIG-I inducible expression.

3.2.9 Chicken IRF7 induces promoter activity of duck RIG-I in DF-1 cells.

To determine whether chicken IRF factors can induce the duck RIG-I gene in chicken cells, we cloned and generated mCherry constructs for chicken IRF1 (pmCherry-chIRF1), chicken IRF7 (pmCherry-chIRF7), duck IRF1 (pmCherry-dIRF1) and mCherry (vector only). We expressed these constructs in DF-1 cells to confirm their expression by fluorescence (Figure. 3.9A). All constructs were expressed, and staining was evident in both cytoplasm and nucleus. To determine which IRFs could drive expression of duck RIG-I, we overexpressed each mCherry tagged protein in DF-1 cells with the RIG-I promoter constructs to determine whether the promoter activity of duck RIG-I is upregulated. Surprisingly, the overexpression of chIRF1 did not induce RIG-I promoter activity. However, overexpression of either chIRF7 or dIRF1 significantly induced duck RIG-I promoter activity (Figure 3.9B). Interestingly, duck IRF1, but not chicken IRF1 or IRF7, induced p73, which was not inducible by factors present in chicken cells.

To confirm that chIRF7 activates using the putative ISRE in the promoter, we transfected wild-type p125 or the construct with deletion of the ISRE on the p125 backbone together with cells overexpressing pmCherry, pmCherry-chIRF7 or pmCherry-dIRF1. The deletion of the ISRE affects the induction by chIRF7, but not the induction by dIRF1 (Figure 3.9C). Therefore, the chIRF7 induces through the putative ISRE, while the duck IRF1 binds a different site within the p73 promoter region, which was not investigated further. Here we show that overexpressed chicken IRF7 activates the duck RIG-I promoter, and this requires a predicted ISRE located near -104 to -90. Thus, duck RIG-I is upregulated downstream of RIG-I signaling by IRF7.

3.3 Summary

To summarize, we identified and analyzed the duck RIG-I promoter sequence. It showed that RIG-I promoters were very poorly conserved and their similarity did not reflect the phylogenetic relationship of vertebrate species. Subsequently, we showed that the promoter activity of duck RIG-I was interferon-inducible downstream of MAVS signaling. Using serial deletion mutants, we demonstrated that the core promoter was within the proximal 250 nucleotides and retained the ability to respond to MAVS signaling. We also identified the essential *cis* elements required for the basal and inducible expression within the core promoter region. The constitutive expression requires both GC-box and ISRE, and the inducible expression requires the ISRE only. Finally, we showed that chicken IRF7 induced the duck RIG-I promoter, and this required the putative ISRE.

3.4 Discussion

Generally, 2 kb of nucleotides upstream of the transcription start site (TSS) is considered to be the full length promoter. TSS is the location where transcription starts at the 5'-end of a gene sequence, alternatively, it is the beginning of 5'-UTR. Comparing the 5'-UTR of duck RIG-I to that of human and mouse RIG-I, it is much shorter, only 19 bp nucleotides. However, the 5'-UTR of human and mouse RIG-I are 158 bp and 129 bp, respectively. In case the online released 5'-UTR of duck RIG-I is not complete, I took 2005 bp upstream of and 19 bp 5'-UTR as the full length of duck RIG-I promoter to study in this project.

The promoters of RIG-I are very poorly conserved, and their similarity does not reflect the phylogenetic relationship of vertebrate species. Poor conservation between human and mouse RIG-I promoters was noted before (Hayakari et al., 2016). This result differs from the phylogenetic analysis of MDA5 promoters, which closely followed the taxonomic relationship among different vertebrates (Zhang et al., 2016), despite RIG-I and MDA5 are in the same PRR family and their structure and function are related. Promoters of immune genes are particularly poorly conserved between orthologues in different species, as are the proteins encoded by the immune genes themselves (Chiba et al., 2008). Enhancers and promoters of immune genes may, nonetheless, conserve function, as does the immunoglobulin heavy chain gene enhancer of fish which differs greatly from mammals (Magor et al., 1994).

In this study, the promoter activity of duck RIG-I was induced by overexpression of 2CARD. The ISRE was responsible for the inducible promoter activity of duck RIG-I. IRF1 and IRF7 were predicted to bind to this element. Additionally, IRF1 and IRF3 were reported to induce the expression of human RIG-I. However, chicken is lack of IRF3. IRF7 is functionally similar to IRF3. Hence, here, I examined whether chIRF7 and chIRF1 transcripts were upregulated in RIG-I 2CARD stimulated DF-1 cells. Unexpectedly, the mRNA levels of both chIRF1 and chIRF7 did not change after adding GST-2CARD expression plasmid. However, the mRNA levels of Mx1 and IFN- β were increased, indicating the MAVS signaling pathway was activated by overexpression of RIG-I 2CARD. Even though the expression level does not change, the transcription factors can perform their functions as long as they were phosphorylated and translocated into nucleus. Therefore, in order to test the activation of transcription factors, we can do Western blot to detect phosphorylated transcription factors, using anti-phosphorylation antibodies, such as anti-phospho-chIRF1 and anti-phospho-chIRF7 antibodies, or look at their translocation after adding RIG-I 2CARD using confocal microscopy. However, the commercial phospho specific antibodies to chicken IRFs are not available. The regular IRF1 antibody, which was supposed to work in chicken, did not work either. Therefore, finally, I constructed mCherry tagged chIRF1 and chIRF7 expression vectors to study their induction of the promoter activity of duck RIG-I.

In this study, I used duck RIG-I 2CARD as the inducer of duck RIG-I promoter. Actually, chicken IFN- β should be a better choice to induce duck RIG-I promoter activity, as human IFN- β did in human RIG-I promoter study (Su et al., 2007).

C

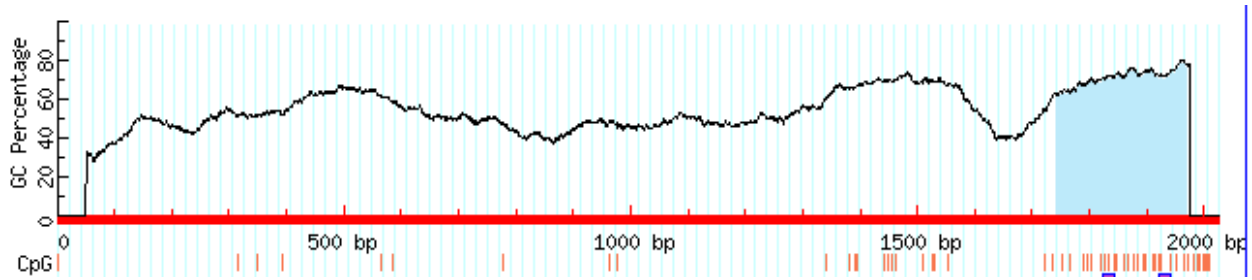


Figure 3.1 The nucleotide sequences of the amplified fragments and CpG island prediction

The amplified segments were sequenced using standard Sanger sequence on ABI 3730. (A) The first amplified fragment of approximately 1.5 kb length was composed of 1121 bp promoter sequence, 19 bp 5' UTR, 106 bp exon1, 108 bp intron 1, and 124 bp partial exon 2. (B) The full-length sequence of duck RIG-I promoter (2024 bp), including 5' UTR. Yellow, green, gray, and purple colors highlight the sequences of 5' UTR, the first exon, the first intron, and partial second exon, respectively. (C) A CpG island highlighted with light blue color was predicted between -284 bp and -55 bp of duck RIG-I promoter by MethPrimer (<http://www.urogene.org/cgi-bin/methprimer/methprimer.cgi>).

promoter 1 AGCTGATGACCTGCAAAAAGTTGGACATGCAAAATTTAAAGCTGAGGAACACAACACTACAC
 Ensembl- 1 AGCTGATGACCTGCAAAAAGTTGGACATGCAAAATTTAAAGCTGAGGAACACAACACTACAC

 promoter 61 ACTATGCTCTGAAAAAGAAAAAATAATAATAACAATCAAGAAAAGCATTATTCCACCA
 Ensembl- 61 ACTATGCTCTGAAAAAGAAAAAATAATAATAACAATCAAGAAAAGCATTATTCCACCA

 promoter 121 GCTGGACCACACTCTCTAAGGCAGGACTTGGTGGGTACACAGGGACCCTTCCAGACAGC
 Ensembl- 121 GCTGGACCACACTCTCTAAGGCAGGACTTGGTGGGTACACAGGGACCCTTCCAGACAGC

 promoter 181 CACAAGTGATTTTGGGAAAAAGTAACATATTTCCCTACACCCTTGCCCTAGAAAGTTCTCCA
 Ensembl- 181 CACAAGTGATTTTGGGAAAAAGTAACATATTTCCCTACACCCTTGCCCTAGAAAGTTCTCCA

 promoter 241 GAAAACCTGCTCAGCACCATGGTTTGCAGTAGCACAAGCAGGTTAAGGTCTTCCCAGTGT
 Ensembl- 241 GAAAACCTGCTCAGCACCATGGTTTGCAGTAGCACAAGCAGGTTAAGGTCTTCCCAGTGT

 promoter 301 GCAGCTTCTCTCACCCGATGTGCTTGGCCACTGCAACCCACAG-----
 Ensembl- 301 GCAGCTTCTCTCACCCGATGTGCTTGGCCACTGCAACCCACAGATACNNNNNNNNNNNN

 promoter 346 -TTACGATGTAGCAATAAAAACAGCCACTGAGGATATGAGCATGAGATACCGCACAGGCCAC
 Ensembl- 361 NNNNCGATGTAGCAATAAAAACAGCCACTGAGGATATGAGCATGAGATACCGCACAGGCCAC

 promoter 405 AACCCATCCCCTGCAACCACTGCCCTGCACCAACAAGCCTGGGAGAGCCTCCTGTGCTC
 Ensembl- 421 AACCCATCCCCTGCAACCACTGCCCTGCACCAACAAGCCTGGGAGAGCCTCCTGTGCTC

 promoter 465 ACCAGGTGCATCTCCAGCCTGGTGGGACTGATCCCTGCTGCCCTCAGTACCCCTCCTGCA
 Ensembl- 481 ACCAGGTGCATCTCCAGCCTGGTGGGACTGATCCCTGCTGCCCTCAGTACCCCTCCTGCA

 promoter 525 GCCACCCTGCCAGCAGGTGCATCCACCTCCTGCATGCACGATCAGAGGTGCTATTCCC
 Ensembl- 541 GCCACCCTGCCAGCAGGTGCATCCACCTCCTGCATGCACGATCAGAGGTGCTATTCCC

 promoter 585 CCGTGCCTCCAGTCCAGCTTTGTTGAAGAGCAGCAGGTCCACTTCACTGGGCAGATTG
 Ensembl- 601 CCGTGCCTCCAGTCCAGCTTTGTTGAAGAGCAGCAGGTCCACTTCACTGGGCAGATTG

 promoter 645 ACTTCTCCATCTAGGGCTGGAGAAGCAGCAAGCAAGGAGTTGATTTCCCTCCTCTCTCA
 Ensembl- 661 ACTTCTCCATCTAGGGCTGGAGAAGCAGCAAGCAAGGAGTTGATTTCCCTCCTCTCTCA

 promoter 705 GGTGAAGGACAAGACTGGGTTTCTGCTTGGCAGAGCAATTGCAACCCACCCTCAGCACTG
 Ensembl- 721 GGTGAAGGACAAGACTGGGTTTCTGCTTGGCAGAGCAATTGCAACCCACCCTCAGCACTG

 promoter 765 ATCTTTGAATCTTCGAACACTCTGTCTGTGAGGAGCAGAACCTGAGTGCTAATATCACTC
 Ensembl- 781 ATCTTTGAATCTTCGAACACTCTGTCTGTGAGGAGCAGAACCTGAGTGCTAATATCACTC

 promoter 825 ATTACTGAATGAAAGCTGTAATAGGCATTTCTCAAGTGAAATAGGCTCAACAGGCACTA
 Ensembl- 841 ATTACTGAATGAAAGCTGTAATAGGCATTTCTCAAGTGAAATAGGCTCAACAGGCACTA

 promoter 885 CCAAGTAAAAATGCCTCTCTGCTATGTTTGTACCTGTCAGGCTAATCACCATGCTCTAC
 Ensembl- 901 CCAAGTAAAAATGCCTCTCTGCTATGTTTGTACCTGTCAGGCTAATCACCATGCTCTAC

promoter 945 **AGGGTGTGTGGGCAACTCACGTAGGGGCTAACGCTTCTTCCTTGTACTCACAGCAA**

Ensembl- 961 **AGGGTGTGTGGGCAACTCACGTAGGGGCTAACGCTTCTTCCTTGTACTCACAGCAA**

promoter 1005 **TTAAGCCCTAAGAGATTACCTTACTGAAAATGCAGGGTGGAGAGATGACTGACAGGGGCT**

Ensembl- 1021 **TTAAGCCCTAAGAGATTACCTTACTGAAAATGCAGGGTGGAGAGATGACTGACAGGGGCT**

promoter 1065 **TGTTACCTGCCCCTTTTCTTGCTGCAGAAGATGTCTCTCTCAGTTGTTTCAGCATTCCCC**

Ensembl- 1081 **TGTTACCTGCCCCTTTTCTTGCTGCAGAAGATGTCTCTCTCAGTTGTTTCAGCATTCCCC**

promoter 1125 **AGTCTAGCAGTGGATAGCCTTTCTGTGTCTTGGTCAGCTGTGCATGATATTTCTCTGGTC**

Ensembl- 1141 **AGTCTAGCAGTGGATAGCCTTTCTGTGTCTTGGTCAGCTGTGCATGATATTTCTCTGGTC**

promoter 1185 **CTTCTCATTGCTCTGGTTAAGCTAACAGCCCAAATGCAAGTCTCTCCTAGCCTAGGGCCA**

Ensembl- 1201 **CTTCTCATTGCTCTGGTTAAGCTAACAGCCCAAATGCAAGTCTCTCCTAGCCTAGGGCCA**

promoter 1245 **TTTGTAGCCTAGGGCAACAGCAGCTGGGAGAGAGTGAGAAAATGTGAGAGAACCTTACAT**

Ensembl- 1261 **TTTGTAGCCTAGGGCAACAGCAGCTGGGAGAGAGTGAGAAAATGTGAGAGAACCTTACAT**

promoter 1305 **TTGGGATCTTTGGGGAGCTGCTGCCCATGGGGACCCGTGCTGGAGCAGTTTGCTCCTGG**

Ensembl- 1321 **TTGGGATCTTTGGGGAGCTGCTGCCCATGGGGACCCGTGCTGGAGCAGTTTGCTCCTGG**

promoter 1365 **GGGATGGATGGATGGACCCCGTGGGACGGAGCCGTGTGGGAGCAGTGTGTAAGAGCTGC**

Ensembl- 1381 **GGGATGGATGGATGGACCCCGTGGGACGGAGCCGTGTGGGAGCAGTGTGTAAGAGCTGC**

promoter 1425 **TGCCTGTGGGCAGCCCCCGGGATCGGTTCCGGGAAGGACGGCATCCCTGGGAGGGACCC**

Ensembl- 1441 **TGCCTGTGGGCAGCCCCCGGGATCGGTTCCGGGAAGGACGGCATCCCTGGGAGGGACCC**

promoter 1485 **CATGGGAGCAGGGGCAGAGAGGGACCCGTGAGGGAGAGGGAGCGCGGAGACAAAGTGCC**

Ensembl- 1501 **CATGGGAGCAGGGGCAGAGAGGGACCCGTGAGGGAGAGGGAGCGCGGAGACAAAGTGCC**

promoter 1545 **AGGGACTGACCGACGCCCCATTCCCCTGCACTGCCTGGGGGGAGAGGTAGAGGAGGG**

Ensembl- 1561 **AGGGACTGACCGACGCCCCATTCCCCTGCACTGCCTGGGG-GGAAGAGGTAGAGGAGGG**

promoter 1605 **TGGATGGTGGGGAAGGTGTTTTTCATTTCCCTTTTATTTTTTCTCACTGCTAGTCTGTTAG**

Ensembl- 1620 **TGGATGGTGGGGAAGGTGTTTTTCATTTCCCTTTTATTTTTTCTCACTGCTAGTCTGTTAG**

promoter 1665 **TGATAGGCAATTAATTCTATTCTCCCCATCCTTGTGCCAACCCCTGAGCCCTTTCCATCG**

Ensembl- 1680 **TGATAGGCAATTAATTCTATTCTCCCCATCCTTGTGCCAACCCCTGAGCCCTTTCCATCG**

promoter 1725 **CATTTTCTCCCCGTTTCCCTTTGAGGAGGCGGAGTGGAGAGCGGCTGTGCTGGA**

Ensembl- 1740 **CATTTTCTCCCCGTTTCCCTTTGAGGAGGCGGAGTGGAGAGCGGCTGTGCTGGA**

promoter 1785 **GGCCCGGTGCTCGGTGTCCCGGTGAGGCTGTGTTGGTGGCGATCCAGGCTCACGAAGCTGC**

Ensembl- 1800 **GC-----TGCCACTCCAGC-----GCAACCAGACA-----**

promoter 1845 **GAGCCGCTGCCTATGCCCTCTGGCGGCCAGAGGCCGGCTGCGGATGGGGCCGCGATCTC**

Ensembl- 1827 **-----CAGGCCTCTAGTT--CCCAAGTCACT-----**

```

promoter 1905 CACACCCCGGGGGCCGCTTTCGTTTCCATTCCCGCGGGCCTCGCTGCCTTCTGT
Ensembl- 1852 -----cctccggccc-----ttct--

promoter 1965 GCCGAGCCGCTTGCGGGCCGGCCGGCCGGCGCCGGCGCGGCCGAGAGCCAGCC
Ensembl- 1866 -----TGTAGTTGGGGTCTCCATTTCCTAGCC-----GCCCTCAGCTGCNNNNNNNN

```

Figure 3.2 The alignment of the identified full-length promoter sequence of duck RIG-I with the published duck RIG-I genome sequence in Ensembl.

The alignment was run using the online Clustal Omega interface and modified in the BoxShade server. The overall percent identity between the identified full-length duck RIG-I promoter sequence and the published RIG-I genome sequence is 96.51%. The yellow color highlights the region of 5' UTR.

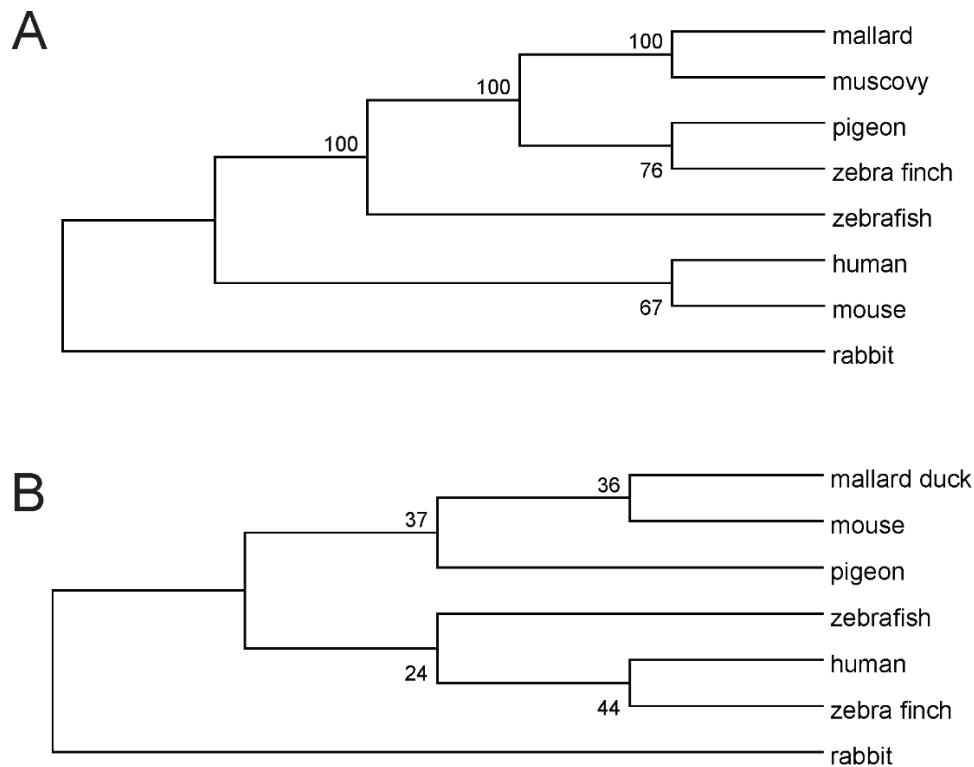


Figure 3.3 Phylogenetic analysis of RIG-I proteins and *DDX58* promoters.

(A) A consensus tree of RIG-I proteins was generated by MEGA7 with bootstrap analysis (Neighbor-Joining method, 1000 replicates, Poisson model). Branches corresponding to partitions reproduced in less than 50% bootstrap replicates are collapsed. There was a total of 224 positions in the final dataset. Protein sequences used include human NP_055129.2, mouse NP_766277.3, mallard duck NP_001297309.1, Muscovy duck AGX27431.1, pigeon AKR15098.1, zebrafish NP_001293024.1, zebra finch XP_012432982.1 and rabbit XP_002708086.1. (B) A consensus tree of RIG-I promoters was generated as above (Neighbor-Joining method, 1000 replicates, Maximum Composite Likelihood model). There were a total of 497 positions in the final dataset. RIG-I promoters have the following accession numbers; human AL353671.6, mouse AL831793.4, mallard duck KY093012, pigeon 102098789, zebrafish NM_001306095, zebra finch NM_001311190, and rabbit ENSOCUG00000004710.

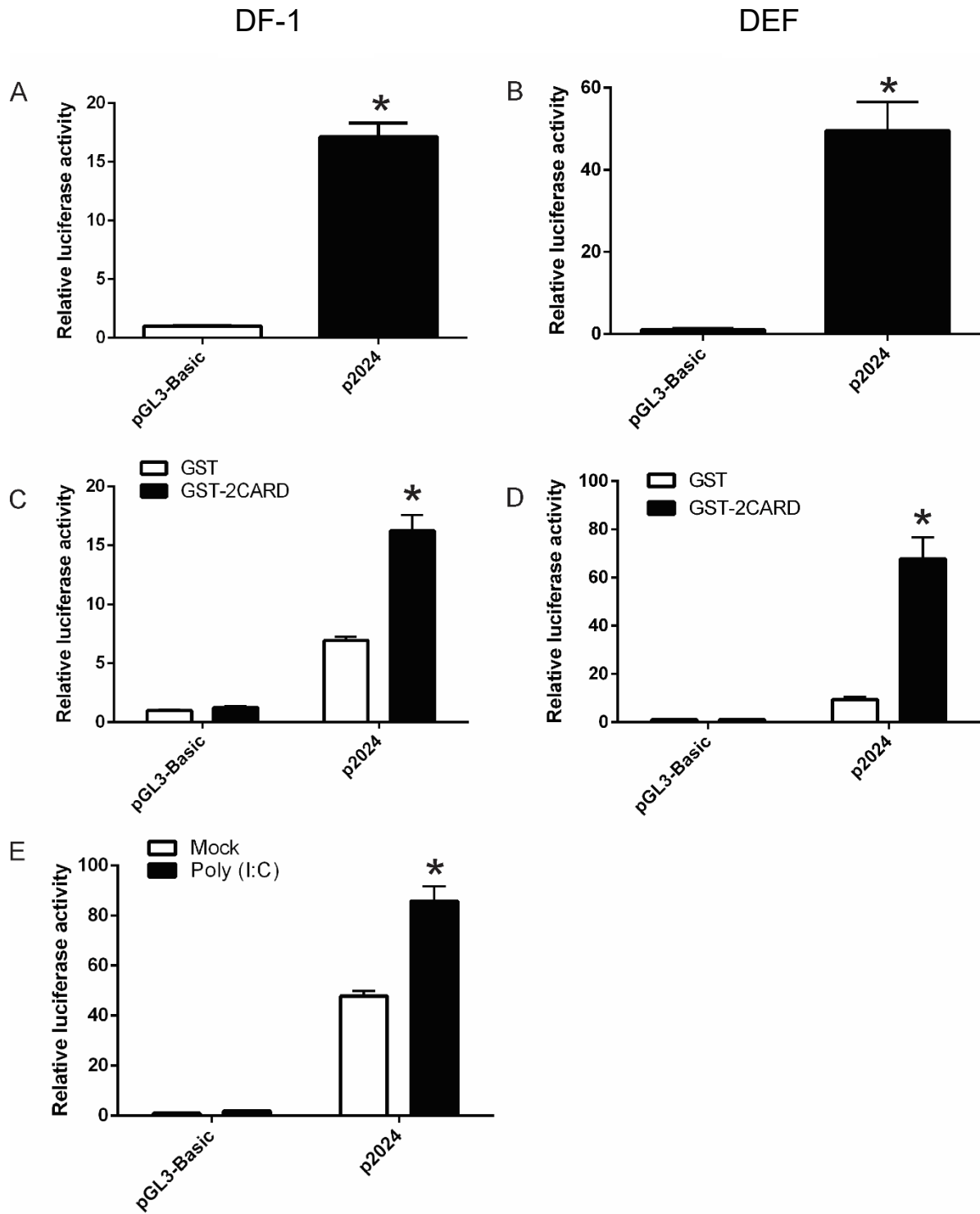


Figure 3.4 The duck RIG-I promoter activity is induced by MAVS signaling downstream of RIG-I 2CARD or poly (I:C) stimulation.

The promoter activity of the 2024 bp upstream of the *DDX58* gene was investigated in comparison to the pGL3-Basic vector in (A) chicken DF-1 cells and (B) primary DEF. Promoter activity was measured using the dual luciferase assay with firefly luciferase activity normalized to *Renilla* luciferase activity. RIG-I promoter activity is induced by MAVS signaling downstream of RIG-I 2CARD, the constitutively active N-terminal fragment of RIG-I. Promoter activity was determined by luciferase assay at 24 h post-transfection in (C) DF-1 cells and (D) DEF. Co-transfections were carried out with pGL3-Basic or RIG-I promoter reporter p2024 with either pcDNA3.1 expressing GST (control) or GST-2CARD (stimulator). (E) Promoter activity is induced by poly (I:C) stimulation. DF-1 cells were transfected with pGL3-Basic or p2024 and 18 h post-transfection they were treated with or without 2 µg/ml poly (I:C) for 6 hours before measuring the relative luciferase activity. The mean of triplicate determinations (\pm SD) was shown, and significance was analyzed with Student's t-test (* $p < 0.05$). Each experiment was repeated at least twice.

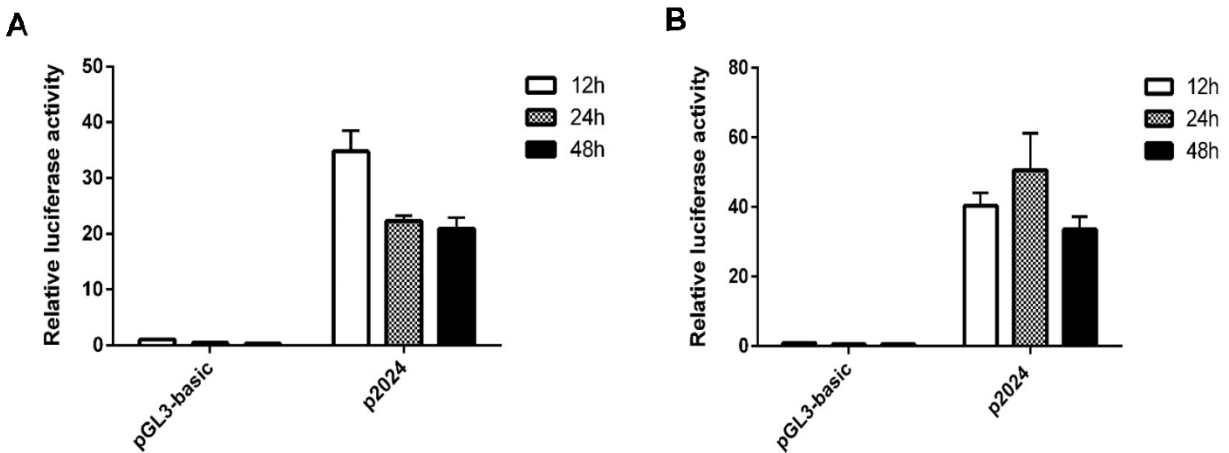


Figure 3.5 RIG-I promoter activity at different time points post-transfection.

(A) The promoter activity of the 2024bp upstream of the *DDX58* gene was investigated in DF-1 cells at the indicated time points post-transfection. (B) DF-1 cells were co-transfected with pGL3-Basic or RIG-I promoter reporter p2024 with GST-2CARD (stimulator). The induction of the RIG-I promoter by 2CARD was determined by dual luciferase assay at the indicated time points post-transfection. These experiments were done only once.

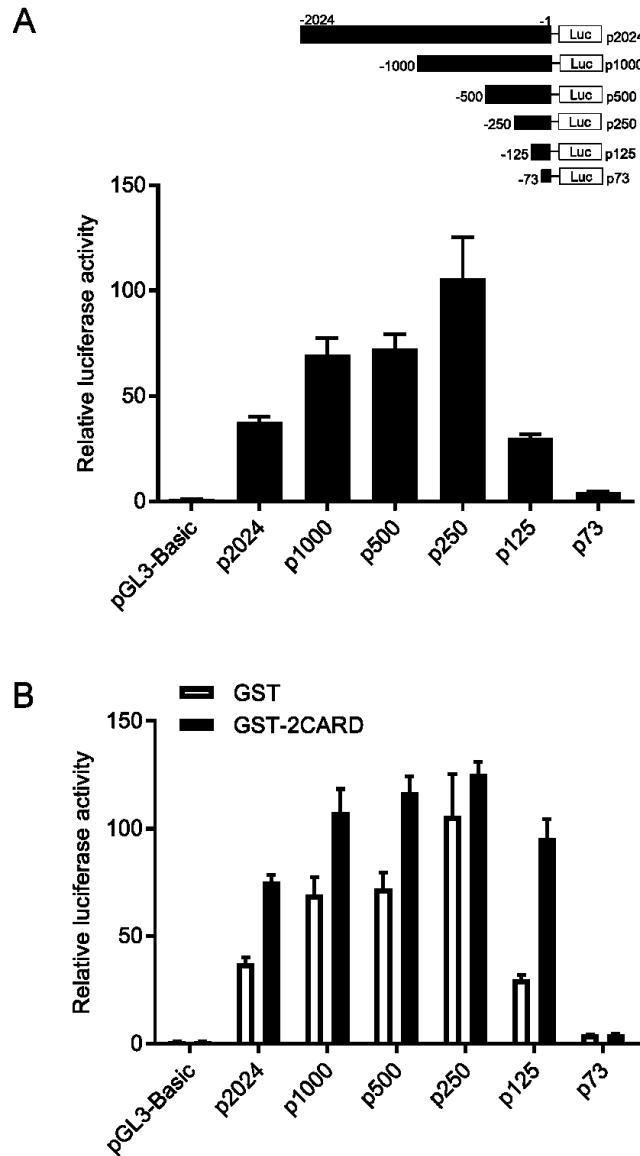


Figure 3.6 The region between -250 and -73 confers basal and IFN- β inducible activity of the duck RIG-I promoter.

(A) Serial deletion constructs were generated from the RIG-I promoter p2024. The serial deletion constructs of the duck RIG-I promoter were individually transfected into DF-1 cells with the *Renilla* luciferase vector. (B) The serial deletion constructs of the duck RIG-I promoter were co-transfected into DF-1 cells with GST (control) or GST-2CARD (stimulator) to assess induction by IFN- β downstream of MAVS signaling. For both experiments, the relative luciferase activities were determined at 24 hours post-transfection, and the data from triplicate determinations was expressed as mean (\pm SD).

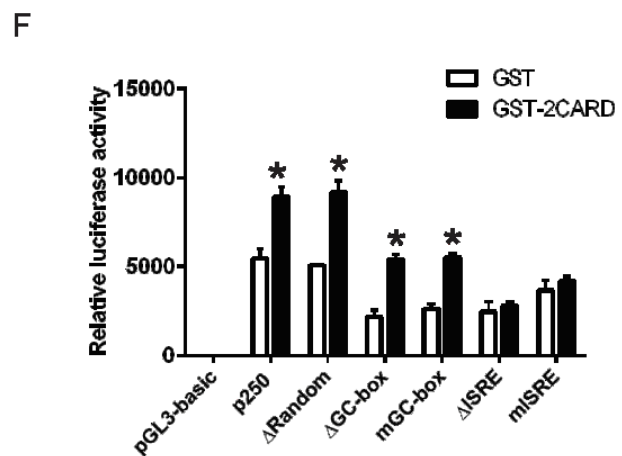
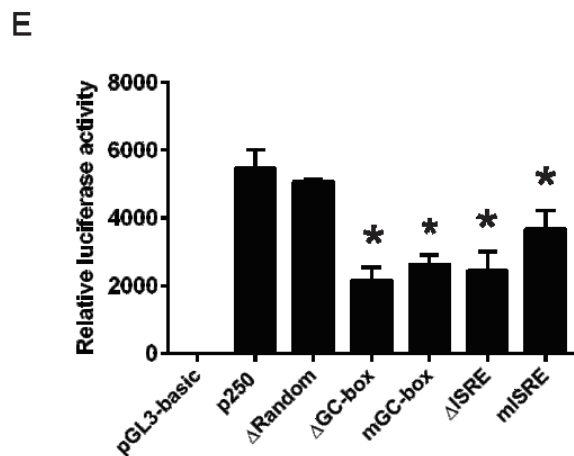
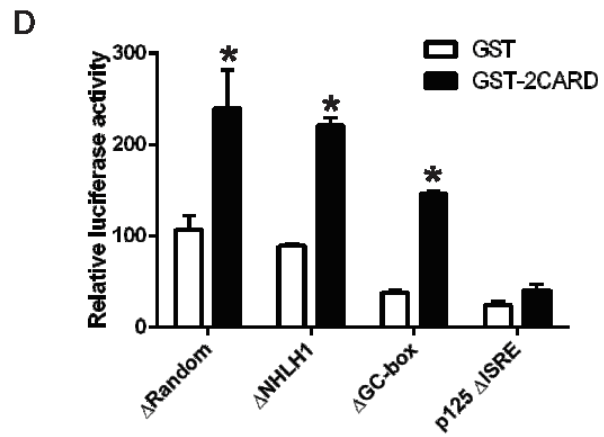
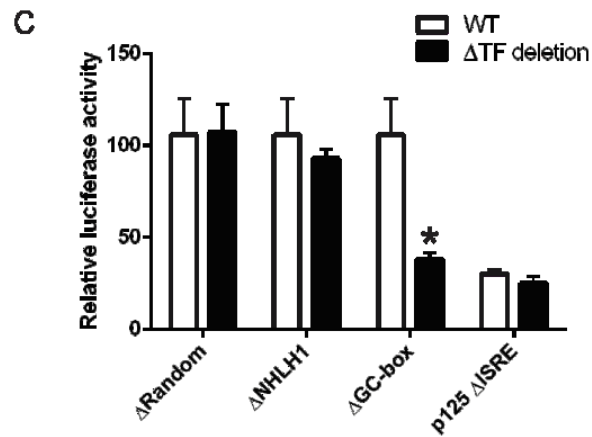
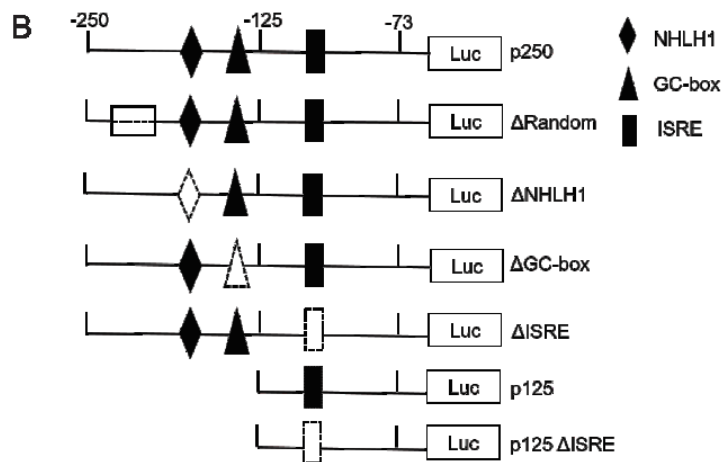


Figure 3.7 Deletion of the GC-box and ISRE *cis* elements decreased the basal and inducible RIG-I promoter activity, respectively.

(A) The putative transcription factor (TF) binding sites in the core promoter of duck RIG-I predicted by JASPAR are indicated by underlining or overlining. Nucleotides deleted are indicated in grey shading. The box indicates the location of a random deletion used as the control. (B) Schematic diagram illustrates the core promoter region with TF binding sites indicated and the deletion constructs created. (C) DF-1 cells were transfected with the wild-type promoter (p250 or p125) or promoter constructs with deletions of *cis* elements to test the influence of the predicted TF binding sites on the basal promoter activity. (D) DF-1 cells were co-transfected with the promoter constructs or element deletion reporter vectors with GST (control) or GST-2CARD (stimulator) to assess which predicted TF binding sites affect the inducible promoter activity. (E) DF-1 cells were transfected with the promoter construct p250 or deletions generated on this backbone, or mutated GC-box or ISRE. Mutation of the wild-type GC-box AGCCCGCCCTC to AGCAAGAACTC, and ISRE GGCCGCTTTCGTTTTCCATTC to GGCCGCTAACGTGAGCCATTC. (F) DF-1 cells were transfected with p250 or promoter mutants with GST or GST-2CARD. For all experiments, firefly luciferase activities were normalized to *Renilla* activity at 24 h post-transfection. The mean of triplicate determinations (\pm SD) of relative luciferase activity is shown, and each experiment was repeated at least twice. Significance was analyzed with Student's t-test (* $p < 0.05$).

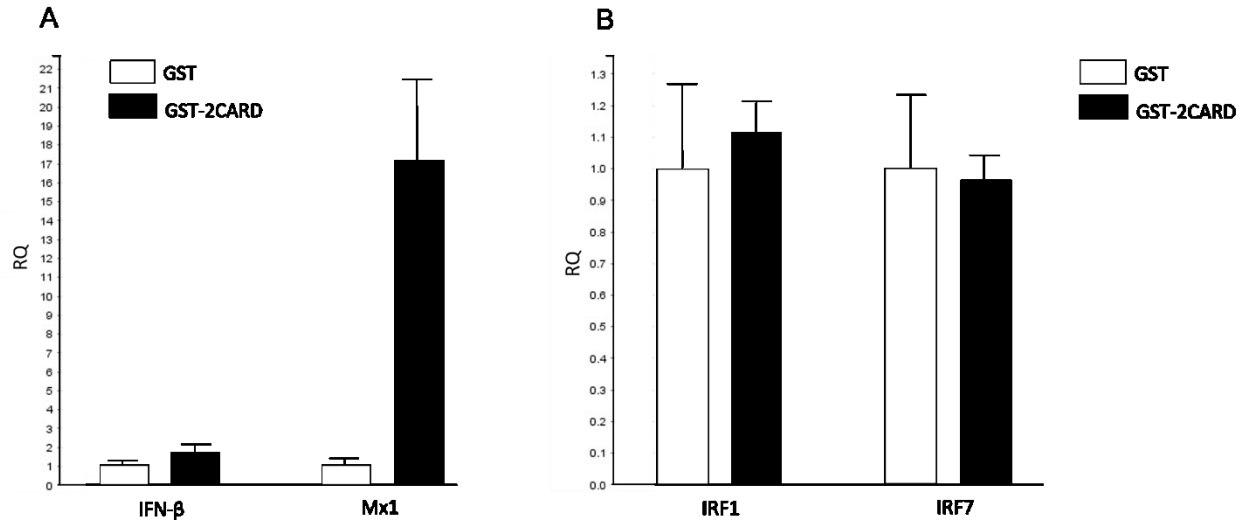


Figure 3.8 Neither IRF1 nor IRF7 was upregulated at the transcriptional level by the stimulation of RIG-I 2CARD.

DF-1 cells were co-transfected with p2024 and GST only (as the negative control) or p2024 and GST-conjugated RIG-I 2CARD (as the stimulator). 24 hours post transfection, the mRNA levels of chicken IFN-β and Mx1 (A) or IRF1 and IRF7 (B) were quantitatively analyzed using TaqMan Realtime-PCR. The experiment was done only once.

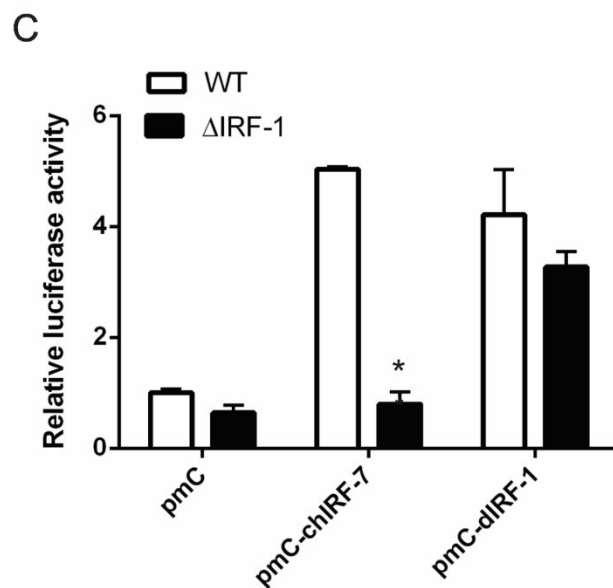
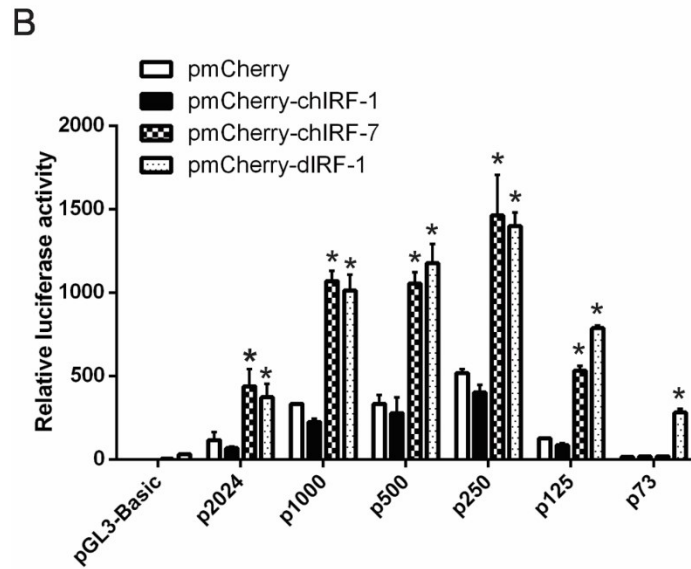
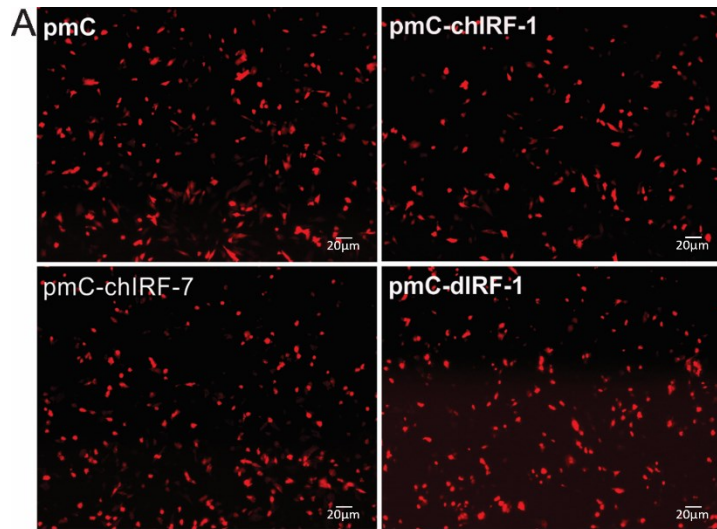


Figure 3.9 Chicken IRF7 and duck IRF1 induce RIG-I promoter activity.

(A) The expression of mCherry control, or mCherry-tagged interferon regulatory factors in DF-1 cells. (B) DF-1 cells were transfected with p250 or the serial deletion constructs of the duck RIG-I promoter and pmCherry (control) or overexpressed pmCherry-IRFs. (C) DF-1 cells were transfected with p125 or p125 with ISRE deleted and pmCherry or chIRF7 or dIRF1. For both experiments, the relative luciferase activities were tested at 24 h post-transfection and the mean of triplicate determinations (\pm SD) is shown and significance was analyzed with Student's *t*-test (* $p < 0.05$). Each experiment was repeated at least twice.

Chapter 4 Results-Part II: Duck MAVS Signaling and Inhibition by PB1-F2

4.1 Rationale

Duck RIG-I is highly induced by influenza infection in ducks. The transfected duck RIG-I could also sense the transcribed 5'ppp RNA and influenza infection and stimulate the production of IFN- β and some key ISGs in naturally RIG-I-deficient chicken cells (Barber et al., 2010). However, the molecular mechanism by which duck RIG-I works in an avian system has not been fully characterized. In mammals, MAVS is the critical adaptor protein to activate the downstream immune factors of RIG-I/MDA5 mediated signaling pathway via interacting with their 2CARD domains (Kawai et al., 2005). RIG-I is absent in chicken, but MDA5 and MAVS are present and functionally conserved (Liniger et al., 2012). Thus, duck RIG-I appears able to interact with both duck and chicken MAVS proteins. It has been recently shown that the RIG-I: MAVS interacting surfaces are not highly conserved between humans and ducks, but the tandem T175K/T176E mutations on duck RIG-I permit interaction with human MAVS in HEK293T cells (Wu et al., 2014). The molecular interactions of duck MAVS in avian cells should also be systematically studied.

Furthermore, it is known that many viruses employ mechanisms to inhibit innate immune signaling via protein-protein interactions with or around the MAVS protein in mammals. The influenza PB2 protein is reported to block interferon by interacting with human MAVS (Graef et al., 2010). Similarly, PB1-F2 from influenza strain PR8 (H1N1) interacts with MAVS in human cells to inhibit interferon production (Varga et al., 2012). Given the apparent strain-specific and species-specific nature of the various PB1-F2 interactions discussed above. I was interested to examine whether PR8 PB1-F2 can interact with duck MAVS as it does with the human MAVS. My colleague, Ximena Fleming, first identified and cloned duck MAVS out of the genome. **I began phylogenetic and functional characterization of duck MAVS, and the examination of its potential interaction with PR8 PB1-F2 and its consequences for type I IFN production in avian cells.**

Four aims were generated in this part:

Aim 1. To perform phylogenetic analysis on duck MAVS

Aim 2. To determine the subcellular distribution of duck MAVS in avian cells

Aim 3. To functionally characterize duck MAVS, focusing on IFN- β induction and interaction with duck RIG-I 2CARD.

Aim 4. To examine the interaction between PR8 PB1-F2 and duck MAVS

4.2 Results

4.2.1 Duck MAVS has only 27.82% amino acid sequence identity to human MAVS.

The full open reading frame of duck MAVS is 1860 base pairs, encoding a peptide of 619 amino acids. The molecular weight of duck MAVS is predicted to be 64 kDa using the online ExPASy program (http://web.expasy.org/compute_pi/). To examine the conserved features of duck MAVS among different species, I did an alignment of duck, chicken, human and mouse MAVS proteins using Clustal Omega (<https://www.ebi.ac.uk/Tools/msa/clustalo/>) and edited it with the Boxshade server (https://embnet.vital-it.ch/software/BOX_form.html). The result showed that avian MAVS (duck or chicken) amino acid sequence was very different from mammalian MAVS (human or mouse) (Figure 4.2.1A). Duck MAVS shares low amino acid identity with chicken MAVS (57.60%) and human MAVS (only 27.82%). However, the caspase activation and recruitment domain (CARD) and the transmembrane (TM) domain of duck and chicken MAVS are highly conserved, as evident from black shading shown in Figure 4.1B. The sequence identities of CARD and TM domain between duck and chicken were up to 80.52% and 80%, respectively. The proline-rich region of duck MAVS only shares 49.15% amino acid identity with the counterpart of chicken MAVS.

4.2.2 Duck MAVS is most closely related to chicken MAVS.

To investigate the evolutionary distance between duck and other vertebrate MAVS, a phylogenetic tree of MAVS was generated using MEGA7. The bootstrap consensus tree was inferred using the Neighbor-Joining method from 1000 replicates. MAVS protein sequences were downloaded from the NCBI protein database. The accession numbers are listed in Appendix II. As expected, duck MAVS has a closer evolutionary distance to bird MAVS than to that of mammals, and the closest evolutionary distance was to chicken MAVS (Figure 4.2.).

4.2.3 Duck MAVS is localized on mitochondria of DF-1 cells.

To investigate the distribution of duck MAVS in avian cells, I transfected V5-tagged MAVS expression vector into DF-1 cells and detected its localization with immunofluorescence (IF) 24h post-transfection. The mitochondria were stained with Mitotracker red. The distribution of V5-MAVS in cells was indicated by Alexa 488 green dye, which was conjugated to the secondary antibody. Through confocal images, we could observe co-localization between V5-dMAVS and mitochondria (Figure 4.3A). Meanwhile, co-localization of V5-dMAVS with mitochondria was also quantitatively analyzed using pixel-based quantitative methods: Pearson's correlation coefficient (PCC), Mander's coefficient A (MCA) and Mander's coefficient B (MCB). The average values of PCC, MCA, and MCB for the co-localization analysis between V5-duck MAVS and mitochondria were 0.79, 0.43 and 0.51, respectively (Figure 4.3B), which indicated V5-duck MAVS and mitochondrial staining had a very high signal correlation. The data suggested duck MAVS had the same distribution pattern as human MAVS. Both proteins were localized to the cell mitochondria, although the amino acid sequences in the TM domains of avian and mammalian MAVS were very different, as shown in Figure 4.1A.

4.2.4 Overexpression of duck MAVS stimulates IFN- β promoter activity in DF-1 cells.

Considering the low sequence identity between duck MAVS and chicken MAVS but with high identity in CARD, we wondered whether duck MAVS is capable of inducing IFN- β production in chicken DF-1 cells. With this question in mind, we transfected V5-dMAVS with chIFN- β reporter vector and the *Renilla* luciferase vector (the internal reference control) into DF-1 cells. GST-2CARD and pcDNA3.1 were individually transfected into DF-1 cells with chIFN- β and *Renilla* luciferase vector as the positive and the negative control, respectively. 24 hours post-transfection, the cells were lysed, and the chIFN- β reporter activities were measured by dual luciferase assay. Compared to pcDNA3.1 vector only, overexpression of V5-dMAVS stimulated chIFN- β promoter activity up to 8-fold in DF-1 cells though not as much as GST-2CARD did, which was up to approximately 50-fold. We also observed that co-transfection of V5-MAVS and RIG-I 2CARD induced the strongest chIFN- β reporter activity (Figure 4.4), suggesting the possible interaction between duck MAVS and duck RIG-I 2CARD. We will test this prediction in the following experiment. Overall, in this part, we observed duck MAVS stimulated chIFN- β

promoter activity in DF-1 cells, which suggested duck MAVS could also upregulate IFN- β production in birds as does human MAVS in mammals.

4.2.5 Human RIG-I 2CARD is not able to interact with avian MAVS to stimulate IFN- β promoter activity in DF-1 cells.

Previous studies have documented that the CARD domain of MAVS interacts with RIG-I 2CARD, which further stimulates the downstream cascade of the immune signaling pathway. Considering the low sequence identity between avian MAVS and mammalian MAVS, including the CARD domain, we want to investigate whether this difference limited their cross-species interaction. To answer this question, DF-1 cells were transfected with duck RIG-I 2CARD or human RIG-I 2CARD expression vectors together with chIFN- β reporter vector and *Renilla* luciferase vector (the internal reference control). 24 hours post-transfection, chIFN- β reporter activities were measured by dual luciferase assay. GST only vector was regarded as the negative control. The result showed that only duck RIG-I 2CARD, not human RIG-I 2CARD, significantly increased chIFN- β promoter activity in DF-1 cells (Figure 4.5A). This finding suggested duck RIG-I 2CARD can interact with chicken MAVS, which might be attributed to the high sequence identity between duck and chicken MAVS CARD domain. While, human RIG-I 2CARD did not support the cross-species interaction between human RIG-I and chicken MAVS. To exclude the possibility of human RIG-I 2CARD was not working because of the expression vector itself, we further tested this vector in the human cell line, AD293T. The result showed that human RIG-I 2CARD stimulated human IFN- β promoter activity up to around 400 times in human cells (Figure 4.5B), indicating this expression construct worked very well. So, this experiment supported the above suggestion that human RIG-I 2CARD did not interact with avian MAVS because of the difference in CARD domain sequences between bird and human.

4.2.6 Duck MAVS has a similar staining pattern to duck RIG-I 2CARD and it can be pulled down by GST tagged duck RIG-I 2CARD.

Our result above in section 4.4 suggested duck MAVS could also stimulate IFN- β promoter activity. Additionally, prior research has shown the activation of human MAVS requires the CARD-CARD interaction between MAVS and the upstream RNA sensor, RIG-I protein (Wu et al., 2014). Thus, to clarify whether duck MAVS interacts with duck RIG-I 2CARD, we

investigated the co-localization of these two proteins using confocal microscopy and further quantitatively analyzed the co-localization using Pearson's correlation coefficient and Mander's coefficient. The confocal images showed GST was diffusely distributed within the whole cytoplasm, not related to the distribution of V5-MAVS. Whereas, GST-2CARD had a similar staining pattern to duck MAVS in DF-1 cells, which demonstrated duck RIG-I 2CARD co-localized with duck MAVS in DF-1 cells. Three out of eleven different DF-1 cells overexpressing V5-MAVS and GST-2CARD used for the qualitative analysis were shown as representative cells in Figure 4.6B. The average values of PCC, MCA, and MCB for the co-localization analysis between duck MAVS and duck RIG-I were 0.83, 0.37 and 0.48, respectively (Figure 4.6C). Our data showed a very high signal correlation between V5-duck MAVS and duck RIG-I.

To see if duck MAVS can be pulled down with GST-2CARD, DF-1 cells were co-transfected with V5-MAVS with GST or GST-2CARD. 24 hours post-transfection, the cell lysate was incubated with Glutathione Sepharose 4B beads overnight. GST-pull down clearly showed V5-MAVS was pulled down only by GST-2CARD, but not by GST, although both proteins could be detected in the whole cell lysate and the elution product (Figure 4.6D). Therefore, this result further suggested an interaction between duck MAVS and duck RIG-I 2CARD.

4.2.7 PB1-F2 (PR8) inhibits duck RIG-I 2CARD and duck MAVS mediated IFN- β promoter activity.

PB1-F2 from mammalian influenza A virus PR8 has been shown to inhibit RIG-I induced type I IFN production at the level of human MAVS in human cell lines (Varga et al., 2011). Based on our data above, despite the vast difference in the amino acid sequence, duck MAVS plays a similar role as human MAVS does in RIG-I signaling pathway, which is an essential host innate immune response to influenza infection. Therefore, to further determine whether PR8 PB1-F2 interferes with IFN- β production in DF-1 cells, we stimulated chicken IFN- β promoter activity using GST-d2CARD or V5-dMAVS, and co-transfected Flag-tagged PB1-F2 (PR8) expression vector into DF-1 cells. Flag-NS1 and pcDNA3.1 were co-transfected as the positive and negative control, respectively. 24 hours post-transfection, chIFN- β activity was measured by dual luciferase assay. Both PR8 PB1-F2 and NS1 significantly decreased duck RIG-I 2CARD and

duck MAVS mediated chicken IFN- β promoter activities (Figure 4.7A & Figure 4.7B), and PR8 PB1-F2 demonstrated a stronger potential to inhibit duck RIG-I 2CARD stimulated chicken IFN- β promoter activity than NS1 (Figure 4.7B).

4.2.8 PB1-F2 (PR8) is localized to the mitochondria of DF-1 cells.

PB1-F2 (PR8) has been shown to be expressed on the mitochondria of human cells, and interacts with mitochondrial proteins, like MAVS and Tom40 (a major mitochondrial outer membrane import channel) (Yoshizumi et al., 2014). To determine whether the above inhibitory activity of PR8 PB1-F2 is due to the interaction with avian MAVS, we first examined the distribution of PR8 PB1-F2 in DF-1 cells by confocal microscopy and co-localization analysis. The distribution of PR8 PB1-F2 in HeLa cells was examined for comparison, as the positive control. The confocal images clearly showed PR8 PB1-F2 had a similar staining pattern to MitoTracker both in DF-1 cells and in HeLa cells (Figure 4.8A). Four representative cell images used for Pearson's correlation coefficient and Mander's coefficient analysis were shown in Figure 4.8B. The average values of PCC, MCA, and MCB for the co-localization analysis between PR8 PB1-F2 and mitochondria were 0.82, 0.61 and 0.32, respectively (Figure 4.8C). The result showed a very high signal correlation between PB1-F2 (PR8) and MitoTracker staining, suggesting PR8 PB1-F2 is also distributed on mitochondria of DF-1 cells, consistent with the distribution in human cells.

4.2.9 PB1-F2 (PR8) has a similar staining pattern to duck MAVS and immunoprecipitated with V5-MAVS.

To determine whether PR8 PB1-F2 inhibits duck RIG-I d2CARD and duck MAVS mediated chIFN- β promoter activity through interacting with avian MAVS, we further tested the interaction between PR8 PB1-F2 and duck MAVS. DF-1 cells were co-transfected with Flag-tagged PB1-F2 (PR8) and V5-dMAVS. 24 hours post-transfection, the cells were used to do confocal microscopy or co-immunoprecipitation (Co-IP).

The confocal images of three representative DF-1 cells used for the following quantitative analysis showed PR8 PB1-F2 had a similar staining pattern to duck MAVS (Figure 4.9A). The average values of PCC, MCA, and MCB were 0.6748, 0.3975, and 0.637929, respectively. It

showed a moderate signal correlation between PR8 PB1-F2 and duck MAVS staining, indicating the co-localization of PR8 PB1-F2 with duck MAVS in DF-1 cells (Figure 4.9B).

To determine whether PB1-F2 co-precipitates with duck MAVS, we performed Co-IP by two different strategies. First, we co-transfected DF-1 cells with both V5-dMAVS and Flag-PB1-F2. Upon overnight incubation of cell lysate with sepharose beads coated with mouse anti-V5 antibody, V5-dMAVS was immunoprecipitated with Flag-PB1-F2 (Figure 4.9C). Second, we transfected DF-1 cells with V5-dMAVS or Flag-PB1-F2 separately, followed by mixing them and incubating the mixture with the mouse anti-V5 antibody-coated sepharose beads overnight. Finally, the same result was observed that V5-dMAVS was immunoprecipitated with Flag-PB1-F2 (Figure 4.9D). To confirm the specificity of the co-immunoprecipitation between PB1-F2 and duck MAVS, I further co-transfected DF-1 cells with GFP or GFP labeled PB1-F2 and V5-dMAVS. GFP only vector was used as the negative control here. As expected, only GFP-PB1-F2 was immunoprecipitated with V5-dMAVS, not for GFP (Figure 4.9E).

4.3 Summary

Here, we identified and characterized duck MAVS protein. Furthermore, we investigated the relationship of duck MAVS and PR8 PB1-F2 by characterizing the subcellular distribution of PR8 PB1F2 and its role in RIG-I or MAVS mediated induction of type I IFN in the avian system. It shows duck MAVS shares a low amino acid identity to human MAVS (only 27.82%) and chicken MAVS (57.60%). Even though, it is conserved in subcellular distribution (mitochondrial membranes) and the role of stimulating RIG-I signaling pathway through interacting with duck RIG-I 2CARD. Additionally, PR8 PB1-F2 interacts with duck MAVS, like human MAVS, and impairs duck RIG-I and duck MAVS stimulated IFN- β promoter activities in DF-1 cells. All these findings in avian cells are consistent with the observations in mammalian species despite low sequence identity.

4.4 Discussion

Despite only 28% amino acid identity between duMAVS and huMAVS, duMAVS was also distributed in the mitochondria of chicken DF-1 cells and contributed to the induction of type I IFN, consistent with a previous report (Li et al., 2016), in which, Li H *et al.* observed the

mitochondrial distribution and the stimulation of IFN- β promoter activity of duMAVS in DEFs. Knocking down duMAVS significantly decreased the induction of IFN- β by poly (I:C) and Sendai virus (SeV) (Li et al., 2016), suggesting the involvement of duMAVS in the duck innate immune system. However, they did not investigate how duMAVS works to induce IFN- β production. Whether it is also involved in RIG-I/MDA5 signaling pathway through interacting with RIG-I 2CARD was not yet elucidated. Here, using co-localization and co-IP techniques, I showed an interaction between duMAVS and duRIG-I 2CARD. Using dual luciferase assay, I showed duMAVS induced IFN- β promoter activity. The induction was augmented when I co-transfected duck RIG-I 2CARD with duMAVS, but not by much. It did not exceed the sum of activity induced by each transfected alone. The co-transfection of DF-1 cells with duMAVS and duck RIG-I 2CARD together induced more IFN promoter activity than by a single transfection with either of them. By microscopy, I observed that some DF-1 cells only expressed one of the co-transfected proteins in the co-transfection experiments.

I also showed that huRIG-I 2CARD did not induce IFN- β production in avian cells, suggesting that huRIG-I 2CARD does not interact with avian MAVS, and vice versa, the duRIG-I 2CARD did not work well in human cells either (Wu et al., 2014). The lack of cross-species interaction of 2CARD::CARD may be attributed to the strict binding between the tandem residues T175/T176 in duck RIG-I 2CARD or K175/E176 in human RIG-I 2CARD and the interacting residues in MAVS CARD, but which residues of human and avian MAVS they bind to are still unclear.

Like in mammalian cells, such as, HeLa cells (Chen et al., 2010; Cheng et al., 2017; Gibbs et al., 2003) and MDBK cells (Chen et al., 2001), PR8 PB1-F2 was also predominantly distributed in the mitochondria of transfected DF-1 cells in my study. These findings suggested the conservative subcellular distribution of PR8 PB1-F2 in different cell types of mammalian and avian species. Through constructing a serial deletion mutants, Gibbs et al. confirmed the C-terminal residues 65-87 to be the mitochondrial targeting sequence of PR8 PB1-F2 (Gibbs et al., 2003). Moreover, similar to the function of modifying human innate immunity (Varga et al., 2012; Varga et al., 2011), PR8 PB1-F2 was found to be able to inhibit duRIG-I 2CARD or duMAVS mediated IFN- β promoter activity in avian cells. The interaction of PR8 PB1-F2 with duMAVS may be responsible for the inhibitory activity of PR8 PB1-F2 in duck MAVS

stimulated signaling pathway. But, the inhibition of duck RIG-I 2CARD mediated IFN- β promoter activity by PR8 PB1-F2 was also observed in DF-1 cells, suggesting that this protein possibly interacts with chicken MAVS, too. PR8 PB1-F2 was found to bind to human MAVS via its C-terminal region (aa 38 to 87), but not the N-terminal region (aa 1 to 37) (Varga et al., 2012). However, which region of PR8 PB1-F2 bind to in avian MAVS is not yet known.

In this study, both duck MAVS and PR8 PB1-F2 were fused with a V5 and a flag tag, respectively. However, I did not have a control to exclude the influence of these tags on their distributions and functions in DF-1 cells. To make the results more convincing, other irrelevant V5 and flag-tagged proteins, which are neither localized to the mitochondria nor interact with duMAVS, should be used as negative controls. Additionally, isotype-matched antibodies should also be used as negative controls to the specific anti tag primary antibodies. However, V5 tag was broadly used in previously publications, such as V5-MAVS (Minassian et al., 2015), TRIM25-V5 (Castanier et al., 2012), etc. PB1-F2 from PR8 was also flag tagged on either N-terminal (Varga et al., 2011) (Chen et al., 2010) or C-terminal (Buehler et al., 2013) in previous *in vivo* studies. Here, GFP-tagged PB1-F2 was immunoprecipitated with V5-dMAVS, but not GFP, also suggesting the specificity of the interaction between PB1-F2 and V5-dMAVS.

Furthermore, due to lack of commercial duck cell line with good proliferation, I had to characterize duck MAVS and investigate PB1-F2 interference with avian MAVS signaling pathway in the chicken cell line, DF-1 cells, which has a higher transfection efficiency and a better proliferative ability, supports the replication of avian influenza A virus, and was previously used for the study of duck innate immune response (Barber et al., 2013; Barber et al., 2010; Blyth et al., 2016).

A

```

Mallard 1 MGFAEDKVVYGHILRNMDKFKNIHVASLVDSLGLCLTEADRDELHTRQEVGRSNATAYKLYQ
Chicken 1 MGFAEDKVVYNHILRNMSRFCDIHVASLVDSLGLCLTDADRDELHTRQDMRGIIRATAYKIFYQ
Human.. 1 MPFAEDKTYKYICRNFSNFCNDVVEILPYLPCLTARDQDRLEATCTLSGNRDTLWHLFN
Mouse.. 1 MTFPAEDKTYKYIRDNHSHKFCNDVLEILPYLSCLTASDQDRLEASYRQIGNRDTLWGLFN

Mallard 61 HVKORRGVWTDLINALHQNNAAGHLAELQVYDLYQTTPPRASAPPAAPNPGAASFPPDA
Chicken 61 HLKORKGWVMDLINALHQNNAAGHLAELQRVYDCYQAPPGVSAPPSASAPAAWP-----
Human.. 61 TLQRRPGWVEYFIAALRGCELDVLADEVASVYHSYQPR-TSDRPFDPLEPP-----
Mouse.. 61 NLQRRPGWVEVFIKALQICELPGLADQVTRVYQSYLPPGTSRSLEPLQLP-----

Mallard 121 RPAVSVSAQLPFGFKPAAAAP-T-----AIPFCCTSSTCGSAA-----T-----SV
Chicken 116 -AVSSSSVFKPFPGENSAAEAP-M-----AEPFRYNPSAGGRPELSPAAT-----TA
Human.. 111 -----SLPAEREPGPTTPAAAHSTPYNSCREKEPSYPMVQETQAPESPGENSEQALQTL
Mouse.. 112 -----DFPAAVSGPSAFAPGHNIFDHGLRE-TFSCPKFVQDTQFPESPVENSEQLLQTN

Mallard 162 SPA-----SRDVPSTDLDAAPVQEKPLEKTSQPPLPLATTYGGESDGFSTAGPL
Chicken 162 TSA-----VSDVSTELDARAPVQETPPEKSPQPLMTSTVC-----DGK--EKPL
Human.. 165 SPRAI PRNPDGPLESSSDLAALSP-----
Mouse.. 165 SGAV--ARMSGSLTSPNQALSP-----

Mallard 215 PCPTEAERVAAGPPGG--LFPWAPPEQGREWLSQRSVPCVADGCFGNSKHLHRAAPGSG
Chicken 208 PYPTESEQEAVETPGTSSVTLPSVSPQQQEWLSHRHPVCVNDGCFGNAHLORGMPNLD
Human.. 190 -LTSSTGHQEKTELGSTHTAGATSS-----LTPSRGPVSPVVS-F---QPLARSTP---
Mouse.. 188 -QPSREHQEQPELGGAAHNVASV-----PATA YGPVSPVVS-F---QPLERTAL---

Mallard 273 LGTSMPLRDPISARCVGQPRNEEQEDVYISAEIPAGLAEPGSGQGR-----QEKEAE
Chicken 268 LRSRIPPRDLAAPGPEQTRNEEQEDVYISSELPVRLVETIDGGPQPPDSVRTQEERAV
Human.. 236 -----RASRL----PGPTGSVVSTGTSFSSSS-PGLASAGAAEGKQGAES----DQAEPI
Mouse.. 234 -----RTNLL----SGVTVSALSADTSSSSS-TGSFAFKGA-----G----DQAKAA

Mallard 325 LGAEHGEAPSSLVDVRSPLLIQQQFDAEQKLAGMLREHQGGDT-----QVETTVPRDT
Chicken 328 HSEFKHDGPPSSVDVRNPLLIQQQFDAEQKQIE--REHEGGGDVVKETTTVSTSAPODI
Human.. 282 LCGSGAEAPANSIPSKVPTTLM-----PVTNVALKVPANP
Mouse.. 273 TCFSTTLTN-----SVTTSSV-----P-----SPRL

Mallard 378 SPSEIDVSWKLPVPEQTL-----PAGKAASSTPPVPAHEKVLVPAS
Chicken 386 SPFCDTSLKPPVREKML-----PEEKAASSTPSMPGKEKVLVSAS
Human.. 317 ASVSTVPSKLPSTSKPPGAVPSNALTNPAPSKLPINSTRAGMVPKSVPTSMVLTKVSAST
Mouse.. 294 VPVPTMSSKLPSSKSTAAMTSTVLTNTAPSKLBSNSVYAGTVPSRVPASVAKAP--ANT

Mallard 417 ASPEFQGSAVGGSFVSPSGRTSCRGSSATSIIW--ASPNGPEEDVELSKPGVLSLPGESPR
Chicken 425 VASLSGMNAGSFEGTAGRTSSQVSSAASIW--ASHDNEEDVELSKPGALQSVVGGESPK
Human.. 377 VP-TDGSSR--NEETPAAPT PACATGGSSAWLDSSFENRGLGSELSKPGVLASQVDSPPFS
Mouse.. 352 LPPERNSKQ--AKETPEGPAIKVTGGNQTPGNSSIRSLHSGPEMSKPGVLSQLDEPFS

Mallard 475 VAARPPGGAATASEATDHLGLSSDFLLMSTDSDFGETHEDSTSGRCSS-----APGRE
Chicken 483 AAARYLGGSP--SSNTSSHLGLSSDFIMVSTDSLRLPGEAQSTANSGLWSATPAVHADPGGE
Human.. 434 GCF-----EDLAISASTSLGMGPCH-----GPE
Mouse.. 410 ACS-----VDLAISPSSSLVSEPNH-----GPE

Mallard 529 EAEETRSCSPLSWRTE----EMRVEHSPSLLQASNELQDAGGVGISPAAAA-----SH
Chicken 541 EAGVSPYPPPLSWADPSVGTHEHVEHHPSPLTA-GNDVPEBAVPYGDSPDSNKGSAAN
Human.. 457 EN-----EYKSEGTGFIHVAENPSQLLEGNPGPPADPDGGPRPQ-----ADR
Mouse.. 433 EN-----EYSS--FRIQVDESPSADL-----LGSPEPL-----AIQ

Mallard 577 SRGGRGVPSPGDSPGFSPLPYPVAVGIALISTVAFLVYARLQK--
Chicken 600 NSSHAEVPTS GDSNGPSLLYIIPAVGIALIS--VFLVYTRLQK--
Human.. 500 KEQEREVPCHRPSP--GALWLVAVTGVLVVTLVVLVYRRRLH--
Mouse.. 462 CPQEEHEHCASSMP--WAKWLGATSA--LLAVFLAVMLYRSRRLAQ

```

B

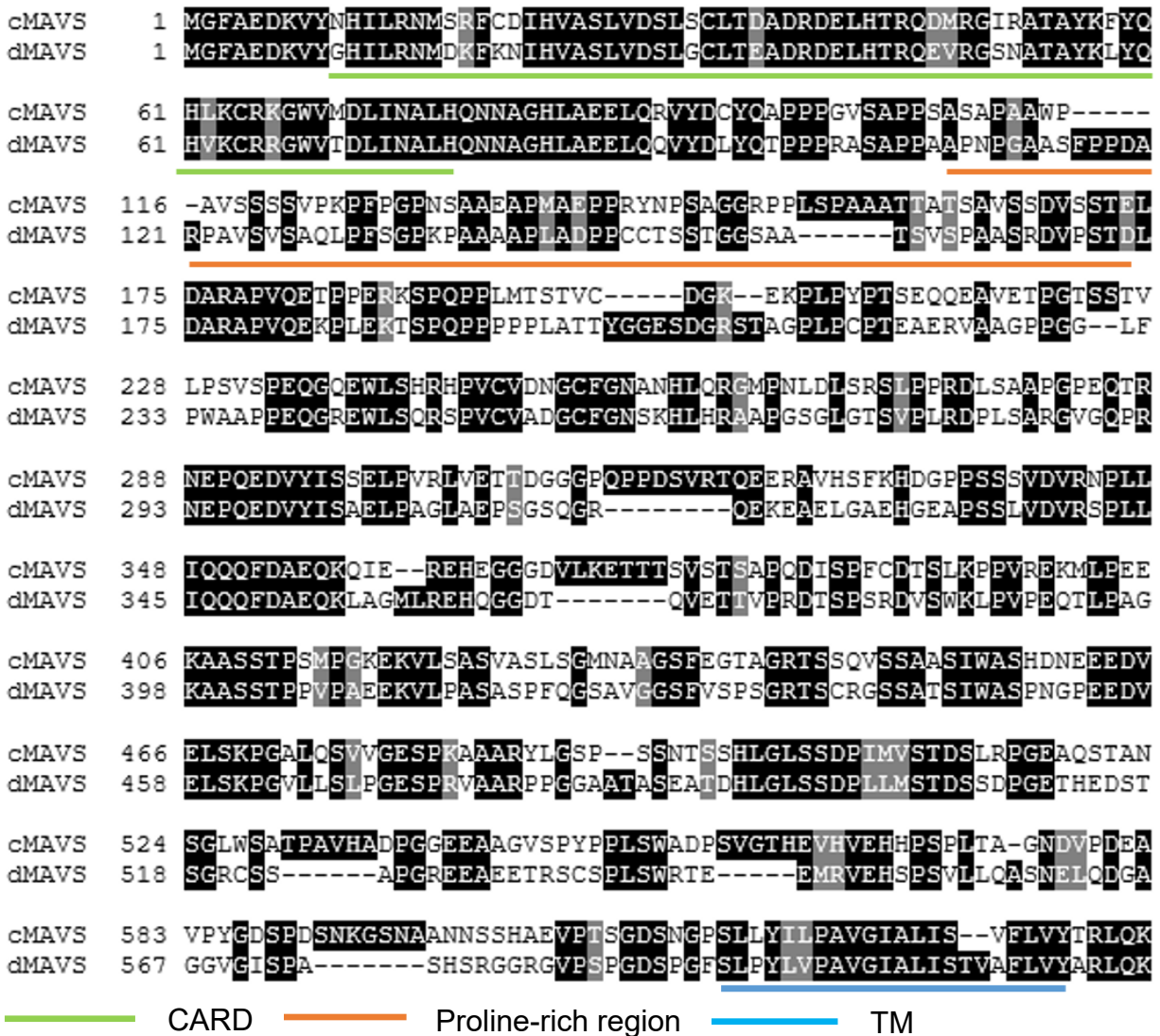


Figure 4.1 MAVS amino acid alignment

The alignments were performed and edited with the Clustal Omega and Boxshade, respectively. (A) MAVS amino acid alignment among duck (accession no. APB08796.1), chicken (accession no. NP_001012911.1), human (accession no. NP_065797.2), and mouse (accession no. NP_001193314.1). (B) The amino acid alignment between duck MAVS (accession no. APB08796.1) and chicken MAVS (accession no. NP_001012911.1). The black shading indicates identical amino acids and the gray shading indicates similar amino acids (50% threshold). The TRAF-interacting motifs (TIMs) of human MAVS were highlighted in purple.

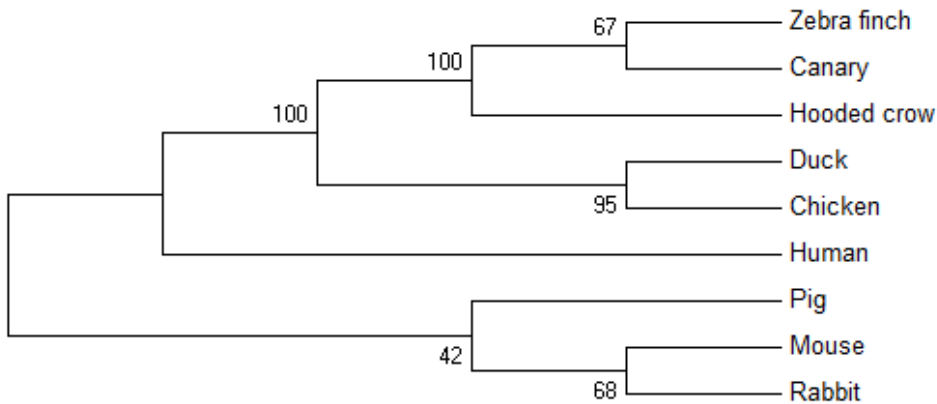


Figure 4.2 Phylogenetic analysis of MAVS proteins.

The evolutionary history of MAVS proteins was inferred using the Neighbor-Joining method. The bootstrap consensus tree inferred from 1000 replicates is taken to represent the evolutionary history of the taxa analyzed. Branches corresponding to partitions reproduced in less than 50% bootstrap replicates are collapsed. The percentage of replicate trees in which the associated taxa clustered together in the bootstrap test (1000 replicates) are shown next to the branches. The evolutionary distances were computed using the Poisson correction method and are in the units of the number of amino acid substitutions per site. The analysis involved 9 amino acid sequences. All positions containing gaps and missing data were eliminated. There was a total of 406 positions in the final dataset. Evolutionary analyses were conducted in MEGA7.

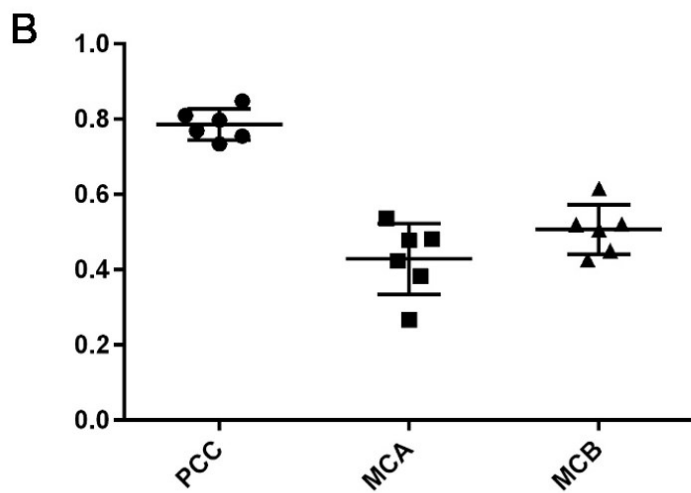
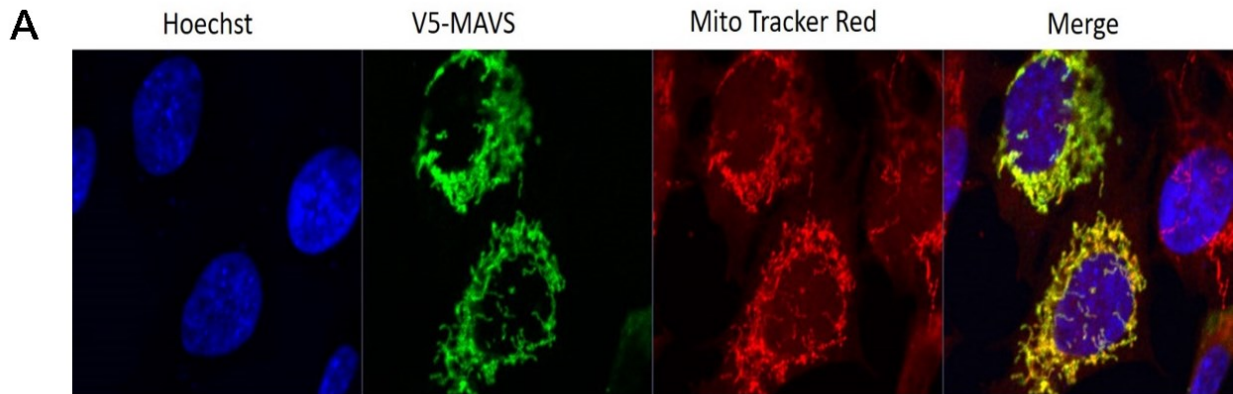


Figure 4.3 Duck MAVS localizes to mitochondria of DF-1 cells.

(A) Representative confocal microscopy image of DF-1 cells overexpressing duck MAVS stained for nuclei (blue), V5-dMAVS (green) and mitochondria (red). (B) Co-localization of V5-dMAVS with mitochondria was analyzed with Pearson's correlation coefficient (PCC) and Mander's coefficient (MCA and MCB). Bar shows the mean value from 6 analyzed cells.

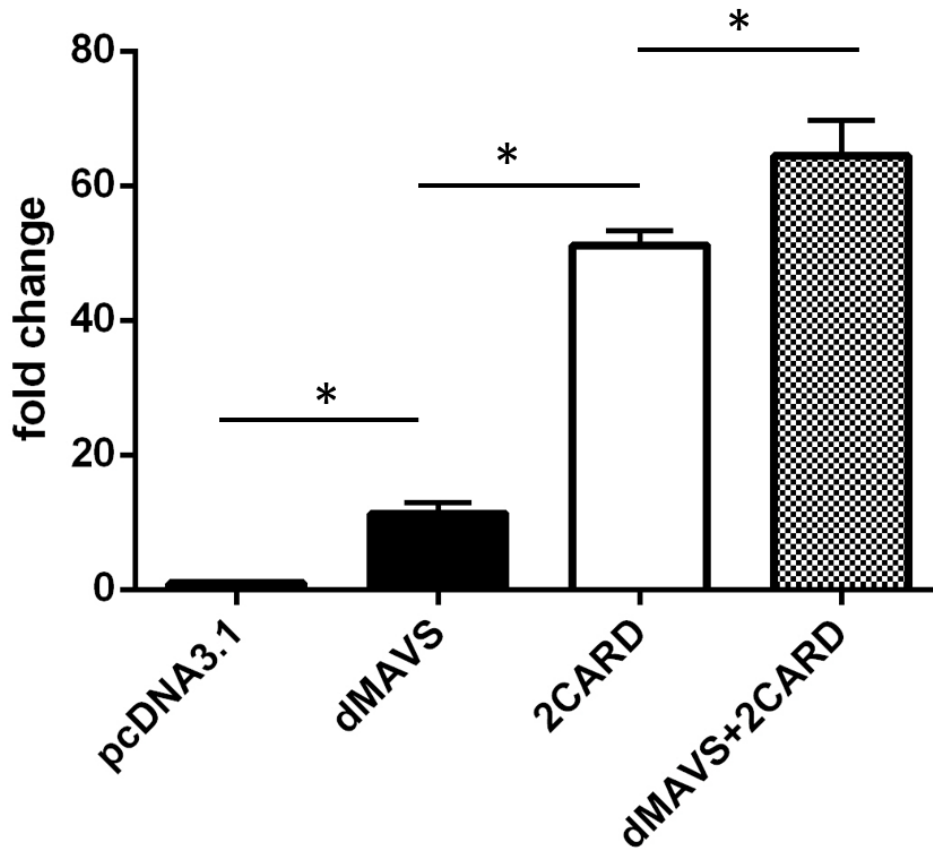


Figure 4.4 Duck MAVS overexpression promotes the IFN- β promoter activity.

DF-1 cells were transfected with 20 ng/well the indicated vectors with chIFN- β reporter vector and *Renilla* luciferase vector (the internal reference control). 24 hours post-transfection, the cells were lysed, and the chIFN- β activity was measured by dual luciferase assay. The pcDNA3.1 transfected cells were used as negative control. The mean of triplicate determinations (\pm SD) was shown in each experiment. The significance was analyzed by Tukey's multiple comparison under one-way analysis of variance (ANOVA) using GraphPad Prism 6 software. (* $p < 0.05$). This experiment was repeated twice.

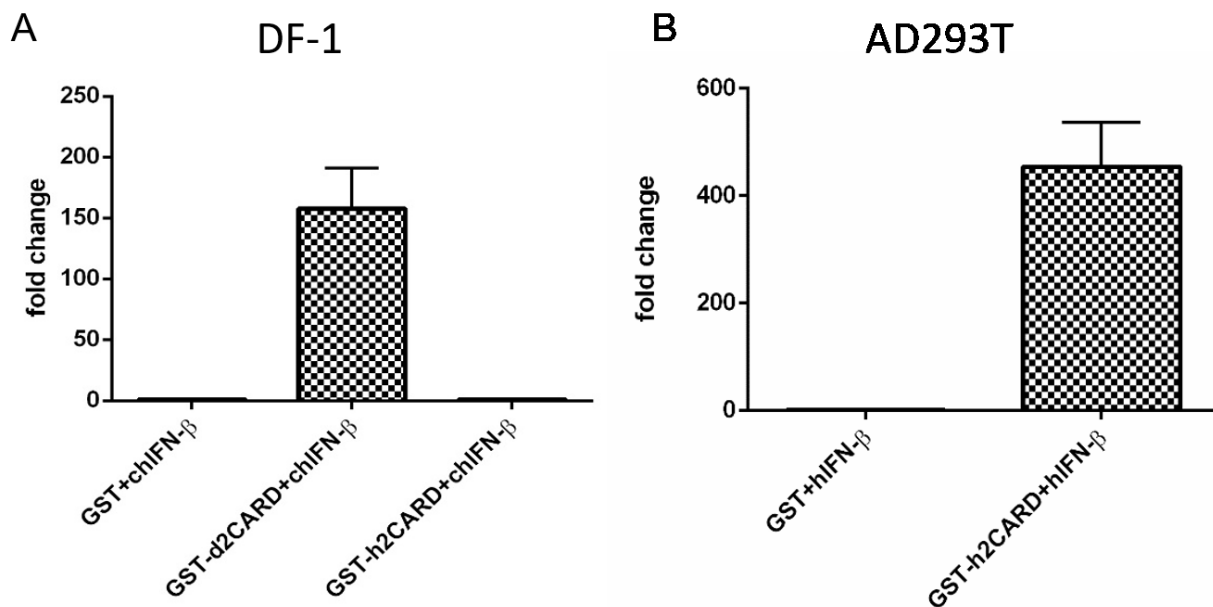


Figure 4.5 The RIG-I 2CARD interaction with MAVS to stimulate IFN- β promoter activity is species-specific.

(A) DF-1 cells were transfected with GST, GST-duck 2CARD (GST-d2CARD) or GST-human 2CARD (GST-h2CARD) individually with chicken IFN- β firefly luciferase reporter vector (chIFN- β) and *Renilla* luciferase vector (the internal reference control). 24 hours post-transfection, the cells were lysed, and the chIFN- β activity was measured by dual luciferase assay. Cells transfected with GST only were regarded as the control. (B) To examine whether GST-h2CARD works in the human cell line, AD293T cells were transfected with GST or GST-h2CARD along with human IFN- β firefly luciferase reporter vector (hIFN- β) and *Renilla* luciferase vector (the internal reference control). 24 hours post-transfection, the cells were lysed, and the hIFN- β activity was measured by dual luciferase assay as above.

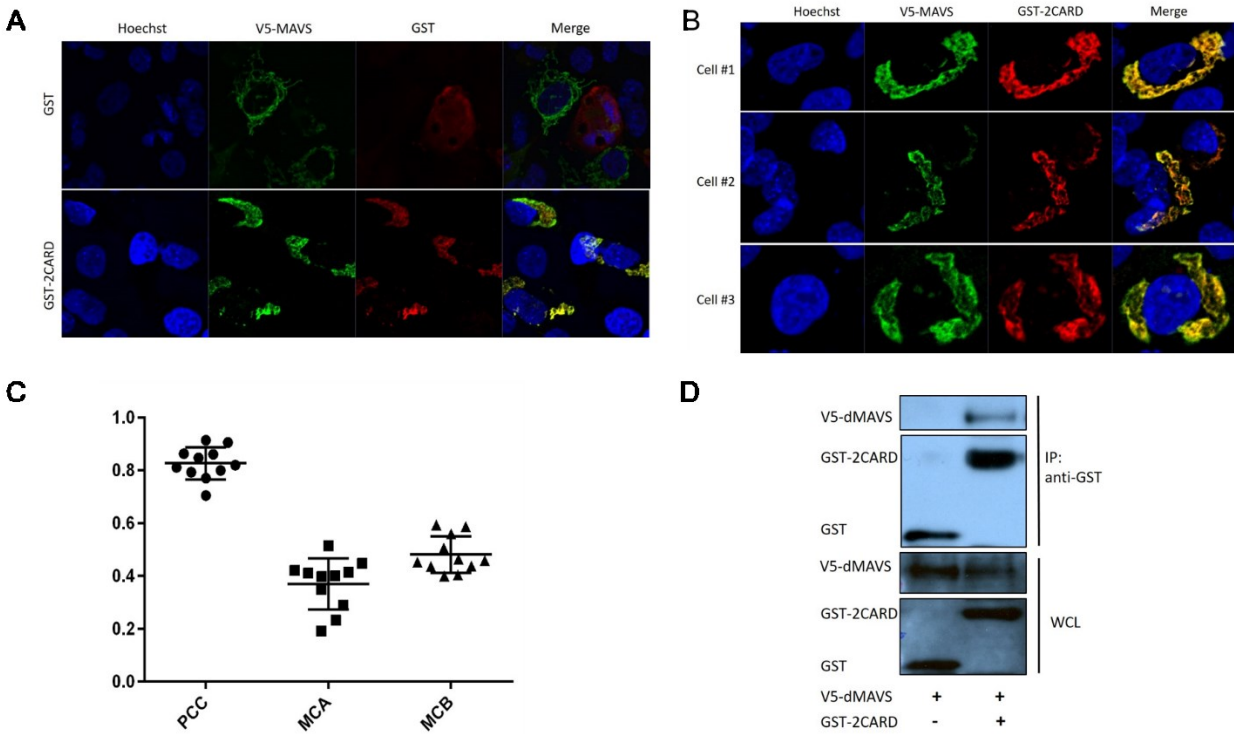


Figure 4.6 Duck MAVS has a similar staining pattern to duck RIG-I 2CARD and can be pulled down by GST tagged duck RIG-I 2CARD.

(A) DF-1 cells were co-transfected with GST or GST-2CARD and V5-MAVS. 24 hours post-transfection, the cells were fixed with 4% PFA and visualized by confocal microscopy. The primary antibodies were mouse anti-V5 antibody and rabbit anti-GST antibody. The secondary antibodies were goat anti-mouse-Alexa 488 antibody and goat anti-rabbit-Alexa 594 antibody. (B) Three representative DF-1 cells overexpressing V5-MAVS and GST-2CARD used for the following quantitative analysis. (C) Co-localization of V5-MAVS with GST-2CARD was analyzed with PCC and Mander's coefficient (MCA and MCB). Bars show the mean value from 11 analyzed cells. (D) DF-1 cells overexpressing V5-MAVS and GST-2CARD were lysed and used to do GST-pull down. The extracted proteins were mixed with glutathione sepharose 4B overnight. Following the washing and elution step, the eluted proteins were used to do Western Blot (WB). The primary antibodies were mouse anti-V5 antibody and rabbit anti-GST antibody. The secondary antibodies were goat anti-mouse-HRP antibody and goat anti-rabbit-HRP antibody.

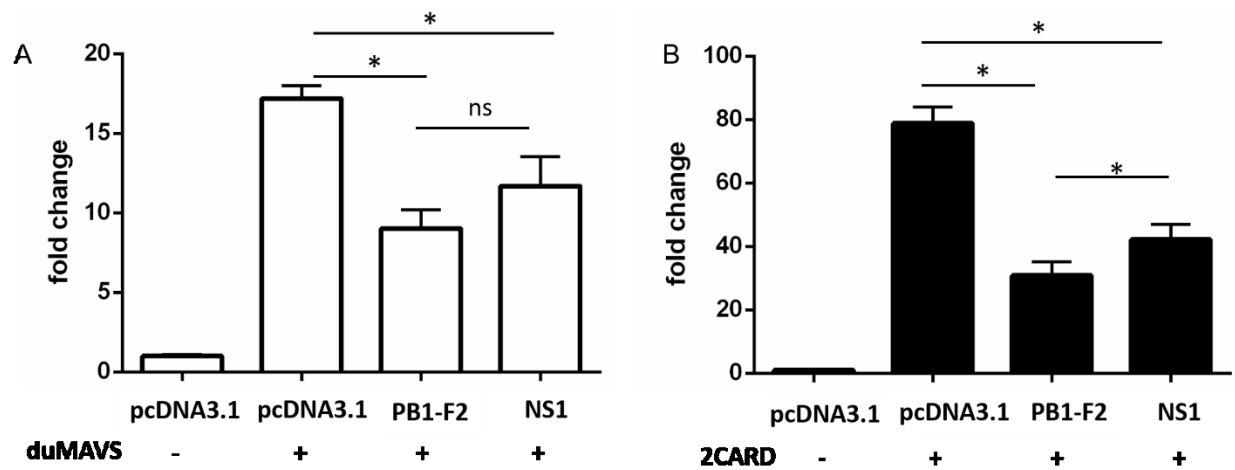


Figure 4.7 PB1-F2 (PR8) inhibits duck RIG-I 2CARD and duck MAVS mediated IFN- β promoter activity.

DF-1 cells were transfected with chIFN- β and *Renilla* luciferase vectors to report IFN- β promoter activity. (A) The stimulator used was V5-dMAVS, and pcDNA3.1 was used as negative control. (B) The stimulator used was GST-d2CARD, and GST only served as negative control. Inhibition of signaling from V5-dMAVS or GST-2CARD were tested by co-transfection with Flag-PB1-F2 (PR8) or Flag-NS1 (as the positive control). 24 hours post-transfection, the cells were lysed, and the chIFN- β activity was measured by dual luciferase assay. The mean of triplicate determinations (\pm SD) was shown in each figure. The significance was analyzed by Tukey's multiple comparison under one-way analysis of variance (ANOVA) using GraphPad Prism 6 software. (* $p < 0.05$, ns: not significant). Experiments were repeated at least twice.

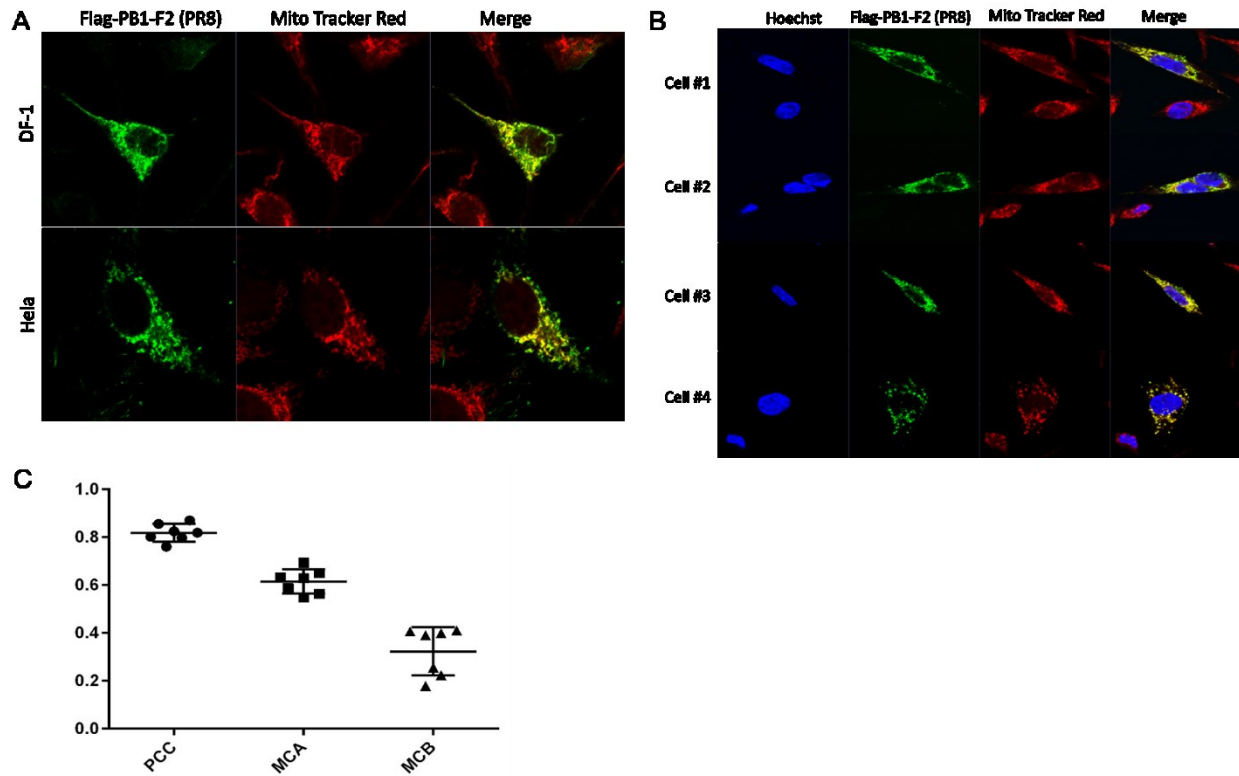


Figure 4.8 PB1-F2 (PR8) is co-localized with the mitochondria of DF-1 cell.

DF-1 or HeLa cells overexpressing Flag-PB1-F2 (PR8) were stained with MitoTracker Red, followed by fixation and immunofluorescence staining, and imaged using confocal microscopy.

(A) PB1-F2 (PR8) distribution in DF-1 and HeLa cells. (B) Four representative DF-1 cells overexpressing PB1-F2 (PR8) used for the following quantitative analysis. (C) Co-localization of PB1-F2 with MitoTracker Red was analyzed with both PCC and Mander's coefficient (MCA and MCB). Bars show the mean value from 7 analyzed cells.

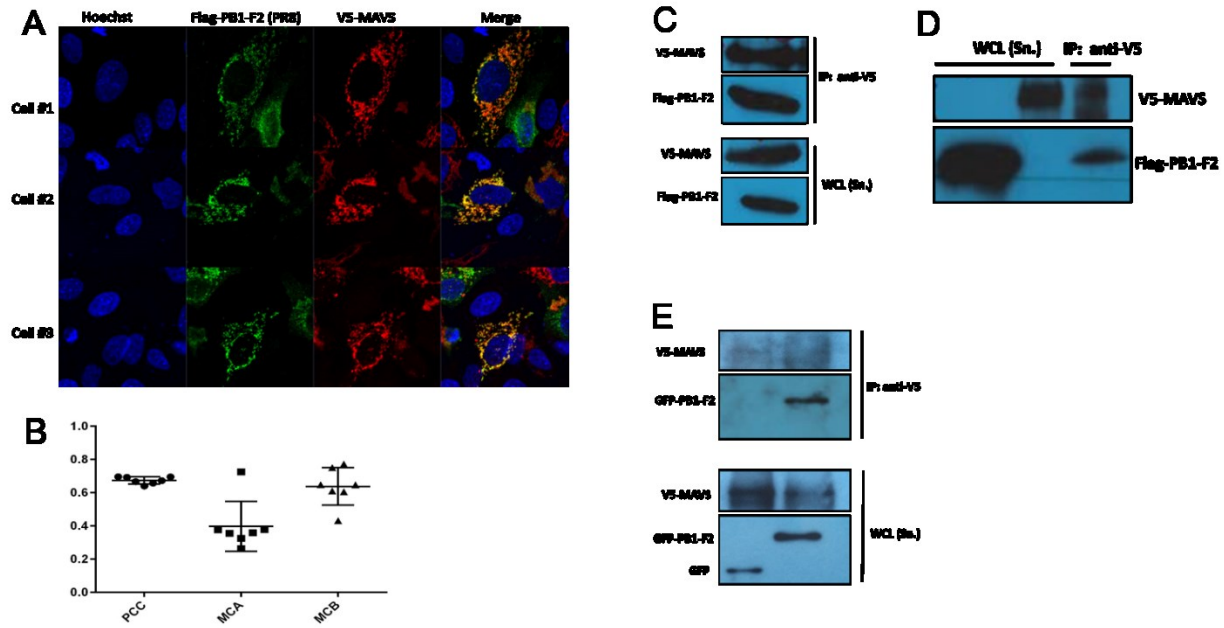


Figure 4.9 PB1-F2 (PR8) has a similar staining pattern to duck MAVS and can be immunoprecipitated with V5-MAVS.

DF-1 cells overexpressing Flag-PB1-F2 (PR8) and V5-MAVS were fixed with 4% PFA for IF staining and imaged with confocal microscopy. (A) The image shows three representative cells used for the following quantitative analysis. (B) Co-localization of V5-MAVS with GST-2CARD was analyzed with PCC and Mander's coefficient (MCA and MCB). Bars show the mean value from 8 examined cells. DF-1 cells were co-transfected with Flag-PB1-F2 (PR8) and V5-MAVS or were transfected with Flag-PB1-F2 (PR8) or V5-MAVS, separately (D). DF-1 cells were co-transfected with GFP or GFP-PB1-F2 (PR8) and V5-MAVS (E). 24 hours post-transfection, the cells were lysed and used for co-immunoprecipitation (Co-IP). The extracted proteins were incubated with mouse anti-V5 antibody-coated beads overnight. Following the washing and elution steps, the eluted proteins were used to do Western Blot (WB). The primary antibodies were rabbit anti-V5 antibody and mouse anti-Flag antibody or mouse anti-GFP antibody. The secondary antibodies were goat anti-mouse-HRP conjugated antibody and goat anti-rabbit-HRP conjugated antibody.

**Chapter 5 Results-Part III: Inhibition of MAVS Signaling by PB1-F2
from H5N1 Highly Pathogenic Avian Influenza Viruses in Avian Cells**

5.1 Rationale

Historically, HPAI H5N1 caused little or no symptoms in the natural reservoirs, including mallard ducks. Since 2002, certain H5N1 strains have become extensively lethal to multiple waterfowl species (tufted ducks, flamingos, geese, and swans) after jumping from natural reservoirs to domestic poultry (Ellis et al., 2004). Due to co-evolution between influenza viruses and ducks, these H5N1 strains rapidly recovered the natural host-pathogen relationship in ducks, although remained highly pathogenic in other waterfowl (Hulse-Post et al., 2005). However, in 2004, two particularly virulent H5N1 strains emerged in Southeast Asia: A/duck/D4AT/2004 (D4AT) and A/Vietnam/1203/04 (VN1203). Both are avian H5N1 viruses, but VN1203 was isolated from an infected person who died (Govorkova et al., 2005). In laboratory infections of mallard ducks, D4AT was the most lethal strain with 100% lethality, while VN1203 was only 50% lethal to ducks at 5 days post infection (Sturm-Ramirez et al., 2005). *In vivo* studies have suggested that polymerase proteins (Salomon et al., 2006) and PB1-F2 (Marjuki et al., 2010) contribute to the unusual lethality of VN1203 in mallard ducks, but the precise molecular mechanism are still unclear. Surprisingly, the reverse-genetics recombinant VN1203 (rgVN1203) with three amino acid mutations (T51M, V56A, and E87G) within PB1-F2 significantly decreased the lethality compared to the original isolate (VN1203) in mallard ducks (Marjuki et al., 2010). As previously discussed, PB1-F2, a viral immune antagonist protein, plays multiple roles in a virus strain-specific, cell type-specific, and species-specific manner, and these functions were mainly characterized in mammalian system. But limited information is available in an avian system. I have shown in objective 2 that PB1-F2 from the PR8 (H1N1) strain interacts with duck MAVS to inhibit RIG-I 2CARD-mediated induction of IFN- β . It is not known whether PB1-F2 from highly pathogenic strains can interact with duck MAVS, and whether sequence differences between them affect this. Thus, the third objective is to compare the functions of PB1-F2 from D4AT, VN1203, and rgVN1203 in avian cells, and to examine whether PB1-F2 contributes to the highly pathogenic nature of these HPAI H5N1 strains in ducks through interfering with duck RIG-I signaling pathway.

Four aims were developed in this part:

Aim1. To characterize the distribution of PB1-F2 derived from HPAI H5N1 viruses in avian cell line (DF-1).

- Aim2. To determine whether H5N1 PB1-F2 interferes with RIG-I mediated signaling pathway through investigating the promoter activity of IFN- β triggered by duck RIG-I 2CARD or duck MAVS overexpression.
- Aim3. To determine whether H5N1 PB1-F2 interacts with duck MAVS using co-IP and confocal microscopy.
- Aim4. To examine whether sequence differences between PB1-F2 proteins alter binding to MAVS.

5.2 Results

5.2.1 The amino acid alignment of PB1-F2 from three similar HPAI H5N1 and PR8 (H1N1).

PB1-F2 proteins investigated in this project were derived from three similar HPAI H5N1 viruses: wild-type A/Vietnam/1203/2004 (H5N1) (VN1203), reverse-genetics recombinant VN1203 (RgVN1203), and A/Thailand 71.1/2004 (D4AT). To better characterize PB1-F2 from HPAI in avian systems, PB1-F2 from A/Puerto Rico/8/1934 (H1N1) (PR8) was used as a control, because it has been extensively studied in mammals, and well-studied in avian cells in my previous work (Chapter 4). The origin and virulence of these virus strains has been mentioned in Chapter 2. VN1203 and D4AT were isolated from a fatal human and an infected duck, respectively. RgVN1203 was the reverse-genetics recombinant version of VN1203. PR8 was isolated from a fatal human, but it is a mouse-adapted strain.

To compare the PB1-F2 proteins from avian strains, we aligned them to PB1-F2 from PR8. PB1-F2 from HPAI H5N1 viruses is 273 base pairs, encoding the full-length peptide of 90 amino acids. PR8 PB1-F2 is 264 base pairs, also encoding a full-length peptide, but only 87 amino acids long. The alignment was run using Clustal Omega online interface (<https://www.ebi.ac.uk/Tools/msa/clustalo/>) and edited with Boxshade server (https://embnet.vital-it.ch/software/BOX_form.html). PB1-F2 proteins from RgVN1203 (Rg) and D4AT share the same amino acid identity (high up to 96.67%) to that in wild-type VN1203 (VN). By comparison with VN PB1-F2, there are only three mutations (T51M, V56A, and E87G) in Rg PB1-F2 and three mutations (Y42C, T51M, and R79Q) in D4AT PB1-F2. PB1-F2 from RgVN1203 and D4AT share a common mutation at position 51 (T51M) (Figure 5.1).

In addition to a shorter length, the amino acid sequence of PR8 PB1-F2 differs greatly from PB1-F2 from HPAI H5N1. It shares only 62.07%, 60.92%, and 63.22% identities to VN, Rg, and D4AT PB1-F2, respectively. The C-terminal of the aligned PB1-F2 look more conserved than the N-terminal, except for four amino acids at positions from 68 to 71, which are supposed to decide the subcellular distribution of PB1-F2 (Figure 5.1). The single point mutation, N66S, has been reported as attributing to the high pathogenicity of H5N1 (Hong Kong/1997) and 1918 pandemic influenza viruses (Conenello et al., 2007). However, this mutation was observed in PB1-F2 neither from the three similar HPAI H5N1 nor PR8.

5.2.2 Expression levels of different tagged PB1-F2 vectors in DF-1 cells.

To characterize PB1-F2 of HPAI H5N1 in avian cells, I generated GST-PB1-F2 (Rg/D4AT/VN) expression constructs and transfected them into DF-1 cells. 24 hours post-transfection, the expression levels of the indicated GST-PB1-F2 fusion proteins in the supernatant and the pellet of cell lysate were detected by Western Blotting (WB). The molecular weight of the full-length peptide of PB1-F2 is around 10.5 kDa, adding GST tag, and the molecular weight of fusion proteins becomes 36 kDa. The result shows the generated GST-PB1-F2 (Rg /D4AT/VN) constructs were expressed well and detected in both the supernatant and the pellet of DF-1 cell lysate at 24 hours post-transfection (Figure 5.2A). Later, it was found GST non-specifically influenced the signal of dual luciferase assay (Figure 5.2B). Hence, I further constructed Flag and GFP conjugated PB1-F2 (Rg/D4AT/VN) expression vectors. To determine whether the newly generated constructs work or not, we transfected them into DF-1 cells and detected their expression levels using WB at 24 hours post-transfection. The blotting for β -actin was used as the protein loading control. These newly generated Flag and GFP expression vectors were expressed well in DF-1 cells at 24 hours post-transfection. With the same amount of transfected DNA, PB1-F2 from three H5N1 virus strains have a similar expression level (Figure 5.2C), but all less than PR8 PB1-F2 (Figure 5.2E), suggesting PR8 PB1-F2 might have a longer half-life. Later, the GFP tag was shown to have a similar behavior to GST, non-specifically inhibiting duck RIG-I 2CARD stimulated chIFN- β promoter activity (Figure 5.2D), but not for Flag tag (Figure 5.2F). Thereafter, only Flag-tagged PB1-F2 (Rg/D4AT/VN) constructs were applied to the following experiments of dual luciferase assay.

5.2.3 PB1-F2 (Rg/D4AT/VN) are distributed throughout DF-1 cells.

Previous research has shown that the region from residues 46 to 75 is both necessary and sufficient for PB1-F2 (PR8) mitochondrial targeting (Yamada et al., 2004). However, the residues in the range from 46 to 75 of PB1-F2 from HPAI H5N1 differs from the counterpart of PR8 PB1-F2, particularly the residues from 45 to 52 and residues from 68 to 71 (Figure 5.1). With this discrepancy, we needed to investigate the distribution of PB1-F2 from HPAI H5N1 in avian cells. GST-tagged PB1-F2 (Rg/D4AT/VN) expression vectors were constructed and transfected into DF-1 cells. GST only vector and V5-tagged duck MAVS expression vector were transfected into DF-1 cells as the negative and the positive control, respectively. 24 hours post-transfection, the cells were stained with MitoTracker Red to display the location of mitochondria. The distributions of GST and the indicated GST-PB1-F2 fusion proteins were detected with rabbit anti-GST primary antibody and FITC conjugated secondary antibody, and the distribution of V5-duck MAVS protein was detected with mouse anti-V5 primary antibody and the same secondary antibody as above. The confocal images showed that PB1-F2 from these three H5N1 virus strains were distributed unevenly throughout DF-1 cells. Whereas, GST tag only, the negative control, was distributed evenly throughout DF-1 cells, and V5-MAVS was co-localized to the mitochondria (Figure 5.3A). Additionally, if PB1-F2 proteins from these three similar H5N1 viral strains were labelled with flag tag, which is much smaller than GST, they were still distributed throughout DF-1 cells, unlike flag-PB1-F2 (PR8), predominantly in the mitochondria (Figure 5.3B). These findings suggested that the residues 45 to 52 or residues 68 to 71, or both were crucial for the mitochondrial distribution of PB1-F2.

5.2.4 VN1203 PB1-F2 is the most potent inhibitory factor to RIG-I 2CARD mediated IFN- β promoter activity.

PB1-F2 has been reported to contribute to the highly pathogenic feature of wild-type VN1203 in ducks (Marjuki et al., 2010). RIG-I mediated type I interferon pathway plays a critical role in the host innate immune response to influenza A virus. Additionally, PR8 PB1-F2 has been shown to attenuate duck RIG-I 2CARD mediated IFN- β promoter activity in Chapter 4. Herein, to determine whether PB1-F2 from HPAI H5N1 also interferes with RIG-I mediated type-I IFN signaling pathway with the different subcellular localization from PR8 PB1-F2, we transfected

the indicated Flag-tagged PB1-F2 (Rg/D4AT/VN), chIFN- β reporter vector, and the *Renilla* luciferase vector (the internal reference control) into DF-1 cells with the stimulator (duck RIG-I 2CARD or duck MAVS). Additionally, NS1 and PR8 PB1-F2 were individually transfected as the positive controls. 24h post-transfection, the cells were lysed, and the chIFN- β reporter activities were measured by dual luciferase assay. Compared to pcDNA3.1 vector only, overexpression either duck RIG-I 2CARD or duck MAVS significantly stimulated chIFN- β promoter activity as observed in Chapter 4. But, the induction mediated by RIG-I 2CARD was substantially attenuated by all three tested H5N1 PB1-F2, and VN1203 PB1-F2 displayed a stronger inhibitory activity than Rg and D4AT PB1-F2, which showed equal inhibitory activities. Despite VN1203 PB1-F2 has the strongest inhibitory activity among these three H5N1 PB1-F2, its inhibitory activity is still lower than that of PR8 PB1-F2 and NS1 (Figure 5.4A-D). However, another two individual experiments showed only VN1203 PB1-F2 had significant inhibitory activity to duck RIG-I 2CARD and duck MAVS induced type I IFN promoter activity, but Rg and D4AT PB1-F2 were unable to do so. Even though, compared to PR8 PB1-F2 and NS1, VN1203 PB1-F2 still had a lower inhibitory activity, which was consistent with the above results (Figure 5.4E-F).

5.2.5 T51M point mutation alone does not change the function of wild-type PB1-F2 (VN)

Since Rg and D4AT PB1-F2 have a similar inhibitory effect to RIG-I and MAVS mediated type I IFN promoter activity, but not as strong as VN1203 PB1-F2, we expanded their sequences, compared to the amino acid sequence of VN1203 PB1-F2, there are only three different amino acids in both Rg PB1-F2 and D4AT PB1-F2. Among the different amino acids of these two viral strains, there is a common difference at position 51: threonine compared to methionine (T51M). Therefore, to determine whether the common difference (T51M) is responsible for the different inhibitory activities of the test three H5N1 PB1-F2 to RIG-I and MAVS stimulated type I interferon production, I generated the point mutation (T51M) construct from the wild-type VN1203 PB1-F2, and transfected them side by side into DF-1 cells with chIFN- β reporter vector and the stimulator RIG-I 2CARD. PR8 PB1-F2 and NS1 were used as the positive controls for the inhibitory activity of PB1-F2. 24 hours post-transfection, the influence of this mutation on the IFN- β induction was examined by comparing the IFN- β reporter activities using dual

luciferase assay. Although not as strong as PR8 PB1-F2 and NS1, T51M mutated and wild-type VN1203 PB1-F2 equally inhibited duck RIG-I-2CARD mediated chIFN- β promoter activities in DF-1 cells, indicating T51M mutation alone could not change the inhibitory function of VN1203 PB1-F2 in the chicken cell line (Figure 5.5A and Figure 5.5B).

5.2.6 The indicated point mutations do not change the inhibiting function of wild-type VN1203 PB1-F2 to RIG-I 2CARD mediated IFN- β promoter activity.

Because the common mutation, T51M, cannot explain the different inhibitory activities of PB1-F2 (Rg and D4AT) from PB1-F2 (VN), we further constructed the vectors with the other four single mutations or the possible double mutations to explore the responsible amino acid for the different inhibitory activity of VN1203 PB1-F2 from PB1-F2 (Rg and D4AT). Like the above experiments, the indicated VN1203 PB1-F2 mutant was co-transfected into DF-1 cells with chicken IFN- β promoter vector, RIG-I 2CARD, and the *Renilla* luciferase vector. 24 hours post-transfection, chIFN- β promoter activities were examined by dual luciferase assay. The results demonstrated all tested mutated VN1203 PB1-F2 and wild-type VN1203 PB1-F2 equally attenuated duck RIG-I 2CARD induced chIFN- β promoter activities in DF-1 cells, except for T51M, which showed the impaired inhibitory activity in one out of four individual experiments (Figure 5.6A-D). This observation on T51M was not consistent with the finding in Figure 5.5. Although it might well explain the lower inhibitory activities of PB1-F2 from Rg and D4AT, it was only observed once in six repeated experiments, a low occurrence rate. No significant difference was detected in the other five times. Hence, the conclusion that all tested single or double mutations did not attribute to the different inhibitory activities of PB1-F2 from similar three HPAI H5N1 was preferred. The three amino acids might work together to make the functional change happen.

5.2.7 PB1-F2 has a similar staining pattern to duck MAVS.

To further investigate the interacting immune factors in duck RIG-I stimulated signaling pathway with H5N1 PB1-F2, we tried to overexpress GST-tagged PB1-F2 from three H5N1 virus strains in DF-1 cells stimulated with RIG-I 2CARD, then, to screen the interacting proteins using GST-pull down and mass spectrometry. However, this trial was not successful because the expression

level of H5N1 PB1-F2 was too low to detect with Coomassie staining. Based on the previous reports and the data obtained in Chapter 4, PR8 PB1-F2 is interacting with MAVS both in mammals and in ducks. Therefore, I first examined whether H5N1 PB1-F2 also interacts with duck MAVS *in vitro*. DF-1 cells were co-transfected with Flag-PB1-F2 (Rg/D4AT/VN) and V5-MAVS. 24 hours post-transfection, the cells were fixed to do immunofluorescence (IF) and finally imaged using confocal microscopy. The primary antibodies were mouse anti-flag and rabbit anti-V5. The secondary antibodies were goat anti-mouse-Alexa 488 and goat anti-rabbit Alexa 594. The confocal images showed that PB1-F2 (Rg/D4AT/VN) had a similar staining pattern to duck MAVS (Figure 5.7A). Several representative DF-1 cells overexpressing Flag-PB1-F2 (Rg/D4AT/VN) and V5-dMAVS of those used for the quantitative analysis were shown in Figure 5.7B, Figure 5.7C, and Figure 5.7D, respectively. In fact, at least eight cells from each group were taken to do co-localization analysis using Pearson's correlation coefficient (PCC), Mander's coefficient (MCA and MCB). The average values of PCC between Flag-PB1-F2 (Rg/D4AT/VN) and V5-dMAVS were 0.6122, 0.521338 and 0.632825, respectively. The average values of MCA between Flag-PB1-F2 (Rg/D4AT/VN) and V5-dMAVS were 0.5576, 0.530175 and 0.641388, respectively. Additionally, the average values of MCB between Flag-PB1-F2 (Rg/D4AT/VN) and V5-dMAVS were 0.5601, 0.687963 and 0.676663, respectively (Figure 5.7E). All these data showed the high signal correlation between all three test H5N1 Flag-PB1-F2 and V5-dMAVS, suggesting the co-localization of H5N1 PB1-F2 and duck MAVS.

5.2.8 PB1-F2 was immunoprecipitated by duck MAVS.

To exam whether PB1-F2 from HPAI H5N1 interacts with duck MAVS *in vitro*, we also performed co-immunoprecipitation (Co-IP). DF-1 cells were co-transfected with the indicated Flag-PB1-F2 (Rg/D4AT/VN/PR8) and V5-MAVS. PR8 PB1-F2 was regarded as the positive control. 24 hours post-transfection, the cells were lysed and separated into two parts (the supernatant and the pellet) by centrifuging. The major supernatant of each Flag-PB1-F2 cell lysate was incubated with sepharose beads coated with mouse anti-V5 antibody overnight. Unexpectedly, only Flag-PB1-F2 (PR8) and V5-duck MAVS were detected both in the whole cell lysate (supernatant and pellet) and the precipitated samples. PB1-F2 proteins from all three H5N1 virus strains were not detected either in the supernatant of the whole cell lysate or the

precipitated samples but was observed in the pellet of the whole cell lysate (Figure 5.8A and Figure 5.8B). Therefore, the Co-IP clearly demonstrated the interaction between PR8 PB1-F2 and duck MAVS, consistent with the previous result in chapter 4. But it was hard to tell the reason not detecting H5N1 PB1-F2 from the precipitated samples was because of no interaction between H5N1 PB1-F2 and duck MAVS, or because of too little amount of H5N1 PB1-F2 released into the supernatant of the whole cell lysate.

To solve this problem, I transfected the indicated Flag-PB1-F2 (Rg/D4AT/VN/PR8) and V5-duck MAVS expression vector separately into DF-1 cells. 24 hours post-transfection, the cells were lysed and separated into the supernatant and the pellet. The expression levels of each tested Flag-PB1-F2 and V5-dMAVS in the supernatant were directly examined by WB (Figure 5.8C). The major supernatant of each Flag-PB1-F2 (Rg/D4AT/VN/PR8) cell lysate was mixed with the supernatant of V5-duck MAVS cell lysate and incubated with mouse anti-V5 coated beads overnight. In contrast to the above result, not only PR8 PB1-F2 was precipitated by V5-MAVS, but also three H5N1 PB1-F2 (Rg/D4AT/VN) (Figure 5.8C), indicating the interaction between all tested H5N1 PB1-F2 and duck MAVS *in vitro*.

Due to lack of the negative control to the flag tag in the above experiments, I further tested whether GFP tagged PB1-F2 (Rg/D4AT/VN) proteins were also precipitated by V5-MAVS, but not GFP tag only. Similar to the above co-transfection protocol, DF-1 cells were co-transfected with the indicated GFP-PB1-F2 (Rg/D4AT/VN/PR8) and V5-MAVS. GFP-PB1-F2 (PR8) and GFP were used as the positive and the negative control, respectively. 24 hours post-transfection, the cells were lysed. The minor supernatant of cell lysate was directly used for Western blot, and the major part was used to do co-IP through incubating with mouse anti-V5 antibody-coated beads overnight. The results showed that GFP-PB1-F2 proteins from H5N1 (Rg/D4AT) were like PR8 PB1-F2, also being precipitated with V5-MAVS, but not GFP. GFP-PB1-F2 (VN) was not detected in the co-IP samples either, but I suppose the reason for not detecting was due to the very little amount of GFP-PB1-F2 (VN) in the supernatant of cell lysate (Figure 5.8D). Taken together, these data suggested the association of PB1-F2 proteins from H5N1 (Rg/D4AT/VN) with duck MAVS was specific.

5.3 Summary

Here, we characterized PB1-F2 from three similar HPAI H5N1 in chicken DF-1 cell line. Unlike PB1-F2 from mammalian influenza viruses, PB1-F2 proteins from three similar HPAI H5N1 were unevenly distributed in DF-1 cells. However, the function of modulating RIG-I mediated innate immune response has shown conserved both in mammals and in birds. Like PR8 PB1-F2 in mammals, three examined H5N1 PB1-F2 also inhibited RIG-I 2CARD stimulated IFN- β promoter activities in DF-1 cells, and VN1203 PB1-F2 has shown the strongest inhibitory activity. The alignment demonstrated that Rg PB1-F2 and D4AT PB1-F2 individually bear three different amino acids from VN1203 PB1-F2, and one common point mutation is T51M. To determine which amino acid responsible for the above discrepancy, we construct every single- and double-point mutations of VN1203 PB1-F2. Unexpectedly, none of the tested single- or double-point mutations attributes to the different virulence of PB1-F2 from three similar H5N1 virus strains. Finally, we observed the interaction between H5N1 PB1-F2 and duck MAVS employing co-localization and immunoprecipitation.

5.4 Discussion

Here, I showed that both GST and flag tagged PB1-F2 from H5N1 viral strains were distributed throughout DF-1 cells, which is consistent to the previous reports about their locations in mammalian cells (Chen et al., 2010): flag-PB1-F2 proteins from avian strains, A/Hong PB1-F2 from Kong/156/1997 (H5N1) (HK156) and A/Netherlands/219/2003 (H7N7) (Neth219), were localized in the cytoplasm and nucleus of HeLa cells. Schmolke et al. also showed that PB1-F2 protein from VN1203 was not predominantly localized in the mitochondria of mouse epithelial cells (Schmolke et al., 2011). Comparing the MitoTracker Red staining patterns of GST-PB1-F2 transfected cells, it seems like that GST-PB1-F2 (D4AT) overexpression changed the mitochondrial morphology of DF-1 cells. 3 \times flag-PB1-F2 (PR8) was reported to change the mitochondrial morphology from a filamentous to a dotted structure and suppressed mitochondrial membrane potential in Vero, HeLa and MDCK cells (Yamada et al., 2004). In this study, I did not observe the predominant co-localization of all tested H5N1 PB1-F2 proteins with mitochondria, but rather a diffuse distribution throughout the DF-1 cells. Additionally, changes in the mitochondrial morphology were not detected in Flag-PB1-F2 (D4AT) transfected cells. Hence, I do not think PB1-F2 from highly pathogenic avian influenza H5N1 viruses are able to

affect the mitochondrial morphology or mitochondrial membrane potential, which is crucial for its pro-apoptotic role (Gibbs et al., 2003).

Both GST and GFP tags were shown interfering with duck RIG-I 2CARD mediated chIFN- β promoter activities in the dual luciferase assay. Therefore, only flag tagged PB1-F2 proteins were used for the following dual luciferase assays. GST and GFP are quite large tags, 220 and 238 amino acids in size, respectively. GST is an active enzyme protein, and GFP is a fluorescent protein. Therefore, both tags might directly affect the luciferase signals or might interact non-specifically with some factors in the RIG-I 2CARD mediated signaling pathway. Finally, it would be better to add a negative control with an irrelevant protein with flag tag in the co-localization and co-IP experiments.

In this study, all tested PB1-F2 proteins from H5N1 inhibited duck RIG-I 2CARD triggered IFN- β promoter activity in four out of five individual experiments. However, I also observed that only PB1-F2 (VN) inhibited IFN- β signaling triggered either by duck RIG-I 2CARD or duck MAVS with the experiment done only once each, respectively. Using co-localization and co-IP, I also showed the interactions between all tested PB1-F2 (Rg/D4AT/VN) and duck MAVS. Taking these data together, I speculate that all three PB1-F2 proteins have inhibitory activities to RIG-I or MAVS mediated IFN- β signaling pathway in avian cells. But, whether the IFN- β signaling inhibition by PB1-F2 was due to the interaction between PB1-F2 and avian MAVS needs to be investigated. The influence of PB1-F2 (Rg/D4AT/VN) on duMAVS mediated IFN- β promoter activity also needs to be repeated. Type I interferon is a vital innate immune factor to control influenza A virus and many other viruses (White et al., 2008). PB1-F2 was an important virulence factor of VN1203 in infected ducks (Marjuki et al., 2010; Schmolke et al., 2011), but the molecular mechanism remained unclear. My findings provided a way to explain the virulence of H5N1 PB1-F2 in ducks: PB1-F2 proteins from H5N1 (Rg/D4AT/VN) inhibit duck RIG-I signaling pathway, possibly via interacting with the adaptor protein, duck MAVS, in turn, inhibit the production of type I IFN and ISGs, finally, finally, result in the decrease of duck innate immune responses against avian influenza viruses. However, our results do not explain the loss of virulence between VN1203 and the attenuated reverse-genetics RgVN1203 in ducks.

Here, overexpression of duck RIG-I 2CARD could stimulate chicken MAVS signaling pathway, which was inhibited by PB1-F2 (Rg/D4AT/VN) in DF-1 cells. However, Leymarie et al. inoculated wildtype and PB1-F2 deleted influenza virus, A/duck/Niger/2090/2006 (H5N1) (Nig06), into chickens, and found the deletion of PB1-F2 led to a higher mortality rate and higher viral titres (Leymarie et al., 2014), suggesting a role of PB1-F2 in attenuating the virulence of Nig06 in chickens. The amino acid sequence of Nig06 PB1-F2 is very similar to VN1203 PB1-F2, with only five substitutions, E2G, D5G, D40G, G50V, and T51M. As the alignment showed in this study, PB1-F2 proteins from rgVN1203 and D4AT also have the substitution T51M, but not the other four. Through constructing the single point mutated vector, I did not see any change of the inhibitory activity of VN1203 PB1-F2 by T51M. Whether the other four substitutions will affect its function of modulating the innate immune response in avian systems needs to be elucidated.

PB1-F2 plays multiple roles, including pro-apoptosis, modulating host innate immunity, exacerbating secondary bacterial infection, and increasing viral replication (reviewed by Kamal et al., 2017). Recently, PB1-F2 from H7N9 was found to induce inflammation in mammalian systems (human and mouse) (Pinar et al., 2017). Therefore, more roles PB1-F2 protein may play in virus-host interaction. These findings further confirmed the viral strain and species specificity of PB1-F2.

There were also some limitations of the study. Similar to the chapter 4, there was no commercial duck cell line with a good proliferative activity. Therefore, all the experiments were performed in chicken DF-1 cells, although my study was to examine how PB1-F2 from H5N1 viruses interact with duck RIG-I signaling pathway. Additionally, the signaling components downstream of MAVS in the duck RIG-I signaling pathway was unavailable, thus, I could only focus on the function of PB1-F2 proteins in this signaling pathway at avian MAVS level.

```

Rg--      1  MEQGQDTPWTQSTEHTNIQKRGSGQQTQRLEHPNSTRIMDHYLRIMSPVGMHKQIAYWKQ
D4AT      1  MEQGQDTPWTQSTEHTNIQKRGSGQQTQRLEHPNSTRIMDHCCLRIMSPVGMHKQIVYWKQ
VN--      1  MEQGQDTPWTQSTEHTNIQKRGSGQQTQRLEHPNSTRIMDHYLRIMSPVGTHTKQIVYWKQ
PR8-      1  MGQEQDTPWILSTGHISTQKREDGQQTPKLEHRNSTRIMGHCQKTMNQVVMPPKQIVYWRR

Rg--      61  WLSLKNPTQGSLKTRVLKRWKLFNKQGIN
D4AT      61  WLSLKNPTQGSLKTRVLKQWKLFNKQEWIN
VN--      61  WLSLKNPTQGSLKTRVLKRWKLFNKQEWIN
PR8-      61  WLSLRNPILVFLKTRVLKRWRFLFSKHE---

```

Figure 5.1 Amino acid alignment of PB1-F2.

The alignment of VN1203 PB1-F2 (accession no. ADD97093.1), Rg PB1-F2 (based on the report (Marjuki et al., 2010)), D4AT PB1-F2 (AFH77081.1), and PR8 PB1-F2 (YP418248.1) was performed using Clustal Omega and edited with BoxShade Server. The black shading indicates identical amino acids and the gray shading indicates similar amino acids (50% threshold). The amino acid at position 66 (N66) was highlighted red.

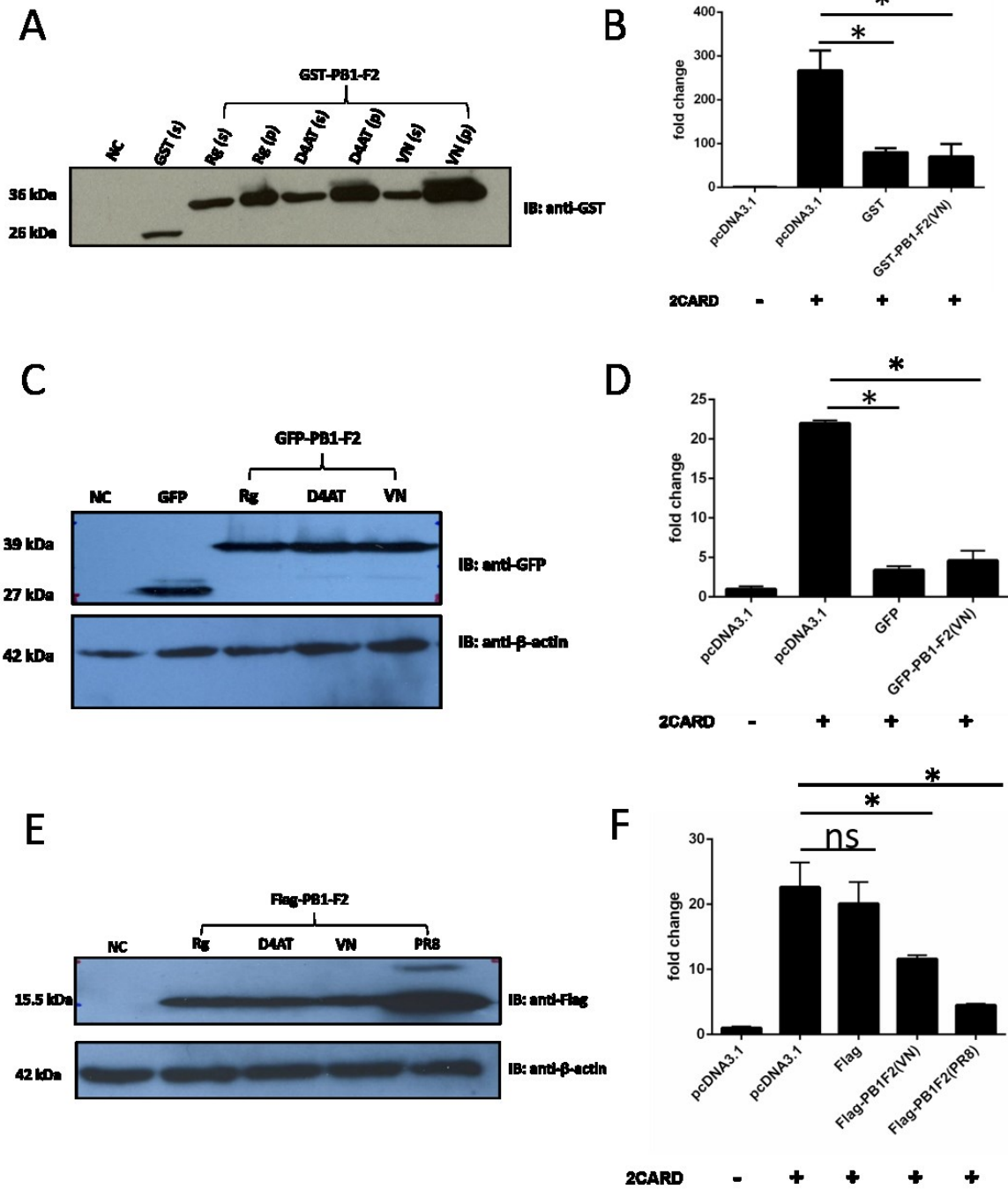
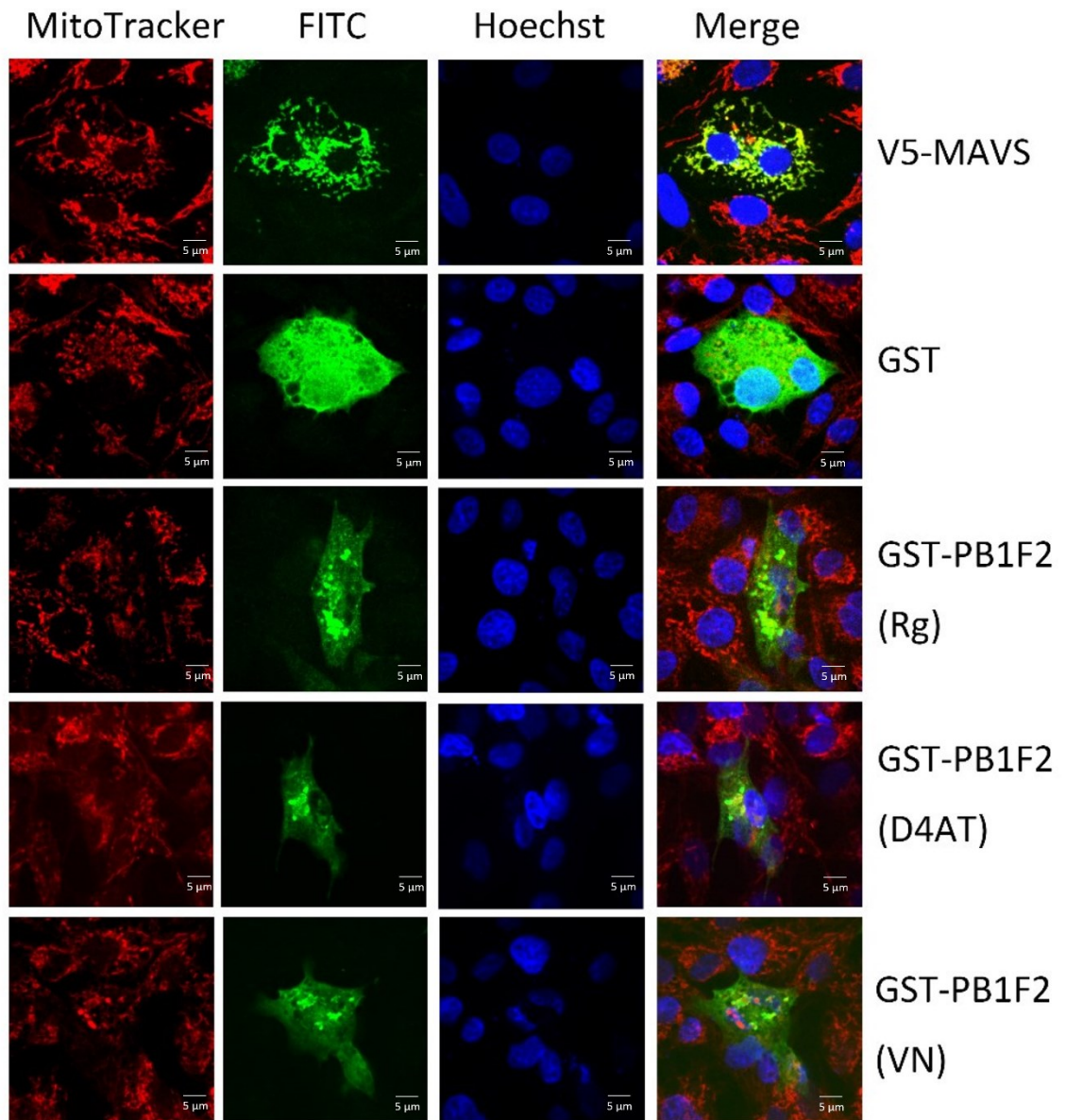


Figure 5.2 Expression levels of PB1-F2 fusion proteins in DF-1 cells.

DF-1 cells were transfected with the indicated PB1-F2 expression vectors. 24 hours post-transfection, the cells were lysed to do a Western Blot (WB). GST-tagged PB1-F2 proteins in the supernatant (s) or the pellet (p) of cell lysates were shown in A. The protein expression levels of GFP and Flag-tagged PB1-F2 in the supernatant of cell lysate were shown in C, and E, respectively. DF-1 cells were co-transfected with the indicated expression vectors and chicken IFN- β reporter vector with GST (the negative control) or GST-d2CARD (the stimuli of IFN- β promoter activity). 24 hours post-transfection, the cells were lysed and the chIFN- β reporter activity was measured using dual luciferase assay. The mean of triplicate determinations (\pm SD) was shown in each figure (B, D and F). The significance was analyzed by Tukey's multiple comparison under one-way analysis of variance (ANOVA) using GraphPad Prism 6 software. (* $p < 0.05$, ns: not significant). DF-1 cells were transfected with only pcDNA3.1 empty vector as negative control (NC) (A, C and E). Actin is blotted as protein loading control (C and E).

A



B

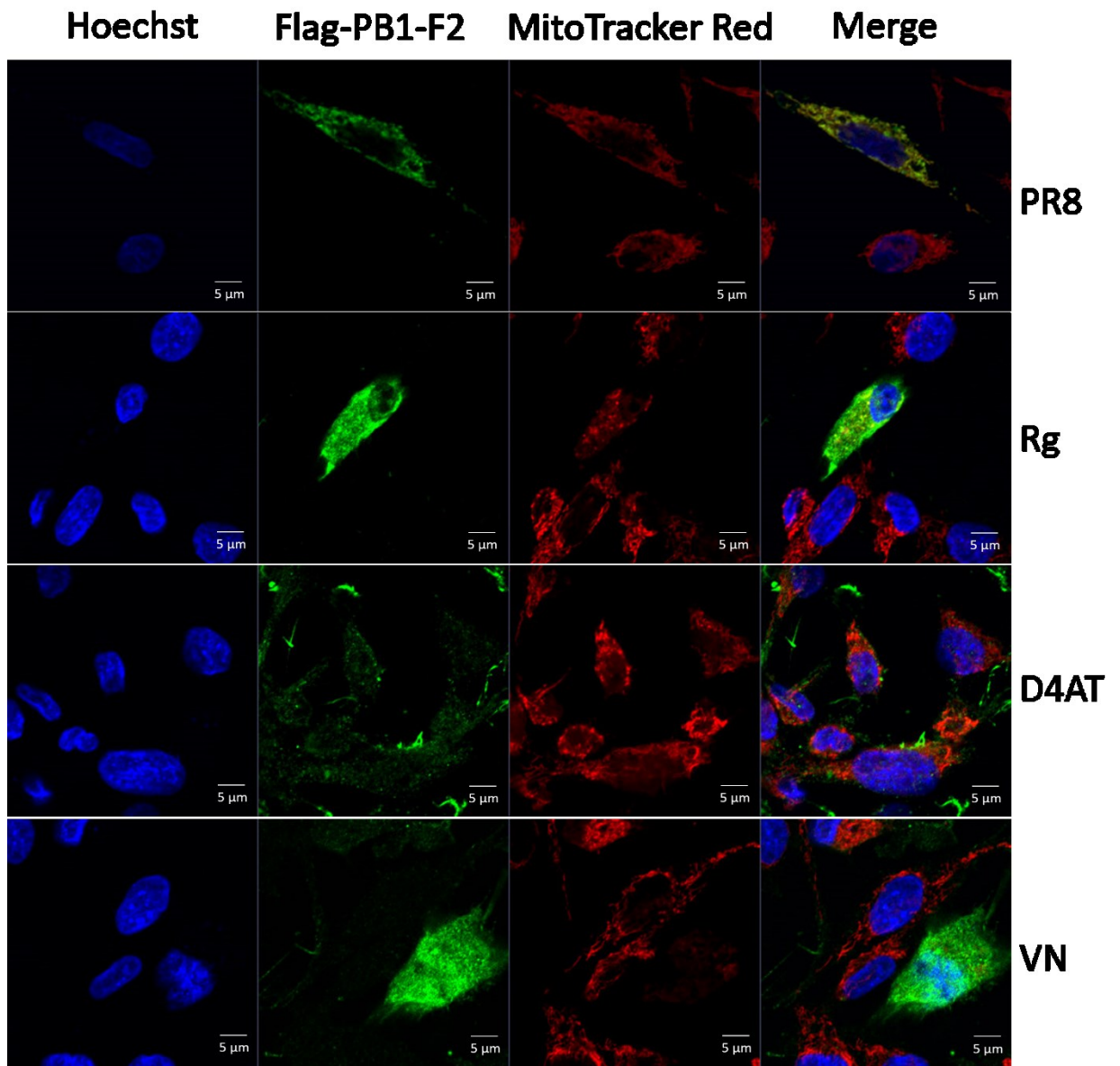


Figure 5.3 The distribution of HPAI H5N1 PB1-F2 in DF-1 cells.

DF-1 cells were transfected with the indicated expression vectors. 24 hours post-transfection, the cells were stained with MitoTracker Red and used to do immunofluorescence (IF) after fixation. The red and green signals indicate the location of mitochondria and the distributions of GST (A) or Flag (B) tagged PB1-F2 proteins, respectively. The distributions of V5-MAVS and GST only were used as the positive and the negative control, respectively in A. Flag-PB1-F2 (PR8) was used as the positive control in B.

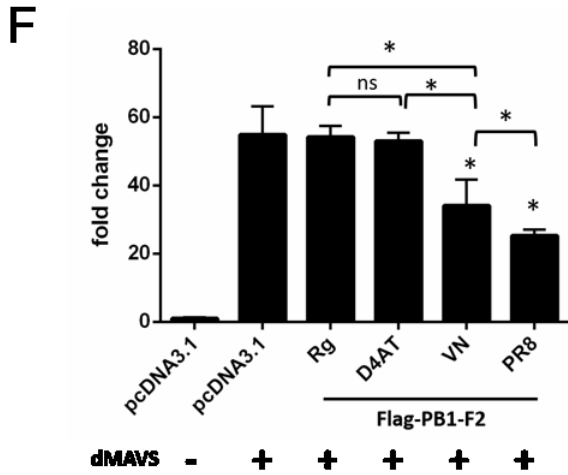
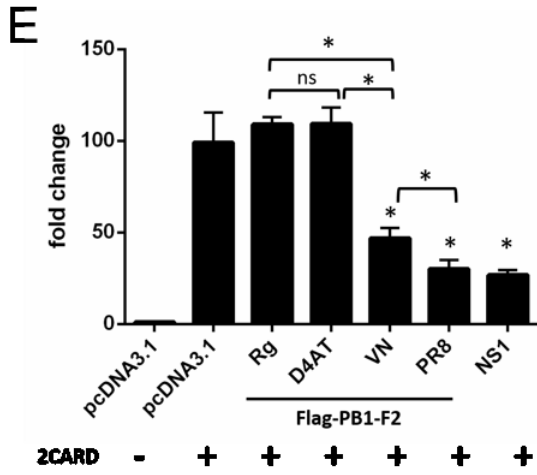
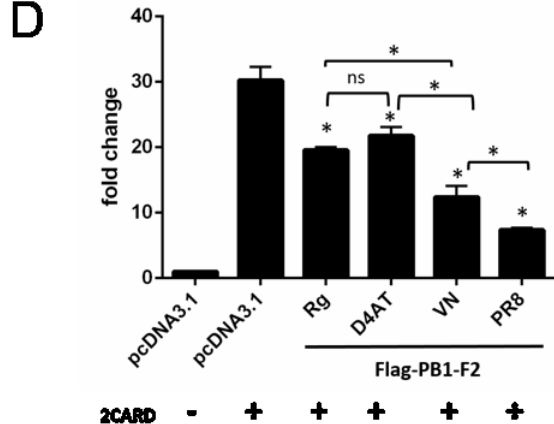
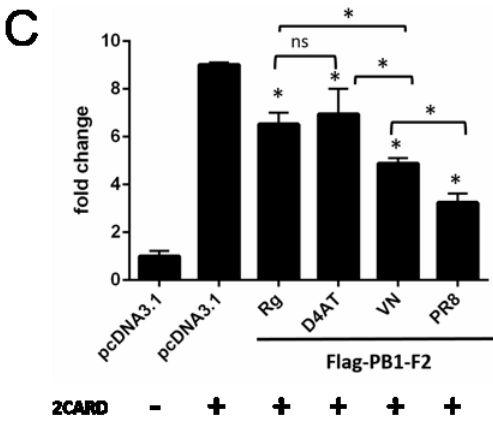
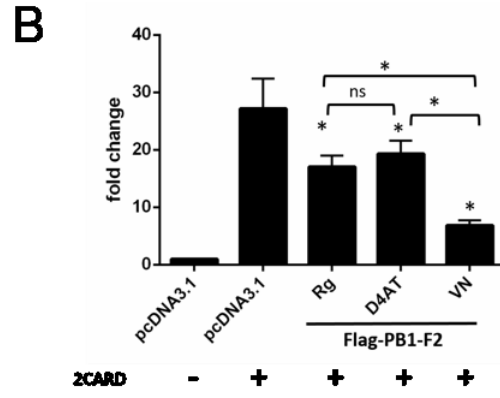
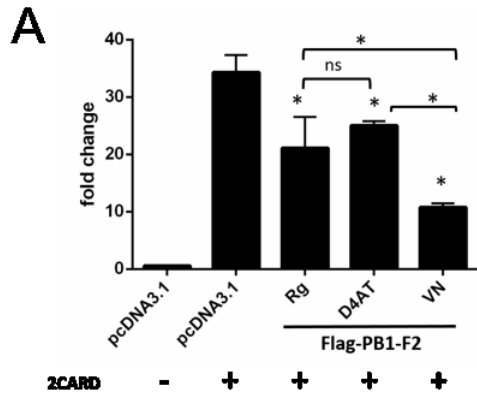


Figure 5.4 Among three tested H5N1 PB1-F2, VN1203 PB1-F2 has the strongest inhibitory activity to RIG-I 2CARD induced IFN- β reporter activity.

DF-1 cells were co-transfected with the expression vectors and chicken IFN- β reporter vector with GST (the negative control), GST-d2CARD (the stimuli of IFN- β promoter activity) (A-E) or V5-dMAVS (the stimuli of IFN- β promoter activity) (F). 24 hours post-transfection, the cells were lysed and the chIFN- β reporter activity was measured using the dual luciferase assay. The amount of transfected expression vectors was 250 ng/well in figure 5.4A, and 500 ng/well in the others. PR8 Flag-PB1-F2 and Flag-NS1 were transfected as the positive controls. The figures A to F show the results of six individual experiments. The mean of triplicate determinations (\pm SD) was shown in each figure. The significance was analyzed by Tukey's multiple comparison under one-way analysis of variance (ANOVA) using GraphPad Prism 6 software. (* $p < 0.05$, ns: not significant).

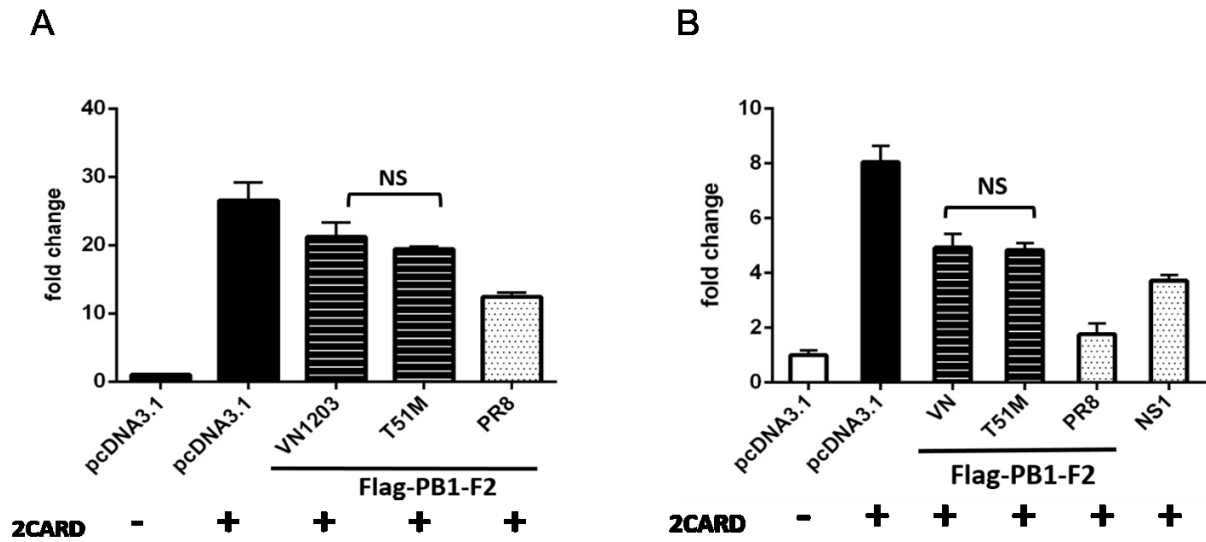


Figure 5.5 T51M point mutation alone does not change the function of wild-type VN PB1-F2.

DF-1 cells were co-transfected with the indicated vectors, chIFN- β , and *Renilla* luciferase vectors with GST or GST-d2CARD (the stimulator). Flag-PB1-F2 (PR8) and Flag-NS1 were used as the positive controls. 24 hours post-transfection, the cells were lysed, and the chIFN- β reporter activity was measured using dual luciferase assay. Significance was analyzed with Student's t-test. (* $p < 0.05$). (A) and (B) are two independent experiments.

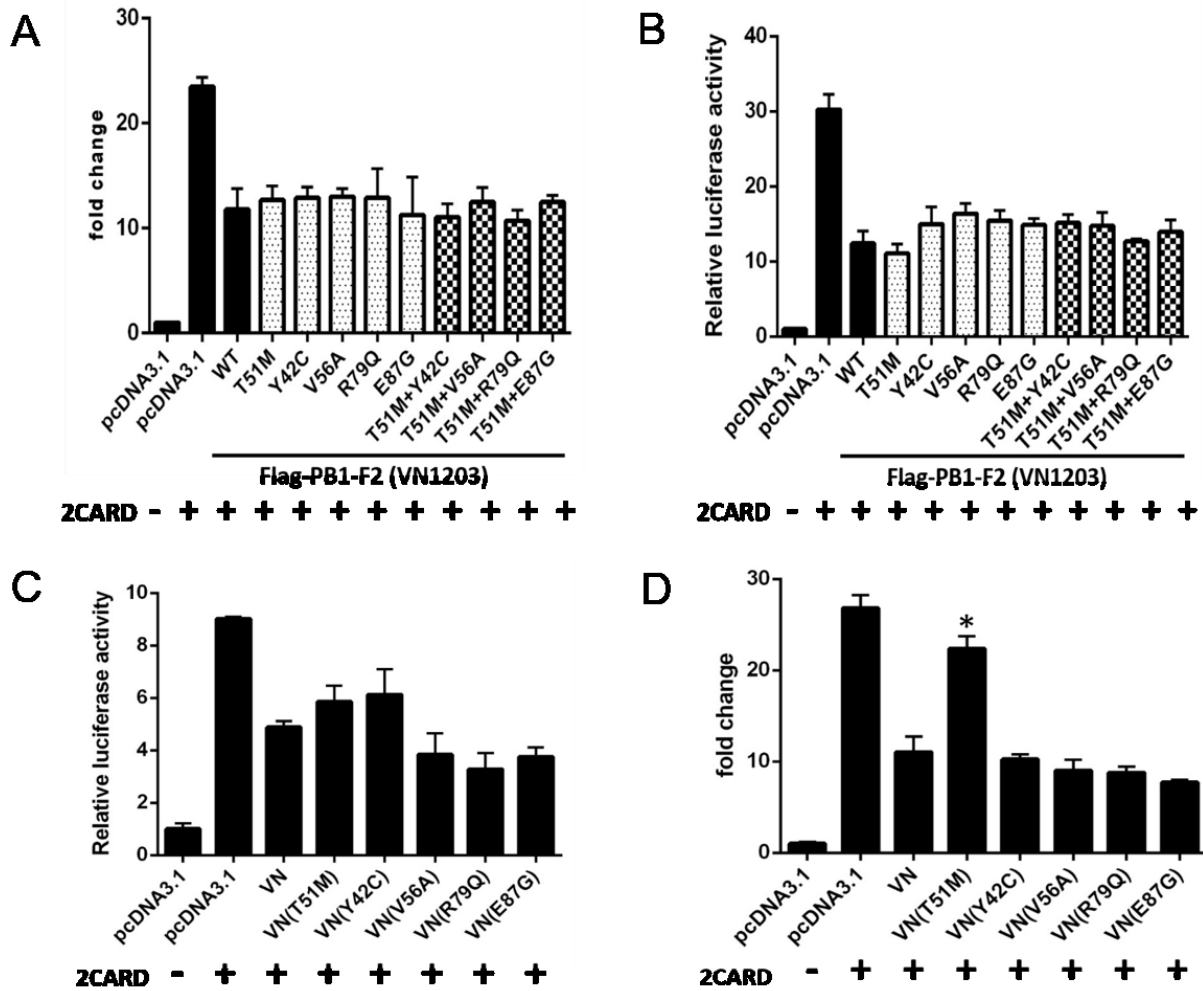
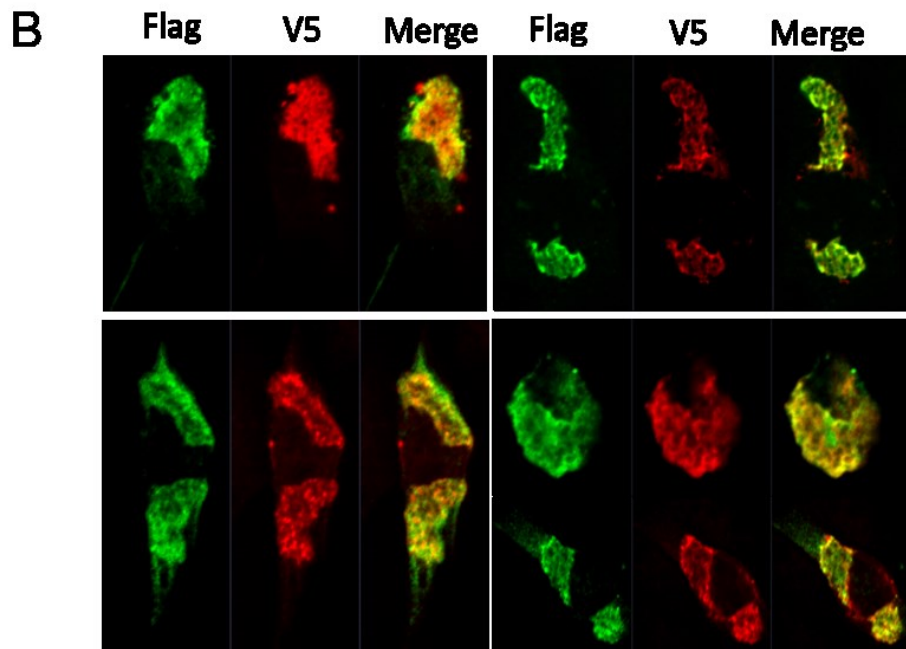
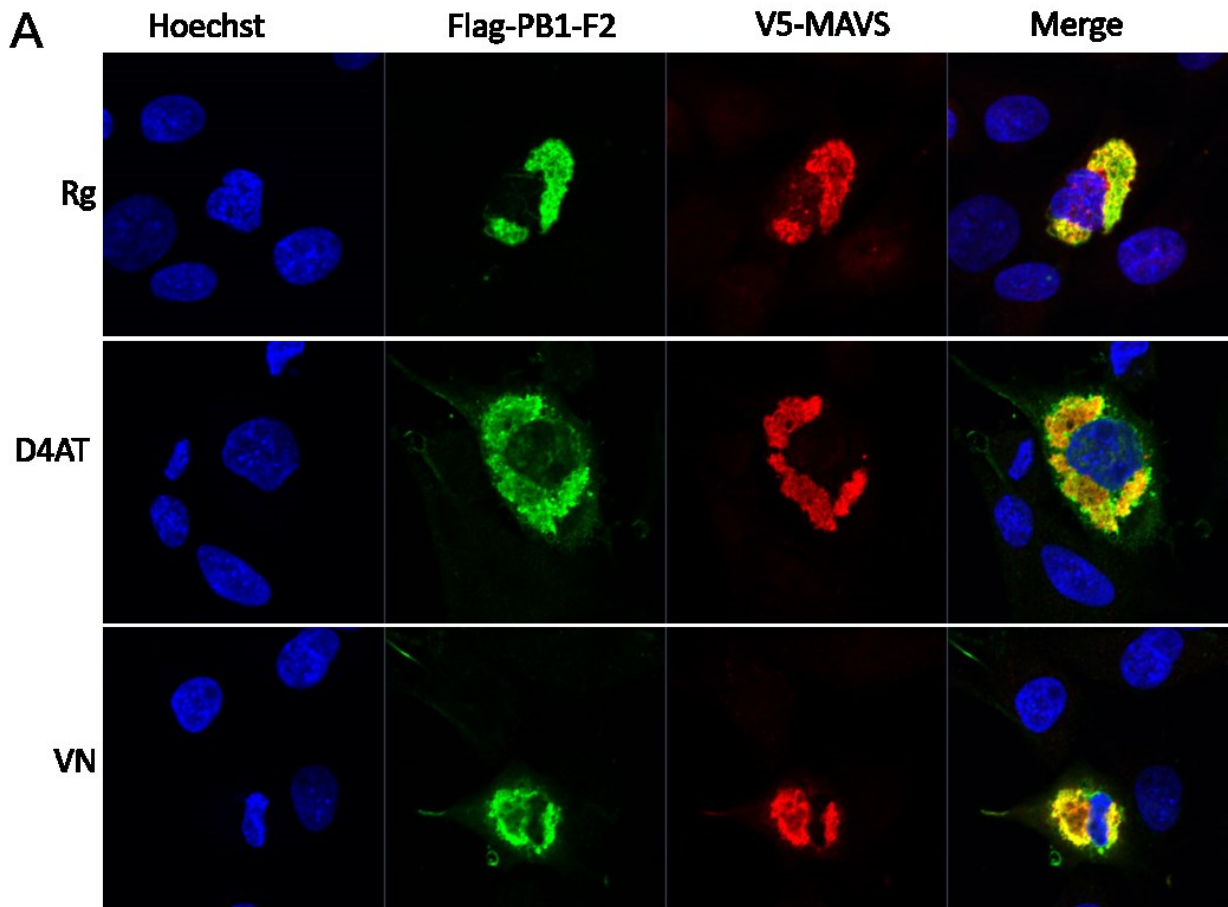


Figure 5.6 The indicated point mutations do not change the inhibiting function of wild-type VN PB1-F2 on RIG-I 2CARD mediated IFN- β reporter activity.

DF-1 cells were co-transfected with the indicated vectors, chIFN- β , and *Renilla* luciferase vectors with GST or GST-d2CARD. 24 hours post-transfection, the cells were lysed, and the chIFN- β activity was measured by dual luciferase assay. The influence of the single point mutations on the inhibitory effect of PB1-F2 from wild-type VN1203 were investigated in two individual experiments (A and B). The influence of both the single point mutations and two-point mutations on the inhibitory effect of PB1-F2 from wild-type VN1203 were tested in the other two experiments (C and D). Significance was analyzed between wild-type VN1203 and each mutation group with Student's t-test. (* $p < 0.05$)



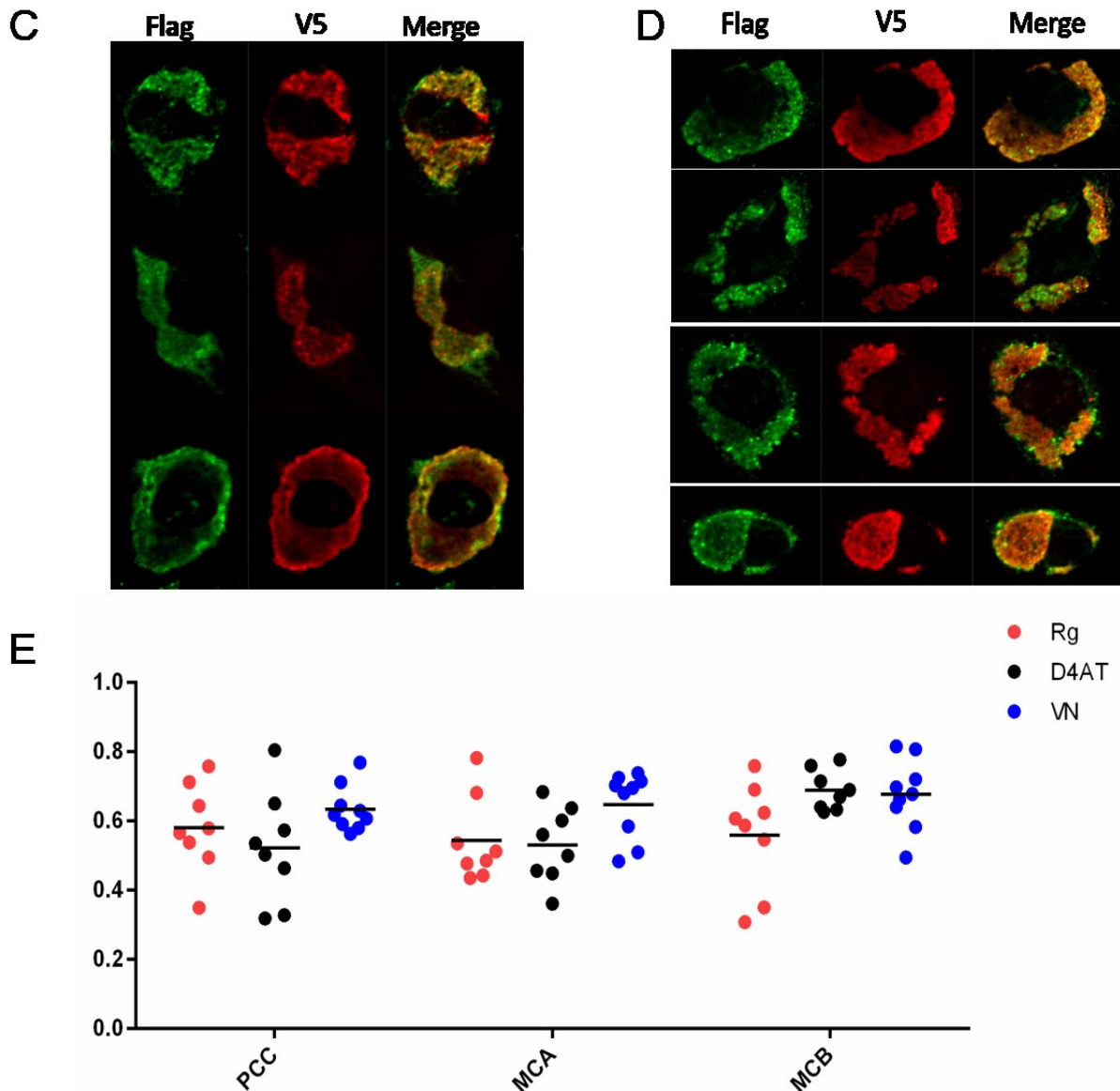


Figure 5.7 PB1-F2 co-localizes with duck MAVS.

(A) DF-1 cells overexpressing the indicated H5N1 Flag-PB1-F2 and V5-MAVS were fixed with 4% PFA and used to do IF staining, finally imaged using confocal microscopy. Blue, green, and red colors indicate nuclei, Flag-PB1-F2, and V5-dMAVS, respectively. (B, C, and D) The representative DF-1 cells of those used for the following quantitative analysis. (E) The co-localization between the indicated H5N1 Flag-PB1-F2 and V5-MAVS was quantitatively analyzed using Pearson's correlation coefficient (PCC) and Mander's coefficient (MCA and MCB). Bars show the mean value from at least 8 analyzed cells.

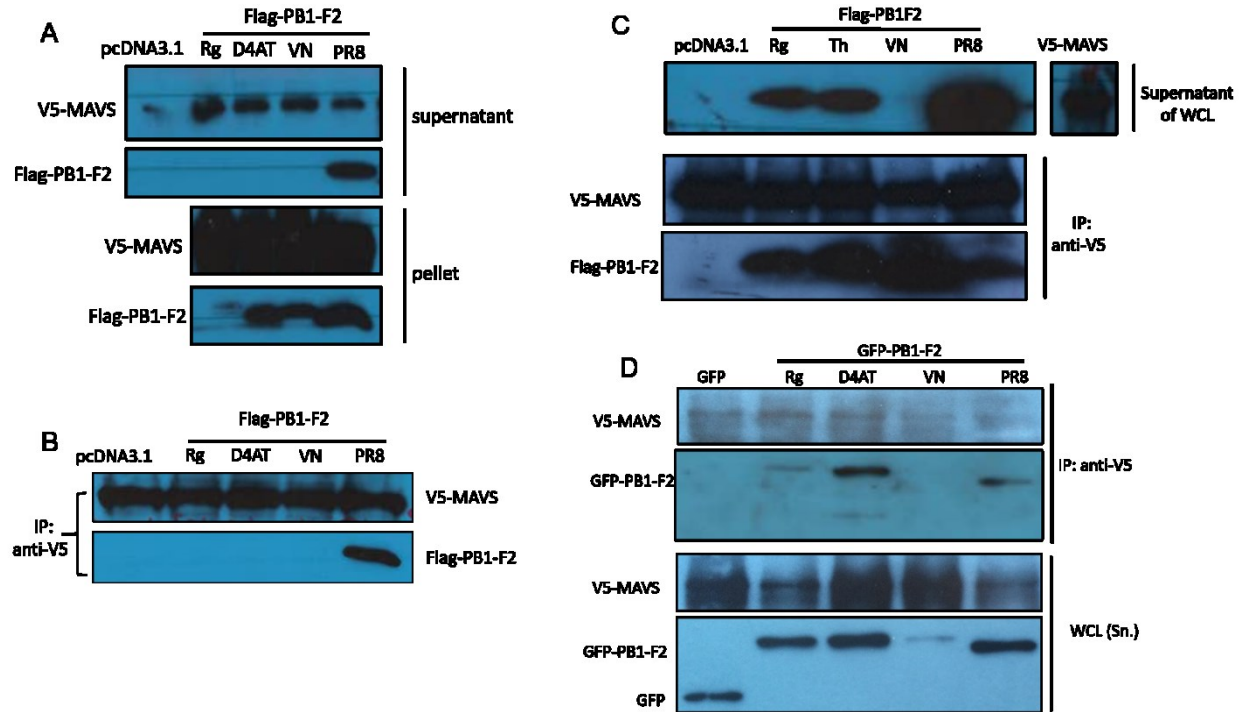


Figure 5.8 PB1-F2 was immunoprecipitated by duck MAVS.

DF-1 cells were co-transfected with the individual Flag-PB1-F2 expression vector and V5-MAVS. 24h post-transfection, the cells were lysed and used for Western Blot (A), or the supernatant of cell lysate was incubated with mouse anti-V5 antibody-coated beads overnight. Following the washing and elution steps, the eluted proteins were used to do Western Blot (B). (C) DF-1 cells were transfected with the indicated Flag-PB1-F2 and V5-MAVS, separately. 24h post-transfection, the supernatants of each Flag-PB1-F2 and V5-MAVS transfected cell lysate were mixed and incubated with mouse anti-V5 antibody-coated beads overnight. (D) DF-1 cells were co-transfected with the indicated GFP-PB1-F2 expression vector and V5-MAVS. 24h post-transfection, the supernatant of cell lysate was used for Western Blot or co-immunoprecipitation using mouse anti-V5 antibody-coated beads. The other steps were the same as above. The primary antibodies were rabbit anti-V5 antibody and mouse anti-Flag antibody or mouse anti-GFP antibody. The secondary antibodies were goat anti-mouse-HRP antibody and goat anti-rabbit-HRP antibody.

Chapter 6 Summary, Discussion and Future Directions

6.1 Summary of results

In this thesis, I studied host-pathogen molecular interactions between ducks and influenza A viruses, focusing on the RIG-I signalling pathway, which plays an essential role in the host innate immune response to influenza infection. When the study was started, only RIG-I was well characterized in ducks, but not the adaptor protein, MAVS, nor the duck RIG-I promoter. The influenza PB1-F2 protein from the PR8 strain had been found to inhibit interferon production in mammalian cells, but no experiments had been done in avian cells. Furthermore, PB1-F2 was found to contribute to the pathogenicity of VN1203, but the underlying molecular mechanism was unknown. In this thesis, I identified and characterized the duck RIG-I promoter, duck MAVS, as well as PB1-F2 from PR8 and three similar H5N1 virus strains, in DF-1 chicken cells. Schematic of my findings and the left questions in avian MAVS signaling pathway was shown in figure 6.1.

I showed that the duck RIG-I promoter activity was interferon-inducible downstream of MAVS signaling. Using serial deletion constructs, I demonstrated that the core promoter lies within the proximal 250 nucleotides and retains the ability to respond to MAVS signaling. I also identified the essential *cis* elements required for basal and inducible expression within this core promoter. Constitutive expression requires a GC-box and inducible expression requires an ISRE. Finally, I showed that chicken IRF7 induced the duck RIG-I promoter, and this required the ISRE site.

Additionally, I showed that duck MAVS has the expected, mitochondrial subcellular localization and conserved function in avian species. Duck MAVS also stimulates type I IFN promoter activity via interaction with duck RIG-I 2CARD. Although H5N1 PB1-F2 has a different subcellular distribution pattern compared to PR8 PB1-F2, I demonstrated that all tested PB1-F2 proteins had the inhibitory activity to duck RIG-I 2CARD mediated type I IFN induction, which may contribute to the virulence of PB1-F2 in ducks. Finally, using confocal microscopy and co-immunoprecipitation, I showed the interaction between duck MAVS and the tested PB1-F2 proteins which may explain the inhibition of RIG-I 2CARD mediated type I IFN promoter activity.

Collectively, these findings improved our understanding of the molecular interactions between influenza A viruses and ducks, as well as the transcriptional regulation of duck RIG-I expression, which may help us decipher therapeutic targets and guide us to make RNA virus-resistant transgenic chickens.

6.2 Discussion and future directions

To move forward the transgenic chicken project

I have identified the duRIG-I promoter and confirmed its constitutive and inducible activity in chicken cells. Using the serial deletion mutant constructs of the duRIG-I promoter, I further identified the core promoter region (250 bp upstream of TSS) and showed its sufficiency for the transcriptional regulation of duRIG-I. This result was consistent with the observation by Zhang Yu and co-workers (Zhang et al., 2018). Now we can move forward to put the full-length duck RIG-I cDNA under the control of the core promoter into chicken DF-1 cells using CRISPR-Cas9, followed by screening the successfully transfected cells and evaluating the character of these cells, to see whether duRIG-I is properly controlled by the duRIG-I promoter and whether it works well in chicken cells with its antiviral immune function, but without changing other features and functions of chicken cells. At the end, repeating the above procedure in chicken embryo cells will be needed to make transgenic chicken. Of course, there must be many challenges associated with this genetic manipulation process of avian embryos, including the location in the chicken genome, off-target, and the transfection efficiency, and so on. Recently, the Roslin Institute of University of Edinburgh and University of Cambridge has developed a genetically modified (GM) chicken expressing the short hairpin RNA molecule, decoy 5, which interferes with influenza virus replication through inhibiting virus polymerase proteins, consequently, successfully prohibits bird flu spreading within poultry flocks (Lyll et al., 2011).

To investigate the transcriptional regulation of duck RIG-I expression at epigenetic and microRNA level.

One CpG island was predicted between -284 bp and -55 bp of the duck RIG-I promoter in this study, which was also recently reported by another paper (Zhang et al., 2018), though they did not mention the exact location of the CpG island. The authors performed sub-bisulphite sequencing to determine the methylation status of the duck RIG-I promoter, but only one

methylation site was observed in one out of ten positive clones, indicating the expression of duck RIG-I was likely not regulated by DNA methylation (Zhang et al., 2018). Due to the repressive function to gene expression, CpG islands have been found to be associated with a majority of gene promoters, but lack DNA methylation. The methylated CpG islands are seen in malignant cells, leading to improper gene silencing, such as the tumor suppressor genes, or related to the tissue-specific gene expression (reviewed by Illingworth and Bird, 2009). RIG-I, as a cytosolic RNA sensor, is extensively expressed in the variety of tissues in a constitutive and inducible manner. Therefore, I speculate their conclusion that *duRIG-I* expression is not regulated by methylation of its promoter is correct, however, we need to do experiments to prove it in the future. Another group demonstrated that priming a human bronchial epithelial cell line with IFN- γ increased the cell resistance to respiratory syncytial virus (RSV) via the epigenetic regulation of human RIG-I expression by reducing the methylation of histone 3 lysine 9 at the RIG-I promoter (Spalluto et al., 2017). Thus, I wonder whether some other inflammatory cytokines or influenza viral proteins can also modulate antiviral gene expression via epigenetic mechanisms. NS1 from H3N2 possesses a histone H3-like sequence, through which NS1 suppresses the antiviral gene expression by interacting with human PAF1 transcription elongation complex (hPAF1C) (Marazzi et al., 2012).

Additionally, research increasingly suggests that microRNA (miRNA) negative gene regulation plays important roles in both healthy and disease states. MicroRNAs are involved in various biological and pathological processes by mediating degradation of mRNA or inhibition of translation via complete or partial binding to the 3'UTR of target gene transcripts (Othumpangat et al., 2014; Zhao et al., 2015). Several miRNAs that are involved in the immune response to influenza have been identified in mammals. For example, miRNA-485 was recently reported to markedly reduce the replication of H5N1 in mammalian cells through targeting the PB1 transcript, and the targeted region is conserved among various influenza A viruses (Ingle et al., 2015). However, when a decreased amount of H5N1 virus is present, it will switch to target the 3' UTR of human RIG-I mRNA to prevent excessive antiviral signaling (Ingle et al., 2015), which provided a basic understanding of the involvement of miRNA both in the maintenance of homeostasis and in restriction of IAV infection. Moreover, the miRNA expression patterns in several other animals infected with different influenza A virus strains have been described as well, for example, H5N1

infected macaque lung (Li et al., 2011), H5N3 infected chicken lung (Wang et al., 2012), H5N1 infected chicken and duck immune organs (spleen, thymus and bursa) (Li et al., 2015), and H1N2 infected pig lung (Skovgaard et al., 2013). Through comparing these reports, we found that miRNA122a, miRNA155 and miRNA146a were conserved miRNAs involved in influenza A virus infection among different species and they were predicted to target immune-related signaling pathways. Therefore, it is promising to elucidate whether duRIG-I expression is also regulated by miRNAs.

To determine whether chIRF7 and duIRF1 regulate duRIG-I expression via directly or indirectly interacting with the duRIG-I promoter.

The duck RIG-I promoter activity is increased downstream of MAVS signaling induced by the constitutively active RIG-I N-terminal 2CARD or the MDA5 agonist, poly (I:C), in a positive feedback loop. Induction may be indirect through elicited interferon-beta or direct through stimulation of an interferon regulatory factor (IRF1 or IRF7), or potentially both. This would be consistent with the induction of human RIG-I by IFN-alpha in A549 lung epithelial cells (Matikainen et al., 2006), and upregulation by IFN-beta or poly (I:C) in a variety of human cell lines (Su et al., 2007).

The interferon-inducible promoter activity of duck RIG-I depends on the presence of the ISRE, which was identified at position -103 to -90 in the duck promoter. Zhang and colleagues also predicted the same IRF1 site in the duck promoter using TRANSFAC 4.0 (Zhang et al., 2018), however, they did not experimentally test it. The duck ISRE bears a strong similarity to the IRF1 binding site in the human RIG-I promoter located between -17 and -4, which has the sequence "ACTTTCGATTTCC" (Su et al., 2007). Because human IRF1 is induced by type-I IFN and directly controls human RIG-I expression (Su et al., 2007), we expected the chIRF1 to activate the duck RIG-I promoter, however, it did not. Unfortunately, we have no assay to confirm that the chIRF1 is functional, however, we did observe both cytoplasmic and nuclear staining with this mCherry tagged protein, suggesting it can access the nucleus. Human IRF1 was shown to directly bind the IRF1 site by EMSA (Su et al., 2007). IRF1 was also confirmed to play a role in RIG-I regulation by knockdown using siRNA in HeLa cells (Hayakari et al., 2016), however, these latter researchers noted nuclear accumulation of IRF1 was not consistent with timing of

RIG-I induction by poly (I:C), while nuclear accumulation of IRF3 was consistent (Hayakari et al., 2016). Using Chromatin immunoprecipitation (ChIP) analysis and electrophoretic mobility shift assay (EMSA) they showed that human IRF3 is bound to the RIG-I promoter in the same region previously predicted as the IRF1 binding site. Downstream of RIG-I and MAVS signaling, IRF3 and IRF7 are activated by phosphorylation, translocate to the nucleus and induce expression of interferon-stimulated genes (Lin et al., 1998; Paz et al., 2006). In avian species, IRF3 is missing (Cormican et al., 2009; reviewed by Magor et al., 2013), and IRF7 is thought to fulfil this role. Indeed, our group showed that mCherry-tagged IRF7 translocated to the nucleus with increased MAVS signaling, which was induced by RIG-I CARD domains. I also demonstrated that chIRF7 activates RIG-I and that this requires the ISRE site, as the mutation or deletion of this site abrogates the inducible promoter activity. I do not yet know whether this is through direct interaction, analogous to IRF3 binding to an ISRE in the human RIG-I promoter (Hayakari et al., 2016), or indirectly through the induction of IFN- β , and induced ISGs. Thus, ChIP and EMSA experiments are necessary to determine whether chIRF7 interacting with duck RIG-I promoter directly in the future.

In contrast, duIRF1 induced activity of the duck RIG-I promoter, and the deletion of ISRE did not impair this function, suggesting like huIRF1, duIRF1 also plays a vital role in the transcriptional regulation of duck RIG-I inducible expression, which requires an element in the most proximal region, 73 bp upstream sequence, rather than the putative ISRE or acts indirectly to induce something. Most recently, duck IRF1 has been reported as a positive regulator of duck antiviral innate immunity to induce the expression of type I IFN- β and ISGs, and is induced by viral infection and poly (I:C) (Qian et al., 2018). In the future, we could further identify whether duIRF1 plays a role in the transcriptional regulation of duRIG-I expression through directly interacting with the promoter region using ChIP and EMSA. If it does, we can further identify the binding sites in the promoter region.

Amino acid residues 68-71 are important for cell expression pattern and function of PB1-F2

In my study, PR8 PB1-F2 and H5N1 PB1-F2 (Rg/D4AT/VN) were predominantly distributed in mitochondria and throughout the cells, respectively, which was consistent with the observation

by Chi-Jene Chen and coworkers in HeLa cells (Chen et al., 2010). The C-terminal residues from 65 to 87 were supposed to be the mitochondrial targeting sequence by Gibbs and coworkers (Gibbs et al., 2003). Compared to H5N1 PB1-F2 (Rg/D4AT/VN) to PR8 PB1-F2, four amino acid residues from 68 to 71 are entirely different, TQGS in H5N1 PB1-F2 (Rg/D4AT/VN), while, ILVF in PR8 PB1-F2. These four residues have been shown to determine the subcellular distribution of PB1-F2 by comparing the distribution of GFP-tagged PB1-F2 from PR8, HK156, and the chimeric PB1-F2 proteins in HeLa cells (Cheng et al., 2017). HK156 is short for another HPAI H5N1 virus strain: A/Hong Kong/156/1997 (H5N1), which is bearing TQDS residues in position 68 to 71 of PB1-F2 protein. In their study, they showed PB1-F2 with ILVF was localized to mitochondria, while PB1-F2 with TQDS was localized to cytoplasm and nucleus (Cheng et al., 2017), which was consistent with our observation. In contrast, another group did not observe the different subcellular localization in MDCK cells infected with wild-type PR8 and PR8 with three mutations (I68T, L69Q, and V70G) in PB1-F2. In both cases, they found PB1-F2 was predominantly distributed in the mitochondria (Alymova et al., 2014). These data again demonstrated the specificity of PB1-F2 from different viral strains and cell types, not to mention the species.

Surprisingly, despite the different subcellular expression patterns, the interactions between PB1-F2 from H5N1 (VN/Rg/D4AT) and PR8 strains with duMAVS were still detected in DF-1 cells using co-localization and co-IP in my study. But the expression patterns of duMAVS and H5N1 PB1-F2 in co-transfected cells became more aggregated than the ones of duMAVS or H5N1 PB1-F2 individually transfected cells, and H5N1 PB1-F2 was not detected in the supernatant, but in the pellet of the cell lysate when we co-transfected with duMAVS into DF-1 cells. These data further confirmed the functional form of MAVS is aggregated structure. It also suggested H5N1 PB1-F2 proteins may undergo re-distribution in DF-1 cells upon activation of MAVS. As reported previously, MAVS can form very large SDS-resistant prion-like aggregates upon activation by Sendai virus infection or overexpression (Hou et al., 2011). Recently, another group also noticed that the overexpression of MAVS triggered the translocation of NLRP3 from the cytosol to the mitochondria and the formation of NLRP3 oligomers in 293T cells (Park et al., 2013). They demonstrated the association between MAVS and NLRP3 using confocal microscopy and co-IP. As mentioned above, PB1-F2 from both avian and mammalian influenza

viruses have been involved in the activation of NLRP3 in mammals, thus, I speculate that H5N1 PB1-F2 proteins may also play a role in duck inflammatory response mediated by the NLRP3 inflammasome complex.

I also noticed that PR8 (H1N1) PB1-F2 had a higher protein expression level and a more significant inhibitory activity to type I IFN induction than H5N1 PB1-F2 proteins. These observations were consistent with the previous findings: PR8 PB1-F2 with ILVF (68-71) had a longer protein half-life than HK156 PB1-F2 with TQDS (68-71), and the mutation of the amino acids at 68 to 71 from ILVF to TQDS significantly decreased the inhibition by PR8 PB1-F2 of Sendai virus-induced IFN- β promoter activity from 81% to 33% (Cheng et al., 2017). Moreover, I68, L69, and V70 of PR8 PB1-F2 have been identified as a cytotoxic sequence because they can induce necrotic death in approximately 80% of MDCK and A549 cells, on the other hand, T68, Q69, and G70 only resulted in 5% cell death (Alymova et al., 2014). These data suggested the importance of these four amino acid residues for determining the protein stability, subcellular expression pattern, and the function of PB1-F2.

To determine the amino acids responsible for the different inhibitory activities of VN1203 PB1-F2 compared to the other two H5N1 PB1-F2 proteins (rgVN1203 and D4AT), I generated all possible PB1-F2 mutants with a single or a double mutation. Unexpectedly, none of the single or double mutants reduced the inhibition of VN1203 PB1-F2 induction of IFN- β promoter activity, suggesting that the inhibitory function is the result of the cooperation of three amino acids. Irina et al. also showed that any single mutation of I68T, L69Q, or V70G did not cause the alteration of the cytotoxicity of the PR8 PB1-F2 indicating that three or at least two amino acids are prerequisites for this function (Alymova et al., 2014).

To determine the domain of duMAVS responsible for its function, distribution and interaction with PB1-F2 by generating chimeric duMAVS constructs.

Like huMAVS, duMAVS is also distributed in the mitochondria of chicken DF-1 cells and contributes to the induction of type I IFN, although they only share 28% amino acid identity. I also observed the interaction of PB1-F2 proteins from PR8 and H5N1 (Rg/D4AT/VN) with duMAVS. However, which domain of duMAVS is responsible for its distribution and function,

and which domain is involved in the interaction with PB1-F2 proteins are still unclear. In the future, we could construct the chimeric plasmids of duMAVS to identify the related domains.

To explore other virulence factors in H5N1 or other functions of PB1-F2 in ducks.

Through comparing the inhibitory activities of PB1-F2 from three similar H5N1 subtypes, we showed that VN1203 PB1-F2 is a stronger inhibitor of type I IFN production than rgVN1203, which provides a plausible explanation of why introducing three amino acid mutations to PB1-F2 attenuated the virulence of wild-type VN1203 (Marjuki et al., 2010). Unexpectedly, VN1203 PB1-F2 also showed a stronger inhibitory activity than D4AT PB1-F2, although D4AT has a higher lethality, which suggested there might be other stronger virulence factors in D4AT than PB1-F2, or PB1-F2 may be involved in other immune-related processes other than modulating the induction of IFN- β . But, this unexpected higher IFN response induced by D4AT than by VN1203 has been observed earlier in ducks infected with both similar H5N1 viruses (Saito et al., 2018). Comparing VN1203 with D4AT, there are several more amino acid substitutions in PB2, PA, HA, NP, NA and NEP in addition to the three in PB1-F2. More importantly, there are five amino acid substitutions and a ten amino acid deletion (from 216 to 225 residues) in the C-terminal region of NS1 in VN1203 viral strain (Saito et al., 2018). Considering the importance of the C-terminal region of NS1 in determining the virulence of influenza A virus, I speculated the higher lethality of D4AT to ducks is due, in part, to the virulence factor, NS1. Zhu et al. reported the five amino acids deletion from 191 to 195 of NS1 significantly attenuated the virulence of A/swine/Fujian/1/01 (SW/FJ/01) (H5N1) in chickens and affected its inhibition of IFN induction (Zhu et al., 2008). In contrast, Zielecki *et al.* showed rescuing the deleted ten amino acids in the C-terminal region of wild type VN1203 NS1 did not change its inhibition to IFN- β promoter activity in MDCK cells, suggesting this deletion was not important to the virulence of H5N1 viruses (Zielecki et al., 2010). Whether the five amino acid substitutions in NS1 affected the virulence of VN1203 needs to be further tested.

“Cytokine storm”, associated with excessive proinflammatory cytokines, such as TNF- α , IL-1 β , and IL-6, is understood to contribute to the severe outcome of HPAI infections by leading to extensive tissue damage (Tisoncik et al., 2012). Recent studies demonstrated that PB1-F2 proteins from both H7N9 and H1N1 strains mediated activation of the NLRP3 inflammasome

and the subsequent inflammatory response in human and mouse models (McAuley et al., 2013). Additionally, the aggregation of PB1-F2 was a prerequisite for the induction of NLRP3 activation (McAuley et al., 2013). PB1-F2 peptide treatment induced robust mitochondrial reactive oxygen production, which can activate NLRP3 (Pinar et al., 2017). Moreover, our lab has also detected the upregulation of the proinflammatory cytokine, IL-1 β , known as the maker for inflammasome complex activation, both in VN1203 and in D4AT-infected ducks (Saito et al., 2018). Thus, to investigate the potential interactions of H5N1 PB1-F2 proteins with the duck NLRP3 inflammasome complex is also of interest.

To further confirm that PB1-F2 proteins inhibit MAVS signaling pathway by interacting with duck MAVS

Here, I observed PB1-F2 proteins from both PR8 and H5N1 inhibited MAVS-signaling pathway in chicken cells, and I also observed the possible interaction between all these PB1-F2 proteins and duck MAVS using confocal microscopy and co-IP. However, these data were not enough to support that inhibition of innate signaling was due to their interaction with duck MAVS, because these inhibitory experiments were done in chicken cells without duck MAVS. Considering the conservation of MAVS in different species, probably these PB1-F2 proteins also interact with chicken MAVS. In order to confirm that the interaction between PB1-F2 proteins and duck MAVS is responsible to their inhibitory activities to duck MAVS signaling pathway, I think, firstly, we should identify the interacting region of PB1-F2 with duck MAVS, and then making mutations to abolish their interactions and to see whether their inhibitory activities will be affected by these mutations. If not, probably, their inhibitory activities are due to some other factors downstream of MAVS in this signaling pathway, such as, IKK- β (Reis and McCauley, 2013) or NDP52 (Leymarie et al., 2017).

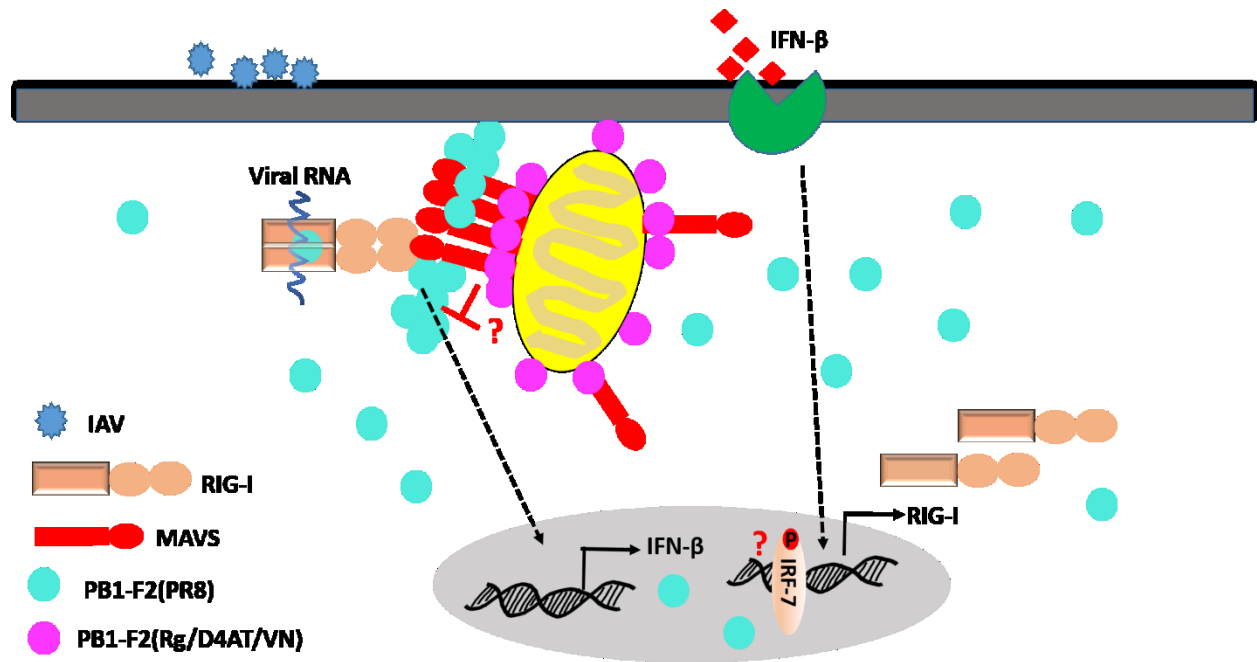


Figure 6.1 Overview of my findings and questions left unanswered

The adaptor protein, duck MAVS, is distributed in the mitochondria of avian cells. Duck MAVS interacts with duck RIG-I 2CARD. PR8 PB1-F2 is distributed in the mitochondria of the avian cells, while, PB1-F2 from H5N1 (Rg/D4AT/VN) are distributed throughout the cells. However, upon activation of duck MAVS through its filamentous conformation, PB1-F2 from H5N1 (Rg/D4AT/VN) will be attracted to MAVS and form aggregates. All tested PB1-F2 proteins were observed to interact with duck MAVS. All tested PB1-F2 proteins inhibit MAVS signaling pathway. However, whether the inhibitory effect is due to their interaction is still unknown. Additionally, chIRF7 induces the promoter activity of duck RIG-I using the ISRE. But, whether it directly binds to this element has not been elucidated. Although duck RIG-I and duck MAVS interactions have been characterized, the downstream signalling cascade is still a puzzle.

References

- 1980a. Antigenic shift and drift. *Nature* 283, 524-525.
- 1980b. A revision of the system of nomenclature for influenza viruses: a WHO memorandum. *Bull World Health Organ* 58, 585-591.
1998. Update: isolation of avian influenza A(H5N1) viruses from humans--Hong Kong, 1997-1998. *MMWR Morb Mortal Wkly Rep* 46, 1245-1247.
- Abderrazak, A., Syrovets, T., Couchie, D., El Hadri, K., Friguet, B., Simmet, T., Rouis, M., 2015. NLRP3 inflammasome: from a danger signal sensor to a regulatory node of oxidative stress and inflammatory diseases. *Redox Biol* 4, 296-307.
- Ablasser, A., Poeck, H., Anz, D., Berger, M., Schlee, M., Kim, S., Bourquin, C., Goutagny, N., Jiang, Z., Fitzgerald, K.A., Rothenfusser, S., Endres, S., Hartmann, G., Hornung, V., 2009. Selection of molecular structure and delivery of RNA oligonucleotides to activate TLR7 versus TLR8 and to induce high amounts of IL-12p70 in primary human monocytes. *J Immunol* 182, 6824-6833.
- Akarsu, H., Burmeister, W.P., Petosa, C., Petit, I., Muller, C.W., Ruigrok, R.W., Baudin, F., 2003. Crystal structure of the M1 protein-binding domain of the influenza A virus nuclear export protein (NEP/NS2). *EMBO J* 22, 4646-4655.
- Akira, S., Uematsu, S., Takeuchi, O., 2006. Pathogen recognition and innate immunity. *Cell* 124, 783-801.
- Alexander, D.J., Parsons, G., Manvell, R.J., 1986. Experimental assessment of the pathogenicity of eight avian influenza A viruses of H5 subtype for chickens, turkeys, ducks and quail. *Avian pathology : journal of the W.V.P.A* 15, 647-662.
- Allen, I.C., Scull, M.A., Moore, C.B., Holl, E.K., McElvania-TeKippe, E., Taxman, D.J., Guthrie, E.H., Pickles, R.J., Ting, J.P., 2009. The NLRP3 inflammasome mediates in vivo innate immunity to influenza A virus through recognition of viral RNA. *Immunity* 30, 556-565.
- Alymova, I.V., Samarasinghe, A., Vogel, P., Green, A.M., Weinlich, R., McCullers, J.A., 2014. A novel cytotoxic sequence contributes to influenza A viral protein PB1-F2 pathogenicity and predisposition to secondary bacterial infection. *J Virol* 88, 503-515.

- Amorim, M.J., Bruce, E.A., Read, E.K., Foeglein, A., Mahen, R., Stuart, A.D., Digard, P., 2011. A Rab11- and microtubule-dependent mechanism for cytoplasmic transport of influenza A virus viral RNA. *J Virol* 85, 4143-4156.
- Anderson, R.J., 1958. Influenza: 1957-1958 pandemic. *GP* 17, 110-114.
- Arzt, S., Baudin, F., Barge, A., Timmins, P., Burmeister, W.P., Ruigrok, R.W., 2001. Combined results from solution studies on intact influenza virus M1 protein and from a new crystal form of its N-terminal domain show that M1 is an elongated monomer. *Virology* 279, 439-446.
- Arzt, S., Petit, I., Burmeister, W.P., Ruigrok, R.W., Baudin, F., 2004. Structure of a knockout mutant of influenza virus M1 protein that has altered activities in membrane binding, oligomerisation and binding to NEP (NS2). *Virus Res* 99, 115-119.
- Atsmon, J., Caraco, Y., Ziv-Sefer, S., Shaikevich, D., Abramov, E., Volokhov, I., Bruzil, S., Haima, K.Y., Gottlieb, T., Ben-Yedidia, T., 2014. Priming by a novel universal influenza vaccine (Multimeric-001)-a gateway for improving immune response in the elderly population. *Vaccine* 32, 5816-5823.
- Balachandran, S., Thomas, E., Barber, G.N., 2004. A FADD-dependent innate immune mechanism in mammalian cells. *Nature* 432, 401-405.
- Barber, M.R., Aldridge, J.R., Jr., Fleming-Canepa, X., Wang, Y.D., Webster, R.G., Magor, K.E., 2013. Identification of avian RIG-I responsive genes during influenza infection. *Mol Immunol* 54, 89-97.
- Barber, M.R., Aldridge, J.R., Jr., Webster, R.G., Magor, K.E., 2010. Association of RIG-I with innate immunity of ducks to influenza. *Proc Natl Acad Sci U S A* 107, 5913-5918.
- Barral, P.M., Sarkar, D., Su, Z.Z., Barber, G.N., DeSalle, R., Racaniello, V.R., Fisher, P.B., 2009. Functions of the cytoplasmic RNA sensors RIG-I and MDA-5: key regulators of innate immunity. *Pharmacol Ther* 124, 219-234.
- Baudin, F., Bach, C., Cusack, S., Ruigrok, R.W., 1994. Structure of influenza virus RNP. I. Influenza virus nucleoprotein melts secondary structure in panhandle RNA and exposes the bases to the solvent. *EMBO J* 13, 3158-3165.
- Beato, M.S., Toffan, A., De Nardi, R., Cristalli, A., Terregino, C., Cattoli, G., Capua, I., 2007. A conventional, inactivated oil emulsion vaccine suppresses shedding and prevents viral

- meat colonisation in commercial (Pekin) ducks challenged with HPAI H5N1. *Vaccine* 25, 4064-4072.
- Berger, M., Ablasser, A., Kim, S., Bekeredjian-Ding, I., Giese, T., Endres, S., Hornung, V., Hartmann, G., 2009. TLR8-driven IL-12-dependent reciprocal and synergistic activation of NK cells and monocytes by immunostimulatory RNA. *J Immunother* 32, 262-271.
- Bergmann, M., Garcia-Sastre, A., Carnero, E., Pehamberger, H., Wolff, K., Palese, P., Muster, T., 2000. Influenza virus NS1 protein counteracts PKR-mediated inhibition of replication. *J Virol* 74, 6203-6206.
- Berke, I.C., Modis, Y., 2012. MDA5 cooperatively forms dimers and ATP-sensitive filaments upon binding double-stranded RNA. *EMBO J* 31, 1714-1726.
- Berke, I.C., Yu, X., Modis, Y., Egelman, E.H., 2012. MDA5 assembles into a polar helical filament on dsRNA. *Proc Natl Acad Sci U S A* 109, 18437-18441.
- Bertram, S., Glowacka, I., Steffen, I., Kuhl, A., Pohlmann, S., 2010. Novel insights into proteolytic cleavage of influenza virus hemagglutinin. *Rev Med Virol* 20, 298-310.
- Bevins, S.N., Pedersen, K., Lutman, M.W., Baroch, J.A., Schmit, B.S., Kohler, D., Gidlewski, T., Nolte, D.L., Swafford, S.R., DeLiberto, T.J., 2014. Large-scale avian influenza surveillance in wild birds throughout the United States. *PLoS One* 9, e104360.
- Blaine, A.H., Miranzo-Navarro, D., Campbell, L.K., Aldridge, J.R., Jr., Webster, R.G., Magor, K.E., 2015. Duck TRIM27-L enhances MAVS signaling and is absent in chickens and turkeys. *Mol Immunol* 67, 607-615.
- Blyth, G.A., Chan, W.F., Webster, R.G., Magor, K.E., 2016. Duck Interferon-Inducible Transmembrane Protein 3 Mediates Restriction of Influenza Viruses. *J Virol* 90, 103-116.
- Brown, J.D., Stallknecht, D.E., Beck, J.R., Suarez, D.L., Swayne, D.E., 2006. Susceptibility of North American ducks and gulls to H5N1 highly pathogenic avian influenza viruses. *Emerg Infect Dis* 12, 1663-1670.
- Brownlie, R., Allan, B., 2011. Avian toll-like receptors. *Cell Tissue Res* 343, 121-130.
- Brownlie, R., Zhu, J.Z., Allan, B., Mutwiri, G.K., Babiuk, L.A., Potter, A., Griebel, P., 2009. Chicken TLR21 acts as a functional homologue to mammalian TLR9 in the recognition of CpG oligodeoxynucleotides. *Molecular Immunology* 46, 3163-3170.
- Bruns, K., Studtucker, N., Sharma, A., Fossen, T., Mitzner, D., Eissmann, A., Tessmer, U., Roder, R., Henklein, P., Wray, V., Schubert, U., 2007. Structural characterization and

- oligomerization of PB1-F2, a proapoptotic influenza A virus protein. *J Biol Chem* 282, 353-363.
- Buehler, J., Navi, D., Lorusso, A., Vincent, A., Lager, K., Miller, C.L., 2013. Influenza A virus PB1-F2 protein expression is regulated in a strain-specific manner by sequences located downstream of the PB1-F2 initiation codon. *J Virol* 87, 10687-10699.
- Bui, M., Wills, E.G., Helenius, A., Whittaker, G.R., 2000. Role of the influenza virus M1 protein in nuclear export of viral ribonucleoproteins. *J Virol* 74, 1781-1786.
- Cady, S.D., Schmidt-Rohr, K., Wang, J., Soto, C.S., Degrado, W.F., Hong, M., 2010. Structure of the amantadine binding site of influenza M2 proton channels in lipid bilayers. *Nature* 463, 689-692.
- Cagle, C., To, T.L., Nguyen, T., Wasilenko, J., Adams, S.C., Cardona, C.J., Spackman, E., Suarez, D.L., Pantin-Jackwood, M.J., 2011. Pekin and Muscovy ducks respond differently to vaccination with a H5N1 highly pathogenic avian influenza (HPAI) commercial inactivated vaccine. *Vaccine* 29, 6549-6557.
- Calder, L.J., Wasilewski, S., Berriman, J.A., Rosenthal, P.B., 2010. Structural organization of a filamentous influenza A virus. *Proc Natl Acad Sci U S A* 107, 10685-10690.
- Capua, I., Alexander, D.J., 2008. Avian influenza vaccines and vaccination in birds. *Vaccine* 26 Suppl 4, D70-73.
- Castanier, C., Zemirli, N., Portier, A., Garcin, D., Bidere, N., Vazquez, A., Arnoult, D., 2012. MAVS ubiquitination by the E3 ligase TRIM25 and degradation by the proteasome is involved in type I interferon production after activation of the antiviral RIG-I-like receptors. *BMC Biol* 10, 44.
- Chen, B.J., Leser, G.P., Morita, E., Lamb, R.A., 2007. Influenza virus hemagglutinin and neuraminidase, but not the matrix protein, are required for assembly and budding of plasmid-derived virus-like particles. *J Virol* 81, 7111-7123.
- Chen, B.J., Takeda, M., Lamb, R.A., 2005. Influenza virus hemagglutinin (H3 subtype) requires palmitoylation of its cytoplasmic tail for assembly: M1 proteins of two subtypes differ in their ability to support assembly. *J Virol* 79, 13673-13684.
- Chen, C.J., Chen, G.W., Wang, C.H., Huang, C.H., Wang, Y.C., Shih, S.R., 2010. Differential localization and function of PB1-F2 derived from different strains of influenza A virus. *J Virol* 84, 10051-10062.

- Chen, I.Y., Ichinohe, T., 2015. Response of host inflammasomes to viral infection. *Trends Microbiol* 23, 55-63.
- Chen, S., Cheng, A., Wang, M., 2013a. Innate sensing of viruses by pattern recognition receptors in birds. *Vet Res* 44, 82.
- Chen, W., Calvo, P.A., Malide, D., Gibbs, J., Schubert, U., Bacik, I., Basta, S., O'Neill, R., Schickli, J., Palese, P., Henklein, P., Bennink, J.R., Yewdell, J.W., 2001. A novel influenza A virus mitochondrial protein that induces cell death. *Nat Med* 7, 1306-1312.
- Chen, X., Liu, S., Goraya, M.U., Maarouf, M., Huang, S., Chen, J.L., 2018. Host Immune Response to Influenza A Virus Infection. *Front Immunol* 9, 320.
- Chen, Y., Xu, Q., Li, Y., Liu, R., Huang, Z., Wang, B., Chen, G., 2016. Gene expression profile after activation of RIG-I in 5'ppp-dsRNA challenged DF1. *Dev Comp Immunol* 65, 191-200.
- Chen, Y., Zhang, Y., Huang, Z., Xu, Q., Zhu, Z., Tong, Y., Yu, Q., Ding, J., Chen, G., 2013b. Molecular characterization, expression patterns, and subcellular localization of RIG-I in the Jinding duck (*Anas platyrhynchos domesticus*). *Dev Comp Immunol* 41, 766-771.
- Cheng, Y.Y., Yang, S.R., Wang, Y.T., Lin, Y.H., Chen, C.J., 2017. Amino Acid Residues 68-71 Contribute to Influenza A Virus PB1-F2 Protein Stability and Functions. *Front Microbiol* 8, 692.
- Chevalier, C., Al Bazzal, A., Vidic, J., Fevrier, V., Bourdieu, C., Bouguyon, E., Le Goffic, R., Vautherot, J.F., Bernard, J., Moudjou, M., Noinville, S., Chich, J.F., Da Costa, B., Rezaei, H., Delmas, B., 2010. PB1-F2 influenza A virus protein adopts a beta-sheet conformation and forms amyloid fibers in membrane environments. *J Biol Chem* 285, 13233-13243.
- Chiba, H., Yamashita, R., Kinoshita, K., Nakai, K., 2008. Weak correlation between sequence conservation in promoter regions and in protein-coding regions of human-mouse orthologous gene pairs. *BMC Genomics* 9, 152.
- Cockburn, W.C., Delon, P.J., Ferreira, W., 1969. Origin and progress of the 1968-69 Hong Kong influenza epidemic. *Bull World Health Organ* 41, 345-348.
- Compans, R.W., Mountcastle, W.E., Choppin, P.W., 1972. The sense of the helix of paramyxovirus nucleocapsids. *J Mol Biol* 65, 167-169.

- Conenello, G.M., Zamarin, D., Perrone, L.A., Tumpey, T., Palese, P., 2007. A single mutation in the PB1-F2 of H5N1 (HK/97) and 1918 influenza A viruses contributes to increased virulence. *Plos Pathogens* 3, 1414-1421.
- Cooley, A.J., Van Campen, H., Philpott, M.S., Easterday, B.C., Hinshaw, V.S., 1989. Pathological lesions in the lungs of ducks infected with influenza A viruses. *Vet Pathol* 26, 1-5.
- Cormican, P., Lloyd, A.T., Downing, T., Connell, S.J., Bradley, D., O'Farrelly, C., 2009. The avian Toll-Like receptor pathway--subtle differences amidst general conformity. *Developmental & Comparative Immunology* 33, 967-973.
- Cornelissen, J.B., Post, J., Peeters, B., Vervelde, L., Rebel, J.M., 2012. Differential innate responses of chickens and ducks to low-pathogenic avian influenza. *Avian pathology : journal of the W.V.P.A* 41, 519-529.
- Costa, T.P., Brown, J.D., Howerth, E.W., Stallknecht, D.E., 2011. Variation in viral shedding patterns between different wild bird species infected experimentally with low-pathogenicity avian influenza viruses that originated from wild birds. *Avian pathology : journal of the W.V.P.A* 40, 119-124.
- Cui, X.F., Imaizumi, T., Yoshida, H., Borden, E.C., Satoh, K., 2004. Retinoic acid-inducible gene-I is induced by interferon-gamma and regulates the expression of interferon-gamma stimulated gene 15 in MCF-7 cells. *Biochem Cell Biol* 82, 401-405.
- Daoust, P.Y., Kibenge, F.S., Fouchier, R.A., van de Bildt, M.W., van Riel, D., Kuiken, T., 2011. Replication of low pathogenic avian influenza virus in naturally infected Mallard ducks (*Anas platyrhynchos*) causes no morphologic lesions. *J Wildl Dis* 47, 401-409.
- De Nardo, D., 2015. Toll-like receptors: Activation, signalling and transcriptional modulation. *Cytokine* 74, 181-189.
- de Zoete, M.R., Bouwman, L.I., Keesstra, A.M., van Putten, J.P., 2011. Cleavage and activation of a Toll-like receptor by microbial proteases. *Proc Natl Acad Sci U S A* 108, 4968-4973.
- Delneste, Y., Beauvillain, C., Jeannin, P., 2007. [Innate immunity: structure and function of TLRs]. *Med Sci (Paris)* 23, 67-73.
- Deng, G., Tan, D., Shi, J., Cui, P., Jiang, Y., Liu, L., Tian, G., Kawaoka, Y., Li, C., Chen, H., 2013. Complex reassortment of multiple subtypes of avian influenza viruses in domestic ducks at the Dongting Lake Region of China. *J Virol* 87, 9452-9462.

- Desselberger, U., Racaniello, V.R., Zazra, J.J., Palese, P., 1980. The 3' and 5'-terminal sequences of influenza A, B and C virus RNA segments are highly conserved and show partial inverted complementarity. *Gene* 8, 315-328.
- Deyde, V.M., Xu, X., Bright, R.A., Shaw, M., Smith, C.B., Zhang, Y., Shu, Y., Gubareva, L.V., Cox, N.J., Klimov, A.I., 2007. Surveillance of resistance to adamantanes among influenza A(H3N2) and A(H1N1) viruses isolated worldwide. *J Infect Dis* 196, 249-257.
- Dixit, E., Boulant, S., Zhang, Y., Lee, A.S., Odendall, C., Shum, B., Hacohen, N., Chen, Z.J., Whelan, S.P., Fransen, M., Nibert, M.L., Superti-Furga, G., Kagan, J.C., 2010. Peroxisomes are signaling platforms for antiviral innate immunity. *Cell* 141, 668-681.
- Doerner, A., Pauschinger, M., Badorff, A., Noutsias, M., Giessen, S., Schulze, K., Bilger, J., Rauch, U., Schultheiss, H.P., 1997. Tissue-specific transcription pattern of the adenine nucleotide translocase isoforms in humans. *FEBS Lett* 414, 258-262.
- Dolin, R., Reichman, R.C., Madore, H.P., Maynard, R., Linton, P.N., Webber-Jones, J., 1982. A controlled trial of amantadine and rimantadine in the prophylaxis of influenza A infection. *N Engl J Med* 307, 580-584.
- Domenech, J., Dauphin, G., Rushton, J., McGrane, J., Lubroth, J., Tripodi, A., Gilbert, J., Sims, L.D., 2009. Experiences with vaccination in countries endemically infected with highly pathogenic avian influenza: the Food and Agriculture Organization perspective. *Rev Sci Tech* 28, 293-305.
- Dudek, S.E., Wixler, L., Nordhoff, C., Nordmann, A., Anhlan, D., Wixler, V., Ludwig, S., 2011. The influenza virus PB1-F2 protein has interferon antagonistic activity. *Biol Chem* 392, 1135-1144.
- Eisfeld, A.J., Kawakami, E., Watanabe, T., Neumann, G., Kawaoka, Y., 2011. RAB11A is essential for transport of the influenza virus genome to the plasma membrane. *J Virol* 85, 6117-6126.
- Eisfeld, A.J., Neumann, G., Kawaoka, Y., 2015. At the centre: influenza A virus ribonucleoproteins. *Nat Rev Microbiol* 13, 28-41.
- Elleman, C.J., Barclay, W.S., 2004. The M1 matrix protein controls the filamentous phenotype of influenza A virus. *Virology* 321, 144-153.
- Ellis, T.M., Bousfield, R.B., Bissett, L.A., Dyrting, K.C., Luk, G.S., Tsim, S.T., Sturm-Ramirez, K., Webster, R.G., Guan, Y., Malik Peiris, J.S., 2004. Investigation of outbreaks of

- highly pathogenic H5N1 avian influenza in waterfowl and wild birds in Hong Kong in late 2002. *Avian pathology : journal of the W.V.P.A* 33, 492-505.
- Elton, D., Simpson-Holley, M., Archer, K., Medcalf, L., Hallam, R., McCauley, J., Digard, P., 2001. Interaction of the influenza virus nucleoprotein with the cellular CRM1-mediated nuclear export pathway. *J Virol* 75, 408-419.
- Escuret, V., Frobert, E., Bouscambert-Duchamp, M., Sabatier, M., Grog, I., Valette, M., Lina, B., Morfin, F., Ferraris, O., 2008. Detection of human influenza A (H1N1) and B strains with reduced sensitivity to neuraminidase inhibitors. *J Clin Virol* 41, 25-28.
- Fahrenkrog, B., Aebi, U., 2003. The nuclear pore complex: nucleocytoplasmic transport and beyond. *Nat Rev Mol Cell Biol* 4, 757-766.
- Fauci, A.S., 2006. Emerging and re-emerging infectious diseases: influenza as a prototype of the host-pathogen balancing act. *Cell* 124, 665-670.
- Ferguson, L., Olivier, A.K., Genova, S., Epperson, W.B., Smith, D.R., Schneider, L., Barton, K., McCuan, K., Webby, R.J., Wan, X.F., 2016. Pathogenesis of Influenza D Virus in Cattle. *J Virol* 90, 5636-5642.
- Fiore, A.E., Fry, A., Shay, D., Gubareva, L., Bresee, J.S., Uyeki, T.M., 2011. Antiviral agents for the treatment and chemoprophylaxis of influenza --- recommendations of the Advisory Committee on Immunization Practices (ACIP). *MMWR Recomm Rep* 60, 1-24.
- Fodor, E., 2013. The RNA polymerase of influenza A virus: mechanisms of viral transcription and replication. *Acta Virologica* 57, 113-122.
- Fouchier, R.A., Munster, V.J., 2009. Epidemiology of low pathogenic avian influenza viruses in wild birds. *Rev Sci Tech* 28, 49-58.
- Francis, J.N., Bunce, C.J., Horlock, C., Watson, J.M., Warrington, S.J., Georges, B., Brown, C.B., 2015. A novel peptide-based pan-influenza A vaccine: a double blind, randomised clinical trial of immunogenicity and safety. *Vaccine* 33, 396-402.
- Friedman, C.S., O'Donnell, M.A., Legarda-Addison, D., Ng, A., Cardenas, W.B., Yount, J.S., Moran, T.M., Basler, C.F., Komuro, A., Horvath, C.M., Xavier, R., Ting, A.T., 2008. The tumour suppressor CYLD is a negative regulator of RIG-I-mediated antiviral response. *EMBO Rep* 9, 930-936.
- Fujii, Y., Goto, H., Watanabe, T., Yoshida, T., Kawaoka, Y., 2003. Selective incorporation of influenza virus RNA segments into virions. *Proc Natl Acad Sci U S A* 100, 2002-2007.

- Fukumi, H., 1959. Summary report on the Asian influenza epidemic in Japan, 1957. *Bull World Health Organ* 20, 187-198.
- Gack, M.U., Albrecht, R.A., Urano, T., Inn, K.S., Huang, I.C., Carnero, E., Farzan, M., Inoue, S., Jung, J.U., Garcia-Sastre, A., 2009. Influenza A virus NS1 targets the ubiquitin ligase TRIM25 to evade recognition by the host viral RNA sensor RIG-I. *Cell Host Microbe* 5, 439-449.
- Gack, M.U., Nistal-Villan, E., Inn, K.S., Garcia-Sastre, A., Jung, J.U., 2010. Phosphorylation-Mediated Negative Regulation of RIG-I Antiviral Activity. *Journal of Virology* 84, 3220-3229.
- Gack, M.U., Shin, Y.C., Joo, C.H., Urano, T., Liang, C., Sun, L., Takeuchi, O., Akira, S., Chen, Z., Inoue, S., Jung, J.U., 2007. TRIM25 RING-finger E3 ubiquitin ligase is essential for RIG-I-mediated antiviral activity. *Nature* 446, 916-920.
- Gale, M., Jr., Katze, M.G., 1998. Molecular mechanisms of interferon resistance mediated by viral-directed inhibition of PKR, the interferon-induced protein kinase. *Pharmacol Ther* 78, 29-46.
- Garten, R.J., Davis, C.T., Russell, C.A., Shu, B., Lindstrom, S., Balish, A., Sessions, W.M., Xu, X., Skepner, E., Deyde, V., Okomo-Adhiambo, M., Gubareva, L., Barnes, J., Smith, C.B., Emery, S.L., Hillman, M.J., Rivaller, P., Smagala, J., de Graaf, M., Burke, D.F., Fouchier, R.A., Pappas, C., Alpuche-Aranda, C.M., Lopez-Gatell, H., Olivera, H., Lopez, I., Myers, C.A., Faix, D., Blair, P.J., Yu, C., Keene, K.M., Dotson, P.D., Jr., Boxrud, D., Sambol, A.R., Abid, S.H., St George, K., Bannerman, T., Moore, A.L., Stringer, D.J., Blevins, P., Demmler-Harrison, G.J., Ginsberg, M., Kriner, P., Waterman, S., Smole, S., Guevara, H.F., Belongia, E.A., Clark, P.A., Beatrice, S.T., Donis, R., Katz, J., Finelli, L., Bridges, C.B., Shaw, M., Jernigan, D.B., Uyeki, T.M., Smith, D.J., Klimov, A.I., Cox, N.J., 2009. Antigenic and genetic characteristics of swine-origin 2009 A(H1N1) influenza viruses circulating in humans. *Science* 325, 197-201.
- Gerdil, C., 2003. The annual production cycle for influenza vaccine. *Vaccine* 21, 1776-1779.
- Gershon, B., 2006. 1918 the influenza pandemic. *Md Med* 7, 7-9.
- Gibbs, J.S., Malide, D., Hornung, F., Bennink, J.R., Yewdell, J.W., 2003. The influenza A virus PB1-F2 protein targets the inner mitochondrial membrane via a predicted basic amphipathic helix that disrupts mitochondrial function. *J Virol* 77, 7214-7224.

- Gilbert, M., Chaitaweesub, P., Parakamawongsa, T., Premashthira, S., Tiensin, T., Kalpravidh, W., Wagner, H., Slingenbergh, J., 2006. Free-grazing ducks and highly pathogenic avian influenza, Thailand. *Emerg Infect Dis* 12, 227-234.
- Glezen, W.P., 1996. Emerging infections: pandemic influenza. *Epidemiol Rev* 18, 64-76.
- Goubau, D., Deddouche, S., Reis e Sousa, C., 2013. Cytosolic sensing of viruses. *Immunity* 38, 855-869.
- Goubau, D., Schlee, M., Deddouche, S., Pruijssers, A.J., Zillinger, T., Goldeck, M., Schuberth, C., Van der Veen, A.G., Fujimura, T., Rehwinkel, J., Iskarpatyoti, J.A., Barchet, W., Ludwig, J., Dermody, T.S., Hartmann, G., Reis e Sousa, C., 2014. Antiviral immunity via RIG-I-mediated recognition of RNA bearing 5'-diphosphates. *Nature* 514, 372-375.
- Govorkova, E.A., Rehg, J.E., Krauss, S., Yen, H.L., Guan, Y., Peiris, M., Nguyen, T.D., Hanh, T.H., Puthavathana, P., Long, H.T., Buranathai, C., Lim, W., Webster, R.G., Hoffmann, E., 2005. Lethality to ferrets of H5N1 influenza viruses isolated from humans and poultry in 2004. *J Virol* 79, 2191-2198.
- Graef, K.M., Vreede, F.T., Lau, Y.F., McCall, A.W., Carr, S.M., Subbarao, K., Fodor, E., 2010. The PB2 subunit of the influenza virus RNA polymerase affects virulence by interacting with the mitochondrial antiviral signaling protein and inhibiting expression of beta interferon. *J Virol* 84, 8433-8445.
- Gu, W., Gallagher, G.R., Dai, W., Liu, P., Li, R., Trombly, M.I., Gammon, D.B., Mello, C.C., Wang, J.P., Finberg, R.W., 2015. Influenza A virus preferentially snatches noncoding RNA caps. *RNA* 21, 2067-2075.
- Guarda, G., Zenger, M., Yazdi, A.S., Schroder, K., Ferrero, I., Menu, P., Tardivel, A., Mattmann, C., Tschopp, J., 2011. Differential expression of NLRP3 among hematopoietic cells. *J Immunol* 186, 2529-2534.
- Guo, X.M., Liu, X.P., Chang, G.B., Xu, L., Bi, Y.L., Wang, H.Z., Zhang, Y., Zhu, P.F., Wu, Y., Chen, G.H., 2016. Characterization of the NLRC5 promoter in chicken: SNPs, regulatory elements and CpG islands. *Anim Genet* 47, 579-587.
- Guo, Z., Chen, L.M., Zeng, H., Gomez, J.A., Plowden, J., Fujita, T., Katz, J.M., Donis, R.O., Sambhara, S., 2007. NS1 protein of influenza A virus inhibits the function of intracytoplasmic pathogen sensor, RIG-I. *Am J Respir Cell Mol Biol* 36, 263-269.

- Hackett, S.J., Kimball, R.T., Reddy, S., Bowie, R.C., Braun, E.L., Braun, M.J., Chojnowski, J.L., Cox, W.A., Han, K.L., Harshman, J., Huddleston, C.J., Marks, B.D., Miglia, K.J., Moore, W.S., Sheldon, F.H., Steadman, D.W., Witt, C.C., Yuri, T., 2008. A phylogenomic study of birds reveals their evolutionary history. *Science* 320, 1763-1768.
- Hai, R., Schmolke, M., Leyva-Grado, V.H., Thangavel, R.R., Margine, I., Jaffe, E.L., Krammer, F., Solorzano, A., Garcia-Sastre, A., Palese, P., Bouvier, N.M., 2013. Influenza A(H7N9) virus gains neuraminidase inhibitor resistance without loss of in vivo virulence or transmissibility. *Nat Commun* 4, 2854.
- Hai, R., Schmolke, M., Varga, Z.T., Manicassamy, B., Wang, T.T., Belser, J.A., Pearce, M.B., Garcia-Sastre, A., Tumpey, T.M., Palese, P., 2010. PB1-F2 expression by the 2009 pandemic H1N1 influenza virus has minimal impact on virulence in animal models. *J Virol* 84, 4442-4450.
- Hale, B.G., Randall, R.E., Ortin, J., Jackson, D., 2008. The multifunctional NS1 protein of influenza A viruses. *J Gen Virol* 89, 2359-2376.
- Harford, C.G., Leidler, H.V., 1947. Pathogenesis of pneumonia secondary to influenza. *J Clin Invest* 26, 1183.
- Hatada, E., Fukuda, R., 1992. Binding of influenza A virus NS1 protein to dsRNA in vitro. *J Gen Virol* 73 (Pt 12), 3325-3329.
- Hause, B.M., Collin, E.A., Liu, R., Huang, B., Sheng, Z., Lu, W., Wang, D., Nelson, E.A., Li, F., 2014. Characterization of a novel influenza virus in cattle and Swine: proposal for a new genus in the Orthomyxoviridae family. *MBio* 5, e00031-00014.
- Hay, A.J., Wolstenholme, A.J., Skehel, J.J., Smith, M.H., 1985. The molecular basis of the specific anti-influenza action of amantadine. *EMBO J* 4, 3021-3024.
- Hayakari, R., Matsumiya, T., Xing, F., Yoshida, H., Hayakari, M., Imaizumi, T., 2016. Critical Role of IRF-3 in the Direct Regulation of dsRNA-Induced Retinoic Acid-Inducible Gene-1 (RIG-I) Expression. *PLoS One* 11, e0163520.
- Heo, Y.A., 2018. Baloxavir: First Global Approval. *Drugs* 78, 693-697.
- Herold, S., Becker, C., Ridge, K.M., Budinger, G.R., 2015. Influenza virus-induced lung injury: pathogenesis and implications for treatment. *Eur Respir J* 45, 1463-1478.
- Hinshaw, V.S., Webster, R.G., Turner, B., 1980. The perpetuation of orthomyxoviruses and paramyxoviruses in Canadian waterfowl. *Can J Microbiol* 26, 622-629.

- Horner, S.M., Gale, M., Jr., 2013. Regulation of hepatic innate immunity by hepatitis C virus. *Nat Med* 19, 879-888.
- Horner, S.M., Liu, H.M., Park, H.S., Briley, J., Gale, M., Jr., 2011. Mitochondrial-associated endoplasmic reticulum membranes (MAM) form innate immune synapses and are targeted by hepatitis C virus. *Proc Natl Acad Sci U S A* 108, 14590-14595.
- Hornung, V., Ellegast, J., Kim, S., Brzozka, K., Jung, A., Kato, H., Poeck, H., Akira, S., Conzelmann, K.K., Schlee, M., Endres, S., Hartmann, G., 2006. 5'-Triphosphate RNA is the ligand for RIG-I. *Science* 314, 994-997.
- Hou, F., Sun, L., Zheng, H., Skaug, B., Jiang, Q.X., Chen, Z.J., 2011. MAVS forms functional prion-like aggregates to activate and propagate antiviral innate immune response. *Cell* 146, 448-461.
- Hsu, W.B., Shih, J.L., Shih, J.R., Du, J.L., Teng, S.C., Huang, L.M., Wang, W.B., 2013. Cellular protein HAX1 interacts with the influenza A virus PA polymerase subunit and impedes its nuclear translocation. *J Virol* 87, 110-123.
- Huang, Q., Sivaramakrishna, R.P., Ludwig, K., Korte, T., Bottcher, C., Herrmann, A., 2003. Early steps of the conformational change of influenza virus hemagglutinin to a fusion active state: stability and energetics of the hemagglutinin. *Biochim Biophys Acta* 1614, 3-13.
- Huang, S., Chen, J., Chen, Q., Wang, H., Yao, Y., Chen, Z., 2013a. A second CRM1-dependent nuclear export signal in the influenza A virus NS2 protein contributes to the nuclear export of viral ribonucleoproteins. *J Virol* 87, 767-778.
- Huang, Y., Li, Y., Burt, D.W., Chen, H., Zhang, Y., Qian, W., Kim, H., Gan, S., Zhao, Y., Li, J., Yi, K., Feng, H., Zhu, P., Li, B., Liu, Q., Fairley, S., Magor, K.E., Du, Z., Hu, X., Goodman, L., Tafer, H., Vignal, A., Lee, T., Kim, K.W., Sheng, Z., An, Y., Searle, S., Herrero, J., Groenen, M.A., Crooijmans, R.P., Faraut, T., Cai, Q., Webster, R.G., Aldridge, J.R., Warren, W.C., Bartschat, S., Kehr, S., Marz, M., Stadler, P.F., Smith, J., Kraus, R.H., Ren, L., Fei, J., Morisson, M., Kaiser, P., Griffin, D.K., Rao, M., Pitel, F., Wang, J., Li, N., 2013b. The duck genome and transcriptome provide insight into an avian influenza virus reservoir species. *Nat Genet* 45, 776-783.
- Huang, Y., Li, Y., Burt, D.W., Chen, H., Zhang, Y., Qian, W., Kim, H., Gan, S., Zhao, Y., Li, J., Yi, K., Feng, H., Zhu, P., Li, B., Liu, Q., Fairley, S., Magor, K.E., Du, Z., Hu, X.,

- Goodman, L., Tafer, H., Vignat, A., Lee, T., Kim, K.W., Sheng, Z., An, Y., Searle, S., Herrero, J., Groenen, M.A.M., Crooijmans, R., Faraut, T., Cai, Q., Webster, R.G., Aldridge, J.R., Warren, W.C., Bartschat, S., Kehr, S., Marz, M., Stadler, P.F., Smith, J., Kraus, R.H.S., Zhao, Y., Ren, L., Fei, J., Morisson, M., Kaiser, P., Griffin, D.K., Rao, M., Pitel, F., Wang, J., Li, N., 2013c. The duck genome and transcriptome provide insight into an avian influenza virus reservoir species. *Nat Genet* 45, 776-783.
- Hufford, M.M., Richardson, G., Zhou, H., Manicassamy, B., Garcia-Sastre, A., Enelow, R.I., Braciale, T.J., 2012. Influenza-infected neutrophils within the infected lungs act as antigen presenting cells for anti-viral CD8(+) T cells. *PLoS One* 7, e46581.
- Hulse-Post, D.J., Sturm-Ramirez, K.M., Humberd, J., Seiler, P., Govorkova, E.A., Krauss, S., Scholtissek, C., Puthavathana, P., Buranathai, C., Nguyen, T.D., Long, H.T., Naipospos, T.S., Chen, H., Ellis, T.M., Guan, Y., Peiris, J.S., Webster, R.G., 2005. Role of domestic ducks in the propagation and biological evolution of highly pathogenic H5N1 influenza viruses in Asia. *Proc Natl Acad Sci U S A* 102, 10682-10687.
- Hurt, A.C., Besselaar, T.G., Daniels, R.S., Ermetal, B., Fry, A., Gubareva, L., Huang, W., Lackenby, A., Lee, R.T., Lo, J., Maurer-Stroh, S., Nguyen, H.T., Pereyaslov, D., Rebelo-de-Andrade, H., Siqueira, M.M., Takashita, E., Tashiro, M., Tilmanis, D., Wang, D., Zhang, W., Meijer, A., 2016. Global update on the susceptibility of human influenza viruses to neuraminidase inhibitors, 2014-2015. *Antiviral Res* 132, 178-185.
- Ichinohe, T., Pang, I.K., Iwasaki, A., 2010. Influenza virus activates inflammasomes via its intracellular M2 ion channel. *Nat Immunol* 11, 404-410.
- Illingworth, R.S., Bird, A.P., 2009. CpG islands--'a rough guide'. *FEBS Lett* 583, 1713-1720.
- Imaizumi, T., Aratani, S., Nakajima, T., Carlson, M., Matsumiya, T., Tanji, K., Ookawa, K., Yoshida, H., Tsuchida, S., McIntyre, T.M., Prescott, S.M., Zimmerman, G.A., Satoh, K., 2002. Retinoic acid-inducible gene-I is induced in endothelial cells by LPS and regulates expression of COX-2. *Biochem Biophys Res Commun* 292, 274-279.
- Ingle, H., Kumar, S., Raut, A.A., Mishra, A., Kulkarni, D.D., Kameyama, T., Takaoka, A., Akira, S., Kumar, H., 2015. The microRNA miR-485 targets host and influenza virus transcripts to regulate antiviral immunity and restrict viral replication. *Sci Signal* 8, ra126.

- Iqbal, M., Philbin, V.J., Smith, A.L., 2005. Expression patterns of chicken Toll-like receptor mRNA in tissues, immune cell subsets and cell lines. *Veterinary Immunology and Immunopathology* 104, 117-127.
- Iwai, A., Shiozaki, T., Kawai, T., Akira, S., Kawaoka, Y., Takada, A., Kida, H., Miyazaki, T., 2010. Influenza A virus polymerase inhibits type I interferon induction by binding to interferon beta promoter stimulator 1. *J Biol Chem* 285, 32064-32074.
- Iwatsuki-Horimoto, K., Horimoto, T., Noda, T., Kiso, M., Maeda, J., Watanabe, S., Muramoto, Y., Fujii, K., Kawaoka, Y., 2006. The cytoplasmic tail of the influenza A virus M2 protein plays a role in viral assembly. *J Virol* 80, 5233-5240.
- Jagadesh, A., Salam, A.A., Mudgal, P.P., Arunkumar, G., 2016. Influenza virus neuraminidase (NA): a target for antivirals and vaccines. *Arch Virol* 161, 2087-2094.
- Jagger, B.W., Wise, H.M., Kash, J.C., Walters, K.A., Wills, N.M., Xiao, Y.L., Dunfee, R.L., Schwartzman, L.M., Ozinsky, A., Bell, G.L., Dalton, R.M., Lo, A., Efstathiou, S., Atkins, J.F., Firth, A.E., Taubenberger, J.K., Digard, P., 2012. An overlapping protein-coding region in influenza A virus segment 3 modulates the host response. *Science* 337, 199-204.
- Janeway, C.A., Jr., 1989. Approaching the asymptote? Evolution and revolution in immunology. *Cold Spring Harb Symp Quant Biol* 54 Pt 1, 1-13.
- Jaworska, J., Coulombe, F., Downey, J., Tzelepis, F., Shalaby, K., Tattoli, I., Berube, J., Rousseau, S., Martin, J.G., Girardin, S.E., McCullers, J.A., Divangahi, M., 2014. NLRX1 prevents mitochondrial induced apoptosis and enhances macrophage antiviral immunity by interacting with influenza virus PB1-F2 protein. *Proc Natl Acad Sci U S A* 111, E2110-2119.
- Jiang, F., Ramanathan, A., Miller, M.T., Tang, G.Q., Gale, M., Jr., Patel, S.S., Marcotrigiano, J., 2011. Structural basis of RNA recognition and activation by innate immune receptor RIG-I. *Nature* 479, 423-427.
- Jiang, X.M., Kinch, L.N., Brautigam, C.A., Chen, X., Du, F.H., Grishin, N.V., Chen, Z.J.J., 2012. Ubiquitin-Induced Oligomerization of the RNA Sensors RIG-I and MDA5 Activates Antiviral Innate Immune Response. *Immunity* 36, 959-973.

- Jiao, P.R., Wei, L.M., Cheng, Y.Q., Yuan, R.Y., Han, F., Liang, J., Liu, W.L., Ren, T., Xin, C.A., Liao, M., 2012. Molecular cloning, characterization, and expression analysis of the Muscovy duck Toll-like receptor 3 (MdTLR3) gene. *Poult Sci* 91, 2475-2481.
- Jiao, P.R., Wei, L.M., Song, Y.F., Cui, J., Zhang, S., Han, F., Yuan, R.Y., Liao, M., 2015. Molecular cloning and immune responsive expression of LGP2 gene, a pivotal member of the RLR gene family from Muscovy duck *Cairina moschata*. *Poult Sci* 94, 1170-1176.
- Jorba, N., Coloma, R., Ortin, J., 2009. Genetic trans-complementation establishes a new model for influenza virus RNA transcription and replication. *PLoS Pathog* 5, e1000462.
- Jourdain, E., Gunnarsson, G., Wahlgren, J., Latorre-Margalef, N., Brojer, C., Sahlin, S., Svensson, L., Waldenstrom, J., Lundkvist, A., Olsen, B., 2010. Influenza virus in a natural host, the mallard: experimental infection data. *PLoS One* 5, e8935.
- Kamal, R.P., Alymova, I.V., York, I.A., 2017. Evolution and Virulence of Influenza A Virus Protein PB1-F2. *Int J Mol Sci* 19.
- Kang, D.C., Gopalkrishnan, R.V., Lin, L., Randolph, A., Valerie, K., Pestka, S., Fisher, P.B., 2004. Expression analysis and genomic characterization of human melanoma differentiation associated gene-5, mda-5: a novel type I interferon-responsive apoptosis-inducing gene. *Oncogene* 23, 1789-1800.
- Kang, D.C., Gopalkrishnan, R.V., Wu, Q., Jankowsky, E., Pyle, A.M., Fisher, P.B., 2002. mda-5: An interferon-inducible putative RNA helicase with double-stranded RNA-dependent ATPase activity and melanoma growth-suppressive properties. *Proc Natl Acad Sci U S A* 99, 637-642.
- Karpala, A.J., Lowenthal, J.W., Bean, A.G., 2008. Activation of the TLR3 pathway regulates IFN beta production in chickens. *Developmental and Comparative Immunology* 32, 435-444.
- Karpala, A.J., Stewart, C., McKay, J., Lowenthal, J.W., Bean, A.G., 2011. Characterization of chicken Mda5 activity: regulation of IFN-beta in the absence of RIG-I functionality. *J Immunol* 186, 5397-5405.
- Kato, H., Takeuchi, O., Mikamo-Satoh, E., Hirai, R., Kawai, T., Matsushita, K., Hiiragi, A., Dermody, T.S., Fujita, T., Akira, S., 2008. Length-dependent recognition of double-stranded ribonucleic acids by retinoic acid-inducible gene-I and melanoma differentiation-associated gene 5. *J Exp Med* 205, 1601-1610.

- Kawai, T., Akira, S., 2009. The roles of TLRs, RLRs and NLRs in pathogen recognition. *Int Immunol* 21, 317-337.
- Kawai, T., Akira, S., 2011. Toll-like receptors and their crosstalk with other innate receptors in infection and immunity. *Immunity* 34, 637-650.
- Kawai, T., Takahashi, K., Sato, S., Coban, C., Kumar, H., Kato, H., Ishii, K.J., Takeuchi, O., Akira, S., 2005. IPS-1, an adaptor triggering RIG-I- and Mda5-mediated type I interferon induction. *Nat Immunol* 6, 981-988.
- Kayagaki, N., Phung, Q., Chan, S., Chaudhari, R., Quan, C., O'Rourke, K.M., Eby, M., Pietras, E., Cheng, G., Bazan, J.F., Zhang, Z., Arnott, D., Dixit, V.M., 2007. DUBA: a deubiquitinase that regulates type I interferon production. *Science* 318, 1628-1632.
- Keestra, A.M., de Zoete, M.R., Bouwman, L.I., Vaezirad, M.M., van Putten, J.P., 2013. Unique features of chicken Toll-like receptors. *Dev Comp Immunol* 41, 316-323.
- Kent, W.J., Sugnet, C.W., Furey, T.S., Roskin, K.M., Pringle, T.H., Zahler, A.M., Haussler, D., 2002. The human genome browser at UCSC. *Genome Res* 12, 996-1006.
- Khanna, M., Sharma, S., Kumar, B., Rajput, R., 2014. Protective immunity based on the conserved hemagglutinin stalk domain and its prospects for universal influenza vaccine development. *Biomed Res Int* 2014, 546274.
- Kilbourne, E.D., Murphy, J.S., 1960. Genetic studies of influenza viruses. I. Viral morphology and growth capacity as exchangeable genetic traits. Rapid in ovo adaptation of early passage Asian strain isolates by combination with PR8. *J Exp Med* 111, 387-406.
- Kim, J.K., Negovetich, N.J., Forrest, H.L., Webster, R.G., 2009. Ducks: the "Trojan horses" of H5N1 influenza. *Influenza Other Respir Viruses* 3, 121-128.
- Kohlway, A., Luo, D., Rawling, D.C., Ding, S.C., Pyle, A.M., 2013. Defining the functional determinants for RNA surveillance by RIG-I. *EMBO Rep* 14, 772-779.
- Koppstein, D., Ashour, J., Bartel, D.P., 2015. Sequencing the cap-snatching repertoire of H1N1 influenza provides insight into the mechanism of viral transcription initiation. *Nucleic Acids Res* 43, 5052-5064.
- Koshiha, T., Yasukawa, K., Yanagi, Y., Kawabata, S., 2011. Mitochondrial membrane potential is required for MAVS-mediated antiviral signaling. *Sci Signal* 4, ra7.

- Kowalinski, E., Lunardi, T., McCarthy, A.A., Loubser, J., Brunel, J., Grigorov, B., Gerlier, D., Cusack, S., 2011. Structural basis for the activation of innate immune pattern-recognition receptor RIG-I by viral RNA. *Cell* 147, 423-435.
- Krauss, S., Walker, D., Pryor, S.P., Niles, L., Chenghong, L., Hinshaw, V.S., Webster, R.G., 2004. Influenza A viruses of migrating wild aquatic birds in North America. *Vector Borne Zoonotic Dis* 4, 177-189.
- Krauss, S., Webster, R.G., 2010. Avian influenza virus surveillance and wild birds: past and present. *Avian Dis* 54, 394-398.
- Kubota, K., Sakaki, H., Imaizumi, T., Nakagawa, H., Kusumi, A., Kobayashi, W., Satoh, K., Kimura, H., 2006. Retinoic acid-inducible gene-I is induced in gingival fibroblasts by lipopolysaccharide or poly IC: possible roles in interleukin-1beta, -6 and -8 expression. *Oral Microbiol Immunol* 21, 399-406.
- Kumar, B., Asha, K., Khanna, M., Ronsard, L., Meseko, C.A., Sanicas, M., 2018. The emerging influenza virus threat: status and new prospects for its therapy and control. *Arch Virol* 163, 831-844.
- Kumar, P., Khanna, M., Kumar, B., Rajput, R., Banerjea, A.C., 2012. A conserved matrix epitope based DNA vaccine protects mice against influenza A virus challenge. *Antiviral Res* 93, 78-85.
- Lang, X.T., Tang, T.T., Jin, T.C., Ding, C., Zhou, R.B., Jiang, W., 2017. TRIM65-catalyzed ubiquitination is essential for MDA5-mediated antiviral innate immunity. *Journal of Experimental Medicine* 214, 459-473.
- Latz, E., Xiao, T.S., Stutz, A., 2013. Activation and regulation of the inflammasomes. *Nat Rev Immunol* 13, 397-411.
- Lavanchy, D., 1998. The WHO update on influenza A (H5N1) in Hong Kong. *Euro Surveill* 3, 23-25.
- Le Goffic, R., Bouguyon, E., Chevalier, C., Vidic, J., Da Costa, B., Leymarie, O., Bourdieu, C., Decamps, L., Dhone-Pollet, S., Delmas, B., 2010. Influenza A virus protein PB1-F2 exacerbates IFN-beta expression of human respiratory epithelial cells. *J Immunol* 185, 4812-4823.

- Lee, C.C., Wu, C.C., Lin, T.L., 2012. Characterization of chicken melanoma differentiation-associated gene 5 (MDA5) from alternative translation initiation. *Comp Immunol Microbiol Infect Dis* 35, 335-343.
- Leymarie, O., Embury-Hyatt, C., Chevalier, C., Jouneau, L., Moroldo, M., Da Costa, B., Berhane, Y., Delmas, B., Weingartl, H.M., Le Goffic, R., 2014. PB1-F2 attenuates virulence of highly pathogenic avian H5N1 influenza virus in chickens. *PLoS One* 9, e100679.
- Leymarie, O., Meyer, L., Tafforeau, L., Lotteau, V., Costa, B.D., Delmas, B., Chevalier, C., Le Goffic, R., 2017. Influenza virus protein PB1-F2 interacts with CALCOCO2 (NDP52) to modulate innate immune response. *J Gen Virol* 98, 1196-1208.
- Li, C., Bu, Z., Chen, H., 2014a. Avian influenza vaccines against H5N1 'bird flu'. *Trends Biotechnol* 32, 147-156.
- Li, H., Jin, H., Li, Y., Liu, D., Foda, M.F., Jiang, Y., Luo, R., 2017. Molecular cloning and functional characterization of duck nucleotide-binding oligomerization domain 1 (NOD1). *Dev Comp Immunol* 74, 82-89.
- Li, H.L., Zhai, Y.J., Fan, Y.F., Chen, H.C., Zhang, A.D., Jin, H., Luo, R., 2016. Molecular cloning and functional characterization of duck mitochondrial antiviral-signaling protein (MAVS). *Developmental and Comparative Immunology* 56, 1-6.
- Li, S., Min, J.Y., Krug, R.M., Sen, G.C., 2006. Binding of the influenza A virus NS1 protein to PKR mediates the inhibition of its activation by either PACT or double-stranded RNA. *Virology* 349, 13-21.
- Li, W., Chen, H., Sutton, T., Obadan, A., Perez, D.R., 2014b. Interactions between the influenza A virus RNA polymerase components and retinoic acid-inducible gene I. *J Virol* 88, 10432-10447.
- Li, Y., Li, J., Belisle, S., Baskin, C.R., Tumpey, T.M., Katze, M.G., 2011. Differential microRNA expression and virulence of avian, 1918 reassortant, and reconstructed 1918 influenza A viruses. *Virology* 421, 105-113.
- Li, Z., Zhang, J., Su, J., Liu, Y., Guo, J., Zhang, Y., Lu, C., Xing, S., Guan, Y., Li, Y., Sun, B., Zhao, Z., 2015. MicroRNAs in the immune organs of chickens and ducks indicate divergence of immunity against H5N1 avian influenza. *FEBS Lett* 589, 419-425.

- Lian, L., Ciraci, C., Chang, G., Hu, J., Lamont, S.J., 2012. NLRC5 knockdown in chicken macrophages alters response to LPS and poly (I:C) stimulation. *BMC Vet Res* 8, 23.
- Liang, Y., Hong, Y., Parslow, T.G., 2005. cis-Acting packaging signals in the influenza virus PB1, PB2, and PA genomic RNA segments. *J Virol* 79, 10348-10355.
- Lin, R., Heylbroeck, C., Pitha, P.M., Hiscott, J., 1998. Virus-dependent phosphorylation of the IRF-3 transcription factor regulates nuclear translocation, transactivation potential, and proteasome-mediated degradation. *Mol Cell Biol* 18, 2986-2996.
- Liniger, M., Summerfield, A., Zimmer, G., McCullough, K.C., Ruggli, N., 2012. Chicken cells sense influenza A virus infection through MDA5 and CARDIF signaling involving LGP2. *J Virol* 86, 705-717.
- Liu, D., Liu, X., Yan, J., Liu, W.J., Gao, G.F., 2009. Interspecies transmission and host restriction of avian H5N1 influenza virus. *Sci China C Life Sci* 52, 428-438.
- Liu, G., Lu, Y., Thulasi Raman, S.N., Xu, F., Wu, Q., Li, Z., Brownlie, R., Liu, Q., Zhou, Y., 2018. Nuclear-resident RIG-I senses viral replication inducing antiviral immunity. *Nat Commun* 9, 3199.
- Liu, T.X., Zhang, J.W., Tao, J., Zhang, R.B., Zhang, Q.H., Zhao, C.J., Tong, J.H., Lanotte, M., Waxman, S., Chen, S.J., Mao, M., Hu, G.X., Zhu, L., Chen, Z., 2000. Gene expression networks underlying retinoic acid-induced differentiation of acute promyelocytic leukemia cells. *Blood* 96, 1496-1504.
- Loo, Y.M., Gale, M., Jr., 2011. Immune signaling by RIG-I-like receptors. *Immunity* 34, 680-692.
- Lu, Y., Wambach, M., Katze, M.G., Krug, R.M., 1995. Binding of the influenza virus NS1 protein to double-stranded RNA inhibits the activation of the protein kinase that phosphorylates the eIF-2 translation initiation factor. *Virology* 214, 222-228.
- Luo, D., Ding, S.C., Vela, A., Kohlway, A., Lindenbach, B.D., Pyle, A.M., 2011. Structural insights into RNA recognition by RIG-I. *Cell* 147, 409-422.
- Lyall, J., Irvine, R.M., Sherman, A., McKinley, T.J., Nunez, A., Purdie, A., Outtrim, L., Brown, I.H., Rolleston-Smith, G., Sang, H., Tiley, L., 2011. Suppression of avian influenza transmission in genetically modified chickens. *Science* 331, 223-226.

- Ma, J.H., Yang, F.R., Yu, H., Zhou, Y.J., Li, G.X., Huang, M., Wen, F., Tong, G., 2013. An M2e-based synthetic peptide vaccine for influenza A virus confers heterosubtypic protection from lethal virus challenge. *Virology* 10, 227.
- MacDonald, M.R., Xia, J., Smith, A.L., Magor, K.E., 2008. The duck toll like receptor 7: genomic organization, expression and function. *Mol Immunol* 45, 2055-2061.
- Magor, B.G., Wilson, M.R., Miller, N.W., Clem, L.W., Middleton, D.L., Warr, G.W., 1994. An Ig heavy chain enhancer of the channel catfish *Ictalurus punctatus*: evolutionary conservation of function but not structure. *J Immunol* 153, 5556-5563.
- Magor, K.E., Navarro, D.M., Barber, M.R.W., Petkau, K., Fleming-Canepa, X., Blyth, G.A.D., Blaine, A.H., 2013. Defense genes missing from the flight division. *Developmental and Comparative Immunology* 41, 377-388.
- Marazzi, I., Ho, J.S., Kim, J., Manicassamy, B., Dewell, S., Albrecht, R.A., Seibert, C.W., Schaefer, U., Jeffrey, K.L., Prinjha, R.K., Lee, K., Garcia-Sastre, A., Roeder, R.G., Tarakhovsky, A., 2012. Suppression of the antiviral response by an influenza histone mimic. *Nature* 483, 428-433.
- Marintcheva, B., 2016. Modeling Influenza Antigenic Shift and Drift with LEGO Bricks. *J Microbiol Biol Educ* 17, 300-301.
- Marjuki, H., Scholtissek, C., Franks, J., Negovetich, N.J., Aldridge, J.R., Salomon, R., Finkelstein, D., Webster, R.G., 2010. Three amino acid changes in PB1-F2 of highly pathogenic H5N1 avian influenza virus affect pathogenicity in mallard ducks. *Arch Virol* 155, 925-934.
- Martin, K., Helenius, A., 1991. Nuclear transport of influenza virus ribonucleoproteins: the viral matrix protein (M1) promotes export and inhibits import. *Cell* 67, 117-130.
- Martinon, F., Mayor, A., Tschopp, J., 2009. The inflammasomes: guardians of the body. *Annu Rev Immunol* 27, 229-265.
- Masoodi, T.A., Shaik, N.A., Shafi, G., Munshi, A., Ahamed, A.K., Masoodi, Z.A., 2012. Comparative analysis of hemagglutinin of 2009 H1N1 influenza A pandemic indicates its evolution to 1918 H1N1 pandemic. *Gene* 491, 200-204.
- Mathelier, A., Fornes, O., Arenillas, D.J., Chen, C.Y., Denay, G., Lee, J., Shi, W., Shyr, C., Tan, G., Worsley-Hunt, R., Zhang, A.W., Parcy, F., Lenhard, B., Sandelin, A., Wasserman,

- W.W., 2016. JASPAR 2016: a major expansion and update of the open-access database of transcription factor binding profiles. *Nucleic Acids Res* 44, D110-115.
- Matikainen, S., Siren, J., Tissari, J., Veckman, V., Pirhonen, J., Severa, M., Sun, Q., Lin, R., Meri, S., Uze, G., Hiscott, J., Julkunen, I., 2006. Tumor necrosis factor alpha enhances influenza A virus-induced expression of antiviral cytokines by activating RIG-I gene expression. *J Virol* 80, 3515-3522.
- Matlin, K.S., Reggio, H., Helenius, A., Simons, K., 1981. Infectious entry pathway of influenza virus in a canine kidney cell line. *J Cell Biol* 91, 601-613.
- Matsumiya, T., Stafforini, D.M., 2010. Function and regulation of retinoic acid-inducible gene-I. *Crit Rev Immunol* 30, 489-513.
- Mazel-Sanchez, B., Boal-Carvalho, I., Silva, F., Dijkman, R., Schmolke, M., 2018. H5N1 Influenza A Virus PB1-F2 Relieves HAX-1-Mediated Restriction of Avian Virus Polymerase PA in Human Lung Cells. *J Virol* 92.
- Mazur, I., Anhlan, D., Mitzner, D., Wixler, L., Schubert, U., Ludwig, S., 2008. The proapoptotic influenza A virus protein PB1-F2 regulates viral polymerase activity by interaction with the PB1 protein. *Cell Microbiol* 10, 1140-1152.
- McAuley, J.L., Chipuk, J.E., Boyd, K.L., Van De Velde, N., Green, D.R., McCullers, J.A., 2010a. PB1-F2 proteins from H5N1 and 20 century pandemic influenza viruses cause immunopathology. *PLoS Pathog* 6, e1001014.
- McAuley, J.L., Hornung, F., Boyd, K.L., Smith, A.M., McKeon, R., Bennink, J., Yewdell, J.W., McCullers, J.A., 2007. Expression of the 1918 influenza A virus PB1-F2 enhances the pathogenesis of viral and secondary bacterial pneumonia. *Cell Host Microbe* 2, 240-249.
- McAuley, J.L., Tate, M.D., MacKenzie-Kludas, C.J., Pinar, A., Zeng, W., Stutz, A., Latz, E., Brown, L.E., Mansell, A., 2013. Activation of the NLRP3 inflammasome by IAV virulence protein PB1-F2 contributes to severe pathophysiology and disease. *PLoS Pathog* 9, e1003392.
- McAuley, J.L., Zhang, K., McCullers, J.A., 2010b. The effects of influenza A virus PB1-F2 protein on polymerase activity are strain specific and do not impact pathogenesis. *J Virol* 84, 558-564.
- Mellman, I., Fuchs, R., Helenius, A., 1986. Acidification of the endocytic and exocytic pathways. *Annu Rev Biochem* 55, 663-700.

- Meylan, E., Curran, J., Hofmann, K., Moradpour, D., Binder, M., Bartenschlager, R., Tschopp, J., 2005. Cardif is an adaptor protein in the RIG-I antiviral pathway and is targeted by hepatitis C virus. *Nature* 437, 1167-1172.
- Mibayashi, M., Martinez-Sobrido, L., Loo, Y.M., Cardenas, W.B., Gale, M., Jr., Garcia-Sastre, A., 2007. Inhibition of retinoic acid-inducible gene I-mediated induction of beta interferon by the NS1 protein of influenza A virus. *J Virol* 81, 514-524.
- Michallet, M.C., Meylan, E., Ermolaeva, M.A., Vazquez, J., Rebsamen, M., Curran, J., Poeck, H., Bscheider, M., Hartmann, G., Konig, M., Kalinke, U., Pasparakis, M., Tschopp, J., 2008. TRADD protein is an essential component of the RIG-like helicase antiviral pathway. *Immunity* 28, 651-661.
- Min, J.Y., Krug, R.M., 2006. The primary function of RNA binding by the influenza A virus NS1 protein in infected cells: Inhibiting the 2'-5' oligo (A) synthetase/RNase L pathway. *Proc Natl Acad Sci U S A* 103, 7100-7105.
- Min, J.Y., Li, S., Sen, G.C., Krug, R.M., 2007. A site on the influenza A virus NS1 protein mediates both inhibition of PKR activation and temporal regulation of viral RNA synthesis. *Virology* 363, 236-243.
- Minassian, A., Zhang, J., He, S., Zhao, J., Zandi, E., Saito, T., Liang, C., Feng, P., 2015. An Internally Translated MAVS Variant Exposes Its Amino-terminal TRAF-Binding Motifs to Deregate Interferon Induction. *PLoS Pathog* 11, e1005060.
- Miranzo-Navarro, D., Magor, K.E., 2014. Activation of duck RIG-I by TRIM25 is independent of anchored ubiquitin. *PLoS One* 9, e86968.
- Mishra, A., Vijayakumar, P., Raut, A.A., 2017. Emerging avian influenza infections: Current understanding of innate immune response and molecular pathogenesis. *Int Rev Immunol* 36, 89-107.
- Mitzner, D., Dudek, S.E., Studtrucker, N., Anhlan, D., Mazur, I., Wissing, J., Jansch, L., Wixler, L., Bruns, K., Sharma, A., Wray, V., Henklein, P., Ludwig, S., Schubert, U., 2009. Phosphorylation of the influenza A virus protein PB1-F2 by PKC is crucial for apoptosis promoting functions in monocytes. *Cell Microbiol* 11, 1502-1516.
- Momose, F., Kikuchi, Y., Komase, K., Morikawa, Y., 2007. Visualization of microtubule-mediated transport of influenza viral progeny ribonucleoprotein. *Microbes Infect* 9, 1422-1433.

- Momose, F., Sekimoto, T., Ohkura, T., Jo, S., Kawaguchi, A., Nagata, K., Morikawa, Y., 2011. Apical transport of influenza A virus ribonucleoprotein requires Rab11-positive recycling endosome. *PLoS One* 6, e21123.
- Moon, D.A., Magor, K.E., 2004. Construction and characterization of a fosmid library for comparative analysis of the duck genome. *Anim Genet* 35, 417-418.
- Moscona, A., 2005. Neuraminidase inhibitors for influenza. *N Engl J Med* 353, 1363-1373.
- Mukherjee, A., Morosky, S.A., Shen, L., Weber, C.R., Turner, J.R., Kim, K.S., Wang, T., Coyne, C.B., 2009. Retinoic acid-induced gene-1 (RIG-I) associates with the actin cytoskeleton via caspase activation and recruitment domain-dependent interactions. *J Biol Chem* 284, 6486-6494.
- Muramoto, Y., Noda, T., Kawakami, E., Akkina, R., Kawaoka, Y., 2013. Identification of novel influenza A virus proteins translated from PA mRNA. *J Virol* 87, 2455-2462.
- Nakajima, K., 2003. [The mechanism of antigenic shift and drift of human influenza virus]. *Nihon Rinsho* 61, 1897-1903.
- Nallagatla, S.R., Toroney, R., Bevilacqua, P.C., 2008. A brilliant disguise for self RNA: 5'-end and internal modifications of primary transcripts suppress elements of innate immunity. *RNA Biol* 5, 140-144.
- Nayak, D.P., Balogun, R.A., Yamada, H., Zhou, Z.H., Barman, S., 2009. Influenza virus morphogenesis and budding. *Virus Res* 143, 147-161.
- Neumann, G., Castrucci, M.R., Kawaoka, Y., 1997. Nuclear import and export of influenza virus nucleoprotein. *J Virol* 71, 9690-9700.
- Nguyen, H.T., Fry, A.M., Gubareva, L.V., 2012. Neuraminidase inhibitor resistance in influenza viruses and laboratory testing methods. *Antivir Ther* 17, 159-173.
- Nieto, A., de la Luna, S., Barcena, J., Portela, A., Ortin, J., 1994. Complex structure of the nuclear translocation signal of influenza virus polymerase PA subunit. *J Gen Virol* 75 (Pt 1), 29-36.
- Noah, D.L., Twu, K.Y., Krug, R.M., 2003. Cellular antiviral responses against influenza A virus are countered at the posttranscriptional level by the viral NS1A protein via its binding to a cellular protein required for the 3' end processing of cellular pre-mRNAs. *Virology* 307, 386-395.
- Noda, T., 2011. Native morphology of influenza virions. *Front Microbiol* 2, 269.

- Noshi, T., Kitano, M., Taniguchi, K., Yamamoto, A., Omoto, S., Baba, K., Hashimoto, T., Ishida, K., Kushima, Y., Hattori, K., Kawai, M., Yoshida, R., Kobayashi, M., Yoshinaga, T., Sato, A., Okamoto, M., Sakoda, Y., Kida, H., Shishido, T., Naito, A., 2018. In vitro characterization of baloxavir acid, a first-in-class cap-dependent endonuclease inhibitor of the influenza virus polymerase PA subunit. *Antiviral Res* 160, 109-117.
- O'Neill, R.E., Talon, J., Palese, P., 1998. The influenza virus NEP (NS2 protein) mediates the nuclear export of viral ribonucleoproteins. *EMBO J* 17, 288-296.
- Okomo-Adhiambo, M., Sleeman, K., Ballenger, K., Nguyen, H.T., Mishin, V.P., Sheu, T.G., Smagala, J., Li, Y., Klimov, A.I., Gubareva, L.V., 2010. Neuraminidase inhibitor susceptibility testing in human influenza viruses: a laboratory surveillance perspective. *Viruses* 2, 2269-2289.
- Olsen, B., Munster, V.J., Wallensten, A., Waldenstrom, J., Osterhaus, A.D., Fouchier, R.A., 2006. Global patterns of influenza A virus in wild birds. *Science* 312, 384-388.
- Opitz, B., Rejaibi, A., Dauber, B., Eckhard, J., Vinzing, M., Schmeck, B., Hippenstiel, S., Suttrop, N., Wolff, T., 2007. IFNbeta induction by influenza A virus is mediated by RIG-I which is regulated by the viral NS1 protein. *Cell Microbiol* 9, 930-938.
- Oshiumi, H., Miyashita, M., Matsumoto, M., Seya, T., 2013. A distinct role of Riplet-mediated K63-Linked polyubiquitination of the RIG-I repressor domain in human antiviral innate immune responses. *PLoS Pathog* 9, e1003533.
- Othumpangat, S., Noti, J.D., Beezhold, D.H., 2014. Lung epithelial cells resist influenza A infection by inducing the expression of cytochrome c oxidase VIc which is modulated by miRNA 4276. *Virology* 468-470, 256-264.
- Pancucharova, H., Russ, G., 2006. PB1-F2 gene in influenza A viruses of different hemagglutinin subtype. *Acta Virol* 50, 269-272.
- Park, S., Juliana, C., Hong, S., Datta, P., Hwang, I., Fernandes-Alnemri, T., Yu, J.W., Alnemri, E.S., 2013. The mitochondrial antiviral protein MAVS associates with NLRP3 and regulates its inflammasome activity. *J Immunol* 191, 4358-4366.
- Patel, J.R., Jain, A., Chou, Y.Y., Baum, A., Ha, T., Garcia-Sastre, A., 2013. ATPase-driven oligomerization of RIG-I on RNA allows optimal activation of type-I interferon. *EMBO Rep* 14, 780-787.

- Paz, S., Sun, Q., Nakhaei, P., Romieu-Mourez, R., Goubau, D., Julkunen, I., Lin, R., Hiscott, J., 2006. Induction of IRF-3 and IRF-7 phosphorylation following activation of the RIG-I pathway. *Cellular & Molecular Biology* 52, 17-28.
- Peisley, A., Wu, B., Yao, H., Walz, T., Hur, S., 2013. RIG-I forms signaling-competent filaments in an ATP-dependent, ubiquitin-independent manner. *Mol Cell* 51, 573-583.
- Pemberton, L.F., Paschal, B.M., 2005. Mechanisms of receptor-mediated nuclear import and nuclear export. *Traffic* 6, 187-198.
- Petrilli, V., Dostert, C., Muruve, D.A., Tschopp, J., 2007. The inflammasome: a danger sensing complex triggering innate immunity. *Curr Opin Immunol* 19, 615-622.
- Pfeiffer, J., Suarez, D.L., Sarmiento, L., To, T.L., Nguyen, T., Pantin-Jackwood, M.J., 2010. Efficacy of commercial vaccines in protecting chickens and ducks against H5N1 highly pathogenic avian influenza viruses from Vietnam. *Avian Dis* 54, 262-271.
- Pflug, A., Guilligay, D., Reich, S., Cusack, S., 2014. Structure of influenza A polymerase bound to the viral RNA promoter. *Nature* 516, 355-360.
- Philbin, V.J., Iqbal, M., Boyd, Y., Goodchild, M.J., Beal, R.K., Bumstead, N., Young, J., Smith, A.L., 2005. Identification and characterization of a functional, alternatively spliced Toll-like receptor 7 (TLR7) and genomic disruption of TLR8 in chickens. *Immunology* 114, 507-521.
- Philpott, D.J., Sorbara, M.T., Robertson, S.J., Croitoru, K., Girardin, S.E., 2014. NOD proteins: regulators of inflammation in health and disease. *Nat Rev Immunol* 14, 9-23.
- Pichlmair, A., Schulz, O., Tan, C.P., Naslund, T.I., Liljestrom, P., Weber, F., Reis e Sousa, C., 2006. RIG-I-mediated antiviral responses to single-stranded RNA bearing 5'-phosphates. *Science* 314, 997-1001.
- Pinar, A., Dowling, J.K., Bitto, N.J., Robertson, A.A., Latz, E., Stewart, C.R., Drummond, G.R., Cooper, M.A., McAuley, J.L., Tate, M.D., Mansell, A., 2017. PB1-F2 Peptide Derived from Avian Influenza A Virus H7N9 Induces Inflammation via Activation of the NLRP3 Inflammasome. *J Biol Chem* 292, 826-836.
- Pinto, L.H., Holsinger, L.J., Lamb, R.A., 1992. Influenza virus M2 protein has ion channel activity. *Cell* 69, 517-528.

- Pizzolla, A., Smith, J.M., Brooks, A.G., Reading, P.C., 2017. Pattern recognition receptor immunomodulation of innate immunity as a strategy to limit the impact of influenza virus. *J Leukoc Biol* 101, 851-861.
- Plotch, S.J., Bouloy, M., Krug, R.M., 1979. Transfer of 5'-terminal cap of globin mRNA to influenza viral complementary RNA during transcription in vitro. *Proc Natl Acad Sci U S A* 76, 1618-1622.
- Plotch, S.J., Bouloy, M., Ulmanen, I., Krug, R.M., 1981. A unique cap(m⁷GpppXm)-dependent influenza virion endonuclease cleaves capped RNAs to generate the primers that initiate viral RNA transcription. *Cell* 23, 847-858.
- Poon, L.L., Pritlove, D.C., Fodor, E., Brownlee, G.G., 1999. Direct evidence that the poly(A) tail of influenza A virus mRNA is synthesized by reiterative copying of a U track in the virion RNA template. *J Virol* 73, 3473-3476.
- Prochnicki, T., Mangan, M.S., Latz, E., 2016. Recent insights into the molecular mechanisms of the NLRP3 inflammasome activation. *F1000Res* 5.
- Qian, W., Wei, X., Guo, K., Li, Y., Lin, X., Zou, Z., Zhou, H., Jin, M., 2017. The C-Terminal Effector Domain of Non-Structural Protein 1 of Influenza A Virus Blocks IFN-beta Production by Targeting TNF Receptor-Associated Factor 3. *Front Immunol* 8, 779.
- Qian, W., Wei, X., Li, Y., Guo, K., Zou, Z., Zhou, H., Jin, M., 2018. Duck interferon regulatory factor 1 acts as a positive regulator in duck innate antiviral response. *Dev Comp Immunol* 78, 1-13.
- Qiu, L.L., Xu, L., Guo, X.M., Li, Z.T., Wan, F., Liu, X.P., Chen, G.H., Chang, G.B., 2016. Gene expression changes in chicken NLRC5 signal pathway associated with in vitro avian leukosis virus subgroup J infection. *Genet Mol Res* 15.
- Quilligan, J.J., Jr., Hirayama, M., Baernstein, H.D., Jr., 1966. The suppression of A2 influenza in children by the chemoprophylactic use of Amantadine. *J Pediatr* 69, 572-575.
- Rajsbaum, R., Albrecht, R.A., Wang, M.K., Maharaj, N.P., Versteeg, G.A., Nistal-Villan, E., Garcia-Sastre, A., Gack, M.U., 2012. Species-specific inhibition of RIG-I ubiquitination and IFN induction by the influenza A virus NS1 protein. *PLoS Pathog* 8, e1003059.
- Reich, S., Guilligay, D., Pflug, A., Malet, H., Berger, I., Crepin, T., Hart, D., Lunardi, T., Nanao, M., Ruigrok, R.W., Cusack, S., 2014. Structural insight into cap-snatching and RNA synthesis by influenza polymerase. *Nature* 516, 361-366.

- Reikine, S., Nguyen, J.B., Modis, Y., 2014. Pattern Recognition and Signaling Mechanisms of RIG-I and MDA5. *Front Immunol* 5, 342.
- Reis, A.L., McCauley, J.W., 2013. The influenza virus protein PB1-F2 interacts with IKKbeta and modulates NF-kappaB signalling. *PLoS One* 8, e63852.
- Reperant, L.A., Moesker, F.M., Osterhaus, A.D., 2016. Influenza: from zoonosis to pandemic. *ERJ Open Res* 2.
- Reuman, P.D., Bernstein, D.I., Keefer, M.C., Young, E.C., Sherwood, J.R., Schiff, G.M., 1989. Efficacy and safety of low dosage amantadine hydrochloride as prophylaxis for influenza A. *Antiviral Res* 11, 27-40.
- Roberts, P.C., Compans, R.W., 1998. Host cell dependence of viral morphology. *Proc Natl Acad Sci U S A* 95, 5746-5751.
- Robertson, J.S., 1979. 5' and 3' terminal nucleotide sequences of the RNA genome segments of influenza virus. *Nucleic Acids Res* 6, 3745-3757.
- Robertson, J.S., Schubert, M., Lazzarini, R.A., 1981. Polyadenylation sites for influenza virus mRNA. *J Virol* 38, 157-163.
- Rothenfusser, S., Goutagny, N., DiPerna, G., Gong, M., Monks, B.G., Schoenemeyer, A., Yamamoto, M., Akira, S., Fitzgerald, K.A., 2005. The RNA helicase Lgp2 inhibits TLR-independent sensing of viral replication by retinoic acid-inducible gene-I. *J Immunol* 175, 5260-5268.
- Runge, S., Sparrer, K.M., Lassig, C., Hembach, K., Baum, A., Garcia-Sastre, A., Soding, J., Conzelmann, K.K., Hopfner, K.P., 2014. In vivo ligands of MDA5 and RIG-I in measles virus-infected cells. *PLoS Pathog* 10, e1004081.
- Saha, S.K., Pietras, E.M., He, J.Q., Kang, J.R., Liu, S.Y., Oganessian, G., Shahangian, A., Zarnegar, B., Shiba, T.L., Wang, Y., Cheng, G., 2006. Regulation of antiviral responses by a direct and specific interaction between TRAF3 and Cardif. *EMBO J* 25, 3257-3263.
- Saito, L.B., Diaz-Satizabal, L., Evseev, D., Fleming-Canepa, X., Mao, S., Webster, R.G., Magor, K.E., 2018. IFN and cytokine responses in ducks to genetically similar H5N1 influenza A viruses of varying pathogenicity. *J Gen Virol* 99, 464-474.
- Saito, T., Hirai, R., Loo, Y.M., Owen, D., Johnson, C.L., Sinha, S.C., Akira, S., Fujita, T., Gale, M., Jr., 2007. Regulation of innate antiviral defenses through a shared repressor domain in RIG-I and LGP2. *Proc Natl Acad Sci U S A* 104, 582-587.

- Salomon, R., Franks, J., Govorkova, E.A., Ilyushina, N.A., Yen, H.L., Hulse-Post, D.J., Humbert, J., Trichet, M., Rehg, J.E., Webby, R.J., Webster, R.G., Hoffmann, E., 2006. The polymerase complex genes contribute to the high virulence of the human H5N1 influenza virus isolate A/Vietnam/1203/04. *J Exp Med* 203, 689-697.
- Sansom, M.S., Kerr, I.D., 1993. Influenza virus M2 protein: a molecular modelling study of the ion channel. *Protein Eng* 6, 65-74.
- Satoh, T., Kato, H., Kumagai, Y., Yoneyama, M., Sato, S., Matsushita, K., Tsujimura, T., Fujita, T., Akira, S., Takeuchi, O., 2010. LGP2 is a positive regulator of RIG-I- and MDA5-mediated antiviral responses. *Proc Natl Acad Sci U S A* 107, 1512-1517.
- Schaefer-Klein, J., Givol, I., Barsov, E.V., Whitcomb, J.M., VanBrocklin, M., Foster, D.N., Federspiel, M.J., Hughes, S.H., 1998. The EV-O-derived cell line DF-1 supports the efficient replication of avian leukosis-sarcoma viruses and vectors. *Virology* 248, 305-311.
- Schlee, M., Roth, A., Hornung, V., Hagmann, C.A., Wimmenauer, V., Barchet, W., Coch, C., Janke, M., Mihailovic, A., Wardle, G., Juranek, S., Kato, H., Kawai, T., Poeck, H., Fitzgerald, K.A., Takeuchi, O., Akira, S., Tuschl, T., Latz, E., Ludwig, J., Hartmann, G., 2009. Recognition of 5' triphosphate by RIG-I helicase requires short blunt double-stranded RNA as contained in panhandle of negative-strand virus. *Immunity* 31, 25-34.
- Schmolke, M., Manicassamy, B., Pena, L., Sutton, T., Hai, R., Varga, Z.T., Hale, B.G., Steel, J., Perez, D.R., Garcia-Sastre, A., 2011. Differential contribution of PB1-F2 to the virulence of highly pathogenic H5N1 influenza A virus in mammalian and avian species. *PLoS Pathog* 7, e1002186.
- Schnell, J.R., Chou, J.J., 2008. Structure and mechanism of the M2 proton channel of influenza A virus. *Nature* 451, 591-595.
- Scholtissek, C., Becht, H., 1971. Binding of ribonucleic acids to the RNP-antigen protein of influenza viruses. *J Gen Virol* 10, 11-16.
- Schrauwen, E.J., de Graaf, M., Herfst, S., Rimmelzwaan, G.F., Osterhaus, A.D., Fouchier, R.A., 2014. Determinants of virulence of influenza A virus. *Eur J Clin Microbiol Infect Dis* 33, 479-490.
- Schroeder, C., Heider, H., Moncke-Buchner, E., Lin, T.I., 2005. The influenza virus ion channel and maturation cofactor M2 is a cholesterol-binding protein. *Eur Biophys J* 34, 52-66.

- Schwartzman, L.M., Cathcart, A.L., Pujanauski, L.M., Qi, L., Kash, J.C., Taubenberger, J.K., 2015. An Intranasal Virus-Like Particle Vaccine Broadly Protects Mice from Multiple Subtypes of Influenza A Virus. *MBio* 6, e01044.
- Seth, R.B., Sun, L., Ea, C.K., Chen, Z.J., 2005. Identification and characterization of MAVS, a mitochondrial antiviral signaling protein that activates NF-kappaB and IRF 3. *Cell* 122, 669-682.
- Shao, Q., Xu, W., Yan, L., Liu, J., Rui, L., Xiao, X., Yu, X., Lu, Y., Li, Z., 2014. Function of duck RIG-I in induction of antiviral response against IBDV and avian influenza virus on chicken cells. *Virus Res* 191, 184-191.
- Shimizu, T., Takizawa, N., Watanabe, K., Nagata, K., Kobayashi, N., 2011. Crucial role of the influenza virus NS2 (NEP) C-terminal domain in M1 binding and nuclear export of vRNP. *FEBS Lett* 585, 41-46.
- Short, K.R., Richard, M., Verhagen, J.H., van Riel, D., Schrauwen, E.J., van den Brand, J.M., Manz, B., Bodewes, R., Herfst, S., 2015. One health, multiple challenges: The inter-species transmission of influenza A virus. *One Health* 1, 1-13.
- Shortridge, K.F., Zhou, N.N., Guan, Y., Gao, P., Ito, T., Kawaoka, Y., Kodihalli, S., Krauss, S., Markwell, D., Murti, K.G., Norwood, M., Senne, D., Sims, L., Takada, A., Webster, R.G., 1998. Characterization of avian H5N1 influenza viruses from poultry in Hong Kong. *Virology* 252, 331-342.
- Silverman, R.H., 2007. Viral encounters with 2',5'-oligoadenylate synthetase and RNase L during the interferon antiviral response. *J Virol* 81, 12720-12729.
- Skehel, J.J., Hay, A.J., 1978. Nucleotide sequences at the 5' termini of influenza virus RNAs and their transcripts. *Nucleic Acids Res* 5, 1207-1219.
- Skehel, J.J., Wiley, D.C., 2000. Receptor binding and membrane fusion in virus entry: the influenza hemagglutinin. *Annu Rev Biochem* 69, 531-569.
- Skovgaard, K., Cirera, S., Vasby, D., Podolska, A., Breum, S.O., Durrwald, R., Schlegel, M., Heegaard, P.M., 2013. Expression of innate immune genes, proteins and microRNAs in lung tissue of pigs infected experimentally with influenza virus (H1N2). *Innate Immun* 19, 531-544.
- Smith, G.J., Vijaykrishna, D., Bahl, J., Lycett, S.J., Worobey, M., Pybus, O.G., Ma, S.K., Cheung, C.L., Raghvani, J., Bhatt, S., Peiris, J.S., Guan, Y., Rambaut, A., 2009. Origins

- and evolutionary genomics of the 2009 swine-origin H1N1 influenza A epidemic. *Nature* 459, 1122-1125.
- Solbak, S.M., Sharma, A., Bruns, K., Roder, R., Mitzner, D., Hahn, F., Niebert, R., Vedeler, A., Henklein, P., Schubert, U., Wray, V., Fossen, T., 2013. Influenza A virus protein PB1-F2 from different strains shows distinct structural signatures. *Biochim Biophys Acta* 1834, 568-582.
- Songserm, T., Jam-on, R., Sae-Heng, N., Meemak, N., Hulse-Post, D.J., Sturm-Ramirez, K.M., Webster, R.G., 2006. Domestic ducks and H5N1 influenza epidemic, Thailand. *Emerg Infect Dis* 12, 575-581.
- Soper, G.A., 1918. The Influenza Pneumonia Pandemic in the American Army Camps during September and October. 1918. *Science* 48, 451-456.
- Spalluto, C.M., Singhania, A., Cellura, D., Woelk, C.H., Sanchez-Elsner, T., Staples, K.J., Wilkinson, T.M.A., 2017. IFN-gamma Influences Epithelial Antiviral Responses via Histone Methylation of the RIG-I Promoter. *Am J Respir Cell Mol Biol* 57, 428-438.
- Stallknecht, D.E., Shane, S.M., 1988. Host range of avian influenza virus in free-living birds. *Vet Res Commun* 12, 125-141.
- Stepien, G., Torroni, A., Chung, A.B., Hodge, J.A., Wallace, D.C., 1992. Differential expression of adenine nucleotide translocator isoforms in mammalian tissues and during muscle cell differentiation. *J Biol Chem* 267, 14592-14597.
- Stewart, M., 2007. Molecular mechanism of the nuclear protein import cycle. *Nat Rev Mol Cell Biol* 8, 195-208.
- Stouffer, A.L., Acharya, R., Salom, D., Levine, A.S., Di Costanzo, L., Soto, C.S., Tereshko, V., Nanda, V., Stayrook, S., DeGrado, W.F., 2008. Structural basis for the function and inhibition of an influenza virus proton channel. *Nature* 451, 596-599.
- Straus, M.R., Whittaker, G.R., 2017. A peptide-based approach to evaluate the adaptability of influenza A virus to humans based on its hemagglutinin proteolytic cleavage site. *PLoS One* 12, e0174827.
- Sturm-Ramirez, K.M., Hulse-Post, D.J., Govorkova, E.A., Humberd, J., Seiler, P., Puthavathana, P., Buranathai, C., Nguyen, T.D., Chaisingh, A., Long, H.T., Naipospos, T.S., Chen, H., Ellis, T.M., Guan, Y., Peiris, J.S., Webster, R.G., 2005. Are ducks contributing to the endemicity of highly pathogenic H5N1 influenza virus in Asia? *J Virol* 79, 11269-11279.

- Stutz, A., Horvath, G.L., Monks, B.G., Latz, E., 2013. ASC speck formation as a readout for inflammasome activation. *Methods Mol Biol* 1040, 91-101.
- Su, Z.Z., Sarkar, D., Emdad, L., Barral, P.M., Fisher, P.B., 2007. Central role of interferon regulatory factor-1 (IRF-1) in controlling retinoic acid inducible gene-I (RIG-I) expression. *J Cell Physiol* 213, 502-510.
- Sugita, Y., Noda, T., Sagara, H., Kawaoka, Y., 2011. Ultracentrifugation deforms unfixed influenza A virions. *J Gen Virol* 92, 2485-2493.
- Suzuki, H., Saito, R., Masuda, H., Oshitani, H., Sato, M., Sato, I., 2003. Emergence of amantadine-resistant influenza A viruses: epidemiological study. *J Infect Chemother* 9, 195-200.
- Swayne, D.E., 2006. Principles for vaccine protection in chickens and domestic waterfowl against avian influenza: emphasis on Asian H5N1 high pathogenicity avian influenza. *Ann N Y Acad Sci* 1081, 174-181.
- Swayne, D.E., Suarez, D.L., 2000. Highly pathogenic avian influenza. *Rev Sci Tech* 19, 463-482.
- Takeuchi, K., Shaughnessy, M.A., Lamb, R.A., 1994. Influenza virus M2 protein ion channel activity is not required to maintain the equine-1 hemagglutinin in its native form in infected cells. *Virology* 202, 1007-1011.
- Tang, E.D., Wang, C.Y., 2010. TRAF5 is a downstream target of MAVS in antiviral innate immune signaling. *PLoS One* 5, e9172.
- Tao, Z.Y., Zhu, C.H., Shi, Z.H., Song, C., Xu, W.J., Song, W.T., Zou, J.M., Qin, A.J., 2015. Molecular characterization, expression, and functional analysis of NOD1 in Qingyuan partridge chicken. *Genet Mol Res* 14, 2691-2701.
- Tarendeau, F., Boudet, J., Guilligay, D., Mas, P.J., Bougault, C.M., Boulo, S., Baudin, F., Ruigrok, R.W., Daigle, N., Ellenberg, J., Cusack, S., Simorre, J.P., Hart, D.J., 2007. Structure and nuclear import function of the C-terminal domain of influenza virus polymerase PB2 subunit. *Nat Struct Mol Biol* 14, 229-233.
- Taubenberger, J.K., Kash, J.C., 2010. Influenza virus evolution, host adaptation, and pandemic formation. *Cell Host Microbe* 7, 440-451.
- Taubenberger, J.K., Morens, D.M., 2006. 1918 Influenza: the mother of all pandemics. *Emerg Infect Dis* 12, 15-22.

- Taubenberger, J.K., Morens, D.M., 2009. Pandemic influenza--including a risk assessment of H5N1. *Rev Sci Tech* 28, 187-202.
- Temperley, N.D., Berlin, S., Paton, I.R., Griffin, D.K., Burt, D.W., 2008. Evolution of the chicken Toll-like receptor gene family: a story of gene gain and gene loss. *BMC Genomics* 9, 62.
- Thomas, P.G., Dash, P., Aldridge, J.R., Jr., Ellebedy, A.H., Reynolds, C., Funk, A.J., Martin, W.J., Lamkanfi, M., Webby, R.J., Boyd, K.L., Doherty, P.C., Kanneganti, T.D., 2009. The intracellular sensor NLRP3 mediates key innate and healing responses to influenza A virus via the regulation of caspase-1. *Immunity* 30, 566-575.
- Ting, J.P., Lovering, R.C., Alnemri, E.S., Bertin, J., Boss, J.M., Davis, B.K., Flavell, R.A., Girardin, S.E., Godzik, A., Harton, J.A., Hoffman, H.M., Hugot, J.P., Inohara, N., Mackenzie, A., Maltais, L.J., Nunez, G., Ogura, Y., Otten, L.A., Philpott, D., Reed, J.C., Reith, W., Schreiber, S., Steimle, V., Ward, P.A., 2008. The NLR gene family: a standard nomenclature. *Immunity* 28, 285-287.
- Tisoncik, J.R., Korth, M.J., Simmons, C.P., Farrar, J., Martin, T.R., Katze, M.G., 2012. Into the eye of the cytokine storm. *Microbiol Mol Biol Rev* 76, 16-32.
- Tong, S., Li, Y., Rivaviller, P., Conrardy, C., Castillo, D.A., Chen, L.M., Recuenco, S., Ellison, J.A., Davis, C.T., York, I.A., Turmelle, A.S., Moran, D., Rogers, S., Shi, M., Tao, Y., Weil, M.R., Tang, K., Rowe, L.A., Sammons, S., Xu, X., Frace, M., Lindblade, K.A., Cox, N.J., Anderson, L.J., Rupprecht, C.E., Donis, R.O., 2012. A distinct lineage of influenza A virus from bats. *Proc Natl Acad Sci U S A* 109, 4269-4274.
- Tong, S., Zhu, X., Li, Y., Shi, M., Zhang, J., Bourgeois, M., Yang, H., Chen, X., Recuenco, S., Gomez, J., Chen, L.M., Johnson, A., Tao, Y., Dreyfus, C., Yu, W., McBride, R., Carney, P.J., Gilbert, A.T., Chang, J., Guo, Z., Davis, C.T., Paulson, J.C., Stevens, J., Rupprecht, C.E., Holmes, E.C., Wilson, I.A., Donis, R.O., 2013. New world bats harbor diverse influenza A viruses. *PLoS Pathog* 9, e1003657.
- Tsigrelis, C., Mohammad, M., Fraimow, H.S., Dellinger, R.P., Marchesani, D., Reboli, A.C., 2010. Secondary bacterial pneumonia due to *Staphylococcus aureus* complicating 2009 influenza A (H1N1) viral infection. *Infection* 38, 237-239.
- Ungchusak, K., Auewarakul, P., Dowell, S.F., Kitphati, R., Auwanit, W., Puthavathana, P., Uprasertkul, M., Boonnak, K., Pittayawonganon, C., Cox, N.J., Zaki, S.R., Thawatsupha,

- P., Chittaganpitch, M., Khontong, R., Simmerman, J.M., Chunsutthiwat, S., 2005. Probable person-to-person transmission of avian influenza A (H5N1). *N Engl J Med* 352, 333-340.
- Varga, Z.T., Grant, A., Manicassamy, B., Palese, P., 2012. Influenza virus protein PB1-F2 inhibits the induction of type I interferon by binding to MAVS and decreasing mitochondrial membrane potential. *J Virol* 86, 8359-8366.
- Varga, Z.T., Ramos, I., Hai, R., Schmolke, M., Garcia-Sastre, A., Fernandez-Sesma, A., Palese, P., 2011. The influenza virus protein PB1-F2 inhibits the induction of type I interferon at the level of the MAVS adaptor protein. *PLoS Pathog* 7, e1002067.
- Vazquez, C., Horner, S.M., 2015. MAVS Coordination of Antiviral Innate Immunity. *J Virol* 89, 6974-6977.
- Velova, H., Gutowska-Ding, M.W., Burt, D.W., Vinkler, M., 2018. Toll-like receptor evolution in birds: gene duplication, pseudogenisation and diversifying selection. *Mol Biol Evol*.
- Viboud, C., Simonsen, L., Fuentes, R., Flores, J., Miller, M.A., Chowell, G., 2016. Global Mortality Impact of the 1957-1959 Influenza Pandemic. *J Infect Dis* 213, 738-745.
- Vreede, F.T., Jung, T.E., Brownlee, G.G., 2004. Model suggesting that replication of influenza virus is regulated by stabilization of replicative intermediates. *J Virol* 78, 9568-9572.
- Vynnycky, E., Edmunds, W.J., 2008. Analyses of the 1957 (Asian) influenza pandemic in the United Kingdom and the impact of school closures. *Epidemiol Infect* 136, 166-179.
- Wang, H., Feng, Z., Shu, Y., Yu, H., Zhou, L., Zu, R., Huai, Y., Dong, J., Bao, C., Wen, L., Yang, P., Zhao, W., Dong, L., Zhou, M., Liao, Q., Yang, H., Wang, M., Lu, X., Shi, Z., Wang, W., Gu, L., Zhu, F., Li, Q., Yin, W., Yang, W., Li, D., Uyeki, T.M., Wang, Y., 2008. Probable limited person-to-person transmission of highly pathogenic avian influenza A (H5N1) virus in China. *Lancet* 371, 1427-1434.
- Wang, P., Palese, P., O'Neill, R.E., 1997. The NPI-1/NPI-3 (karyopherin alpha) binding site on the influenza A virus nucleoprotein NP is a nonconventional nuclear localization signal. *J Virol* 71, 1850-1856.
- Wang, X., Basler, C.F., Williams, B.R., Silverman, R.H., Palese, P., Garcia-Sastre, A., 2002. Functional replacement of the carboxy-terminal two-thirds of the influenza A virus NS1 protein with short heterologous dimerization domains. *J Virol* 76, 12951-12962.

- Wang, Y., Brahmakshatriya, V., Lupiani, B., Reddy, S.M., Soibam, B., Benham, A.L., Gunaratne, P., Liu, H.C., Trakooljul, N., Ing, N., Okimoto, R., Zhou, H., 2012. Integrated analysis of microRNA expression and mRNA transcriptome in lungs of avian influenza virus infected broilers. *BMC Genomics* 13, 278.
- Weber, F., Elliott, R.M., 2002. Antigenic drift, antigenic shift and interferon antagonists: how bunyaviruses counteract the immune system. *Virus Res* 88, 129-136.
- Webster, R.G., Bean, W.J., Gorman, O.T., Chambers, T.M., Kawaoka, Y., 1992. Evolution and ecology of influenza A viruses. *Microbiol Rev* 56, 152-179.
- Wei, L., Cui, J., Song, Y., Zhang, S., Han, F., Yuan, R., Gong, L., Jiao, P., Liao, M., 2014. Duck MDA5 functions in innate immunity against H5N1 highly pathogenic avian influenza virus infections. *Vet Res* 45, 66.
- Wendel, H.A., Snyder, M.T., Pell, S., 1966. Trial of amantadine in epidemic influenza. *Clin Pharmacol Ther* 7, 38-43.
- Wertz, I.E., O'Rourke, K.M., Zhou, H., Eby, M., Aravind, L., Seshagiri, S., Wu, P., Wiesmann, C., Baker, R., Boone, D.L., Ma, A., Koonin, E.V., Dixit, V.M., 2004. De-ubiquitination and ubiquitin ligase domains of A20 downregulate NF-kappaB signalling. *Nature* 430, 694-699.
- White, M.R., Doss, M., Boland, P., Tecele, T., Hartshorn, K.L., 2008. Innate immunity to influenza virus: implications for future therapy. *Expert Rev Clin Immunol* 4, 497-514.
- Wies, E., Wang, M.K., Maharaj, N.P., Chen, K., Zhou, S., Finberg, R.W., Gack, M.U., 2013. Dephosphorylation of the RNA sensors RIG-I and MDA5 by the phosphatase PP1 is essential for innate immune signaling. *Immunity* 38, 437-449.
- Wise, H.M., Foeglein, A., Sun, J., Dalton, R.M., Patel, S., Howard, W., Anderson, E.C., Barclay, W.S., Digard, P., 2009. A complicated message: Identification of a novel PB1-related protein translated from influenza A virus segment 2 mRNA. *J Virol* 83, 8021-8031.
- Wise, H.M., Hutchinson, E.C., Jagger, B.W., Stuart, A.D., Kang, Z.H., Robb, N., Schwartzman, L.M., Kash, J.C., Fodor, E., Firth, A.E., Gog, J.R., Taubenberger, J.K., Digard, P., 2012. Identification of a novel splice variant form of the influenza A virus M2 ion channel with an antigenically distinct ectodomain. *PLoS Pathog* 8, e1002998.
- Wong, S.S., Webby, R.J., 2013. Traditional and new influenza vaccines. *Clin Microbiol Rev* 26, 476-492.

- Wu, B., Hur, S., 2015. How RIG-I like receptors activate MAVS. *Curr Opin Virol* 12, 91-98.
- Wu, B., Peisley, A., Richards, C., Yao, H., Zeng, X., Lin, C., Chu, F., Walz, T., Hur, S., 2013. Structural basis for dsRNA recognition, filament formation, and antiviral signal activation by MDA5. *Cell* 152, 276-289.
- Wu, B., Peisley, A., Tetrault, D., Li, Z., Egelman, E.H., Magor, K.E., Walz, T., Penczek, P.A., Hur, S., 2014. Molecular imprinting as a signal-activation mechanism of the viral RNA sensor RIG-I. *Mol Cell* 55, 511-523.
- Wu, J., Chen, Z.J., 2014. Innate immune sensing and signaling of cytosolic nucleic acids. *Annu Rev Immunol* 32, 461-488.
- Xiao, Y., Reeves, M.B., Caulfield, A.F., Evseev, D., Magor, K.E., 2018. The core promoter controls basal and inducible expression of duck retinoic acid inducible gene-I (RIG-I). *Mol Immunol* 103, 156-165.
- Xu, L.G., Wang, Y.Y., Han, K.J., Li, L.Y., Zhai, Z., Shu, H.B., 2005. VISA is an adapter protein required for virus-triggered IFN-beta signaling. *Mol Cell* 19, 727-740.
- Xu, X., Subbarao, Cox, N.J., Guo, Y., 1999. Genetic characterization of the pathogenic influenza A/Goose/Guangdong/1/96 (H5N1) virus: similarity of its hemagglutinin gene to those of H5N1 viruses from the 1997 outbreaks in Hong Kong. *Virology* 261, 15-19.
- Yamada, H., Chounan, R., Higashi, Y., Kurihara, N., Kido, H., 2004. Mitochondrial targeting sequence of the influenza A virus PB1-F2 protein and its function in mitochondria. *FEBS Lett* 578, 331-336.
- Yang, C., Bolotin, E., Jiang, T., Sladek, F.M., Martinez, E., 2007. Prevalence of the initiator over the TATA box in human and yeast genes and identification of DNA motifs enriched in human TATA-less core promoters. *Gene* 389, 52-65.
- Yasuda, J., Nakada, S., Kato, A., Toyoda, T., Ishihama, A., 1993. Molecular assembly of influenza virus: association of the NS2 protein with virion matrix. *Virology* 196, 249-255.
- Ye, J., Yu, M., Zhang, K., Liu, J., Wang, Q., Tao, P., Jia, K., Liao, M., Ning, Z., 2015. Tissue-specific expression pattern and histological distribution of NLRP3 in Chinese yellow chicken. *Vet Res Commun* 39, 171-177.

- Yi, C., Zhao, Z., Wang, S., Sun, X., Zhang, D., Zhang, A., Jin, M., 2017. Influenza A Virus PA Antagonizes Interferon-beta by Interacting with Interferon Regulatory Factor 3. *Front Immunol* 8, 1051.
- Yoneyama, M., Fujita, T., 2004. [RIG-I: critical regulator for virus-induced innate immunity]. *Tanpakushitsu Kakusan Koso* 49, 2571-2578.
- Yoneyama, M., Kikuchi, M., Matsumoto, K., Imaizumi, T., Miyagishi, M., Taira, K., Foy, E., Loo, Y.M., Gale, M., Jr., Akira, S., Yonehara, S., Kato, A., Fujita, T., 2005. Shared and unique functions of the DExD/H-box helicases RIG-I, MDA5, and LGP2 in antiviral innate immunity. *J Immunol* 175, 2851-2858.
- Yoshizumi, T., Ichinohe, T., Sasaki, O., Otera, H., Kawabata, S., Mihara, K., Koshihara, T., 2014. Influenza A virus protein PB1-F2 translocates into mitochondria via Tom40 channels and impairs innate immunity. *Nat Commun* 5, 4713.
- Zamarin, D., Garcia-Sastre, A., Xiao, X., Wang, R., Palese, P., 2005. Influenza virus PB1-F2 protein induces cell death through mitochondrial ANT3 and VDAC1. *PLoS Pathog* 1, e4.
- Zdanov, V.M., Antonova, I.V., 1969. The Hong Kong influenza virus epidemic in the USSR. *Bull World Health Organ* 41, 381-386.
- Zell, R., Krumbholz, A., Eitner, A., Krieg, R., Halbhuer, K.J., Wutzler, P., 2007. Prevalence of PB1-F2 of influenza A viruses. *J Gen Virol* 88, 536-546.
- Zhai, Y., Luo, F., Chen, Y., Zhou, S., Li, Z., Liu, M., Bi, D., Jin, H., 2015. Molecular characterization and functional analysis of duck TRAF6. *Dev Comp Immunol* 49, 1-6.
- Zhang, M., Song, K., Li, C., Chen, Z., Ding, C., Liu, G., 2015. Molecular cloning of Peking duck Toll-like receptor 3 (duTLR3) gene and its responses to reovirus infection. *Virol J* 12, 207.
- Zhang, W.X., Zuo, E.W., He, Y., Chen, D.Y., Long, X., Chen, M.J., Li, T.T., Yang, X.G., Xu, H.Y., Lu, S.S., Zhang, M., Lu, K.H., Lu, Y.Q., 2016. Promoter structures and differential responses to viral and non-viral inducers of chicken melanoma differentiation-associated gene 5. *Mol Immunol* 76, 1-6.
- Zhang, Y., Chen, Y., Xu, Q., Liu, R., Wu, N., Chen, G., 2018. Identification of DNA methylation and transcriptional regulatory regions in the promoter of duck retinoic acid inducible gene I (RIG-I). *Br Poult Sci* 59, 40-44.

- Zhao, L., Zhu, J., Zhou, H., Zhao, Z., Zou, Z., Liu, X., Lin, X., Zhang, X., Deng, X., Wang, R., Chen, H., Jin, M., 2015. Identification of cellular microRNA-136 as a dual regulator of RIG-I-mediated innate immunity that antagonizes H5N1 IAV replication in A549 cells. *Sci Rep* 5, 14991.
- Zhao, Z., Yi, C., Zhao, L., Wang, S., Zhou, L., Hu, Y., Zou, W., Chen, H., Jin, M., 2014. PB2-588I enhances 2009 H1N1 pandemic influenza virus virulence by increasing viral replication and exacerbating PB2 inhibition of beta interferon expression. *J Virol* 88, 2260-2267.
- Zhu, Q., Yang, H., Chen, W., Cao, W., Zhong, G., Jiao, P., Deng, G., Yu, K., Yang, C., Bu, Z., Kawaoka, Y., Chen, H., 2008. A naturally occurring deletion in its NS gene contributes to the attenuation of an H5N1 swine influenza virus in chickens. *J Virol* 82, 220-228.
- Zielecki, F., Semmler, I., Kalthoff, D., Voss, D., Mael, S., Gruber, A.D., Beer, M., Wolff, T., 2010. Virulence determinants of avian H5N1 influenza A virus in mammalian and avian hosts: role of the C-terminal ESEV motif in the viral NS1 protein. *J Virol* 84, 10708-10718.

Appendix I-Commonly Used Buffers and Solutions

- 20×PBS (1L)

<i>Chemical</i>	<i>Weight/Volume</i>
NaCl (EMD Millipore)	160 g
KCl (Sigma)	4 g
Na ₂ HPO ₄ (Merck)	28.8 g
KH ₂ PO ₄ (Merck)	4.8 g
ddH ₂ O	1 L
pH=7.4	

- 1% TritonX-100 lysis buffer (500 ml)

<i>Chemical</i>	<i>Weight/Volume</i>
Tris Base (Fisher)	3.029 g (50 mM)
NaCl (EMD Millipore)	0.633 g (150 mM)
TritonX-100 (Sigma)	5 ml
ddH ₂ O	adjust to 500 ml
pH=7.2	

- 4×Laemmli buffer (10 ml)

<i>Chemical</i>	<i>Volume</i>
1 M Tris-HCL (pH 6.8)	2.5 ml
β-mercaptoethanol	2 ml
80% Glycerol	4.7 ml
Bromophenol blue	2 mg
SDS	0.8 g
ddH ₂ O	adjust to 10 ml

- 12% SDS-PAGE resolving gel buffer (×2 gels)

<i>Chemical</i>	<i>Volume</i>
ddH ₂ O	4.3 ml
40% acrylamide (BioRad)	3 ml
1.5 M Tris-HCl (pH 8.8)	2.5 ml
10% (w/v) SDS (Fisher)	100 μl
10% (w/v) APS (Sigma)	100 μl
TEMED (BioRad)	6 μl

- 12% SDS-PAGE stacking gel buffer (×2 gels)

<i>Chemical</i>	<i>Volume</i>
ddH ₂ O	2.87 ml
40% acrylamide (BioRad)	500 μl
1 M Tris-HCl (pH 6.8)	500 μl
10% (w/v) SDS (Fisher)	40 μl
10% (w/v) APS (Sigma)	40 μl
TEMED (BioRad)	4 μl

- 10×SDS-PAGE running buffer (2 L)

<i>Chemical</i>	<i>Weight/Volume</i>
Tris Base (Fisher)	60.6 g
Glycine (BioShop)	300 g
SDS (Fisher)	20 g
ddH ₂ O	2 L

- 1×transferring buffer (1 L)

<i>Chemical</i>	<i>Volume</i>
ddH ₂ O	700 ml
10×SDS-PAGE running buffer stock	100 ml
Methanol	200 ml

➤ LB media (1 L)

<i>Chemical</i>	<i>Weight/Volume</i>
NaCl (EMD Millipore)	10 g
Bacto-tryptone (BD)	10 g
Bacto yeast extract (BD)	5 g
ddH ₂ O	1 L

➤ LB plus agar media (1 L)

<i>Chemical</i>	<i>Weight/Volume</i>
NaCl (EMD Millipore)	10 g
Bacto-tryptone (BD)	10 g
Bacto yeast extract (BD)	5 g
Select Agar (invitrogen)	15 g
ddH ₂ O	1 L

➤ SOC media (1 L)

<i>Chemical</i>	<i>Weight/Volume</i>
Bacto-tryptone (BD)	20 g
Bacto yeast extract (BD)	5 g
5 M NaCl (EMD Millipore)	2 ml
1 M KCl (Sigma)	2.5 ml
1 M MgCl ₂ (Sigma)	10 ml
1 M MgSO ₄ (Sigma)	10 ml
1 M glucose (Sigma)	20 ml
ddH ₂ O	adjust to 1 L

➤ MOWIOL mounting media for fluorescence microscopy

<i>Chemical</i>	<i>Weight/Volume</i>
Mowiol (Aldrich)	2.4 g
Glycerol (Fisher)	6 ml
0.2 M Tris-HCl (pH 8.5)	12 ml
Dabco (Aldrich)	450 µl

➤ 10×TBE buffer (1L)

<i>Chemical</i>	<i>Weight/Volume</i>
Tris Base (Fisher)	108 g
Boric acid (Sigma)	55 g
0.5 M EDTA (pH 8.0) (EMD Millipore)	40 ml
ddH ₂ O	adjust to 1 L

Appendix II-Sequence ID

Table App-1 The sequence ID of RIG-I proteins

Number	Common name	Accession #
1	human	NP_055129.2
2	mouse	NP_766277.3
3	mallard duck	NP_001297309.1
4	Muscovy duck	AGX27431.1
5	pigeon	AKR15098.1
6	zebrafish	NP_001293024.1
7	zebra finch	XP_012432982.1
8	rabbit	XP_002708086.1

Table App-2 The sequence ID of RIG-I promoters

Number	Common name	Accession #	Range
1	human	AL353671.6	1: 64121 to 66144
2	mouse	AL831793.4	1: 106557 to 108580
3	mallard duck	KY093012	
4	pigeon	102098789	NW_004973627.1 (322091..324114)
5	zebrafish	NM_001306095	chrUn_KN149959v1:42380-44403
6	zebra finch	NM_001311190	chrZ:31917390-31919413
7	rabbit	ENSOCUG00000004710	OryCun2.0:1:20942020:20944246

Table App-3 the sequence ID of MAVS proteins

Number	Common name	Accession #
1	human	NP_065797.2
2	mouse	NP_001193314.1
3	pig	NP_001090898.1
4	rabbit	XP_017197245.1
5	duck	XP_021130364.1
6	chicken	NP_001012911.1
7	canary	XP_018778718.1
8	hooded crow	XP_010400416.1
9	zebra finch	XP_002188030.1